Self-organized branching morphogenesis

Study of a related FKPP-system, and a case study of prostate cancer

Dissertation
zur
Erlangung des Doktorgrades (Dr. rer. nat.)
der
Mathematisch-Naturwissenschaftlichen Fakultät
der
Rheinischen Friedrich-Wilhelms-Universität Bonn

vorgelegt von
Florian Paul Kreten
aus
Prüm

Bonn, September 2023

Angefertigt mit Genehmigung der Mathematisch-Naturwissenschaftlichen
Fakultät der Rheinischen Friedrich-Wilhelms-Universität Bonn

Erstgutachter: Prof. Dr. Anton Bovier
Zweitgutachter: Prof. Dr. Juan Velázquez

Tag der Promotion: 16.11.2023
Erscheinungsjahr: 2024

Abstract

The group of E. Hannezo et al. proposed "*A Unifying Theory of Branching Morphogenesis*" in glandular epithelial tissues in 2017, based on a stochastic model related to branching and annihilating random walks. In this stochastic model, the individual branches of a tree-like structure grow and branch independently. A hard-coded self-avoiding mechanism makes an analytic treatment of the stochastic model challenging.

In the first part of this PhD thesis, we investigate a related PDE which describes the evolution of two densities of particles: The so-called *active* particles diffuse and branch and become inactive upon collision with a particle of arbitrary type. The *inactive* particles do not react and are of low diffusivity. In the absence of active particles, this system is in a steady state, irrespectively of the inactive particles. The resulting continuum of non-hyperbolic steady states complicates the analysis of the PDE.

We construct the non-negative traveling waves of the PDE and show that they share many similarities with those of the classical FKPP-equation. Among the constructed pulled heteroclinic waves, those with minimal possible speed – referred to as *critical* – are of particular relevance. Subject to compact initial data, simulations of the PDE always show the same behavior: The front of the solution converges to the critical traveling wave.

We then show that the critical traveling waves are asymptoticly stable. To overcome the problem that the limits of the traveling waves are not hyperbolic, we operate in a weighted space where the perturbations can grow exponentially at the back of the wave, but vanish point-wise, a phenomenon referred to as *convective stability*. In order to control the unbounded nonlinear terms of the perturbation equations, we establish a new type of a-priori estimate, based on a Feynman-Kac formula. Our stability results for the PDE support the numerical results found for the stochastic model.

In the second part of this thesis, we investigate the growth and the clonal evolution of *prostate adeconarcinoma* (PCA). These tumors form branched self-avoiding structures, we hypothesize that their growth follows the rules for branching morphogenesis formulated by Hannezo et al. We formulate a mathematical model for the growth and the stochastic genotypic evolution of PCA. Via simulations, we explore in detail the possible evolutionary patterns and clonal architectures, and demonstrate that the tumour architecture represents a major bottleneck for a divergent clonal evolution. As a result, we hypothesize that strong genomic driver mutations cause the evolution

of the tumors into more aggressive variants, contrasting the idea of a gradual, continuous evolution. We validate the results of our simulations using multiregional next generation DNA sequencing of the primary tumours from five patients, and find close similarities between our predictions of clonal development and real-world data from the patient samples.

Acknowledgments

First of all, I want to thank my advisor, Anton Bovier, for giving me the opportunity to do my PhD under his supervision. His feedback, though sometimes a bit uncomfortable, was always honest and helpful. Anton was one the one hand demanding, but on the other hand he has supported and guided my work without pressure of time. It is also thanks to Anton that I could work on an interdisciplinary project, and this biological background was a major motivation for me.

Yuri Tolkach initiated our collaboration on prostate cancer when I was still a Master's student, and our work took quite some turns over the last six years. Yuri, who never sleeps and is extremely stubborn, continuously pushed our project. I want to thank him also for our long discussions and teaching sessions.

Juan Velázquez gave a small, but very critical input for this thesis. He took the time for some discussions with me and reviewed a preprint of mine. I also want to thank the other two members of my committee, Martin Rumpf and Michael Hölzel, for taking their time to review my work.

Among all members of the probability theory group, I first want to thank Mei-Ling for holding the group together and for wearing her heart on her sleeve (... and for helping me with all sorts of paperwork in no time). Thanks to my office mate Luis for sharing a part of the journey, for encouragement and wonderful food, and also to Manuel and Annabell, who all three read proof some parts of this thesis. Thanks also to Adrien, Anna, Joy, Katharina, Kaveh, Maximilian and Saeda, for making the time in the group enjoyable.

Inga, my wonderful partner for life, knows all the ups and downs I had over the last years. I want to thank her and my family for the constant love and support.

Contents

1 Introduction

Biology and mathematics have a long history of interplay, dating back at least over two centuries [32], but over the last fifty years, the conversion of biology into a more quantifiable science has increased the payoff for both fields [80]. On the one hand, biological data can be interpreted and organized only with the help of the computational sciences, and applied mathematics can foster new biological theories. On the other hand, the use of mathematical modelling in biology leads to the development of new computational approaches [57], as well as it gives rise to theoretical problems.

In a *self-organized* system, the emergence of a macroscopic structure is determined solely by the behavior of its microscopic components. These components interact with and react to their local environment, without any additional global guiding mechanism. Biology abounds with phenomena that can be explained (at least partially) via self-organization of groups of individuals: Bacterial populations express pattern formation depending on their environment [88, 116], ant colonies are able to build nests, the coat patterns of zebra and giraffe can be explained via the interplay of different cell types during the growth phase of the animal [27], and corals and sponges which are built of repeated small units, form complex organisms [82].

Cells have countless ways to communicate and interact with each other. As such, cellular systems constitute a huge playground for possible self-organization phenomena and are able to express all different kinds of behavior: spontaneous pattern formation, traveling waves, oscillations and metastable states with fast switching [87, 109, 159]. It is believed that self-organization is vital for the robustness and the adaptability of cellular organization and the maintenance of tissues in general, though many of the underlying mechanisms are still unexplored [74, 159].

Our understanding of cellular systems increases rapidly since the 1990s. Mathematics plays an important role in this process by formalizing and quantifying the intracellular metabolism and the intercellular interactions, and by exploring possible outcomes. Mathematical models can bridge the gap between the different scales and shed light on one of the central questions: How do instructions that are encoded into the behavior of the individual cells translate into tissues with complex and heterogeneous shapes and functions? There exists a large and fast growing body of mathematical literature regarding organ formation, wound healing or tumor growth [37, 46, 74, 83, 99, 106].

1.1 Branching Morphogenesis

Branched structures are ubiquitous in biology. Often, they can be observed if a tubular system needs to maximize its surface per volume, in order to be able to efficiently exchange substances with its environment. In trees, corals, and many fungi [34, 82], repeatedly branched structures are visible to the naked eye. More hidden within the internal anatomy, branched structures are vital for the functionality of different mammalian organs. Prominent examples are the lung, the capillary blood vessels, the mammary glandular system and the kidney. It is a fascinating and unresolved question how the shape of these structures is encoded into the evolutionary program. Countless publications identify related genes and molecular signaling pathways that directly influence the cellular behavior. The critical pathways depend on the system under investigation. Many known results are gathered by Davies [38]. However, there is evidence for universal design principles that apply to a wider class of branched structures, even though their implementation differs from case to case [34, 74, 98]. This is where mathematical modeling comes into play: A mechanistic mathematical model can explain a phenomenon if it operates on the appropriate level of abstraction.

Figure 1.1: Gorgonian coral. Photo by Jesus Cobaleda @ Shutterstock.com.

Regarding branching morphogenesis, many mathematical works focus on the local decision process of the proliferating cells during the growth phase. Growth and branching of the cellular tubes can be explained via reaction-diffusion systems, in which cells consume and secrete different activator and inhibitor signals [68, 81, 113]. These models can explain different local morphologies (i.e. side-branching vs. branching only at the tips, frequency of branchings, etc.) via Turing patterns.

Witten and Sander [163] proposed a model named *Diffusion limited aggregation* (DLA), which resists attempts to be solved analytically since 1981. In this model, particles are randomly placed in space, and diffuse until they

stick to the existing (static) structure upon first contact. This process has been used successfully to produce fractal branched structures, depending on the precise formulation and the chosen parameters: Simulations of DLA can quantitatively reproduce patterns found in river networks, lightning, bacterial colonies, and corals [129], and can give rise to physiologies as in Figure 1.1. It is perplexing that this physical aggregation model also works in biological contexts, where some sort of reproduction drives growth.

There exists a (heuristic) connection between DLA and viscous fingering [107], a phenomenon that originally was observed at the border of two fluids of different viscosity under pressure. Several models related to viscous fluid mechanics have been proposed that consider tissues as "active fluids": on the one hand, tissues are subject to physical pressures, on the other hand, they consist of cells that reproduce, die, consume nutrients and secrete signals [121, 122]. These models can show branched behavior, for example they can explain the fingering invasion of tumors into the surrounding healthy tissue [17]. To our best knowledge, the current understanding of these models is limited to the arise of certain local patterns that can be observed in simulations.

In 2017, Hannezo et al. proposed *A Unifying Theory of Branching Morphogenesis* [73]. They modeled the branching morphogenesis of glandular structures in organs via a stochastic system that is based on branching and annihilating random walks. The aim of this study was to find a set of coherent microscopic rules that can explain the growth of the branched structure on the macroscopic scale. The proposed algorithm is based on simple local mechanisms, and generates a randomly growing binary tree that is able to fill a given volume (e.g. open, bounded sets in $\mathbb{R}^2$ or $\mathbb{R}^3$). A schematic representation in $\mathbb{R}^2$ is shown in Figure 1.2:

A vertex v of the network that is labeled as *active* can either spawn a single connected child-vertex u_1 ahead (referred to as growth-event), or spawn two child-vertices u_1, u_2 (referred to as branch-event), and the u_i are connected to v via edges as depicted. The directions of the new edges are random variables that depend on the direction of the previous edge, whereas the length of the edges is uniform. In both cases (growth or branch), the new edges and vertices must keep a certain minimal distance from all existing structures. After the new possible coordinates of the u_i are drawn randomly, it is checked if they are admissible: if they are not, the growth- or branch-event is not executed (termination-event). Not depending on the outcome, the vertex v becomes irreversibly *inactive* after an event was triggered, and the possibly generated vertices u_i are labeled as active. To keep the algorithm as simple as possible, all active vertices act independently and have their own two random exponential clocks with constant rates $r_g, r_b \geq 0$, that trigger a growth- and branch-event, respectively.

The numerical results of Hannezo et al. suggest that this stochastic sys-

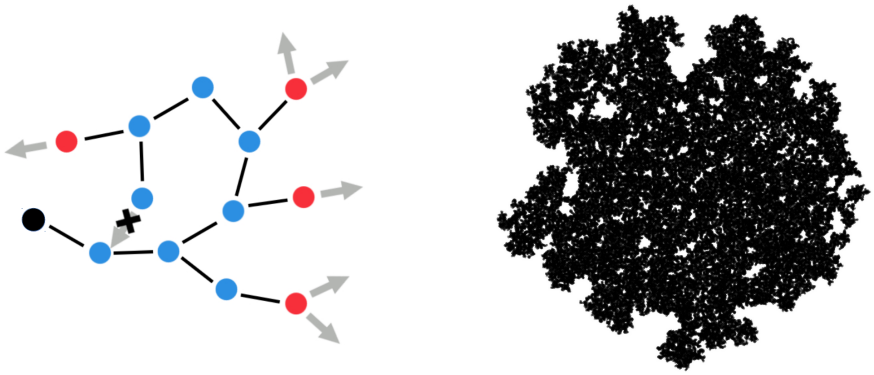

Figure 1.2: The left picture shows a schematic representation of an annihilating branching random walk. Starting with a single vertex (black), the active vertices (red) either grow or branch randomly, and become inactive afterwards. If the space ahead is already occupied, the vertex becomes also inactive. The right picture shows the result of a simulation in $\mathbb{R}^2$ *with* 100.000 *vertices.*

tem generates a spatially homogeneous, space-filling tree-structure; see Figure 1.2 for an example in $\mathbb{R}^2$. They observed the following behavior: The active vertices form a rather sharp layer at the boundary of the network, and this boundary invades into the empty space with constant speed. Contrarily, the interior of the network is almost entirely static. It consists mostly of inactive vertices, which fill the space with a constant density of vertices (subject to local fluctuations). The density and the geometry of the network depend on few key parameters, the most important one being the relative frequency of branchings r_b/r_g.

The authors of [73] verified that their model reproduces very well the growth-phase of the mouse mammary gland epithelium – where they had precise data for different time-points - and also compared their results to the mouse kidney and the human prostate, which are physiologically related. The results suggest that annihilating branching random walks are a suitable framework for formulating the development of branched epithelial tissues as self-organized processes. The proposed rather simple stochastic mechanism is robust against smaller errors of its individual components [74].

1.2 The PDE under investigation

Branching and annihilating random walks have been studied mathematically [23], but adding self-avoiding paths complicates a theoretical analysis, due to the non-Markovian nature of self-avoiding structures. In order to study the dynamics in [73] analytically, Hannezo et al. proposed the PDE (1.1) as a heuristic hydrodynamic limit of the stochastic system. Considering the one-dimensional case $z \in \mathbb{R}, t \in \mathbb{R}_0^+$, two densities of active and inactive

particles $A(t,z), I(t,z) \geq 0$ follow dynamics

$$\begin{aligned} \frac{\partial}{\partial t} A &= \frac{\partial^2}{\partial z^2} A + A - A(A+I), \\ \frac{\partial}{\partial t} I &= d\frac{\partial^2}{\partial z^2} I + rA + A(A+I), \end{aligned} \tag{1.1}$$

for some fixed parameters $r, d \geq 0$. Given the normalized System (1.1), the case with general reaction rates and diffusion speeds can be obtained by rescaling, see the appendix in [92]. For $d = 0$, the PDE (1.1) encapsulates all mechanisms of the stochastic branching system in a simplified way: Active, diffusing particles spawn inactive particles with rate r and branch into two active particles with rate 1, and become irreversibly inactive upon collision with a particle of arbitrary type. The inactive particles do not react themselves, and keep their position in a strict sense if $d = 0$. We consider also the case of low diffusivity $0 < d \ll 1$, which is analytically beneficial since the PDE is parabolic.

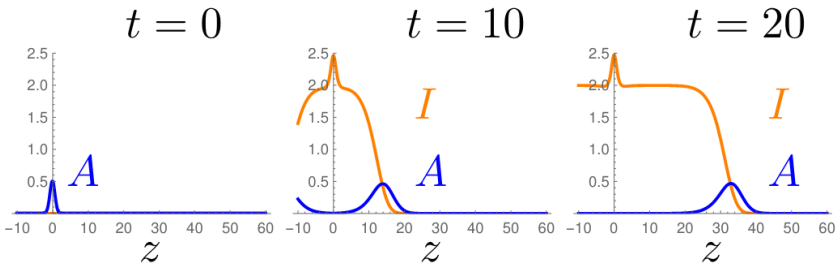

Figure 1.3: Simulation of System (1.1) *for* $r, d = 0$. *Given an initial heap of active particles* $A(z,0) = 1/2\exp(-z^2)$, *and* $I(z,0) = 0$, *two identical traveling fronts arise, the right one is shown. After the separation of the two fronts away from the origin, the density of the remaining inactive particles is given by* $I = 2$ *and the front moves asymptotically with speed* $c = 2$.

For the analysis of System (1.1), the behavior of the inactive particles poses the major difficulty: It gives rise to the continuum of steady states

$$P_I = \{A = 0, I = K \mid K \in \mathbb{R}\}. \tag{1.2}$$

Without further knowledge, we do not know which of these steady states are relevant. Additionally, this continuum implies that none of the points in (1.2) is a hyperbolically stable fixed point of the reaction, which further complicates the analysis.

If we set $I \equiv 0$, the remaining equation for $A(x,t)$ simplifies to the well-known FKPP-Equation (2.1). Despite the additional structure, we will see that System (1.1) shares many properties with the classical FKPP-equation. We postpone the discussion to Section 2.1.

Figure 1.3 depicts the result of a simulation: Given a small initial heap of active particles, two identical fronts arise, we concentrate on the right-traveling one. After a small burn-in time, the front of the system admits an almost fixed shape: The active particles form a traveling pulse, that moves with linear speed $c = 2$, and generate a monotone front of inactive particles which saturates at $I = 2$. Qualitatively, this reflects the behavior of the stochastic system very well, where the active vertices form a sharp layer of growth at the boundary of the network, and where the resulting network has a constant density of vertices per volume.

The front with fixed shape which can be observed in Figure 1.3, is a particular traveling wave of the PDE. In this PhD thesis, we construct and analyze the non-negative traveling wave solutions of System (1.1). Among all the constructed solutions, which can have different limits in P_I (1.2), we focus on the slowest non-negative wave that invades into the empty space, which characterizes uniquely the wave which we observe in Figure 1.3. We show that this wave is stable against small perturbations. Since its limits are not hyperbolic, we need to extend the existing stability theory to this degenerate case. It is worth mentioning that some of our results were predicted numerically and heuristically by Hannezo et al. [73].

The outline of this thesis is given in Section 1.4. Before, we explain how we got interested in branching morphogenesis in the first place:

1.3 The branched growth of prostate cancer

It was observed by Tolkach et al. that a particular class of prostate adeno carcinoma (PCA) does form glandular systems, at least as long as they are classified as low or intermediate aggressive types. A three-dimensional reconstruction revealed that these glandular systems form a self-avoiding branched structure, which belongs precisely to the class of objects that can be generated by the model of Hannezo et al. [146]. As such, the tumor-cells seem to mimic the behavior of the surrounding healthy tissue: The normal prostate glandular system is also known to be highly branched [142]. However, Tolkach et al. could analyze only samples taken via prostatectomy, where the entire prostate or at least substantial parts are removed surgically. There is no available time series data.

Cancer is seen as a disease that mainly develops via a chain of (stochastic) somatic mutations, emanating from healthy cells with normal behavior. These mutations lead to cell-lines which on the one hand show increased proliferation and on the other hand are able to escape the regulatory mechanisms of the immune system [31]. It is a clinically important question how long these evolutionary processes take, and if there are prevalent evolutionary patterns, since progression of the tumors into more aggressive variants

continues after the occurrence of the first malignant cells.

The existing theoretical approaches do not present a coherent picture, since the statistical evaluation of the data as well as the deduction of any underlying theory is complex. Most mutations do not seem to affect the behavior of the cells, but are merely passengers or might even have deleterious effects – from the perspective of the cancer [26, 139]. There is an ongoing debate if the evolution of cancer is a more continuous accumulation of rather weak mutations, or if it is a consequence of few decisive mutation events [162].

PCA is a relatively slow growing cancer, typically age-related, and becomes aggressive and dangerous only in some cases [164]. Its evolution is not understood, even its cell-of-origin remains to be determined [110, 157]. Based on the findings of Tolkach et al. [146], we developed a mathematical model that describes the evolution of well-differentiated PCA via stochastic mutations, and its growth via self-avoiding annihilating random walks in the sense of Hannezo et al. [73] – note that the latter remains to be an assumption, though a reasonable one. We focused on the question which implications this special spatial structure could possibly have on the evolution of the tumor.

As a result, we hypothesize that the spatial structure of prostate cancer serves as a bottleneck for its evolution [94]: As long as the tumor is restrained to follow the rules of branching morphogenesis, its cells – being encased in the glandular network of the tumor – are subject to constant competition. This competition implies that new, fitter genotypes can spread only if they either have a high fitness advantage, or if they break up the spatial structure of the tumor. Concluding, the evolution of well-differentiated PCA is more likely to be driven by few, strong driver mutations.

We simulated the resulting process, which includes both the growth via branching and annihilating random walks, and the stochastic emergence of the new genotypes. Importantly, we only chose the parameters from the literature and by good reasoning, and did not fit them a-priori. We then compared our numerical results to biological data (from five cases), and found a qualitative agreement. Our findings should be seen as preliminary, as this work is under review at the time of writing of this thesis. The unpublished preprint [94] can be found in appendix C.

1.4 Outline

The remainder of this thesis is structured as follows. First, we present the mathematical background of our theoretical work in Chapter 2. In Chapter 3, we construct the traveling wave solutions of System (1.1) in the case $d = 0$. In Chapter 4, we then extend this result via continuation techniques to the case $d > 0$, and analyze the stability of the resulting waves against small perturbations. In chapter 5, we summarize our work on growth and

evolution of prostate cancer. We conclude with a summary of our results in Chapter 6. The Appendices contain the publication, the preprint, and the unpublished work summarized in Chapter 3, 4 and 5: the publication [92] can be found in appendix A, the preprint [93] in appendix B, and the unpublished work [94] in C.

2 Mathematical background: stability of traveling waves

2.1 Traveling waves of FKPP-systems

Reaction-diffusion systems provide the natural framework for the mathematical analysis of the spatiotemporal patterns that can arise from a set of local interaction rules, there exists an extensive literature that focuses on systems with a biological motivation [24, 114, 156]. Two works presumably constitute the foundation of the field. The first is Turings *The Chemical basis of Morphogenesis* [147], describing the arise of complex spatiotemporal patterns due to the instability of a homogeneous rest state.

The second, which is of importance for the present thesis, is the analysis of the FKPP-equation in the 1930s by Fisher [50] and Kolmogorov, Petrovski and Piscunov [91]. This equation describes the spreading of a fitter population. In its simplest form and in one spatial dimension $z \in \mathbb{R}$, this equation describes the evolution over time of a density of diffusing particles $A(t, z) \geq 0$ that undergo dampened growth:

$$\frac{\partial}{\partial t} A = \frac{\partial^2}{\partial z^2} A + F(A), \tag{2.1}$$

where $F : \mathbb{R} \to \mathbb{R}$ is a reaction that satisfies

$$F(0) = F(1) = 0, F'(0) > 0, F'(1) \leq 0, F''(u) < 0 \quad \forall u \in (0, 1). \tag{2.2}$$

The classical example for F is the logistic growth function $F(A) = A - A^2$. Given the FKPP-Equation (2.1), a (right-) traveling wave with speed $c > 0$ is a bounded solution that is constant in the moving frame $x = z - ct$. We only consider twice differentiable waves $\phi(x) : \mathbb{R} \to \mathbb{R}$, which solve the resulting ordinary differential equation

$$0 = \frac{\partial^2}{\partial x^2} \phi(x) + c \frac{\partial}{\partial x} \phi(x) + F\big(\phi(x)\big) \tag{2.3}$$

in a strong sense. The Equation (2.3) has heteroclinic solutions $\phi(x)$ that connect the unstable steady state $\phi = 0$ (at $x = +\infty$) with the stable steady state $\phi = 1$ (at $x = -\infty$). Non-negative solutions, which are the physically relevant ones, exist for all speeds

$$c \geq c_{\min} := 2\sqrt{F'(0)}, \tag{2.4}$$

where the critical value $c_{\min}$ is determined by the linearization of $\phi(x)$ around the unstable state $\phi = 0$, if the reaction satisfies (2.2) [50, 148]. It can easily be seen that Condition (2.4) is necessary: Asymptotically as $x \to +\infty$,

solutions oscillate and thereby become negative if the eigenvalues of the linearized system,

$$\lambda_{\pm} = -\frac{c}{2} \pm \sqrt{\frac{c^2}{4} - F'(0)}, \tag{2.5}$$

are not real-valued, which is true for all $c < c_{\min}$.

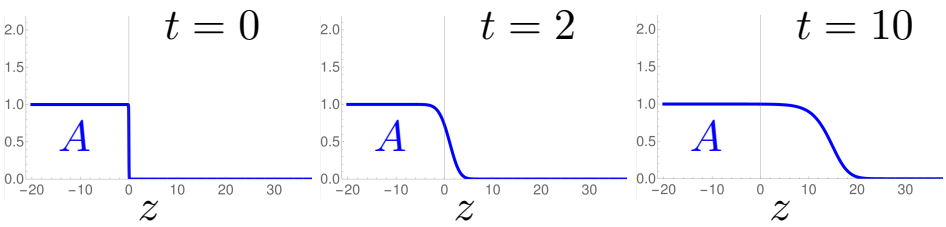

Figure 2.1: Simulation of the FKPP-Equation (2.1) *with logistic growth, given Heaviside initial data* $A(0, z) = \mathbb{1}_{z \leq 0}$. *The front converges to the traveling wave with speed* $c_{\min} = 2$, *which is well-approximated already for* $t = 10$.

The solutions of (2.3) with Reaction (2.2) are referred to as *pulled* traveling waves, since their wave speed is determined uniquely by the tail of $\phi(x)$ as $x \to +\infty$, corresponding to the asymptotic growth speed. The wave with speed $c_{\min}$ is referred to as the *critical* traveling wave; the other waves with speed $c > c_{\min}$ are called *supercritical*. As we will see, the critical traveling wave is the most important one, but also the most intricate to study.

For the FKPP-equation, several proofs show that the traveling waves are the global attractors of the system. Kolmogorov, Petrovski and Piscunov proved in 1937 that if the PDE starts in Heaviside initial data, then its front converges to the critical traveling wave as $t \to \infty$ [91], as depicted in Figure 2.1. Extensions of this result to more general initial data and a more precise description of the speed of the front have been provided by Uchiyama [148], and in particular by Bramson [22], who proved that the front of the PDE with Heaviside initial data actually moves slightly slower – with a difference of order $\log(t)$ – then its limiting traveling wave.

Given that the initial data decays fast enough, then it is always the critical wave which arises in the large time limit. The proofs of Kolmogorov et al. and Uchiyama rely on a comparison principle and on the fact that if the initial data is monotone, then the front remains monotone for all $t \geq 0$. Bramson used a Feynman-Kac formula to relate solutions of the FKPP-equation to branching Brownian motion, which yields very precise estimates on the speed and decay of the front. Both methods work particularly well for systems with a single reactant.

FKPP-related systems often show a similar behavior: They form heteroclinic fronts that connect an unstable state to a stable one and have a certain

minimal speed [41, 48]. However, convergence results are sparse for systems with more than one reactant, and essentially rely on monotonicity and comparison techniques. Given that all reactants move with different asymptotic speeds such that the fronts separate, each front is monotone and satisfies a comparison principle during its own phase of invasion [41]. Figuratively, the authors named these consecutive fronts *propagating terraces*. Under the assumption that the reactants are cooperative and form a monotone front of a single speed [66], one can construct suitable super- and sub-solutions. More recently, Bovier and Hartung used a Feynman-Kac formula to derive precise results on the spreading speeds in a model of two competing species with mutation [19]. Different applications of the Feynman-Kac formula are suitable for analyzing the asymptotic speeds of FKPP-systems, but even given the invasion speed, it remains challenging to prove convergence of the front towards a particular traveling wave.

The (right-) traveling waves of System (1.1) are a pair of functions

$$a : \mathbb{R} \to \mathbb{R}, \quad i : \mathbb{R} \to \mathbb{R}, \tag{2.6}$$

that solve System (1.1) via the ansatz $A(z,t) = a(z-ct), I(z,t) = i(z-ct)$, for a speed $c > 0$ to be determined. As such, they are solutions of a system of coupled ODEs:

$$\begin{aligned} 0 &= a'' + ca' + a - a(a+i), \\ 0 &= di'' + ci' + a(a+i+r). \end{aligned} \tag{2.7}$$

In this thesis, we construct those solutions of (2.7) where $a, i \geq 0$, which we call non-negative, and prove that they share many similarities with those of classical FKPP-systems. We call a non-negative solution of (2.7) an *invading front*, if

$$\lim_{x \to +\infty} a(x) = \lim_{x \to +\infty} i(x) = 0. \tag{2.8}$$

This additional restriction is required due to the continuum of fixed points (1.2), since there are also solutions that are associated to other fixed points.

The minimal speed $c_{\min} = 2$ of an invading front turns out to be determined by the asymptotic growth speed of the active particles and not affected by the inactive particles. The details are given in Chapter 3. The invading front with minimal speed can be observed in the simulation depicted in Figure 1.3: The active particles form a non-monotone pulse and are accompanied by a monotone front of inactive particles of the very same speed.

Proving convergence of solutions the PDE (1.1) towards the traveling waves of the PDE for general classes of initial data is difficult, since the waves are not monotone. Moreover, the inactive particles accumulate only as a by-product of the active ones, thus the system is in lack of useful comparison

principles. However, all our simulations indicate that under initial data that decay sufficiently fast, it is always the critical invading front which arises in the large time limit (as for the classical FKPP-equation). This critical invading is in the focus of our studies. Its stability against small perturbations in analyzed in Chapter 4.

2.2 Stability of traveling waves: setting and notation

For systems that lack any comparison principle, one can still analyze the stability of a traveling front against small perturbations. A classical introduction to the field was written by Sandstede [130], a more recent survey is due to Ghazaryan et al. [63]. As we will see after a recap of the existing results, analyzing the stability of the critical traveling waves of System (1.1) requires for a new approach, which we present in Chapter 4.

In the following, we consider a reaction-diffusion system

$$\frac{\partial}{\partial t}Y(t,z) = D \cdot \frac{\partial^2}{\partial z^2}Y + R(Y), \tag{2.9}$$

where $Y \in \mathbb{R}^n, z \in \mathbb{R}, t \geq 0, D = \mathrm{diag}(d_1, \ldots, d_n)$ with $d_i \geq 0$, and a smooth reaction $R : \mathbb{R}^n \to \mathbb{R}^n$. If $det(D) > 0$, the equation is called *parabolic*, otherwise it is called *partly parabolic* or with *degenerate diffusion*. For speeds $c > 0$, we consider the moving frame $x = z - ct$, where the system reads

$$\frac{\partial}{\partial t}Y = D \cdot \frac{\partial^2}{\partial x^2}Y + c\frac{\partial}{\partial x}Y + R(Y). \tag{2.10}$$

A right-traveling wave $\phi(x) : \mathbb{R} \to \mathbb{R}^n$ with speed c is a constant solution of Equation (2.10). In the following, we assume without further mentioning that $\phi(x)$ is a bounded and twice differentiable wave that converges exponentially fast at both ends.

For analyzing the stability of the wave, we write the solution of the PDE (2.10) as the sum of a (possibly shifted) wave and a perturbation $\tilde{Y}$:

$$Y(t,x) = \phi\big(x + \gamma(t)\big) + \tilde{Y}(t,x), \tag{2.11}$$

for a shift $\gamma(t)$ to be determined. The dynamics of the perturbation are then decomposed into a linear and nonlinear part

$$\frac{\partial}{\partial t}\tilde{Y} = \mathcal{L}\tilde{Y} + N\tilde{Y}. \tag{2.12}$$

We focus on the case without shift, where $\gamma \equiv 0$, but want to mention that most of the following results are not restricted to this case. The shift is for example analyzed in detail in [14, 63, 132].

For $\gamma \equiv 0$, the linear part $\mathcal{L}$ is obtained by linearizing the equation for the perturbation $\tilde{Y}$ around to the constant wave ϕ:

$$\mathcal{L}\tilde{Y} = D \cdot \frac{\partial^2}{\partial x^2}\tilde{Y} + c\frac{\partial}{\partial x}\tilde{Y} + JR(\phi) \cdot \tilde{Y}, \tag{2.13}$$

where $JR(\phi)$ is the Jacobian of the reaction R, evaluated at ϕ. The term $N\tilde{Y}$ is the remainder of the reaction and nonlinear in $\tilde{Y}$.

In order to select for specific types of perturbations, that are for example spatially localized, we introduce the following notion:

Definition 2.1 (Weight)**.** A smooth function

$$w : \mathbb{R} \to \mathbb{R}_{>0} \tag{2.14}$$

is called a *conservative weight* if it is bounded, otherwise it is called *degenerate*. A degenerate weight is called *convective* if $w(x)|_{x\leq 0}$ is unbounded while $w(x)|_{x\geq 0}$ is bounded.

Given a weight w, one writes the Perturbation (2.12) as

$$\tilde{Y}(t,x) = w(x)u(t,x), \tag{2.15}$$

and then analyzes the behavior of $u(t,x)$. If the unweighted perturbation solves $\frac{\partial}{\partial t}\tilde{Y} = \mathcal{L}\tilde{Y} + N(\tilde{Y})$, the weighted one solves

$$\begin{aligned} \frac{\partial}{\partial t}u(t,x) &= \mathcal{L}u + 2\frac{w'}{w}D \cdot u_x + \big(c\frac{w'}{w} + \frac{w''}{w}\big)u + \frac{1}{w}N(wu), \\ &=: \mathcal{L}_w u + \frac{1}{w}N(wu). \end{aligned} \tag{2.16}$$

Using weights that grow or decay exponentially, the spectrum of $\mathcal{L}_w$ is typically shifted compared that of $\mathcal{L}$, possibly changing the stability of the perturbations [64, 118, 130, 132].

Remark: In the literature, the roles of w and w^{-1} are sometimes interchanged. In the course of this thesis, a *weight* corresponds to Equation (2.15) and describes the growth or decay of the perturbation.

We assume that $\mathcal{L}_w$ defined by (2.16) is a bounded, closed and densely defined operator. For $Y \in \mathbb{R}^n$, we consider

$$\mathcal{L}_w : \mathcal{D}^n \to \mathcal{B}^n, \tag{2.17}$$

acting on an $n-$dimensional vector of perturbations, typically for one of the classical pairs of Banach spaces

$$\begin{aligned} &\mathcal{D} = BC^i(\mathbb{R}) \subset \mathcal{B} = BC^{i-2}(\mathbb{R}),\ i \in \mathbb{N}_{\geq 2}, \\ &\mathcal{D} = H^2(\mathbb{R}) \subset \mathcal{B} = L^2(\mathbb{R}), \end{aligned} \tag{2.18}$$

where H^2 is the L^2 Sobolev space with derivative up to the second order, and BC^i is the space of functions that are bounded and continuous up to the i-th derivative, with norm

$$||u||_{BC^i} = \sum_{j=0}^{i} ||u_j||_\infty. \tag{2.19}$$

In both cases, $\mathcal{D}$ lies dense in $\mathcal{B}$. The product-structure of H^2 allows for energy based estimates [118, 153]. However, the first results were proven in BC [132], which seems like a more natural choice. Without further mentioning, the operator $\mathcal{L}_w$ is defined as above.

The spectrum of a bounded linear operator $\mathcal{L}$ is the set of complex numbers λ such that $\mathcal{L} - \lambda\mathbb{1}$ has no bounded inverse. It can be decomposed into the discrete spectrum Σ_d, where solutions of

$$(\mathcal{L} - \lambda\mathbb{1})u = 0,\ u \in \mathcal{D}, \tag{2.20}$$

exist. The rest is called the essential spectrum (Σ_{ess}).

Definition 2.2. The linear operator $\mathcal{L}_w$ is called *spectrally stable with spectral gap* if its spectrum is contained in a sector of type

$$\{\lambda \in \mathbb{C} | \, \mathfrak{Re}\lambda \leq a\}, \tag{2.21}$$

for some $a < 0$, with the possible exception of an isolated simple eigenvalue $0 \in \Sigma_d$ that is associated to ϕ'. We call $\mathcal{L}_w$ *marginally spectrally stable* if the same is true for $a = 0$.

If 0 is a simple discrete eigenvalue of $\mathcal{L}_w$, denote by $\mathcal{Y} \in \mathcal{D}$ the null space of the Riesz spectral projection onto the span of ϕ', otherwise let $\mathcal{Y} = \mathcal{D}$. We say that $\mathcal{L}_w$ is *linearly stable*, if solutions of the linear equation

$$\frac{\partial}{\partial t} u = \mathcal{L}_w u, \tag{2.22}$$

with $u(0) \in \mathcal{Y}$ obey

$$\lim_{t \to +\infty} u(t) = 0, \tag{2.23}$$

where the type of convergence is to be specified. If (2.23) holds, we call $\mathcal{L}_w$ *exponentially linearly stable* if there exist constants $C, \beta > 0$ such that

$$||u(t)||_{\mathcal{D}} \leq Ce^{-\beta t}||u(0)||_{\mathcal{D}} \quad \forall t \geq 0, u(0) \in \mathcal{Y}. \tag{2.24}$$

Lastly, the wave ϕ is called *asymptotically nonlinearly stable*, if there exists a weight w, such that any solution of the PDE (2.10) in the moving frame $x = z - ct$ with initial data

$$Y(0, x) = \phi(x) + w(x)u(0, x), \tag{2.25}$$

where $u(0,x)$ is a sufficiently small perturbation (to be specified), converges to a shift of ϕ. This means, there exists a shift $\gamma \in \mathbb{R}$, such that

$$\lim_{t\to\infty} Y(t,x) = \phi(x+\gamma), \tag{2.26}$$

again in a sense to be specified. We differentiate between stability with shift and without shift (if $\gamma = 0$), both are sometimes also referred to as *orbital stability*.

Remark: For the unweighted perturbation, the equation $\mathcal{L}\phi' = 0$ holds in all cases. It is determined solely by the choice of the weight if $0 \in \Sigma_d(\mathcal{L}_w)$. If $0 \notin \Sigma_d(\mathcal{L}_w)$, the perturbations under consideration decay faster than the wave itself, typically resulting in (non-)linear stability without shift. This setting is used for studying the stability of pulled FKPP-fronts [48, 89, 132] as in the present case, see Section 2.3. If $0 \in \Sigma_d$, then the wave is typically stable with shift [14, 63, 132].

Given a wave ϕ, one tries to find a space and a weight w such that $\mathcal{L}_w$ is spectrally stable, and such that spectral stability implies also linear stability. The relationship between the spectrum of a linear operator and the associated semigroup is rather complex. We focus on the case where $\mathcal{L}_w$ is sectorial, see Definitions 2.3. In this case, there exists an efficient connection between the spectrum of $\mathcal{L}_w$ and its generated analytic semigroup via a Laplace inversion. Note that by Equation (2.16), the operator $\mathcal{L}_w$ is affected only by w'/w and w''/w. Thereby, weights with exponential asymptotics essentially result in some additional constants in $\mathcal{L}_w$, but on a theoretical level do not change the properties of the operator. However, the weight heavily influences how one can deal with the nonlinearity $N(uw)/w$.

If w is bounded or even integrable, the nonlinearity can be dealt with in great generality since $\mathcal{O}(N(uw)/w) = \mathcal{O}(u^2 w)$ [14, 63, 132], whereas proving nonlinear stability is much more difficult if w is unbounded. See [131] for a motivation to use convective weights, and [64, 118] for rigorous results.

The various approaches for proving nonlinear stability highly depend on the chosen space and the precise form of the spectrum [47, 63, 124, 130]. In this thesis we prove stability without shift via a classical Duhamel's principle: Denoting as $S(t)$ the semigroup generated by $\mathcal{L}_w$, the solution $\tilde{Y}(t)$ of the full nonlinear problem (2.16) has a unique weak representation:

$$u(t) = S(t)u_0 + \int_0^t S(t-s)\frac{N\big(wu(s)\big)}{w}\,ds. \tag{2.27}$$

Equation (2.27) holds if the nonlinearity is locally Lipschitz, see e.g. Pazy [117, p. 185 ff.]. The integral can be controlled if the nonlinearity is small enough [47, 48, 132], which is straightforward if the weight is integrable. We analyze a case where w is unbounded, but where we can still control the nonlinearity.

2.3 The spectrum of the system under investigation

We present a short interlude on the spectrum of $\mathcal{L}_w$ for the critical waves of System (1.1). An in-depth review of the underlying theory and related techniques was written by Sandstede [130]; the detailed calculations and results announced in this paragraph can be found in Section B.2.3.

There is no universal approach for evaluating the point spectrum $\Sigma_d(\mathcal{L}_w)$. If the considered wave is monotone, comparison techniques can be used to prove that $\Sigma_d(\mathcal{L}_w)$ is stable, we cite [48, 132] for FKPP-fronts. Another possible approach is to use singular perturbation techniques, if the spectrum of the unperturbed system is known [55]. For System (1.1), a numerical analysis shows that $\Sigma_d(\mathcal{L}_w)$ is stable for the critical invading fronts, for a suitable weight w described in the following. We refer to appendix B.4.2 for a description of the numerical approach.

Contrarily, the essential spectrum Σ_{ess} can be computed: Given that the wave ϕ converges exponentially fast at both ends, it holds that Σ_{ess} is bounded to the right by the two spectra Σ_- and Σ_+ of the two operators $\mathcal{L}_-$ and $\mathcal{L}_+$, which are the limits of (2.13) at the steady states. This is a classical result, see e.g. [130, Thm. 3.2], relying on exponential dichotomies. These two operators have constant coefficients, and thereby their spectra can be computed directly.

Pulled FKPP-fronts connect an unstable state to a stable one. The perturbation must decay faster than the front itself, otherwise Σ_+ cannot be stable, see [132, Sec. 6]. The critical invading fronts of System (1.1) have minimal speed $c = 2$ and decay as fast as $x \cdot e^{-x}$ as $x \to +\infty$, see Theorems 3.1 and 4.1. Consider a weight $w(x)|_{x\geq 1} = e^{-\alpha_+ x}$. Decisive for the stability of Σ_+ is the set $\Sigma_\nu \subset \Sigma_+$, defined as

$$\Sigma_\nu(\alpha_+) := \big\{\lambda \in \mathbb{C} \big| \, \mathfrak{Re}\big(\nu_+(\lambda)\big) = 0 \vee \mathfrak{Re}\big(\nu_-(\lambda)\big) = 0\big\}, \tag{2.28}$$

for the pair of eigenvalues

$$\nu_\pm(\lambda, \alpha_+) = -1 \pm \sqrt{\lambda} + \alpha_+. \tag{2.29}$$

In order to stabilize Σ_+, the weight must obey $w(x)|_{x\geq 1} = e^{-x}$, which is the only possible choice. This can easily be seen from (2.29). This phenomenon occurs for all pulled critical FKPP-fronts, consider also the classical literature [132]. The front of the weighted perturbations is only marginally spectrally stable in this case, since

$$\Sigma_\nu(\alpha_+ = 1) = \big\{\lambda \in \mathbb{C} \big| \mathfrak{Re}\lambda \leq 0, \mathfrak{Im}\lambda = 0\big\} \subset \Sigma_+. \tag{2.30}$$

The situation is different for supercritical fronts, where a conservative weight can be found such that $\mathcal{L}_w$ is spectrally stable with spectral gap [132].

To further complicate the situation, the limit of the wave as $x \to -\infty$ is not hyperbolic, due to the continuum of fixed points (1.2). In a space with

weight $e^{-\alpha x}|_{x\leq -1}$, the spectrum Σ_- contains the parabola

$$\mathcal{P}(\alpha_-) := \Big\{\lambda \in \mathbb{C}\Big|\, \mathfrak{Re}\lambda = \frac{1}{d}\big(2(1-d\alpha_-)^2 - 1 - |\lambda+1|\big)\Big\}. \tag{2.31}$$

This parabola is marginally stable for $\alpha_- = 0$, touching the origin in a quadratic fashion. In order to stabilize it, we consider a convective weight:

$$w(x) = \begin{cases} e^{-x} & x \geq 1, \\ e^{-\alpha x} & x \leq -1, \\ 1 & x = 0 \end{cases} \quad \text{with fixed } \alpha \in (0,1), \tag{2.32}$$

which allows the perturbations to grow exponentially as $x \to -\infty$. Still, $\mathcal{L}_w$ is only marginally stable due to (2.30), as depicted in Figure 2.2.

We continue with a review of the classical results for nonlinear stability. The phenomenon of convective stability are discussed in Section 2.6.

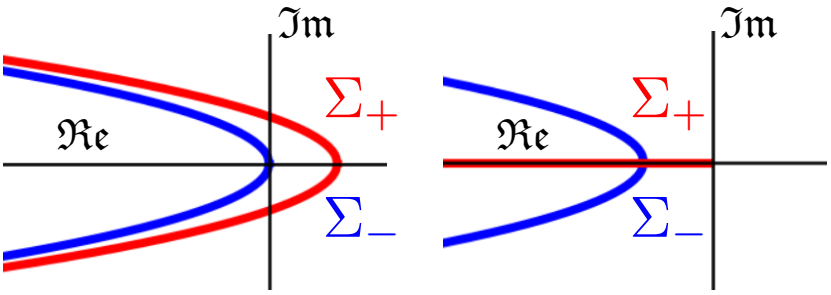

Figure 2.2: Two parts of the essential spectrum of $\mathcal{L}_w$ for a critical invading front of System (1.1). On the left, the essential spectrum is unstable in an unweighted space (with $w \equiv 1$). On the right, the essential spectrum is stabilized via the weight (2.32). The spectrum is contained in the strictly negative half-plane and bounded away from the origin, except that the half-line $\{\lambda \in \mathbb{C}|\mathfrak{Re}\lambda \leq 0, \mathfrak{Im}\lambda = 0\}$ goes up to the origin.

2.4 Classical results for nonlinear stability

The concept of local nonlinear stability of a traveling wave is probably due to Evans, who proved the local stability of a traveling pulse of a FitzHugh-Nagumo system in 1972; we cite a summary by the same author [45]. In this series of papers, Evans introduced the so-called Evans function (it got named so by others), an analytic function whose zeros correspond to the discrete eigenvalues of the linearized perturbation. The Evans function is the basis for many proofs of spectral stability, it also allows for a numerical evaluation of the discrete spectrum [12]. However, Evans' proof of local nonlinear stability uses some very specific properties of the system.

Inspired by Evans, the first generally applicable result was given by Sattinger in 1976 [132]. Sattinger took a more theoretical functional analytic approach, lying the foundations for many subsequent works [14, 48, 167]. Two key concepts form the basis of his proof:

First, Sattinger introduces conservatively weighted perturbations, see Definition 2.1. Exponentially decaying weights are necessary if one limit of the wave is unstable. The weight restricts the perturbations to be of a specific local type, and can thereby shift the spectrum of $\mathcal{L}_w$ into the left half-plane.

Second, Sattinger considers the situation that the operator $\mathcal{L}_w$ is *sectorial*. For parabolic reaction-diffusion systems (2.9), this is true if the wave is smooth and converges exponentially fast to its limit states – a rather mild assumption – see e.g. [167, Prop. 7.3]:

Definition 2.3 (Sectorial Linear Operator)**.** Given a Banach space $\mathcal{B}$, we call a densely defined, closed operator $\mathcal{L} : \mathcal{D} \to \mathcal{B}$ *sectorial*, if there exist numbers $a \in \mathbb{R}$ and $b > 0$, such that the resolvent set of $\mathcal{L}$ is contained in the set

$$\mathcal{P} := \left\{\lambda \in \mathbb{C} : \mathfrak{Re}\lambda > a + b\,|\mathfrak{Im}\lambda|\right\}, \tag{2.33}$$

and there exists a constant K, such that within $\mathcal{P}$, the resolvent satisfies the extimate

$$||(\mathcal{L} - \lambda)^{-1}u||_{\mathcal{D}} \leq \frac{K}{|\lambda - a|}||u||_{\mathcal{B}}. \tag{2.34}$$

If $\mathcal{L}$ is sectorial, then the evolution of the linear problem (2.22) can be described by an inverse Laplace transformation of the pointwise operator. There are different ways to express this result [76, 130]. Since we need it in the following, we adopt the notation used in [48]. We introduce the temporal Green's function $\mathcal{G}(t, x, y)$, the solution kernel of the linear Problem $\partial_t \tilde{Y} = \mathcal{L}\tilde{Y}$ with initial value $\tilde{Y}(0, x) \in \mathcal{D}$:

$$\tilde{Y}(t, x) = \int_{\mathbb{R}} \mathcal{G}(t, x, y)\, \tilde{Y}(0, y)\, dy. \tag{2.35}$$

Moreover, we denote as $\mathcal{G}_\lambda(x, y)$ the pointwise Green's function of $\mathcal{L}$, defined as the negative right-inverse of $(\mathcal{L} - \lambda\mathbb{1})$, meaning that $\mathcal{G}_\lambda(x, y)$ solves

$$(\mathcal{L} - \lambda\mathbb{1})\, \mathcal{G}_\lambda(x, y) = -\delta_{(x-y)}\mathbb{1}. \tag{2.36}$$

The following proposition establishes a connection between $\mathcal{G}_\lambda$ and $\mathcal{G}(t)$, for a proof see e.g. the appendix in [132]:

Proposition 2.4. *Let $\mathcal{L}$ be sectorial. Then, the temporal Green's function $\mathcal{G}(t)$ is given by an inverse Laplace transformation of the pointwise Green's*

function $\mathcal{G}_\lambda$ along a contour $\mathcal{C}$, that lies within the resolvent set $\mathcal{P} \subset \mathbb{C}$ of $\mathcal{L}$ and tends to infinity along rays in the negative half-plane:

$$\mathcal{G}(t,x,y) = \frac{1}{2\pi \mathbf{i}} \int_{\mathcal{C}} e^{\lambda t} \mathcal{G}_\lambda(x,y)\, d\lambda. \tag{2.37}$$

An example is depicted in Figure 2.3, for more details see [132, Lem. 3.4] or [48, Prop. 4.1].

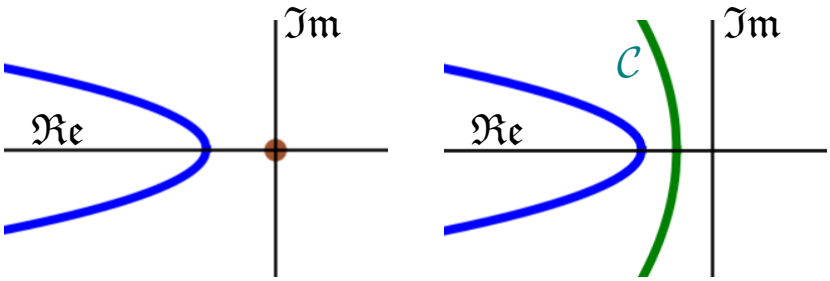

Figure 2.3: The right figure shows an exemplary contour $\mathcal{C}$ along which the temporal Green's function of a linear operator $\mathcal{L}$ can be computed if $\mathcal{L}$ is sectorial, see Equation (2.37). The left figure depicts the situation where the null space of $\mathcal{L}$ is one-dimensional. After projecting $\mathcal{L}$ into the complement of its null space, see Definition 2.2, the remaining part of $\mathcal{L}$ can be dealt with as in the right picture, see e.g. [132].

In words, Sattinger's result for nonlinear stability reads as follows: If a traveling wave ϕ of a parabolic reaction-diffusion System (2.9) is sufficiently smooth and if there exists a conservative weight w such that $\mathcal{L}_w$ is spectrally stable with spectral gap, then the wave is nonlinearly stable. If $0 \notin \Sigma_d$, the wave is nonlinearly stable without shift, and if $0 \in \Sigma_d$, it is stable with shift, see Theorems 4.1 and 4.3 in [132] for the precise formulation.

The family of shifted waves

$$\mathcal{M}_\phi := \{\phi(x+\gamma) | \, \gamma \in \mathbb{R}\} \tag{2.38}$$

is a one-parameter manifold in a suitable function space. Sattinger constructs a smooth local coordinate system in the neighborhood of $\mathcal{M}_\phi$, where one can split $\mathcal{L}_w$ into two orthogonal parts: one part operates on the null space of $\mathcal{L}_w$, and the other on its orthogonal complement.

For proving the decay of the perturbations orthogonal to the null space of $\mathcal{L}_w$, Sattinger uses Proposition 2.4 with a contour $\mathcal{C}$ as depicted in Figure 2.3: An exponential decay of the temporal Green's function of the linearized perturbation can easily be proven via (2.37), choosing $\mathcal{C}$ such that $\mathfrak{Re}\lambda \leq -\beta < 0$ for all $\lambda \in \mathcal{C}$, and by bounding $\mathcal{G}_\lambda$ via (2.34). The full nonlinear problem has a representation similar to (2.27), incorporating also the shift $\gamma(t)$ along (2.38). If the weight w is conservative, one can control the nonlinearity.

For conservative weights, Bates and Jones analyze the geometry of the flow in the neighborhood of $\mathcal{M}_\phi$ in more detail and greater generality [14]. The flow unfolds into three distinct parts acting on a stable, center and unstable (if the wave is not stable) manifold. The (un-)stable manifold can be separated clearly from the center manifold if it satisfies an exponential decay condition. This is crucial, since Gronwall's lemma is used in almost every step of the proof.

One important corollary of the Theorems 1-3 in [14] is the following: If $\mathcal{L}_w$ is exponentially linearly stable and has at most a simple eigenvalue $0 \in \Sigma_d$, then ϕ is nonlinearly stable. The flow along the center manifold corresponds to the shift along $\mathcal{M}_\phi$, and the perturbations vanish exponentially fast along the stable manifold. The general formulation of this result, which essentially only relies on linear exponential stability, allows for several important extensions. In particular, exponential linear stability was proven for a class of partly parabolic PDEs (where $\mathcal{L}_w$ is not sectorial) by Ghazaryan, Latushkin and Schecter [62] and Rottmann-Matthes [124].

For critical FKPP-fronts, there is no weight w such that $\mathcal{L}_w$ is spectrally stable with spectral gap, as explained in Section 2.3. The best we can get is a marginally stable spectrum as depicted in Figure 2.4. The choice of the weight implies that $0 \notin \Sigma_d$, indicating stability without shift, but the stable manifold cannot be separated clearly from the center manifold.

The first general result was not published until 1994. Gallay [53] proved the local stability of a critical pulled front of a one-dimensional FKPP-system with Reaction (2.2). Given the critical traveling wave ϕ of the one-dimensional FKPP-equation, Gallay writes the perturbation as

$$\tilde{Y}(x,t) = \phi'(x) \cdot u(t,x). \tag{2.39}$$

Finding an appropriate weight for the perturbation is quite tricky, since one has to modify also the sub-exponential terms. For all $\beta \geq \beta_0$, where $\beta_0 > 0$ is determined by the left-limit of the wave and not of interest here [53], consider the weight

$$w_{[\beta]}(x) = \begin{cases} (1+x)^{-3} & x \geq 0, \\ e^{-\beta x} & x \leq 0, \end{cases} \tag{2.40}$$

and, for $L \geq 1$, define the weighted space $\mathcal{B}_L \subset L^1(\mathbb{R}) \cap L^\infty(\mathbb{R})$ with norm

$$||g||_{\mathcal{B}_L} := \operatorname*{ess\,sup}_{x \in \mathbb{R}} \frac{|g(x)|}{w_{[\beta L]}(x)} + \int_{\mathbb{R}} \frac{|g(x)}{w_{[\beta L]}(x)}| \, dx. \tag{2.41}$$

Central for Gallay's proof is a renormalization group method. For a fixed $L \geq 1$, one single iteration of this renormalization is given by

$$R_{(L)}\big[g(x)\big] = L^3 \cdot u(L^2, Lx), \tag{2.42}$$

where $u(t,x)$ is the solution of the perturbation equation (2.39) with initial data $u(0,x) = g(x)$. Given the function

$$\psi(x) := \frac{1}{\sqrt{4\pi}} \begin{cases} e^{-x^2/4} & \text{if } x \geq 0, \\ 1 & \text{if } x \leq 0, \end{cases} \tag{2.43}$$

Gallay proves that there exists an $\epsilon > 0$, such that for all initial data subject to $||g||_{\mathcal{B}_1} \leq \epsilon$, there exists a constant $A(g) > 0$ such that

$$||R_{(L^n)}g(x) - A \cdot \psi(x)||_{\mathcal{B}_{L^n}} \to 0 \qquad \text{as } n \to \infty. \tag{2.44}$$

See [53, Thm 1.1] for the precise result. The function $A \cdot \psi$ is a fixed point limit of (2.44), and the analysis of the asymptotics of $R_{(L^n)}$ becomes an analysis of the stability of the fixed point under the transformation. After an additional interpolation argument to rectify the discrete limit, and after undoing the rescaling, Equation (2.44) has two implications. First, it implies stability of the critical front in the following sense:

Theorem 2.5 (Corollary 1.2 in [53]). *Using the previous notation, there exists an $\epsilon > 0$, such that for all initial data $u(0,x)$ with $||u(0,x)||_{\mathcal{B}_1} \leq \epsilon$, it holds that the perturbation $(\phi' u)$ vanishes as $t \to \infty$:*

$$\sup_{x \in \mathbb{R}} \left(1 + \frac{e^{\frac{c}{2}x}}{1+|x|}\right) |\phi'(x)u(x,t)| = \mathcal{O}(t^{-3/2}). \tag{2.45}$$

Second, this result yields a precise estimate of the asymptotic behavior of u. Again, after undoing the rescaling, Equation (2.44) tells us that the leading term of u is given by

$$u(x,t) \sim t^{-3/2} A\psi(xt^{-1/2}) \qquad \text{as } t \to +\infty, \tag{2.46}$$

which shows that the decay $t^{-3/2}$ is optimal for perturbations of critical pulled FKPP-fronts. As far as we know, the proof in [53] has not been modified to other systems and the technique seems to be restricted to case of a single reactant.

Results for the stability of critical fronts with more than one reactant are rare. We want to mention two results by Kan-On and Fang [85], and Gardner [54] concerning the stability of the traveling waves of a Lotka-Volterra system that connect two stable fixed points of the reaction.

More recently, Faye and Holzer proved the *Asymptotic stability of the critical pulled front in a Lotka-Volterra competition model* [48], where the front connects indeed an unstable state to a stable one.

2.5 Critical FKPP-fronts: The results of Faye and Holzer

Faye and Holzer deal with a spectrum of $\mathcal{L}_w$ which is classical for critical FKPP-fronts, as depicted in Figure 2.4: The negative half-line that goes up

to the origin is the critical part of Σ_+, and w is chosen such that $0 \notin \Sigma_d(\mathcal{L}_w)$. Given that $\mathcal{L}_w$ is sectorial, it is in principle possible to calculate the time-dependent Green's function via a Laplace inversion, see Equation (2.37); but the contour must cross the imaginary axis in order to keep a small distance from Σ_+. For this reason, a good estimate on the pointwise Green's function in the neighborhood of the origin is crucial.

Such an estimate is obtained for a system of two species by the authors [48]. We can use this result for studying System (1.1), since it depends only on the shape of the spectrum. A similar analysis of an FKPP-system with a single reactant was presented two years earlier by the same authors [47]. The idea is essentially the same, while the notation is simplified considerably due to the lower dimensionality of the system. In principle, a similar analysis should be possible also for $n \geq 3$ reactants, but the notation becomes quite tedious.

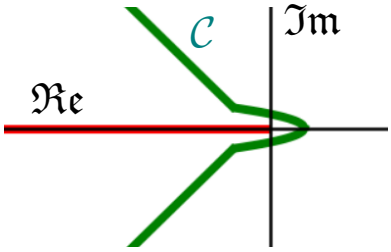

Figure 2.4: Representation of a contour $\mathcal{C}$ along which the temporal Green's function of the linear problem can be computed if the essential spectrum is marginally stable due to the half-line (2.52)*, see Lemma 2.7 and Proposition 2.8.*

For the rest of this section, we consider a critical pulled traveling wave of an FKPP-system of a single reactant, that connects an unstable state $\phi(+\infty) = 0$ to a stable state $\phi(-\infty) = 1$. With a reaction of type (2.2), the critical speed is given by $c^* = 2\sqrt{F'(0)}$, and the critical wave decays like

$$\phi(x) \sim x e^{-\frac{c^*}{2}x}, \quad \text{as } x \to +\infty. \tag{2.47}$$

Consider a conservative and integrable weight that fulfills

$$w(x) = \begin{cases} e^{-\frac{c^*}{2}x} & x \geq 1, \\ e^{\alpha x} & x \leq -1, \\ 1 & x = 0, \end{cases} \quad \text{with fixed } \alpha \in (0, \kappa), \tag{2.48}$$

where $\kappa > 0$ is an upper bound that is dictated by Σ_-, see [47, p.3], and where the weight implies $0 \notin \Sigma_d$. The following holds:

Theorem 2.6 (Thm. 1 in [47]). *Consider a solution of the one-dimensional FKPP-equation with initial data $Y(0,x) = \phi(x) + u(0,x)w(x)$ satisfying*

$$0 \leq Y(0,x) \leq 1, \tag{2.49}$$

for a critical wave ϕ, and perturbations with weight given by (2.48). There exist constants $C, \epsilon > 0$ such that if the weighted perturbation $u(0,x)$ satisfies

$$||u(0,x)||_\infty + ||(1+|\cdot|)u(0,x)||_{L^1} < \epsilon, \tag{2.50}$$

then the wave ϕ is nonlinearly stable in the sense that

$$\sup_{x\in\mathbb{R}} \left| \frac{u(t,x)}{(1+|x|}\right| \leq C\frac{1}{1+t^{3/2}} \quad \forall t \geq 0. \tag{2.51}$$

Note that the decay is of order $t^{-3/2}$, which we know to be optimal (in case of a single reactant).

For proving Theorem 2.6, Faye and Holzer first express the pointwise Green's function (2.36) via fundamental solutions of the eigenvalue problem $\mathcal{L}_w u = \lambda u$. A pair of fundamental solutions becomes co-linear when approaching the essential spectrum

$$\Sigma_+ = \left\{\lambda \in \mathbb{C} \middle| \mathfrak{Re}\lambda \leq 0, \mathfrak{Im}\lambda = 0\right\} \subset \Sigma_{ess}. \tag{2.52}$$

By providing a precise formulation for this co-linearity, Faye and Holzer prove the following:

Proposition 2.7 (Lem. 3.2 in [47]). *For some $\epsilon > 0$, there exists a neighborhood of the origin*

$$\Omega := \left\{\lambda \in \mathbb{C} \middle| \, |\lambda| \leq \epsilon, \lambda \notin \Sigma_+\right\}, \tag{2.53}$$

such that for all $\lambda \in \Omega$, it holds that

$$\mathcal{G}_\lambda(x,y) \; = e^{-\sqrt{\lambda}|x-y|} \cdot H(\sqrt{\lambda}, x, y), \tag{2.54}$$

where H is bounded uniformly in (x,y), and is analytic in $\sqrt{\lambda}$.

Given this estimate on $\mathcal{G}_\lambda$, the estimate for the temporal Green's function follows. There are several regimes for $\mathcal{G}(t,x,y)$ to be considered; we present only the result which covers the critical short-range interaction:

Proposition 2.8 (Prop. 4.1 in [47]). *There exist constants $C, K, r, \kappa > 0$ such that the Green's function $\mathcal{G}(t,x,y)$ for $\partial_t u = \mathcal{L}u$ satisfies the following estimate:*

For all $t \geq 1$ and $|x-y| \leq Kt$:

$$|\mathcal{G}(t,x,y)| \leq C\frac{1+|x-y|}{1+t^{3/2}} e^{-\frac{|x-y|^2}{\kappa t}} + Ce^{-rt}. \tag{2.55}$$

Proof. We briefly explain how this estimate can be gained from (2.54), for the details we refer to the original paper [47]. According to Proposition 2.4, it holds that

$$\mathcal{G}(t,x,y) = \frac{1}{2\pi\mathbf{i}} \int_{\mathcal{C}} e^{\lambda t} \mathcal{G}_\lambda(x,y)\, d\lambda, \tag{2.56}$$

considering a contour $\mathcal{C}$ as depicted in Figure 2.4. Its part $\mathcal{C}_1$ around the origin is defined via a parabola, where

$$\sqrt{\lambda} = \rho + \mathbf{i}k, \tag{2.57}$$

for some $\rho > 0$ and small $k \in [-k^*, k^*]$ such that $\sqrt{\lambda} \in \Omega$. Focusing on the regime $|x-y| \leq Kt$, choose

$$\rho = \frac{|x-y|}{Lt}, \tag{2.58}$$

for L sufficiently large such that the contour lies within Ω. Along this contour, it holds that

$$d\lambda = 2\mathbf{i}\Big(\frac{(x-y)}{Lt} + \mathbf{i}k\Big)\, dk, \quad \lambda = \frac{(x-y)^2}{L^2t^2} - k^2 + 2\frac{x-y}{Lt}\mathbf{i}k. \tag{2.59}$$

We expand the integral into its real and imaginary part. Then, since $\mathcal{G}_\lambda$ is holomorphic and the contour is symmetric with respect to the real axis, several of the terms in the contour-integral cancel. We denote as H_R and H_I the real and imaginary part of H (see Prop. 2.7). It holds that

$$\begin{aligned} &\frac{1}{2\pi\mathbf{i}} \int_{\mathcal{C}_1} e^{\lambda t} \mathcal{G}_\lambda(x,y)\, d\lambda \\ &= \frac{1}{\pi} e^{\rho^2 t - \rho(x-y)} \int_{-k^*}^{k^*} e^{-k^2 t} \big(\rho H_R(x,y,k) + \mathbf{i} H_I(x,y,k)\big)(\rho + \mathbf{i}k)\, dk. \end{aligned} \tag{2.60}$$

As H_R is bounded, the first part of the integral can easily be bounded:

$$\Big| \frac{1}{\pi} e^{\rho^2 t - \rho(x-y)} \int_{-k^*}^{k^*} e^{-k^2 t} \rho H_R(x,y,k)\, dk \Big| \leq C \frac{\rho}{t^{1/2}} e^{-\rho^2 t - \rho(x-y)}. \tag{2.61}$$

Now H_I is odd in k, so it can be written as $H_I(x,y,k) = k\tilde{H}_I(x,y,k)$, where $\tilde{H}_I(x,y,k)$ is again bounded. These estimates imply

$$\Big| \frac{1}{\pi} e^{\rho^2 t - \rho(x-y)} \int_{-k^*}^{k^*} e^{-k^2 t} k^2 H_I(x,y,k)\, dk \Big| \leq C \frac{\rho}{t^{3/2}} e^{-\rho^2 t - \rho(x-y)}. \tag{2.62}$$

Inserting $\rho = \frac{|x-y|}{Lt}$, we arrive at the first part of (2.55). The remainder of the contour $\mathcal{C}$ lies in the strict negative half-plane, so exponential decay of $\mathcal{G}(t)$ along this part of $\mathcal{C}$ follows since $\mathcal{L}$ is sectorial (2.34). □

Given the bound of (2.55) for an integrable weight w, nonlinear stability follows by a Duhamel's principle (2.27), since one can integrate over the nonlinearity of order $\mathcal{O}(wu^2)$. The weighted perturbation decays pointwise like $t^{-3/2}$. Note that due to the additional weighting $1/(1+|x|)$, this result does not imply decay in L^∞. Check Theorem 2.6 for the precise formulation in the scalar case, and [48, Thm. 1] for the case of two reactants.

2.6 Convective stability

Physicists distinguish between *absolute instability* and *convective instability*, which are very natural concepts for analyzing wave propagation in fluids:

"*Briefly, an instability is called convective if it is advected downstream so that at any fixed location in the laboratory frame a perturbation decays asymptotically to zero. In contrast when the instability is absolute it grows at every point in the laboratory frame. Heuristically, absolute instability requires that the growth rate of the instability be faster than the advection rate, and consequently we expect a transition with increasing driving from convective to absolute instability.*" — Tobias, Proctor, Knobloch [143]

Remark: The terms *convective instability* and *convective stability* are both used in the literature, describing the same phenomenon. We use the latter one, since it emphasizes the pointwise stability of the wave, as also mentioned by Ghazaryan et al. [63].

A good introduction to the topic was written by Sandstede and Scheel [131], with an emphasis on numerical examples for convective stability, and an analysis of the spectrum of $\mathcal{L}_w$ in different bounded and unbounded domains.

Proving convective stability is difficult since it requires the use of a degenerate weight. A first rigorous treatment is due to Pego and Weinstein [118], who proved convective stability of solitary traveling waves – locally concentrated waves in fluids that can pass each other without interaction – of the Korteweg-de Vries equation

$$\frac{\partial}{\partial t}Y + Y \cdot \frac{\partial}{\partial z}Y + \frac{\partial^3}{\partial z^3}Y = 0. \tag{2.63}$$

There exists a family of (right-)traveling wave solitons $\phi_c(x)$, continuous in their speed $c > 0$, that solve (2.63) via $Y(t,z) = \phi_c(z - ct + \gamma)$, where $\gamma \in \mathbb{R}$ is an arbitrary shift. Given such a wave ϕ_c, a perturbation results in the arise of several small amplitude waves, that either are slower than ϕ_c or even travel to the left, and an additional correction within the family $\phi_c(\cdot + \gamma)$. In [118], it is proven that the family of waves

$$M_{\phi,c,\gamma} = \{\phi_c(\cdot + \gamma), \gamma \in \mathbb{R}, c > 0\}, \tag{2.64}$$

is a convectively stable manifold, in a space with weight

$$w_\alpha(x) = e^{-\alpha x}, \tag{2.65}$$

for some well-chosen $\alpha > 0$ [118].

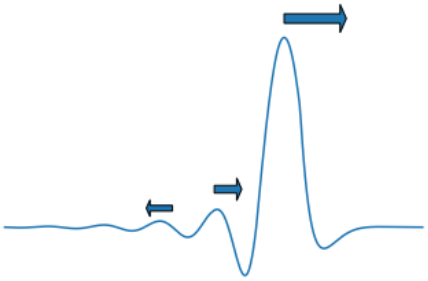

Figure 2.5: Schematic representation of a convectively stable solitary wave, similar to Figure 1 in [118]. The perturbed wave moves to the right, the perturbations either move slower than the wave or move to the left. In both cases, they vanish in the weighted norm.

Controlling the nonlinearity in a space with degenerate weight requires some detours, typically involving and intertwining estimates on both the weighted perturbations, and the evolution of the unweighted full PDE. There are typically three steps involved: First, find a suitable open set of functions $E \subset \mathcal{B}$ such that we can control the nonlinearity as long as $\tilde{Y} \in E$, and choose initial data under which $\tilde{Y}(t) \in E$, for some positive time $t \in [0, T^*)$, where T^* is the first exit time of E. Second, prove that the weighted perturbation $u(t) = \tilde{Y}(t)/w$ decays while $\tilde{Y}(t) \in E$. Third, use the decay of $u(t)$ to prove that $T^* = +\infty$, i.e. we can control the nonlinearity $\tilde{Y} \in E$ for all $t \geq 0$.

Pego and Weinstein control the weighted nonlinearity, which is of order $\mathcal{O}(u^2 w)$, via

$$||u^2 e^{-\alpha x}||_{H^1} \leq ||e^{-\alpha x} u||_{H^1} \cdot ||u||_{H^1} = ||\tilde{Y}||_{H^1} \cdot ||u||_{H^1}. \tag{2.66}$$

In words: The weighted quadratic term $u^2 w$ can be treated like a linear one as long as the unweighted perturbation $uw = \tilde{Y}$ remains bounded. The term $||\tilde{Y}||_{H^1}$ is controlled via energy methods that are tailored precisely to the PDE (2.63). As a result, two stability statements sustain each other: If the initial perturbations are sufficiently small in both the weighted and the unweighted sense, that is

$$||u(0,x)||_{H^1} + ||\tilde{Y}(0,x)||_{H^1} < \epsilon, \tag{2.67}$$

for some $\epsilon > 0$, then the unweighted perturbations $\tilde{Y}$ remain bounded, while the weighted perturbations u decay. The wave is convectively stable with

shift, see [118, Thm. 1] for the precise formulation.

In 2009, Ghazaryan proved convective stability of a traveling wave of a reaction-diffusion system whose structure is quite similar to that of System (1.1). This PDE is a model for a combustion front without heat-loss [61], in one spatial dimension it reads

$$\begin{aligned} \frac{\partial}{\partial t}Y_1 &= \frac{\partial^2}{\partial z^2}Y_1 + Y_2 f(Y_1), \\ \frac{\partial}{\partial t}Y_2 &= \epsilon\frac{\partial^2}{\partial z^2}Y_2 - \kappa Y_2 f(Y_1), \end{aligned} \tag{2.68}$$

where $Y_1(t,z) \geq 0$ is the (rescaled) temperature and $Y_2(t,z) \geq 0$ is the concentration of a viscous fuel, with burning reaction

$$f(Y_1) = e^{-1/Y_1}\mathbb{1}_{\{Y_1 \geq 0\}}, \tag{2.69}$$

for $0 < \epsilon \ll 1, \kappa > 0$. This model has a right-traveling wave solution $\phi(z-ct)$ that invades into the region with fuel, and burns it all while reaching a limiting temperature ζ, thereby connecting the two steady states

$$(\phi_1, \phi_2) = (\zeta, 0) \quad \text{at } x = -\infty, \text{ and } (\phi_1, \phi_2) = (0, 1) \quad \text{at } x = +\infty. \tag{2.70}$$

The left limit of the wave is a non-hyperbolic equilibrium (there is no reaction in absence of fuel). This implies that the linearized perturbation is only spectrally stable with spectral gap if one uses a convective weight – the situation is the same as for the present System (1.1), see the spectral analysis in Section 2.3 for the details. The following holds:

Theorem 2.9 (Thm. 1.3.1 in [61]). *For some values of $\kappa > 0$, there exists a traveling wave ϕ with speed $c > 0$ of System (2.68), whose linearized perturbation $\mathcal{L}_w$ with exponential weight*

$$w(x) = e^{-\alpha x}, \tag{2.71}$$

is spectrally stable with spectral gap (as an operator $H^3 \otimes H^3 \to H^1 \otimes H^1$), for some positive $\alpha > 0$, except that $0 \in \Sigma_d$ is a single eigenvalue that corresponds to ϕ'.

This wave ϕ is convectively stable with shift. There exist constants $\epsilon_0 > 0, K > 0, \beta > 0$ such that the following is true: If both the weighted and unweighted perturbation are initially small,

$$||\tilde{Y}(0,\cdot)||_{H^1} + ||\frac{\tilde{Y}(0,\cdot)}{w(\cdot)}||_{H^1} \leq \epsilon \leq \epsilon_0, \tag{2.72}$$

then the solution of Equation (2.68) with initial data $Y(0,x) = \phi(x) + \tilde{Y}(0,x)$ exists for all $t \geq 0$, and can be expressed as

$$Y(t,x) = \phi\big(x + \gamma(t)\big) + \tilde{Y}(t,x), \tag{2.73}$$

for a shift $|\gamma(t)| \leq K\epsilon$ *with finite limit* $\gamma_+ \in \mathbb{R}$. *It holds that*

$$||\frac{\tilde{Y}(t,\cdot)}{w(\cdot)}||_{H^1} + |\gamma(t) - \gamma_+| \leq K\epsilon e^{-\beta t} \quad \forall t \geq 0. \tag{2.74}$$

For the unweighted perturbations, it holds that

$$\begin{aligned} &||\tilde{Y_2}(0,\cdot)||_{H^1} \leq K\epsilon e^{-\beta t}, \\ &||\tilde{Y_1}(0,\cdot)||_{H^1} \leq K\epsilon \qquad \forall t \geq 0. \end{aligned} \tag{2.75}$$

If, in addition to (2.72), *it holds that* $\tilde{Y}(0,\cdot) \in L^1$, *then*

$$||\tilde{Y_1}(t,\cdot)||_\infty \leq K\frac{1}{t^{1/2}} \qquad \forall t > 0. \tag{2.76}$$

We want to highlight the control of the unweighted perturbations (2.75): The perturbation $\tilde{Y_2}$ of the fuel vanishes, whereas the perturbation $\tilde{Y_1}$ of the temperature remains only bounded. However, $\tilde{Y_1}$ decays algebraically, naturally like a heat kernel, under an additional integrability assumption.

In fact, the boundedness of $\tilde{Y_1}$ stems from an a-priori estimate, which is again needed to control the nonlinearity under a degenerate weight. The idea is motivated by the estimate of Pego and Weinstein (2.66). In view of the Reaction (2.69), again ignoring the shift $\gamma(t)$, the crucial part in the remaining nonlinearity is

$$N(t,x) = u_2(t,x)\exp\Big(-\frac{1}{u_1(t,x)e^{-\alpha x} + \phi_1(x)}\Big) = u_2(t,x)\exp\Big(-\frac{1}{Y_1}\Big). \tag{2.77}$$

Using the explicit structure of the reaction-diffusion PDE (2.68), Ghazaryan is able to get an a-priori bound on the temperature: $||Y_1||_{BC^1} \leq M$. Then, the nonlinear term (2.77) can be estimated by

$$||u_2\exp\Big(-\frac{1}{Y_1}\Big)||_{H^1} \leq L \cdot ||u_2||_{H^1}. \tag{2.78}$$

Again, the nonlinearity can be treated like a linearity in u_2, as long as the a-priori estimate (2.78) holds. The detailed construction is more difficult and involves several Gronwall estimates, using the Lipschitz-continuity of the nonlinearity and the fact that the linear operator is sectorial, see [61, Sec. 3].

Under additional assumptions, it can be shown that $\tilde{Y_1}$ decays algebraically, as it is smoothened by a diffusion [61]. A reader-friendly discussion of these results is given in [63], in particular the authors present a result for more general reaction terms, under the assumption of a "defect" structure similar to Equation (2.68). Moreover, the authors generalize their findings to

partly parabolic systems [62, 63] that exhibit exponential spectral stability.

Using the linear estimates by Faye and Holzer (see Proposition 2.8), we prove convective stability of the critical invading fronts of System (1.1). The energy based Estimate (2.66) or the C^1-Estimate (2.78) are not compatible with the pointwise decay presented in Proposition 2.8. However, we see from (2.78) that it is possible to exploit the explicit nonlinearity: For the defect nonlinearity of System (1.1), which depends only on the A-component as long as the I-component remains bounded, we develop a new type of a-priori estimate via a Feynman-Kac formula.

3 The traveling waves of the system with degenerate diffusion

In this chapter, we introduce and summarize the content of the paper "Traveling waves of an FKPP-type model for self-organized growth", which was published in the *Journal of Mathematical Biology, 84(6):42, 2022, https://doi.org/10.1007/s00285-022-01753-z* by the author of this thesis, with help and supervision of Anton Bovier and Muhittin Mungan.

3.1 Short summary

We begin with the analysis of the PDE (1.1). For $d = 0$, we explicitly construct all non-negative traveling wave solutions of the system and describe their shape. The paper ends with a short heuristic discussion regarding the stability of the traveling waves.

Notation: *For consistency within this thesis, the notation in this chapter deviates from that in [92]. We refer to $z \in \mathbb{R}$ as the spatial variable of the PDE, and to $z - ct = x \in \mathbb{R}$ as the phase of the wave. In the original publication, their roles are vice versa.*

3.2 Results

We construct the traveling waves of the partly parabolic system

$$\begin{aligned} \frac{\partial}{\partial t}A &= \frac{\partial^2}{\partial z^2}A + A - A(A+I), \\ \frac{\partial}{\partial t}I &= rA + A(A+I), \quad r \geq 0. \end{aligned} \tag{3.1}$$

A right-traveling wave of System (3.1) is a pair of bounded functions

$$a : \mathbb{R} \to \mathbb{R}, \quad i : \mathbb{R} \to \mathbb{R}, \tag{3.2}$$

that solve (3.1) via the ansatz $A(z,t) = a(z-ct), I(z,t) = i(z-ct)$, with $c > 0$ being the speed of the wave. Thus, a traveling wave of (3.1) solves the system of coupled ODEs

$$\begin{aligned} 0 &= a'' + ca' + a - a(a+i), \\ 0 &= ci' + a(a+i+r), \end{aligned} \tag{3.3}$$

where we denote by a prime the differentiation w.r.t. the phase-variable $x = z - ct$. We give necessary and sufficient conditions for the existence of

smooth non-negative traveling wave solutions, and analyze the shape of the wave form. Our main result characterizes a family of pulled traveling waves:

Theorem 3.1 (Thm. 1.1 in [92]). *Let $r \geq 0, c > 0$ and define*

$$i_c := \max\{0, 1 - c^2/4\}. \tag{3.4}$$

For each pair $i_{-\infty}, i_{+\infty} \in \mathbb{R}_0^+$ such that

$$i_{+\infty} \in [i_c, 1), \qquad i_{-\infty} = 2 - i_{+\infty}, \tag{3.5}$$

there exists a unique non-negative traveling wave $a, i \in C^\infty(\mathbb{R}, \mathbb{R}^2)$ that solves Equation (3.3), such that

$$\lim_{x \to \pm\infty} a(x) = 0, \qquad \lim_{x \to \pm\infty} i(x) = i_{\pm\infty}. \tag{3.6}$$

The function $i(x)$ is decreasing, whereas $a(x)$ has a unique local and global maximum. If $\frac{c^2}{4} + i_{+\infty} - 1 = 0$, then the wave converges as fast as $x \cdot e^{-\frac{c}{2}x}$ as $x \to +\infty$. If $\frac{c^2}{4} + i_{+\infty} - 1 > 0$, then convergence as $x \to +\infty$ is purely exponential. Convergence as $x \to -\infty$ is purely exponential in all cases. The rates of convergence are given by

$$\begin{aligned} \mu_{-\infty} &= -\frac{c}{2} + \sqrt{\frac{c^2}{4} + i_{\pm\infty} - 1} > 0, \\ \mu_{+\infty} &= \frac{c}{2} - \sqrt{\frac{c^2}{4} + i_{\pm\infty} - 1} > 0. \end{aligned} \tag{3.7}$$

Moreover, these are all bounded, non-negative, non-constant and twice differentiable solutions of Equation (3.3).

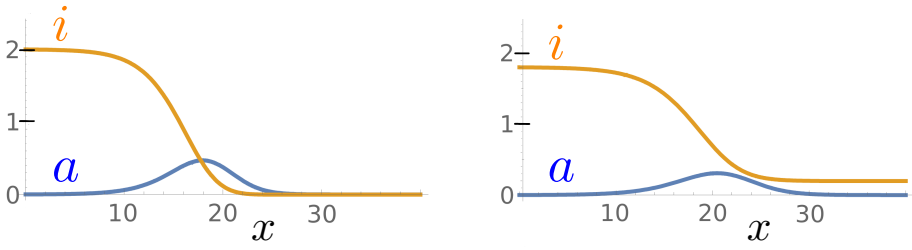

Figure 3.1: Two different traveling waves with speed $c = 2$. The limits of the left wave are given by $i_{-\infty} = 2$ and $i_{+\infty} = 0$. The limits of the right wave are given by $i_{-\infty} = 1.8$ and $i_{+\infty} = 0.2$.

Notice that this result is independent of the reproduction rate r, which affects the shape of the wave, but neither the limits nor the minimal speed of a positive solution. All non-negative and bounded traveling waves resemble the ones depicted in Figure 3.1, consisting of a pulse of active particles which

is accompanied by a monotone wave of inactive particles. We refer to the non-negative waves that fulfill

$$\lim_{x\to+\infty} a(x) = \lim_{x\to+\infty} i(x) = 0, \tag{3.8}$$

as *invading fronts*. In view of Equation (3.5), the invading fronts have minimal speed $c = 2$, and in this case converge as fast as xe^{-x} as $x \to +\infty$. This coincides with the behavior of the associated FKPP-equation in the absence of inactive particles [22, 50, 91].

In the following, we present the main steps of the proof of Theorem 3.1.

3.3 Analysis of the asymptotics

We reformulate the System (3.3) for a traveling wave as an equivalent system of first-order ODEs. We introduce the auxiliary variable $a' = b$, so that (3.3) becomes

$$\begin{aligned} a' &= b, \\ b' &= a(a+i) - a - cb, \\ i' &= -\frac{1}{c} a\,(a+i+r)\,, \end{aligned} \tag{3.9}$$

with $c > 0, r \geq 0$. This equation has a continuum of non-negative fixed points, similar to that of the PDE, see Equation (1.2):

$$a = b = 0, \quad i \in \mathbb{R}^+. \tag{3.10}$$

The continuum of fixed points (3.10) implies that many of the classical approaches – that are topologically motivated and search for certain unique trajectories in the space of waves – can not be applied to the present case, for an introduction see [138, Ch. 22]. Instead, the proof of Theorem 3.1 is mainly based on a detailed analysis of the phase-space of Equation (3.9). We explicitly construct the traveling waves and as a bonus, this approach leads to the conclusion that we have indeed found all bounded and non-negative traveling waves.

In the first place, we need to find out which of the fixed points (3.10) can be considered as limits of right-traveling waves. Any bounded and non-negative solution of System (3.9) can not be periodic and must converge since $ci' = -a(a+i+r) \leq 0$. It is now evident that the limits at $x = \pm\infty$ must be fixed points, thus we denote them as $(a, b, i) = (0, 0, i_{\pm\infty})$. Under mild assumptions regarding integrability, we can interrelate any two different points on a given traveling wave via an integral equation, where we make use of the logistic nature of the growth process, see [92, Sec. 3]. Most importantly, this leads to the correspondence of the limits

$$i_{+\infty} + i_{-\infty} = 2. \tag{3.11}$$

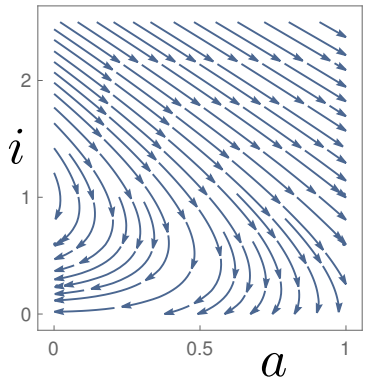

Figure 3.2: Two-dimensional representation of the family of traveling waves presented in Theorem 3.1, for parameters $c = 2$ and $r = 0$. A unique trajectory emerges from each point where $i_{-\infty} > 1$, and converges to a limit where $i_{+\infty} < 1$, where $i_{-\infty} + i_{+\infty} = 2$. For $i_{-\infty} > 2$, the trajectory eventually becomes negative (even though it still seems to converge).

In view of this, monotonicity of i implies that $i_{-\infty} \in (1, 2]$ and $i_{+\infty} \in [0, 1)$.

A short computations reveals that at a fixed point $(a, b, i) = (0, 0, K)$ of the ODE System (3.9), the eigenvalues of its Jacobian are given by

$$\lambda_0 = 0, \qquad \lambda_\pm = -\frac{c}{2} \pm \sqrt{\frac{c^2}{4} + K - 1}. \tag{3.12}$$

This is due to the fact that the fixed points form the Continuum (3.10), therefore the Jacobian at the fixed points must be degenerate. As such, we can not apply the classical theory of Grobmann-Hartmann to linearize the asymptotic behavior. We apply center manifold theory [30, 90] to work out the higher moments of the approximation, see [92, Sec. 4]. Our analysis reveals a suitable *unstable set*

$$S_{-\infty} := \big\{(0, 0, i) \,\big|\, i > 1\big\}, \tag{3.13}$$

and a suitable *stable set*

$$S_{+\infty} := \big\{(0, 0, i) \,\big|\, i \in [0, 1)\big\}. \tag{3.14}$$

Each point $(0, 0, i_{-\infty}) \in S_{-\infty}$ has an unstable manifold of dimension one. Its restriction to $a \geq 0$ is the only possible candidate for the tail of a non-negative traveling wave as $x \to -\infty$, we need to find out under which circumstances these trajectories converge and stay non-negative. Each point $(0, 0, i_{+\infty}) \in S_{+\infty}$ is Lyapunov stable, as depicted in Figure 3.2.

The analysis of the asymptotic behavior also yields a necessary condition on the speed of a non-negative wave. A traveling wave can only be non-negative if $a(x)$ does not spiral while converging to 0. Therefore, the two

eigenvalues $\lambda_\pm$ at the limiting fixed point must be real-valued. In view of (3.12), for a fixed point $(0, 0, K)$, this is given if

$$\frac{c^2}{4} + K - 1 \geq 0. \tag{3.15}$$

Thus, if the stable fixed point $(0, 0, i_{+\infty})$ is the limit of a non-negative traveling wave, where $i_{+\infty} \in [0, 1)$, it is necessary by (3.15) that

$$\frac{c^2}{4} + i_{+\infty} - 1 \geq 0 \quad \Rightarrow \quad i_{+\infty} \geq i_c = \max\{0, 1 - \frac{c^2}{4}\}, \tag{3.16}$$

which is precisely the condition in Theorem 3.1.

3.4 Construction of the traveling waves

For finding a suitable attractor of $S_{+\infty}$, we first analyze solutions that start in points of type $(a, b, i) = (a_0, 0, i_0)$. We start with an analsis of the two-dimensional subsystem in coordinates (a, b), that results from the full System (3.9) by imposing a fixed value of i. In [92, Sec. 5], we construct a trapping region, wherein a converges and stays non-negative: the triangle $T_c(i)$, depicted in Figure 3.3.

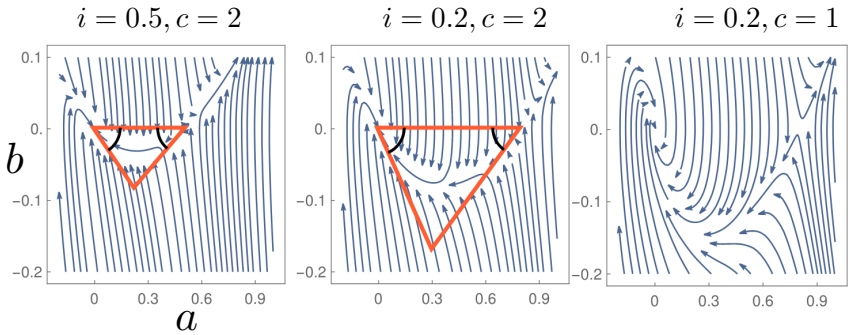

Figure 3.3: The phase plot of the two-dimensional system with coordinates (a, b), that results from the full System (3.9) by imposing a fixed value of i. The only two fixed points are $(a, b) = (0, 0)$ and $(a, b) = (1-i, 0)$. For $i \in [i_c, 1)$, check Definition (3.4), the orange triangles $T_c(i)$ are invariant regions, wherein $a \searrow 0$. The region $T_c(i)$ increases in $-i$: The point $(1-i, 0)$ moves to the right and the two highlighted internal angles increase. In the third case, $i < i_c$ implies that the system spirals around $(0, 0)$. The detailed statements are presented in [92, Sec. 5].

The already mentioned monotonicity of $i(x)$ allows us to lift this result to the full system. Here, the continuum of fixed points comes at help. Still analyzing solutions that start in points of type $(a, b, i) = (a_0, 0, i_0)$, we first prove the existence of almost constant solutions that stay non-negative and converge monotonously, subject to the conditions

$$\begin{aligned} \forall x \geq 0: \quad & 0 \leq a(x) \leq a_0 \ll 1, \\ & i_c \leq i(x) \sim i_0, \\ & a'(x), i'(x) \leq 0. \end{aligned} \tag{3.17}$$

We continuously deform these solutions along their limit: The Lyapunov-stability of the points in $S_{+\infty}$ implies continuity of the entire trajectory up to $x = +\infty$ in initial data. We use this to derive sharp conditions regarding $(a_0, 0, i_0)$ such that the trajectory stays non-negative and converges as $x \to +\infty$, resulting in [92, Thm. 6.10].

We then construct the claimed traveling waves. Therefore, we consider a fixed point $(0, 0, i_{-\infty}) \in S_{-\infty}$, where $i_{-\infty} \in (1, 2 - i_c]$, and follow the unique trajectory that leaves the fixed point in positive direction of a. We prove that there exists a finite phase-time x_0 such that $b(x_0) = 0$: The trajectory reaches a first local (and in fact global) maximum of active particles $(a_{x_0}, 0, i_{x_0})$, see the phase-plot in Figure 3.2. We show that $(a_{x_0}, 0, i_{x_0})$ lies in the previously constructed non-negative attractor of $S_{+\infty}$, see [92, Prop. 7.6], and thereby have constructed a non-negative wave.

4 Convective stability of the critical traveling waves

In this chapter, we introduce and summarize the content of the preprint "Convective stability of the critical waves of an FKPP growth process", which was uploaded to arxiv.org by the author of this thesis in May 2023 [93]. This work was supervised by Anton Bovier, moreover the author wants to thank Juan Velázquez for vital input.

4.1 Short summary

This work continues the analysis of the PDE (1.1). We prove the existence of traveling waves of the system for $d > 0$ that are similar to those in the case $d = 0$. Now that both densities of particles undergo a diffusion, we are able to analyze the stability of the critical invading fronts – the non-negative waves with minimal possible speed that vanish at one end – against small perturbations. In order to stabilize the essential spectrum of the linearized perturbation equation, we operate in a space where the perturbations can grow exponentially at the back of the wave. We present a new approach for dealing with the unbounded non-linear terms. The novelty is that we use a Feynman-Kac formula to get an exponential a-priori estimate for the left tail of the PDE, in the regime where the weight is unbounded. This new type of a-priori estimate is compatible with the pointwise decay that we prove.

4.2 Results

For $d > 0$, the (right-)traveling waves with speed $c > 0$ of the PDE (1.1) solve the system of couples ODEs

$$\begin{aligned} 0 &= a'' + ca' + a - a(a+i), \\ 0 &= di'' + ci' + a(a+i+r). \end{aligned} \tag{4.1}$$

We use the main result in [92] (see Theorem 3.1), which describes the traveling waves for $d = 0$, to construct the traveling waves for $d > 0$. Via perturbation techniques, we prove the existence of a family of traveling wave solutions similar to those of the system for $d = 0$, see [93, Thm. 3.18] for the full statement. Concentrating on the *invading fronts*, those non-negative waves that vanish at one end, the result reads as follows:

Theorem 4.1 (Thm. 1.1 in [93]). *For $r \geq 0, c > 0$, consider the Wave System* (4.1) *with*

$$0 < d < \min\{1, \frac{3c}{2}, \frac{c^2}{2(r+1)}\}. \tag{4.2}$$

If and only if $c \geq 2$, there exists an invading front. The function $i(x)$ is decreasing, and $a(x)$ has a unique local and global maximum. As $x \to -\infty$, the front converges exponentially fast to a fixed point $(a, i) = (0, i_{-\infty})$, where

$$1 < 2 - d \cdot \frac{2(r+1)}{c} < i_{-\infty} < 2. \tag{4.3}$$

The rate of convergence is a function of $i_{-\infty}$, given by

$$\mu_{-\infty} = -\frac{c}{2} + \sqrt{\frac{c^2}{4} + i_{-\infty} - 1} > 0. \tag{4.4}$$

As $x \to +\infty$, both $a(x)$ and $i(x)$ vanish. There are two possibilities for the speed of convergence. In the critical case $c = 2$, the front behaves as $x \cdot e^{-x}$. If $c > 2$, convergence is purely exponential, with rate

$$\mu_{+\infty} = \frac{c}{2} - \sqrt{\frac{c^2}{4} - 1} > 0. \tag{4.5}$$

We refer to the invading fronts with minimal possible speed $c = 2$ as *critical*. Their behavior as $x \to +\infty$ again reproduces the behavior of the critical waves of an FKPP-equation with a single type of branching particles [22, 91].

This fact is crucial when analyzing the stability of the critical invading front, as explained in detail in Section 2.2. In the moving frame $x = z - 2t$, we write a solution of the full PDE (1.1) as the sum of the front $a(x), i(x)$ and the perturbations $\tilde{A}(t, x), \tilde{I}(t, x)$:

$$A(t, x) = a(x) + \tilde{A}(t, x), \quad I(t, x) = i(x) + \tilde{I}(t, x). \tag{4.6}$$

The system is not attracted towards a particular limit, as none of the steady states (1.2) of the PDE is hyperbolically stable. To overcome this, we operate in a space where we allow the perturbations to grow exponentially as $x \to -\infty$. To stabilize the front as $x \to +\infty$, perturbations must vanish exponentially fast, which is typical for FKPP-fronts [130, 132]. Given a smooth weight $w(x) > 0$, subject to

$$w(x) = \begin{cases} e^{-x} & x \geq 1, \\ e^{-\alpha x} & x \leq -1, \\ 1 & x = 0, \end{cases} \quad \text{with fixed } \alpha \in (0, 1), \tag{4.7}$$

we prove that if the weighted perturbations

$$\frac{\tilde{A}(t, x)}{w(x)}, \quad \frac{\tilde{I}(t, x)}{w(x)} \tag{4.8}$$

are initially small, they vanish pointwise with algebraic decay $t^{-3/2}$. We use the result for the linear operator published in [48], and adapt the resulting semi-group estimates for the full nonlinear problem to a space with the unbounded Weight (4.7).

We have to assume that the discrete spectrum of the linearized perturbation equation contains no elements with non-negative real-part, check Section 4.4. Since we could not prove this analytically, we verified this condition numerically, via the library STABLAB [13, 12], which computes contours of the Evans-function, see appendix B in [93].

Theorem 4.2 (Thm. 1.2 in [93]). *For a pair $d > 0, r \geq 0$ as in Theorem 4.1, consider the critical invading front with speed $c = 2$. If we assume that the discrete spectrum of the weighted linearized perturbation equation contains no elements with non-negative real-part (see (4.26)), then the critical invading front is locally stable in a space with weight w as above (4.7):*

Fix a pair of constants $C, \mu_0 > 0$. For all $\epsilon > 0$, there exists a $\delta > 0$, such that if the unweighted perturbations fulfill

$$(i) \qquad \forall x \leq 0: \quad |\tilde{A}(0,x)| \leq Ce^{\mu_0 x}, \quad |\tilde{I}(0,x)| \leq \delta, \tag{4.9}$$

and if the weighted perturbations $\tilde{A}(0,x)/w(x), \tilde{I}(0,x)/w(x)$ are elements of $H^2(\mathbb{R})$, and

$$(ii) \qquad \int_{\mathbb{R}} (1+|x|)\Big[\Big|\frac{\tilde{A}(0,x)}{w(x)}\Big| + \Big|\frac{\tilde{I}(0,x)}{w(x)}\Big|\Big]\, dx \leq \delta, \tag{4.10}$$

$$(iii) \qquad \Big|\Big|\frac{\tilde{A}(0,x)}{w(x)}\Big|\Big|_\infty + \Big|\Big|\frac{\tilde{I}(0,x)}{w(x)}\Big|\Big|_\infty \leq \delta, \tag{4.11}$$

then the weighted perturbations decay pointwise with algebraic speed $t^{-3/2}$:

$$\sup_{t\geq 0}\sup_{x\in\mathbb{R}} \frac{(1+t)^{3/2}}{w(x)(1+|x|)}\Big(|\tilde{A}(t,x)| + |\tilde{I}(t,x)|\Big) \leq \epsilon. \tag{4.12}$$

In the following, we briefly explain the construction of the traveling waves, see Section 4.3. Their asymptotic behavior is identical to those in the case $d = 0$, we omit the discussion here. The stability of the critical invading fronts is analyzed in Section 4.4.

4.3 Construction of the traveling waves

For passing continuously from $d = 0$ to $d \sim 0$, the theory of *geometric singular perturbations* due to Fénichel [49, 84] provides a suitable framework. We introduce two auxiliary variables, $b = a'$ and $j = i'$ and reformulate the Wave-System (4.1) as an equivalent system of four first-order ODEs:

$$\frac{d}{dx}\begin{pmatrix} a \\ b \\ i \\ j \end{pmatrix} = \begin{pmatrix} b \\ a(a+i) - a - cb \\ j \\ -\frac{1}{d}\big[cj + ra + a(a+i)\big] \end{pmatrix}. \tag{4.13}$$

This system features a singularity: As $d \to 0$, a separation of time-scales occurs. Intuitively speaking, the drift $j' = -\frac{1}{d}[cj + ra + a(a+i)]$ becomes so strong that the system remains close to the smooth manifold $\mathcal{M}_0$, where $j' = 0$, which is given by

$$\mathcal{M}_0 := \Big\{(a,b,i,j) \in \mathbb{R}^4 \Big| \, j = -\frac{a(a+i+r)}{c}\Big\}. \tag{4.14}$$

Since $\frac{\partial}{\partial j}\frac{\partial}{\partial x} j = -\frac{c}{d}$, the manifold $\mathcal{M}_0$ is indeed stable against perturbations in j. After the fast variable j is quickly pushed towards its equilibrium, the system continues to evolve along $\mathcal{M}_0$. However, the restriction of the System (4.13) to the manifold $\mathcal{M}_0$ simply reduces to the three-dimensional system

$$\frac{d}{dx}\begin{pmatrix} a \\ b \\ i \end{pmatrix} = \begin{pmatrix} b \\ a(a+i) - a - cb \\ -\frac{a(a+i+r)}{c} \end{pmatrix}, \tag{4.15}$$

which is precisely the Wave-System for $d = 0$, see Equation (4.15).

The theory of geometric singular perturbations [49, 84] makes this reasoning rigorous. One can prove that for $d \neq 0, d \sim 0$, there exists an invariant manifold $\mathcal{M}_d$ of the System (4.13), which is of distance $\mathcal{O}(d)$ to the manifold $\mathcal{M}_0$ on any bounded subset of $\mathbb{R}^4$. The details are explained in appendix C in [93].

We analyze the flow along this manifold $\mathcal{M}_d$ and prove the existence of traveling waves within $\mathcal{M}_d$ – non-negative and bounded solutions of Equation (4.13). By regular perturbation techniques, that allow to vary the parameter $d \gg 0$ and continuously track the solutions of Equation (4.13), we extend this result to non-asymptotic values of d, up to Bound (4.2). The details can be found in [93, Sect. 3.3 and 3.4]. We prove the existence of a family of traveling wave solutions, that are similar to those of the system for $d = 0$, see [93, Thm. 3.18]. This result only yields an estimated correspondence of the limits of the waves, which we can roughly summarize as

$$i_{-\infty} + i_{+\infty} = 2 + \mathcal{O}(d). \tag{4.16}$$

This estimate is explained in detail in [93, Sec 3.4]. In order to prove the existence of an invading front, where $i_{+\infty} = 0$, we use an intermediate value approach: Via a continuity argument, we show that among the constructed waves, there also must exist an invading front. This is proven in [93, Sec. 3.5].

4.4 Stability of the critical invading fronts

We analyze the long-time behavior of the weighted perturbations u, v, defined via (4.8). If the weight w is twice differentiable with derivatives w', w'', they

solve

$$\begin{aligned}\frac{\partial}{\partial t}u &= \frac{\partial^2}{\partial x^2}u + \frac{\partial}{\partial x}u\cdot\big(c+2\frac{w'}{w}\big) + u\cdot\big(c\frac{w'}{w}+\frac{w''}{w}\big)\\ &\quad + u(1-2a-i) - va - wu(u+v),\\ \frac{\partial}{\partial t}v &= d\frac{\partial^2}{\partial x^2}v + \frac{\partial}{\partial x}v\cdot\big(c+2d\frac{w'}{w}\big) + v\cdot\big(c\frac{w'}{w}+d\frac{w''}{w}\big)\\ &\quad + u(2a+i+r) + va + wu(u+v).\end{aligned} \tag{4.17}$$

We summarize this as

$$\frac{\partial}{\partial t}(u,v) = \mathcal{L}_w(u,v) + N(u,v), \tag{4.18}$$

with the linear part

$$\begin{aligned}\mathcal{L}_w u &:= \frac{\partial^2}{\partial x^2}u + \frac{\partial}{\partial x}u\cdot\big(c+2\frac{w'}{w}\big) + u\cdot\big(c\frac{w'}{w}+\frac{w''}{w}\big)\\ &\quad + u(1-2a-i) - va,\\ \mathcal{L}_w v &:= d\frac{\partial^2}{\partial x^2}v + \frac{\partial}{\partial x}v\cdot\big(c+2d\frac{w'}{w}\big) + v\cdot\big(c\frac{w'}{w}+d\frac{w''}{w}\big)\\ &\quad + u(2a+i+r) + va,\end{aligned} \tag{4.19}$$

and the nonlinear part

$$Nu := -wu(u+v), \qquad Nv := wu(u+v). \tag{4.20}$$

The choice of the weight w was explained in Section 2.3:

$$w(x) := \begin{cases} e^{-x} & x \geq 1,\\ e^{-\alpha_- x} & x \leq -1,\ \alpha_- \in (0,1),\\ 1 & x = 0.\end{cases} \tag{4.21}$$

The effect of w on the essential spectrum of $\mathcal{L}_w$ is explained in the introductory Section 2.3 and depicted in Figure 2.2:

Proposition 4.3 (Prop. 2.2 in [93]). *For $d \in (0,1)$ and exponents*

$$\alpha_- \in (0,1), \quad \alpha_+ = 1, \tag{4.22}$$

consider a convective weight w as in (4.21). Then, for a critical invading front as in Theorem 4.1, the essential spectrum of the linear operator $\mathcal{L}_w$:

$$\mathcal{L}_w : H^2(\mathbb{R}) \times H^2(\mathbb{R}) \to L^2(\mathbb{R}) \times L^2(\mathbb{R}), \tag{4.23}$$

defined by (4.19), is bounded to the right by the union of three parabolas that lie in the strict negative half-plane, with the exception of the negative half-line

$$\Sigma_\nu = \big\{\lambda \in \mathbb{C}\big|\, \mathfrak{Re}\lambda \leq 0, \mathfrak{Im}\lambda = 0\big\}. \tag{4.24}$$

This type of essential spectrum is considered in [48], and we can use their estimates regarding the long-time behavior of solutions of $u_t = \mathcal{L}_w u$. We make the following

Assumption on the discrete spectrum: In the Setting of the above Proposition 4.3, let Σ_d be the discrete spectrum of $\mathcal{L}_w$. Assume that there exist $\delta_0, \delta_1 > 0$, such that for the region

$$\Omega := \left\{ \lambda \in \mathbb{C} \middle| \, \mathfrak{Re}\lambda \geq -\delta_0 - \delta_1 \cdot |\mathfrak{Im}\lambda| \right\} \tag{4.25}$$

it holds that

$$\Omega \cap \Sigma_d = \emptyset. \tag{4.26}$$

We verify this assumption numerically, see appendix B.4.2. Note that we assume that $0 \notin \Sigma_d$. For an invading front $a(x), i(x)$, it is easy to see that the symbolic equation $\mathcal{L}(a', i') = 0$ holds. However, the critical front behaves like xe^{-x} as $x \to +\infty$, so its derivative is not an element of the considered weighted space. We expect that this implies $0 \notin \Sigma_d$, which can be proven in some cases, see e.g. [48, App. B].

For compactness of notation, we introduce the vectorial notation

$$p(t,x) := \begin{pmatrix} u(t,x) \\ v(t,x) \end{pmatrix}, \; N(p)(t,x) := w(x)u(t,x) \cdot \begin{pmatrix} -u(t,x) - v(t,x) \\ u(t,x) + v(t,x) \end{pmatrix}, \tag{4.27}$$

and write $|p(x,t)| = |u(x,t)| + |v(x,t)|$. We define as $\mathcal{G}(t,x,y)$ the Kernel of $\mathcal{L}_w$:

$$\mathcal{G}(t,x,y) := \begin{pmatrix} \mathcal{G}_{11}(t,x,y) & \mathcal{G}_{12}(t,x,y) \\ \mathcal{G}_{21}(t,x,y) & \mathcal{G}_{22}(t,x,y) \end{pmatrix}. \tag{4.28}$$

In this compact notation, we want to estimate the long-time behavior of $p(t,x)$ with a Duhamel principle:

$$p(t,x) = \int_{\mathbb{R}} \mathcal{G}(t,x,y)p(0,y)\,dy + \int_0^t ds \int_{\mathbb{R}} \mathcal{G}(t-s,x,y)N(p)(s,y)\,dy. \tag{4.29}$$

We can use a result of Fayé and Holzer [48] to estimate the long-time behavior of $\mathcal{G}(t,x,y)$. Roughly, this result states that for all $x \in \mathbb{R}$ and for large t:

$$\int_{\mathbb{R}} \left| \mathcal{G}(t,x,y) \cdot p(y) \right| dy \leq C \cdot \frac{1+|x|}{(1+t)^{3/2}} \int_{\mathbb{R}} |p(y)|\,dy, \tag{4.30}$$

the precise statement is given in [48, Prop. 4.1, Lem. 5.1]. For estimating the evolution of the full nonlinear system via (4.29), we need to control the nonlinear integral

$$\int_{\mathbb{R}} w(x)u(t,x)\cdot\big(u(t,x)+v(t,x)\big)\,dx. \tag{4.31}$$

We treat the cases $x\le 0$ and $x\ge 0$ separately. Assuming that $w(x)$ vanishes exponentially fast as $z\to+\infty$, the front satisfies the classical estimate

$$\begin{aligned}&\Big|\int_0^\infty w(x)u(t,x)\cdot\big(u(t,x)+v(t,x)\big)\,dx\Big|\\ &\le \sup_{x\ge 0}\Big\{\big(|u(t,x)|+|v(t,x)|\big)^2\Big\}\cdot\int_0^\infty w(x)\,dx\\ &\le C\cdot\sup_{x\ge 0}\big\{|p(t,x)|^2\big\}.\end{aligned} \tag{4.32}$$

Since $w(x)$ grows exponentially as $x\to-\infty$, we take a different approach for $x\le 0$. We use the following a-priori estimate:

Proposition 4.4 (Prop. 2.1. in [93]). *Let $A(t,x), I(t,x)$ be a non-negative solution of the PDE* (1.1) *in the moving frame $x=z-ct$, for a speed $c>0$. Assume that there exist constants $K,\delta,\mu_0>0$, such that the initial data fulfill*

$$\begin{aligned} I(0,x)&\ge 1+\delta && \forall x\le 0,\\ A(0,x)&\le Ke^{\mu_0 x} && \forall x\le 0,\\ A(0,x)+I(0,x)&\le K && \forall x\in\mathbb{R}.\end{aligned} \tag{4.33}$$

Moreover, assume that for some time $t\in(0,\infty]$, it holds that

$$I(s,x=0)\ge 1+\delta \qquad \forall s\in[0,t). \tag{4.34}$$

Then, there exist $C,\zeta>0$ that are independent of t, such that:

$$\forall s\in[0,t),\ x\le 0:\quad i)\qquad I(s,x)\ge 1+\delta, \tag{4.35}$$

$$ii)\qquad A(s,x)\le Ce^{\zeta x}. \tag{4.36}$$

The proof is given in [93, App. A]. It relies on the fact that the inactive particles do not degrade, and that in the regime $I(x,t)\ge 1+\delta$, the solution of the PDE

$$S_t=S_{xx}+cS_x-\delta S \tag{4.37}$$

is a super-solution for $A(t,x)$, which can be seen to decay exponentially fast. The tail of (4.37) is controlled via a Feynman-Kac formula driven by

a Brownian motion with shift equal to the speed $c = 2$ of the critical wave, for the mathematical background we refer to [86, Ch. 4.4].

For an invading front, it holds that $\lim_{x\to-\infty} i(x) > 1$, where $i(x)$ is monotone. We first shift the front such that $i(0) = 1 + 2\delta$ for a fixed $\delta > 0$. It suffices to choose initial data such that

$$|\tilde{I}(0,x)| \leq \delta \qquad \forall x \leq 0, \tag{4.38}$$

and to control the perturbation over time:

$$|\tilde{I}(t,x=0)| \leq \delta \qquad \forall t \geq 0, \tag{4.39}$$

then, it holds that $I(t,x=0) \geq 1+\delta$, and in view of Proposition 4.4, there exist constants $C, \zeta > 0$ such that

$$|\tilde{A}(t,x)| \leq A(t,x) \leq Ce^{\zeta x} \qquad \forall x \leq 0,\, t \geq 0, \tag{4.40}$$

since $A \geq 0$. We re-substitute $wu = \tilde{A}$ to estimate

$$\begin{aligned}
&\Big| \int_{-\infty}^{0} w(x)u(t,x) \cdot \big(u(t,x) + v(t,x)\big) \Big|\, dx \\
&\leq \int_{-\infty}^{0} |\tilde{A}(t,x)| \cdot |u(t,x) + v(t,x)|\, dx \\
&\leq \sup_{x\leq 0} \Big\{ |u(t,x)| + |v(t,x)| \Big\} \cdot \int_{-\infty}^{0} |\tilde{A}(t,x)|\, dx \\
&\leq C \cdot \sup_{x\leq 0} \big\{ |p(t,x)| \big\}.
\end{aligned} \tag{4.41}$$

Given both Estimates (4.32) and (4.41), we can control the nonlinear Evolution (4.29). This is carried out in [93, Sec. 2.4]. Briefly, after introducing

$$\Theta(t) := \sup_{s\leq t} \sup_{x\in\mathbb{R}} \frac{(1+s)^{3/2}}{1+|x|} |p(s,x)|. \tag{4.42}$$

we prove that for all $\epsilon > 0$, we can find suitable conditions regarding the initial data $p(0,x)$ such that

$$\Theta(t) < \epsilon \tag{4.43}$$

holds as long as (4.39) is valid for some fixed $\delta > 0$. Notice that (4.43) is equivalent to the pointwise decay claimed in Theorem 4.2. However, if we choose $\epsilon \leq \delta$ for δ as in (4.39), then the above Estimate (4.43) also implies that

$$|\tilde{I}(t,0)| \leq \Theta(t) < \delta, \tag{4.44}$$

and we can prove that both (4.39) and (4.43) are jointly valid for all $t \geq 0$, given sufficiently small initial data.

5 Tumour architecture and emergence of strong genetic alterations are bottlenecks for clonal evolution in primary prostate cancer

In this chapter, we summarize the content of the work "Tumour architecture and emergence of strong genetic alterations are bottlenecks for clonal evolution in primary prostate cancer", authored by Nima Abedpour, Anton Bovier, Reinhard Büttner, Christian Harder, Axel Hillmer, Florian Kreten, Martin Peifer and Yuri Tolkach [94]. This work is under review at the time of writing. In agreement with all authors, the unpublished preprint can be found in appendix C.

5.1 Background

Cancer is seen as a disease that develops via a chain of (stochastic) somatic mutations, emanating from healthy cells with normal behavior. These mutations lead to cell-lines which on the one hand show increased proliferation, and on the other hand are able to escape the regulatory mechanisms of the immune system [31]. It is a clinically important question how long these evolutionary processes take, and if there are prevalent evolutionary patterns, since progression of the tumors into more aggressive variants continues after the occurrence of the first malignant cells. Prostate adeno carcinoma (PCA) is a relatively slow growing cancer, typically age-related, and becomes aggressive and dangerous only in some cases [164]. However, PCA reveals high levels of intratumoural heterogeneity, which is a major obstacle for the selection of individualized therapies for patients [69, 95, 152].

PCA does form glandular structures, at least as long as it is classified as low or intermediate aggressive, as depicted in Figure 5.1. Recently, a three-dimensional reconstruction by Tolkach et al. revealed that these glandular systems form a self-avoiding branched structure, which belongs precisely to the class of objects that can be generated by the model of Hannezo et al. [146]. As such, the tumor-cells seem to mimic the surrounding healthy cells [142]. Based on these findings, we make the assumption that branched PCA follow the rules of branching morphogenesis proposed by Hannezo et al. [73], and develop a mathematical model to study the growth and the genetic evolution of PCA from the time of the formation of the first malignant cell up to its evolution into a full-size PCA.

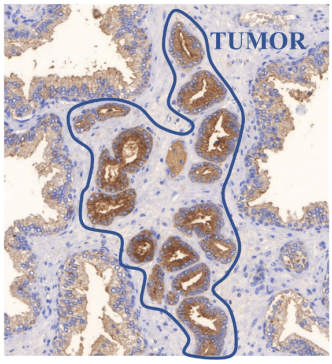

Figure 5.1: A two dimensional section of prostatic tissue. The cancer cells form a glandular system. Picture used with permission by Yuri Tolkach.

5.2 Model

We model PCA as a network with binary tree structure. Every node of the network represents a transversal section of a hollow channel of cells at a fixed position in $\mathbb{R}^3$. The cells of a node are assumed to have the same genotype, as such the nodes are the base entities of our model. In this way, we reduce the cellular movements by one dimension and simplify the hollow nature of the tumour channels-glands (the reconstruction of channels as hollow structures with interactions of the cells on the luminal surface is extremely complex). This simplification preserves the biological sense of the cell interactions: Any significant propagation of a fitter clone within the channels must occur in the axial direction, along the edges of the network (Figure 5.2).

Up to small modifications, the growth dynamics follow the model by Hannezo et al. [73]. Regarding the clonal dynamics, we concentrate on driver mutations and ignore neutral or deleterious mutations. We refer to a *mutation* as any type of genetic alteration that brings fitness advantage to a cell by increasing its rate of cell division. Moreover, we assume that mutations are unique, ignoring the possibility of parallel evolution of independent subpopulations. A *genotype* has a unique combination of consecutive mutations.

Growth and evolution of the system are formulated as a time-continuous stochastic jump process [44] that can be simulated using a Gillespie algorithm [65]. At each node, we differentiate four types of possible events: *growth, branching, mutation and competition* (Figure 5.2). Each event is triggered at exponential rates denoted as R_g, R_b, R_μ, R_c. The first occurring event is executed, then the rates are adjusted to the new situation. All the rates depend on the rate of cell division, which effectively acts as fitness in this model and as such is denoted as $f(v,t)$, the fitness of the genotype present at node v at time t. The details are given in [94].

At a vertex v, a fitter genotype with fitness $f_{new} = (1+\Delta)f_{old}$ occurs with rate of mutation R_μ. This new genotype then is in competition with

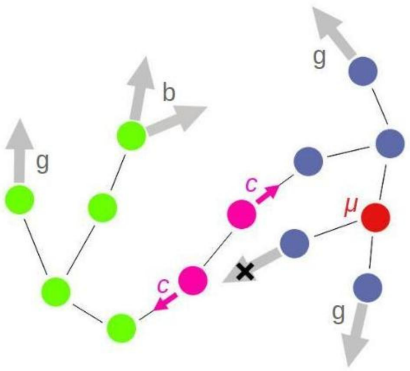

Figure 5.2: A schematic representation of the proposed model for the growth and the evolution of PCA. The growth of the network follows the rules of branching morphogenesis described by Hannezo et al. [73]. Each node of the network hosts a certain genotype (here, the different genotypes are depicted via different colors). Fitter genotypes spread along the edges of the network and replace their unfit neighbors. With a rate of mutation R_μ that depends on the fitness of the genotype at a node, new genotypes can occur anywhere within the network.

its neighboring genotypes, a relabeling process along the edges of the network follows, where the fitter genotype replaces its unfitter neighbors. This relabeling process is of speed $\mathcal{O}(\Delta)$ along the edges of the network and thus slow for small $\Delta > 0$ (see Section C.5.7).

5.3 Results

The parameters that we chose for the simulations are discussed in detail in [94], but we want to emphasize that qualitatively, our theoretical predictions are a result of the structure of the model. We explore the possible evolutionary patterns and demonstrate that the tumour architecture represents a major bottleneck for a divergent gradual clonal evolution: The rather strong competition negates any significant spreading of new genotypes that have only a small fitness advantage over their locally resident ancestor – in the literature, typical estimates for the fitness advante of driver mutations in more well-mixed cancers are values of Δ between 1 and 4% [21, 139]. As a result, *we hypothesize that strong genomic driver alterations drive the evolution of PCA*, and that the spatial structure of PCA impedes its evolution into more aggressive variants. This hypothesis is strongly supported by the fact that the spatial structure of PCA is clearly correlated with its aggressiveness: For clinicians, the different architectural patterns (the so-called Gleason patterns) of PCA are one of the most important indicators for estimating its malignancy, and the clear branched structure is lost in aggressive tumors [42, 126]. Its prevalently slow growth and the fact that PCA can be indolent for decades, are both well reproduced by our model: For large

times $t \geq 0$, the number of nodes in the network is of order $\mathcal{O}(t^3)$, opposing many models that result in exponential growth. Moreover, even mutations with large Δ must arrive rather early, otherwise they can never take over a significant fraction of the network. While the network is still small, the time of arrival as well as the amount of occurring mutations is much more stochastic than in the later phases. This leads to the hypothesis that in PCA, it is decided in the early stages of the tumor if the disease will turn harmful to the patient, however the aftermath of this evolution is will be observed only in later stages.

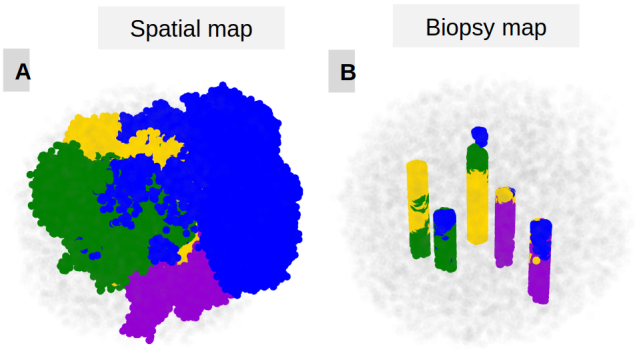

Figure 5.3: An exemplary result of a simulation, indicating different genotypes in different colors, and a biopsy consisting of five cores.

Next, we sought to analyse the spatial relationships between clonal populations (genotypes that can be found in at least 5% of the tumors) within synthetic tumours in a clinically relevant context. Approximately 10–12 biopsy cores are usually acquired during systematic multifocal prostate biopsy in patients with PCA suspicion, with (according to our estimation) on average five cores containing a tumour. We set up a comparable virtual biopsy, containing five cores (Figure 5.3), and selected a 5% volume threshold for the detection of genotypes in the biopsy. In clinical practice, 5% is often considered a threshold for reliable detection using next-generation sequencing. Evaluating the results of 150 simulated cases, we saw that it is extremely relevant to have biopsies from different regions of the tumor, in order not to miss any of the relevant advanced genotypes, which can be spatially localized (the detailed evaluations are given in Section C.2.5). Even in the case of such an extensive biopsy, there is a certain chance (depending on the parameters up to $\sim 20\%$) to miss one or more of the important clonal populations.

In the last step, we performed deep whole-exome multiregional next generation DNA sequencing (WES) of the primary tumours from five patients to validate our theoretical predictions. WES was performed from at least 5 large, neighboring areas of each tumour with a coverage of up to 400x. Copy number alterations were assessed for all tumour samples, then the somatic

point mutations were clustered according to resulting cancer cell fractions (CCFs). The clonal hierarchies of the tumors were reconstructed by using the CCFs, which yield a particularly detailed picture for clones that are present in several samples (due to the different distributions in the different samples). We found a qualitative agreement between real-world data and the results of the simulations (Section C.2.6): The reconstructed phylogenetic trees of the cancers showed clearly distinct generations with at most four evolutionary steps after the initiation of the tumor, and all cases expressed spatially localized, genetically divergent populations.

The code for the simulations, written in Python3, as well as a visual demonstration are available under `https://github.com/floriankreten/Prostate_Cancer_Publication.git`. They will be made publicly available upon publication.

Authors' contributions

Study concept: YT. Model design: YT, FK, AB. Mathematical implementation / simulations: FK. Data analysis, statistics: YT, FK, NA. Data interpretation: all authors. Manuscript drafting: YT, FK. Patient samples acquisition and processing: YT, AH. NGS analysis: NA, YT. Supervision, administrative support: RB, MF, AH. Manuscript editing, critical revision for important intellectual context: all authors.

6 Summary of the thesis

In the first parts of this PhD thesis, we studied the traveling wave solutions the Reaction-Diffusion System (6.1), motivated by the question why a certain stochastic branching system exhibits the property to self-organize. We analyzed the shape of the traveling waves, and found the traveling waves reflect the behavior of the stochastic system. After constructing the waves and anylyzing theis shape analytically, we could verify that these traveling waves are stable against perturbations. Our findings strengthen the observation that the stochastic system which was proposed by Hannezo et al. [73] generates a particular class of branched structures in a self-organized fashion, and that this process is robust against small errors. In the second part of this thesis, we studied a model of the branched growth and the possible evolution of prostate cancer, and found that its evolution is likely to be driven by strong driver mutations, contrasting the idea of a slow, gradual evolution of the tumor.

The introductory Chapter 1 of this thesis contains examples of self-organized systems in biology. One problem that has long fascinated both biologists and modelers is the morphogenesis of branched structures, that can be found for example in corals, fungi, and different mammalian tissues. We gave a first overview over different existing mathematical models, that explain the differentiation of the branches via Turing-patterns [68], or use diffusion-limited aggregation to simulate branched structures in general [129], and then focussed on a particular approach. Hannezo et al. proposed a stochastic system based on branching and annihilating random walks as a model for *A Unifying Theory of Branching Morphogenesis* [73]. In their publications, the authors illustrate why this process can be considered as a good model for the growth of several different branched tissues [73, 74] – the mammary glandular system or the kidney, to mention some.

This stochastic system is difficult to study, since it is not Markovian: The diffusing particles represent the tips of paths that must strictly avoid each other. In this thesis, we studied the heuristic hydrodynamic limit of the stochastic dynamics:

$$\begin{aligned} \frac{\partial}{\partial t}A &= \frac{\partial^2}{\partial z^2}A + A - A(A+I), \\ \frac{\partial}{\partial t}I &= d\frac{\partial^2}{\partial z^2}I + rA + A(A+I), \qquad r, d \geq 0, \end{aligned} \tag{6.1}$$

which describes the evolution of two densities $A(t,z), I(t,z) \geq 0$ of particles on the line $z \in \mathbb{R}$. This equation is related to the well-known FKPP-equation [22, 50, 91], which is also regained upon substituting $I \equiv 0$.

In Chapter 2, we presented the mathematical background of this thesis. FKPP-related systems and their traveling waves have been an active

field of research since the initial works of Fisher [50] and Kolmogorov et al. [91] in the 1930s. In the case of a single reactant, the convergence of the front of the PDE towards the traveling wave solutions is well-understood [22]. For two or more reactants, only local stability results can be obtained in most cases [130], that show that the traveling waves are robust against small perturbations. The stability of the critical traveling waves, those non-negative solutions with minimal possible speed c_{min}, is particularly difficult to study [48, 53], since the spectrum of the linearized perturbations is only marginally stable. At the end of the introductory Chapter 2, we reviewed the phenomenon of convective stability, where perturbations vanish pointwise relative to the traveling wave, in the moving frame $x = z - ct$, but may grow when they are convected away from the front as $x \to -\infty$. This concept originates from the physics of waves in fluids [118], but is now also considered more and more for studying traveling wave solutions of reaction-diffusion systems [63, 131].

We proceeded with a summary of the results of this thesis, which are contained in two papers. The first has been published, the second has appeared as a preprint on *arxiv.org* and has not been peer-reviewed yet:

1. [92] *Traveling waves of an FKPP-type model for self-organized growth*;
2. [93] *Convective stability of the critical waves of an FKPP growth process.*

Review of [92]

In the publication [92], summarized in Chapter 3, we constructed the non-negative traveling wave solutions of System (6.1) in the case $d = 0$. One major difficulty when studying System (6.1) is the continuum of steady state solutions

$$P_I = \{A = 0, I = K \mid K \in \mathbb{R}\}, \tag{6.2}$$

which reflects the fact the the inactive particles do not react. Using the logistic nature of the growth-terms of System (6.1), we could prove via certain integral equations that any bounded and non-negative traveling wave $a(x), i(x)$ of System (6.1) with $d = 0$ must obey the equality

$$\lim_{x\to-\infty} i(x) + \lim_{x\to+\infty} i(x) = 2. \tag{6.3}$$

Given the Identity (6.3), the continuum of fixed points turned out to be advantageous: We could first construct almost constant non-negative traveling wave solutions, where $a \ll 1$ and $i(x) \sim 1$, and then continuously deformed these waves along their Limits (6.2). This resulted in a continuous family of traveling wave solutions.

We used center manifold theory for analyzing the asymptotic behavior of the traveling waves around their limits, and thereby identified the non-negative trajectories. The minimal speed of a non-negative wave where both the active and inactive particles vanish as $x \to +\infty$, is given by $c_{min} = 2$, as in the case of the classical FKPP-equation [22].

Simulations indicate that it is always the wave with speed $c_{min} = 2$ that arises in the large-time limit of the PDE (6.1) under compact initial data. Therefore, we wanted to study their stability. We could not prove a stability result, since the operator that corresponds to the linearized perturbation equation is only marginally stable, see Section 2.3, and additionally is not sectorial for $d = 0$.

Review of [93]

We overcame these problems in the preprint [93], summarized in Chapter 4. First, we introduced a diffusion to the inactive particles, and constructed the non-negative traveling wave solutions of System (6.1) for $d \neq 0$. Second, we analyzed the local stability of the waves with minimal possible speed and found that they are convectively stable. We relied on a numerical evaluation of the point spectrum of the linearized equation.

Given the traveling waves of System (6.1) with $d = 0$ as a starting point, we applied geometric singular perturbation theory by Fénichel [49, 84] to prove the existence of similar traveling waves for $d \sim 0$. We then could again use the continuum of fixed points, together with regular perturbation theory, to improve this result and construct non-negative traveling waves of System (6.1) up to $d \sim 1$. In particular, we could prove that qualitatively, the behavior of the constructed traveling waves is not affected by the diffusion of the inactive particles.

For the fully parabolic system, we could then analyze the stability of the critical invading fronts, since the operator that corresponds to the linearized perturbation equation is now sectorial, as opposed to the case $d = 0$. Since the limits of the traveling waves are non-hyperbolic fixed points, we had to operate in a weighted space where there perturbations can grow exponentially as they are shifted towards the back of the wave. This stabilizes one part of the essential spectrum, see Section 2.3.

The resulting linearized equation falls into a category which was already analyzed by Faye and Holzer [48]. Their result yields linear stability of the critical invading fronts, proving a pointwise decay of solutions of the linearized perturbation equation. However, since our chosen weight is unbounded to the left, we needed an additional a-priori estimate in order to control the full nonlinear problem. To our best knowledge, no such a-priori estimate did exist yet, that is compatible with a pointwise control of the

linear problem. The a-priori bounds which are proven for related cases use energy-based estimates in H^1 [61, 118].

We therefore developed a new approach, tailored to the pointwise estimate that we have for the Green's function of the linear problem. A Feynman-Kac formula driven by a shifted Brownian motion which is stopped at the origin yields a suitable representation of a linear super-solution of $A(t, x)$ at the back of the wave. The central ideas are presented in Section 4.4. The result is an estimate of type $A(t, x) \leq C \exp(\zeta x)$ as $x \to -\infty$, for some $\zeta > 0$. Using the explicit form of the nonlinear terms, inspired by the works of Ghazaryan [61], this estimate turned out to be sufficient for controlling the full non-linear evolution of the weighted perturbations. We use this to prove a decay of the weighted perturbation: Given that the initial perturbations are sufficiently small, they decay pointwise like $t^{-3/2}$.

Review of [94]

In Chapter 5, we investigated the possible effect of the branched structure of prostate cancer (PCA) on its clonal evolution. The unpublished work [94] is based on the findings of Tolkach et al. [146], who did a reconstruction of the three-dimensional glandular structure of PCA. We developed a mathematical model where the growth of well-differentiated PCA obeys the rules for branching morphogenesis proposed by Hannezo et al. [73], and where stochastic mutations and a competition between the different genotypes drive its evolution.

We simulated the resulting stochastic growth and evolutionary process, and explored the possible evolutionary patterns. We hypothesize that the spatial structure of PCA is a bottleneck for its clonal evolution: As along as the tumor follows the rules of branching morphogenesis, its cells are subject to constant local competition, being encased in the glandular network of the tumor. This competition implies that new genotypes can spread significantly only if they either have a high fitness advantage (or if they break up the spatial structure of the tumor, which we do indeed observe in more aggressive PCA). Concluding, the evolution of well-differentiated PCA is more likely to be driven by few, strong driver mutations.

We then performed biopsies of the simulated tumors. As the spatial structure of the cancer implies that cells of different genotypes are not well-mixed over the tumor, but rather can be spatially localized, there is indeed a significant chance to miss one or more relevant driver mutations, even under an extensive biopsy. In the last step, we performed deep whole-exome multiregional next generation DNA sequencing of the primary tumours from five patients to validate our theoretical predictions, and found a qualitative agreement between real-world data and the results of the simulations.

Appendices

A Publication: Traveling waves of an FKPP-type model for self-organized growth

This appendix reproduces exactly the content of the paper "Traveling waves of an FKPP-type model for self-organized growth", published by the author of this thesis in *Journal of Mathematical Biology, 84(6):42, 2022, https://doi.org/10.1007/s00285-022-01753-z.* This publication was summarized in Chapter 3.

A.1 Motivation and result

The mechanics of tissue-growth have drawn the attention of the scientific community. A central question is, how the cells are organized, how they react to and communicate with their environment on the microscopic level, and how their behavior during the growth phase gives rise to distinct macroscopic structures. Mathematical models can help to understand these processes and works regarding organoids, wound healing or tumor growth are abundant [111, 106, 46, 37, 83]. However, for most of these models, our numerical skills far predominate the possibility to analyze them rigorously. Hence, for understanding the basic mechanics of the underlying biological processes, the need for simplified models arises.

Especially when studying spatiotemporal effects and macroscopic pattern formation, reaction-diffusion systems and their traveling waves have proven insightful. One of the oldest and most studied models is the FKPP-equation [50, 91], describing the advance of an advantageous population. The arise of more complex spatial patterns due to the instability of a homogeneous state was first described in Turings groundbreaking paper *The Chemical basis of Morphogenesis* [147]. More recently, systems of Keller-Segel type have been studied extensively, where growth, movement and self-organization of a population are driven by chemotactic guidance [88, 120, 116]. Broad introductions to mathematical modeling of pattern formation in developmental biology have been written by Painter [116] and Othmer et al. [114], among others.

The group of Hannezo et al. proposed *A Unifying Theory of Branching Morphogenesis* in epithelial tissues [73]. They introduced a stochastic model, related to branching and annihilating random walks [29]. In this model, a branched structure is represented by a network. This network undergoes

stochastic growth dynamics, where each branch of the network grows independently from the others and follows a set of simple, local rules. At its tip, each branch elongates or splits up at certain rates and these tips are called *active*. When an active tip comes too close to a different branch, it irreversibly ceases any activity and becomes *inactive*. The numerical results of Hannezo et al. reveal that this stochastic growth process self-organizes: the active tips concentrate at the boundary of the network and form a rather sharp layer of growth. The center of the network is static and – rather surprisingly – exhibits a homogenous geometry, in particular a constant density of branches. Remarkably, as mentioned by the authors, this model self-organizes without any signaling gradients. Even a directional bias of the branches can be achieved, as the result of an appropriate spatial boundary. Moreover, the authors observed that their simulations were in good agreement with biological data from mammary glands, kidneys and the human prostate [73].

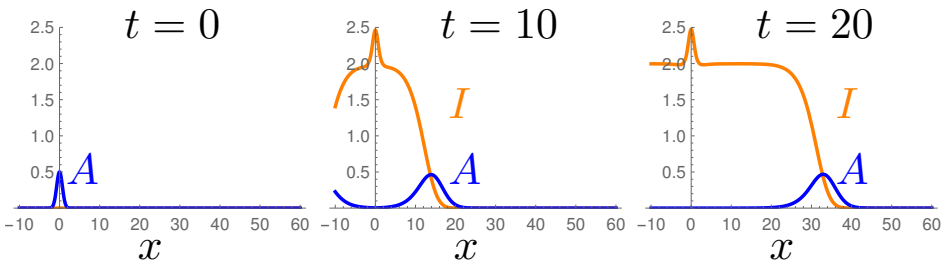

Figure A.1: Simulation of the Reaction-Diffusion System (A.1) *for* $r = 0$. *Given a small initial heap of active particles* $A(x, 0) = 1/2 \exp(-x^2)$ *and* $I(x, 0) = 0$, *two identical traveling fronts arise, the right one is shown. After the separation of the two fronts away from the origin, the density of the remaining inactive particles is given by* $I = 2$ *and the front moves asymptotically with speed* $c = 2$.

To study their model analytically, Hannezo et al. proposed the following system, which corresponds to the diffusive limit of the above stochastic dynamics. We restrict ourselves to the one-dimensional case. Due to a simple linear rescaling (Appendix A.10.3), we only need to consider the normalized reaction-diffusion system

$$\begin{aligned} A_t &= A_{xx} + A - A(A + I), \\ I_t &= A(A + I) + rA. \end{aligned} \tag{A.1}$$

Here, $A, I : \mathbb{R} \times \mathbb{R}^+ \to \mathbb{R}^+$ are the densities of *active particles* and *inactive particles*.

The System (A.1) can be interpreted as a twofold degenerate Keller-Segel system [88, 6]: the active particles are not guided by a chemotactic gradient, but explore the space solely diffusively, and the inactive particles do not

diffuse at all. Still, simulations of System (A.1) show that general solutions of (A.1) self-organize, a phenomenon which is typical for many different Keller-Segel systems [116]. The invading front of the system converges to a fixed shape: a pulse of active particles, that represents a layer of growth, is accompanied by a monotone wave of inactive particles, the resulting static tissue, as demonstrated in Figure A.1. This self-organization of the Reaction-Diffusion System (A.1) resembles that of the stochastic dynamics.

For a wave speed $c > 0$, a right-traveling wave solves Eq. (A.1) via the Ansatz $A(x,t) = a(x-ct), I(x,t) = i(x-ct)$. We substitute $z = x - ct$, such that any traveling wave must be a solution of

$$\begin{aligned} 0 &= a_{zz} + ca_z + a - a(a+i), \\ 0 &= ci_z + a(a+i) + ra. \end{aligned} \tag{A.2}$$

The occurrence of these seemingly stable traveling waves is quite surprising, since the System (A.1) features a continuum of steady state solutions:

$$A = 0,\ I = K,\ K \in \mathbb{R}^+, \tag{A.3}$$

which is due to the fact that the inactive particles do not degrade. This continuum of steady states represents the difficulty when studying the system: we first need to find out which limiting states are chosen by the growth process.

Hannezo et al. presented a rich discussion of the Wave-Equation (A.2) along with numerics and several heuristics that show a deep connection with the original FKPP-equation, and predicted some of the following results. The goal of this paper is to give necessary and sufficient conditions for the existence of such traveling wave solutions and to analyze the shape of the wave form. Our main result characterizes a family of pulled traveling waves:

Theorem A.1. *Let $r \geq 0, c > 0$ and consider the System (A.1) and its traveling wave solutions given by (A.2). Set $i_c := \max\{0, 1 - c^2/4\}$. For each pair $i_{-\infty}, i_{+\infty} \in \mathbb{R}^+$ such that*

$$i_{+\infty} \in [i_c, 1), \qquad i_{-\infty} = 2 - i_{+\infty}, \tag{A.4}$$

there exists a unique bounded and positive traveling wave $a, i \in C^\infty(\mathbb{R}, \mathbb{R}^2)$ with speed c such that

$$\lim_{x \to \pm\infty} a(z) = 0, \qquad \lim_{x \to \pm\infty} i(z) = i_{\pm\infty}. \tag{A.5}$$

The function $i(z)$ is decreasing, whereas $a(z)$ has a unique local and global maximum. If $\frac{c^2}{4} + i_{+\infty} - 1 = 0$, then convergence as $z \to +\infty$ is sub-exponentially fast and of order $z \cdot e^{-\frac{c}{2}z}$. If $\frac{c^2}{4} + i_{+\infty} - 1 > 0$, then convergence as $z \to +\infty$ is exponentially fast. Convergence as $z \to -\infty$ is exponentially fast in all cases. The corresponding rates are

$$\mu_{\pm\infty} = -\frac{c}{2} + \sqrt{\frac{c^2}{4} + i_{\pm\infty} - 1}. \tag{A.6}$$

Moreover, these are all bounded, non-negative, non-constant and twice differentiable solutions of Eq. (A.2).

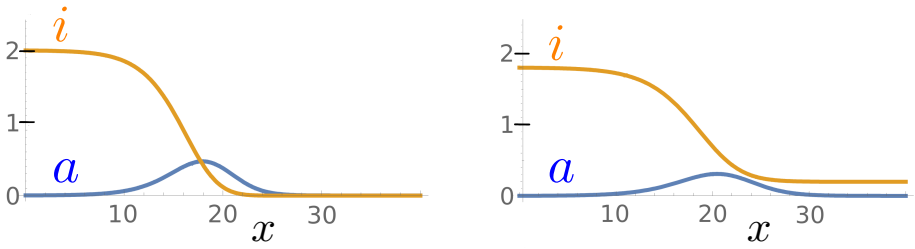

Figure A.2: Two different traveling waves with speed $c = 2$. The limits of the left wave are given by $i_{-\infty} = 2$ and $i_{+\infty} = 0$. The limits of the right wave are given by $i_{-\infty} = 1.8$ and $i_{+\infty} = 0.2$.

Notice that this result is independent of the reproduction rate r, which affects the shape of the wave, but neither its limits nor the minimal speed of a positive solution. Hence, all non-negative and bounded traveling waves resemble the ones depicted in Figure A.2, consisting of a pulse of active particles and a monotone wave of inactive particles. These traveling wave solutions share many similarities with classical FKPP-waves of a single type of particles. Among other mathematical aspects, this will be discussed at the end of the paper, in Section A.9. Notably, Theorem A.1 analytically connects two continua of fixed points via a continuum of traveling waves. Our constructive approach is a novelty: we first prove the existence of almost constant solutions and then continuously deform these solution along the continuum of possible limits.

Figure A.1 shows a simulation of the System (A.1), starting with a small initial amount of active particles. After a short transition phase, we observe a front with fixed shape. Asymptotically, it equals the unique traveling wave with limits $i_{-\infty} = 2, i_{+\infty} = 0$ and speed $c = 2$, which is the minimal possible wave speed for this pair of limits. We observed this behavior for all compact initial data that we chose. Moreover, this wave seems to be stable against perturbations, as briefly discussed in the concluding Section A.9. Even though it is only a first step into this direction, this paper sheds light at the ability of the Growth-Process (A.1) to self-organize and at the robustness of this mechanism, e.g. against errors of individual particles. Our theoretical analysis fortifies the numerical and biological findings of Hannezo et al., where a simple set of local rules organizes the growth of a complex epithelial structure. The underlying assumption of a logistic growth is quite natural, so similar rules might drive and regulate other growth processes as well, without the need for guiding gradients.

A.2 Outline of the paper

A sketch of the central ideas and techniques is presented in Section A.2. The identity $i_{-\infty} + i_{+\infty} = 2$ is proved in Section A.3. The asymptotic behavior around the stable and unstable set of the traveling waves is analyzed in Section A.4. A non-negative trapping region of a lower-dimensional sub-system is analyzed in Section A.5. We use our knowledge about the sub-system to construct a suitable attractor of the full system in Section A.6. Then, we connect the unstable manifold of the unstable set with this attractor, see Section A.7. We complete the proof of Theorem A.1 in Section A.8. In Section A.9, we highlight the similarity of the traveling waves with those of the original FKPP-equation and give a short outlook at their stability.

A.2.1 Identifying the correct limits

We reformulate the System (A.2) for a traveling wave as an equivalent system of first-order ODEs. Denoting differention with respect to z by a prime, we introduce the auxiliary variable $a' = b$, so that (A.2) becomes

$$\begin{aligned} a' &= b, \\ b' &= a(a+i) - a - cb, \\ i' &= -\frac{1}{c} a\,(a+i+r)\,, \end{aligned} \tag{A.7}$$

with $c > 0, r \geq 0$. We call a solution of Eq. (A.7) non-negative if $a, i \geq 0$. If a solution is in $C^1(\mathbb{R}, \mathbb{R}^3)$, then it is also in C^∞ by a simple induction. This equation has a continuum of non-negative fixed points, similar to that of the PDE, cf. (A.3):

$$a = b = 0, \quad i \in \mathbb{R}^+. \tag{A.8}$$

Thus, in the first place, we need to find out which of these fixed points can be considered as limits of right-traveling waves. Any bounded and non-negative solution of System (A.7) can not be periodic and must converge since $ci' = -a(a+i+r) \leq 0$. It is now evident that the limits at $z = \pm\infty$ must be fixed points of Eq. (A.7), thus we denote them as $(a, b, i) = (0, 0, i_{\pm\infty})$. Under mild assumptions regarding integrability, we can interrelate two different points on a given traveling wave, see Section A.3. Most importantly, this leads to the correspondence of the limits

$$i_{+\infty} + i_{-\infty} = 2. \tag{A.9}$$

In view of this, monotonicity of i implies that $i_{-\infty} \in (1, 2]$ and $i_{+\infty} \in [0, 1)$.

The fixed points of the ODE System (A.7) are not isolated, hence its Jacobian D is degenerate there. It is easily verified that D is given by

$$D_{(a,b,i)} = \begin{pmatrix} 0 & 1 & 0 \\ 2a+i-1 & -c & a \\ -\frac{1}{c}(2a+i+r) & 0 & -\frac{a}{c} \end{pmatrix}. \tag{A.10}$$

At a fixed point $(a, b, i) = (0, 0, K)$, the eigenvalues of $D_{(0,0,K)}$ are

$$\lambda_0 = 0, \qquad \lambda_\pm = -\frac{c}{2} \pm \sqrt{\frac{c^2}{4} + K - 1}. \tag{A.11}$$

Hence, we can not apply the classical Theorem of Grobmann-Hartmann to linearize the asymptotic behavior around the fixed points. We apply center manifold theory to work out the higher moments of the approximation, see Section A.4. The center manifold coincides with the continuum of fixed points. This implies that asymptotically, there is no flow along the direction of the eigenvector $(a, b, i) = (0, 0, 1)$ with zero eigenvalue. Hence, the asymptotic flow around any fixed point is two-dimensional and the stability of the fixed point $(0, 0, K)$ is dictated by the two eigenvalues $\lambda_\pm$. When $K > 1$, the fixed point is unstable, while for $K < 1$, it is stable.

At the same time, the analysis of the asymptotic behavior also yields a necessary condition on the speed c of a non-negative wave. A traveling wave can only be non-negative if $a(x)$ does not spiral while converging to 0. Therefore, the two eigenvalues $\lambda_\pm$ at the limiting fixed point must be real-valued. In view of (A.11), for a fixed point $(0, 0, K)$, this is given if

$$\frac{c^2}{4} + K - 1 \geq 0. \tag{A.12}$$

Thus, if the stable fixed point $(0, 0, i_{+\infty})$ is the limit of a non-negative traveling wave, where $i_{+\infty} \in [0, 1)$, it must by (A.12) further hold that

$$\frac{c^2}{4} + i_{+\infty} - 1 \geq 0 \quad \Leftrightarrow \quad i_{+\infty} \geq i_c = \max\{0, 1 - \frac{c^2}{4}\}, \tag{A.13}$$

as in Theorem A.1. In other words, i_c is the minimal limiting density of inactive particles that is necessary for the existence of a non-negative traveling wave with speed c.

A.2.2 Construction of a traveling wave

We will explicitly construct a non-negative traveling wave such that the two necessary conditions $i_{+\infty} \geq i_c$ and $i_{+\infty} + i_{-\infty} = 2$ are fulfilled. Two key features of the model make it tractable: first, the monotonicity of $i(z)$ allows us to investigate the convergence of the sub-system that arises for a fixed value of i, and then lift our result to almost constant solutions of the full system. Second, for extending this result to non-small solutions, we lean on an integral equation that allows us to interrelate two points on a given trajectory. However, the central Proposition A.3 depends essentially on the logistic growth of the active particles. Apart from this, our general approach seems to be applicable to a broader class of systems.

Regarding the ODE System (A.7), our analysis of the flow around the fixed points in Section A.4 reveals a suitable *unstable set*

$$S_{-\infty} := \big\{(0,0,i) : i \in (1,2]\big\}, \tag{A.14}$$

and a suitable *stable set*

$$S_{+\infty} := \big\{(0,0,i) : i \in [0,1)\big\}. \tag{A.15}$$

Each point $(0,0,i_{-\infty}) \in S_{-\infty}$ has an unstable manifold of dimension one. Its restriction to $a \geq 0$ is the only possible candidate for the tail of a non-negative traveling wave as $x \to -\infty$. Each point $(0,0,i_{+\infty}) \in S_{+\infty}$ is Lyapunov stable, which can also be seen in Figure A.3.

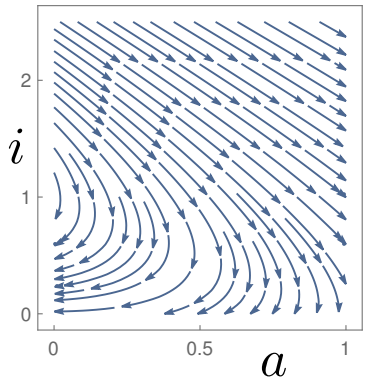

Figure A.3: Two-dimensional phase portrait of (a,i) of traveling waves (A.7) *for $c = 2$ and $r = 0$, omitting the coordinate $b = a'$. A unique trajectory emerges from each point in $S_{-\infty}$ (where $i_{-\infty} > 1$) in positive direction of a and converges to $S_{+\infty}$ (where $i_{+\infty} < 1$). Notice the correspondence $i_{-\infty} + i_{+\infty} = 2$ of the limits.*

To begin with, we let $(0,0,i_{-\infty}) \in S_{-\infty}$, where $i_{-\infty} \in (1, 2 - i_c]$, and follow its unstable manifold in positive direction of a. We prove that there exists a finite phase-time x_0 such that $b(x_0) = 0$: the trajectory reaches a local maximum of active particles, again see Figure A.3. We denote it as $(a_{x_0}, 0, i_{x_0})$. This is carried out in Section A.7.

Thus, for finding a suitable attractor of $S_{+\infty}$, we analyze solutions that start in points of type $(a,b,i) = (a_0, 0, i_0)$. We first analyze the lower-dimensional subsystem in coordinates (a,b), imposing a fixed value of i, which is done Section A.5. We construct a trapping region, wherein a converges and stays non-negative. The monotonicity of $i(z)$ allows us to lift this result to the full system, see Section A.6. Here, the continuum of fixed points comes at help: we first prove the existence of almost constant solutions, where $a \ll 1$ and $i \sim i_0$, that stay non-negative and converge. Then, we continuously deform these solutions: the Lyapunov-stability of the limits in $S_{+\infty}$ implies continuity of the entire trajectory up to $z = +\infty$ in initial

data. We use this to derive sharp conditions regarding $(a_0, 0, i_0)$ such that the trajectory stays non-negative and converges.

We show that the first local maximum $(a_{x_0}, 0, i_{x_0})$ along the instable manifold of $(0, 0, i_{-\infty})$ does fulfill these conditions, see again Section A.7. The technique is the same as for proving the identity $i_{+\infty} + i_{-\infty} = 2$, which is the starting point of our analysis and presented in the next section. The proof of Theorem A.1 is completed in Section A.8, where we bring together all the different pieces. The resulting continuous family of solutions is sketched in Figure A.3.

A.3 The mapping of the limits $i_{-\infty} + i_{+\infty} = 2$

We first verify global integrability of a non-negative solution:

Lemma A.2. *Let $a(x), b(x), i(x)$ be a smooth, bounded and non-negative traveling wave that solves the ODE System (A.7). Then, as $x \to \pm\infty$, $a(x)$ vanishes and $i(x)$ converges, and $a, b, b', i' \in L^1(\mathbb{R})$. Moreover, $i(x)$ is decreasing and $a(x)$ has a unique global and local maximum.*

Proof. Let $a(x), b(x), i(x)$ be a smooth, bounded and non-negative solution of Eq. (A.7). Since $ci' = -a(a + i + r) \leq 0$, it holds that $i(x)$ is decreasing and by boundedness must converge as $x \to \pm\infty$, so $i' \in L^1(\mathbb{R})$. The two limits must be fixed points and given by some $(a, b, i) = (0, 0, i_{-\infty})$ and $(0, 0, i_{+\infty})$. Equality is only given if $a(x) \equiv 0$. If not $a(x) \equiv 0$, then there is at least one local maximum of active particles, which we denote as $(a_0, 0, i_0)$.

At this point, $a'' = b' = a_0(a_0 + i_0 - 1) \leq 0$, so either $a_0 = 0$ and the wave is constant, or $a_0 + i_0 \leq 1$. In the second case case, assume that there is also a local minimum of $a(x)$, denoted as $(a_m, 0, i_m)$. Since $a(x)$ vanishes as $x \to \pm\infty$, we may assume that this be the first local minimum after passing through $(a_0, 0, i_0)$. As before, $(a_m, 0, i_m)$ is already a fixed point or $a_m + i_m \geq 1$. Since $i(x)$ is decreasing, $a(x)$ must have been increasing, a contradiction to the assumption that this is the first local minimum after the maximum $(a_0, 0, i_0)$. Thus, there is only one local maximum of active particles, which is also the global one. Further, this implies $a' = b \in L^1(\mathbb{R})$. By $ci' = -a(a + i + r) \leq 0$, we know that $a(a + i + r)$ is also in $L^1(\mathbb{R})$. We integrate $b' + cb + a = a(a + i)$ over the finite interval $[-M, M]$, then send the boundaries to $\pm\infty$:

$$\int_{-M}^{M} b'(x) + cb(x) + a(x)\, dx = \int_{-M}^{M} a(x) \cdot \big[a(x) + i(x)\big]\, dx. \tag{A.16}$$

We know that the right-hand is integrable since $i' \in L^1(\mathbb{R})$, and that both $a(\pm M)$ and $b(\pm M)$ vanish as $M \to +\infty$. This implies

$$\int_{\mathbb{R}} a(x)\ dx = \lim_{M \to +\infty} \Big[b(M) - b(-M) + c \cdot \big[a(M) - a(-M)\big] + \int_{-M}^{M} a(x)\, dx\Big]$$

$$= \int_{\mathbb{R}} a(x) \cdot \big[a(x) + i(x)\big]\, dx. \tag{A.17}$$

Hence also $a \in L^1(\mathbb{R})$, since $a \geq 0$. Finally, as a sum of integrable terms, also $b' \in L^1(\mathbb{R})$. □

The following Proposition A.3 will be used several times to interrelate two points $(a_1, 0, i_1), (a_2, 0, i_2)$ on a traveling wave, where $b_i = 0$. By the previous Lemma, the necessary conditions regarding integrability are always verified for non-negative and bounded solutions.

Proposition A.3. *Let $a(x), b(x), i(x)$ be a smooth and bounded solution of the ODE System (A.7) on some interval $[z_1, z_2]$, where $-\infty \leq z_1 \leq z_2 \leq +\infty$. Assume that $b(z_1) = b(z_2) = 0$. Further, assume that a, b, b', i' are integrable and define $\mathscr{A}(t) := \int_{z_1}^{t} a(x)\, dx$. The following three identities hold:*

$$\int_{z_i}^{z_2} a(z)\big[a(z) + i(z)\big]\, dz = \mathscr{A}(z_2) + c \cdot \big[a(z_2) - a(z_1)\big], \tag{A.18}$$

$$i(z_1) - i(z_2) = \frac{1+r}{c}\mathscr{A}(z_2), \tag{A.19}$$

$$\begin{aligned}\int_{z_i}^{z_2} a(z)\big[a(z) + i(z)\big] &= \big[i(z_2) + a(z_2)\big] \cdot \mathscr{A}(z_2), \\ &\quad + \frac{1+r}{2c}\mathcal{A}(z_2)^2 + \frac{a(z_1)^2 - a(z_2)^2}{2c}.\end{aligned} \tag{A.20}$$

Proof. Any solution of the ODE System (A.7) also fulfills the original Wave Equations (A.2). We integrate these over $[z_1, z_2]$, substitute $a' = b$ and use that $b(z_i) = 0$. This directly proves (A.18) and (A.19). Regarding Eq. (A.20), note that by integration by parts:

$$\begin{aligned}\int_{z_1}^{z_2} a(x) \cdot \big[a(x) + i(x)\big]\, dx &= \Big|_{z_1}^{z_2} \mathscr{A} \cdot (a + i) \\ &\quad - \int_{z_1}^{z_2} \mathscr{A}(x) \cdot \big[b(x) + i'(x)\big]\, dx \\ &= \big[i(z_2) + a(z_2)\big] \cdot \mathscr{A}(z_2) + \int_{z_1}^{z_2} \mathscr{A}(x) \cdot \frac{1}{c}\big[(1+r)a(x) + b'(x)\big]\, dx \\ &= \big[i(z_2) + a(z_2)\big] \cdot \mathscr{A}(z_2) + \frac{1+r}{2c}\Big|_{z_1}^{z_2} \mathscr{A}^2 + \frac{1}{c}\int_{z_1}^{z_2} \mathscr{A}(x) b'(x)\, dx \\ &= \big[i(z_2) + a(z_2)\big] \cdot \mathscr{A}(z_2) + \frac{1+r}{2c}\mathscr{A}(z_2)^2 + \frac{a(z_1)^2 - a(z_2)^2}{2c}.\end{aligned} \tag{A.21}$$

□

Remark: Equations (A.18) and (A.19) encode a mass transfer from the active to the inactive particles and are not specific for the chosen reactions.

It is the quadratic Eq. (A.20) that relies on a logistic saturation mechanism, we do not see a (direct) way to generalize this result.

Given Proposition, the identity $i_{-\infty} + i_{+\infty} = 2$ is a mere

Corollary A.4 (Limits of traveling waves). *Let $a(x), b(x), i(x)$ be a non-negative and bounded traveling wave that solves the ODE System* (A.7)*, and denote its limits as $(a, b, i) = (0, 0, i_{\pm\infty})$. Either $\int_{\mathbb{R}} a(z)\,dz = 0$ implies $i_{+\infty} = i_{-\infty}$, or the following identity holds:*

$$i_{-\infty} + i_{+\infty} = 2. \tag{A.22}$$

Proof. We apply Proposition (A.3). Since $a(\pm\infty) = 0$, the Equations (A.18), (A.19) and (A.20) can be simplified to

$$\mathscr{A}(+\infty) = i_{+\infty} \cdot \mathscr{A}(+\infty) + \frac{1+r}{2c}\mathscr{A}(+\infty)^2, \tag{A.23}$$

$$\frac{(1+r)}{c}\mathscr{A}(+\infty) = i_{-\infty} - i_{+\infty}. \tag{A.24}$$

Either $\mathscr{A}(+\infty) = 0$ implies $i_{+\infty} = i_{-\infty}$, or we divide the first equation by $\mathscr{A}(+\infty)$ and solve the resulting linear system, which proves the claim. □

A.4 Asymptotics around the fixed points

Let us recall that the Jacobian $D_{(0,0,K)}$ of the ODE System (A.7) at a fixed point $(0, 0, K)$ has eigenvalues

$$\lambda_0 = 0, \qquad \lambda_\pm = -\frac{c}{2} \pm \sqrt{\frac{c^2}{4} + K - 1}. \tag{A.25}$$

The existence of λ_0 implies the existence of a center manifold. In the present case, it locally coincides with the set of fixed points $a = b = 0$. This implies that there is no flow along the center manifold, so the asymptotics are fully described by the remaining two linear terms. The calculations are standard and presented in Appendix A.10.1, along with a short review of the underlying theory. We only state the results here. First, regarding the unstable set $S_{-\infty}$, as defined in (A.14):

Theorem A.5 (Unstable set). *For $i_{-\infty} > 1$, the point $(a, b, i) = (0, 0, i_{-\infty})$ is an unstable fixed point of Dynamics* (A.7)*. Locally, there exists a smooth unstable manifold of dimension one. Its restriction to $\{a \geq 0\}$ is the unique trajectory that emerges from the fixed point such that $a(x), i(x) > 0$ as $x \to -\infty$. It has the following properties:*

$$\begin{aligned} &\bullet \lim_{x\to-\infty} a(x) = 0, \\ &\bullet \lim_{x\to-\infty} i(x) = i_{-\infty}, \\ &\bullet\ b(x) > 0,\ b'(x) > 0,\ i'(x) < 0 \quad \text{as } x \to -\infty. \end{aligned} \tag{A.26}$$

Proof. By choice of $i_{-\infty} > 1$, the eigenvalue λ_+ is positive, whereas λ_- is negative. Denote by u, v, w the coordinates in the system of eigenvectors e_0, e_+, e_- of the Jacobian at the fixed, where the fixed point is shifted to the origin. This transformation is done explicitly in Lemma A.44. By Theorem A.45, the dynamics in an open neighborhood around the fixed point are equivalent to

$$\begin{aligned} u' &= 0, \\ v' &= \lambda_+ \, v, \\ w' &= \lambda_- \, w. \end{aligned} \tag{A.27}$$

Hence, there is a stable and an unstable manifold, each of dimension one. The eigenvector e_+ describes the asymptotic direction of the unstable manifold, in coordinates a, b, i it is given by

$$e_+ = \begin{pmatrix} -\lambda_- \\ i_{-\infty} - 1 \\ \frac{1}{c}(r + i_{-\infty}) \cdot \frac{\lambda_-}{\lambda_+} \end{pmatrix}. \tag{A.28}$$

Since $\lambda_- < 0$ and $\lambda_+ > 0$, asymptotically along the branch of the unstable manifold in direction e_+, where $a > 0$ and $b > 0$, it also holds that $b' = \lambda_+ \, (i_{-\infty} - 1) > 0$ and that $ci' = \lambda_- \, (r + i_{-\infty}) < 0$. □

Next, we prove Lyapunov-stability of the points in $S_{+\infty}$, defined in (A.15). Figure A.4 shows how the phase lines converge to $(0, 0)$ in the (a, b)-plane. For technical reasons, we require that $\lambda_+ \neq \lambda_-$. Later, we deal with this degenerate case via a continuity argument.

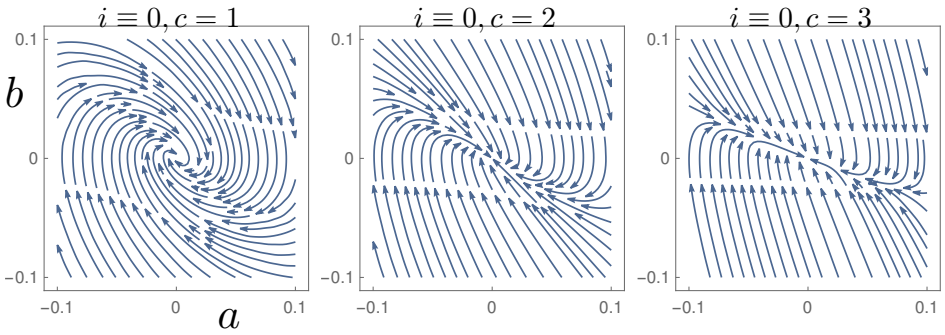

Figure A.4: Phase portrait of (a, b) of the Wave Eq. (A.7) if we impose a fixed value of $i(x) = 0$, see also Section A.5. The choices of c change the type of convergence towards the origin: spiraling for $c = 1$, one stable manifold with with eigenvalue $-c/2$, which has algebraic multiplicity 2 and geometric multiplicity 1 for $c = 2$, two stable manifolds for $c = 3$.

Theorem A.6 (Stable set)**.** *For all $c > 0$ and $i_{+\infty} \in [i_c, 1)$, such that $i_{+\infty} > c^2/4 - 1$, the point $(a, b, i) = (0, 0, i_{+\infty})$ is Lyapunov stable under Dynamics (A.7). In a neighborhood of the fixed point, $(a, b) \to (0, 0)$ exponentially fast.*

Proof. By choices of c and $i_{+\infty}$, both non-zero eigenvalues (A.25) of the Jacobian are real-valued and negative and it holds that $\lambda_+ \neq \lambda_-$. As before, denote by u, v, w the coordinates in the system of eigenvectors e_0, e_+, e_- of the Jacobian at the fixed point, see Lemma A.44. By Theorem A.45, the dynamics of the system in a neighborhood around the fixed point are equivalent to

$$\begin{aligned} u' &= 0, \\ v' &= \lambda_+ v, \\ w' &= \lambda_- w. \end{aligned} \tag{A.29}$$

Take some small enough initial data $(\epsilon_u, \epsilon_v, \epsilon_w)$: in view of Eq. (A.29), ϵ_u does not vanish, but also does not propagate, whereas v and w converge to zero exponentially fast. Since a and b are represented in terms of v and w, see (A.104), they vanish exponentially fast. □

Proposition A.7. *Let $c > 0$ and $i_{+\infty} < i_c$. There is no non-negative and non-constant traveling wave that converges to $(a, b, i) = (0, 0, i_{+\infty})$ as $x \to +\infty$.*

Proof. As in the previous Theorem, the asymptotic behavior of Eq. (A.7) around the limiting fixed point $(a, b, i) = (0, 0, i_{+\infty})$ is described by the linear System (A.29). But now, since $i_{+\infty} < i_c = \max\{0, 1 - c^2/4\}$, either $i_{+\infty} < 0$ or both eigenvalues $\lambda_\pm$ have a non-vanishing imaginary part and thus, v and w spiral. Since a and b are represented in terms of v and w, see (A.104), any trajectory that converges to $(0, 0, i_{+\infty})$ can not stay non-negative in its a-component. □

A.5 Attractor of a sub-system

A.5.1 Construction and result

We begin our search for a non-negative attractor of $S_{+\infty}$ in an easier setting: we fix $i(x) = i = const.$ and investigate the two-dimensional sub-system in the remaining coordinates. To separate it from the full system, we write it as $\bar{a}(x), \bar{b}(x)$. For this system, we prove the existence of a suitable attractor. This set will be denoted as $T_c(i)$, to emphasize that it depends on the chosen value of i, which will be constant only in this section. The flow of the sub-system and the region $T_c(i)$ are drawn in Figure A.5.

Definition A.8 (Two-dimensional sub-system)**.** For $c > 0$ and $i \in [i_c, 1)$, denote by $\bar{a}(x), \bar{b}(x)$ the two-dimensional flow defined by

$$\begin{aligned} \bar{a}' &= \bar{b}, \\ \bar{b}' &= \bar{a}(\bar{a} + i - 1) - c\bar{b}, \end{aligned} \tag{A.30}$$

which results from the Wave System (A.7) by fixing $i(z) = i$.

There are only two fixed points of (A.30), $(\bar{a}, \bar{b}) = (0, 0)$ and $(\bar{a}, \bar{b}) = (1 - i, 0)$. We denote the eigenvalues and eigenvectors of the Jacobian at $(0, 0)$ as

$$\lambda_\pm(i) := -\frac{c}{2} \pm \sqrt{\frac{c^2}{4} + i - 1}, \qquad l_\pm(i) := \begin{pmatrix} \lambda_\mp \\ 1 - i \end{pmatrix}. \tag{A.31}$$

It holds that $\lambda_-(i) \leq \lambda_+(i) < 0$, we see that $(0, 0)$ is a stable fixed point. Moreover, for $i > i_c$, it holds that $\lambda_-(i) \neq \lambda_+(i)$. Note that $\lambda_\pm$ are identical to the non-zero eigenvalues of the full system around the fixed point $(0, 0, i)$, see (A.25). The eigenvectors $l_\pm$ are the projections of the corresponding three-dimensional eigenvectors into the (a, b)-plane.

The Jacobian at $(1 - i, 0)$ has eigenvalues and eigenvectors

$$\beta_\pm(i) := -\frac{c}{2} \pm \sqrt{\frac{c^2}{4} + 1 - i}, \qquad r_\pm(i) := \begin{pmatrix} -\beta_\mp \\ 1 - i \end{pmatrix}, \tag{A.32}$$

and it holds that $\beta_-(i) < 0 < \beta_+(i)$. These have no direct correspondence to the three-dimensional system.

We now define the region $T_c(i)$. It is a triangle, spanned by the two fixed points $(0, 0)$ and $(1 - i, 0)$ and two adjacent eigenvectors:

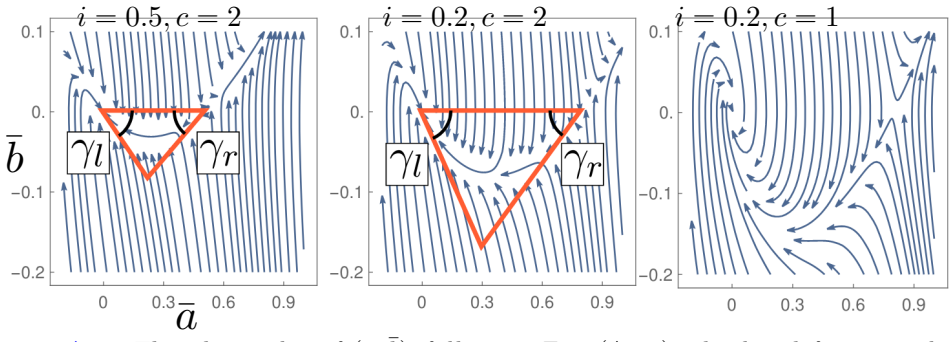

Figure A.5: The phase plot of $(\bar{a}, \bar{b})$ following Eq. (A.30), displayed for several values of i and c. The only two fixed points are $(0, 0)$ and $(1 - i, 0)$. For $i \geq i_c$, the orange triangles $T_c(i)$ are invariant regions of Dynamics (A.30), see Prop. A.10. They increase in $-i$: the point $(1 - i, 0)$ moves to the right and the two internal angles $\gamma_l(i)$ and $\gamma_r(i)$ increase. In the third case, $i < i_c$ implies that the system spirals around $(0, 0)$ while converging.

Definition A.9 (The triangle $T_c(i)$)**.** For $c > 0$ and $i \in [i_c, 1)$, let $T_c(i)$ be the convex hull of the three points $(0, 0), (1 - i, 0)$ and $C(i)$. Here, the point $C(i)$ is the unique intersection of the two half-lines

$$\left\{ \begin{pmatrix} 0 \\ 0 \end{pmatrix} - p \cdot l_+(i) \,\middle|\, p \geq 0 \right\} \quad \text{and} \quad \left\{ \begin{pmatrix} 1 - i \\ 0 \end{pmatrix} - q \cdot r_+(i) \,\middle|\, q \geq 0 \right\}, \tag{A.33}$$

with $l_+(i)$ and $r_+(i)$ defined in (A.31) and (A.32). We denote the internal angles of $T_c(i)$ at $(0, 0)$ and $(1 - i, 0)$ as $\gamma_l(i)$ and $\gamma_r(i)$, respectively.

Visually, it can easily be seen in Figure A.5 that the set $T_c(i)$ is invariant under Dynamics (A.30): the flow at the boundary of $T_c(i)$ points inwards.

Proposition A.10 (Invariant region of the reduced system)**.** *The set $T_c(i)$ is an invariant region of Dynamics* (A.30)*. If $(\bar{a}_0, \bar{b}_0) \in T_c(i)$, then*

$$\bar{a}(x), \bar{b}(x) \in T_c(i) \qquad \forall x \geq 0. \tag{A.34}$$

It holds that $\bar{a} \geq 0$ and $\bar{b} \leq 0$ within $T_c(i)$. Hence, if $(\bar{a}_0, \bar{b}_0) \neq (1-i, 0)$, then $\bar{a}(z)$ converges to 0 monotonically as $z \to +\infty$.

For any non-negative solution of the full Wave System (A.7), it holds that $i' \leq 0$. Thus, we are interested in how $T_c(i)$ changes when i decreases:

Proposition A.11 (Nested invariant regions)**.** *For a fixed $c > 0$, the set $T_c(i)$ is increasing in $-i, i \in [i_c, 1)$. Thus, $T_c(i) \subseteq T_c(i_c)$ for all $i \in [i_c, 1)$.*

This proposition holds due to an easy geometric argument, again take a look at Figure A.5: when i decreases, the point $(1-i, 0)$ moves to the right and the two internal angles $\gamma_l(i)$ and $\gamma_r(i)$ increase. The computations for both propositions are performed in the following Section A.5.2. The reader might skip those and proceed with Section A.6, where we investigate the full system.

A.5.2 Invariance and monotonicity of $T_c(i)$

We analyze the $(\bar{a}, \bar{b})$-system and the set $T_c(i)$ in detail. We prove that the Flow (A.30) at the boundary of $T_c(i)$ points inwards, and that the sets $T_c(i)$ are increasing in $-i$. We formalize what is sketched Figure A.5, and begin by examining the eigenvector $l_+(i)$ at the fixed point $(\bar{a}, \bar{b}) = (0, 0)$:

Lemma A.12. *Let $1 > i > i_c$, and let $l_+(i) = (\lambda_-(i), 1-i)$ be defined as in* (A.31)*. The quotient of the absolute values of the $\bar{b}$-component and $\bar{a}$-component of $l_+(i)$ is increasing in $-i$.*

Proof. The claim is equivalent to

$$\frac{d}{di} \frac{|\lambda_-(i)|}{1-i} > 0. \tag{A.35}$$

Recall that $\alpha_-(i) = -c/2 - \sqrt{c^2/4 + i - 1} < 0$. A computation reveals that

$$\begin{aligned} \frac{d}{di} \frac{|\lambda_-(i)|}{1-i} &= -\frac{d}{di} \frac{\lambda_-(i)}{1-i} \\ &= \frac{\frac{1-i}{2\sqrt{c^2/4+i-1}} + \frac{c}{2} + \sqrt{c^2/4+i-1}}{(1-i)^2} \\ &= \frac{1-i+c\sqrt{c^2/4+i-1} + 2(\frac{c^2}{4}+i-1)}{2(1-i)^2\sqrt{c^2/4+i-1}} > 0, \end{aligned} \tag{A.36}$$

the last inequality holds since $i_c < i$ implies $i > 1 - c^2/4$. □

Now, since $\gamma_l(i)$ is the angle between the two vectors $(1,0)$ and $-l_+(i)$, the previous Lemma directly implies

Corollary A.13. *Let $c > 0$ and $i_c \leq i_1 < i_2 < 1$. It holds that $\gamma_l(i_1) > \gamma_l(i_2)$, the angle $\gamma_l(i)$ is increasing in $-i$.*

For the invariance of $T_c(i)$, we need

Lemma A.14. *For any $p > 0$, the Flow (A.30) at the point $(\bar{a}, \bar{b}) = -p \cdot l_+(i)$ points inwards $T_c(i)$.*

Proof. Let $L_{inw} := \big(1-i, -\lambda_-(i)\big)$ be orthogonal to $l_+(i)$ and point inwards $T_c(i)$. The claim of the Lemma is now equivalent to

$$\left\langle \begin{pmatrix} \bar{a}' \\ \bar{b}' \end{pmatrix}, L_{inw} \right\rangle > 0. \tag{A.37}$$

Let $(\bar{a}, \bar{b}) = -p \cdot l_+(i)$. First compute the Flow (A.30):

$$\begin{aligned} \begin{pmatrix} \bar{a}' \\ \bar{b}' \end{pmatrix} &= \begin{pmatrix} -p(1-i) \\ -p\lambda_-(-p\lambda_- + i - 1) - c\big(-p(1-i)\big) \end{pmatrix} \\ &= p \begin{pmatrix} -(1-i) \\ p\lambda_-^2 + (1-i)(\lambda_- + c) \end{pmatrix}. \end{aligned} \tag{A.38}$$

Its part in direction L_{inw} is given by

$$\begin{aligned} \left\langle \begin{pmatrix} \bar{a}' \\ \bar{b}' \end{pmatrix}, L_{inw} \right\rangle &= -p\Big[(1-i)\big(1-i+\lambda_-(\lambda_- + c)\big) + p\lambda_-^3\Big] \\ &= -p\Big[(1-i)\big(1-i+i-1\big) + p\lambda_-^3\Big] = -p^2\lambda_-^3 > 0. \end{aligned} \tag{A.39}$$

□

For the fixed point $(\bar{a}, \bar{b}) = (1-i, 0)$, we get similar results concerning its unstable eigenvector $r_+(i)$:

Lemma A.15. *Let $1 > i > i_c$, and let $r_+(i) = (-\beta_-(i), 1-i)$ be defined as in (A.32). The quotient of the absolute values of the $\bar{b}$-component and $\bar{a}$-component of $r_+(i)$ is increasing in $-i$:*

$$\frac{d}{di} \frac{1-i}{|\beta_-(i)|} < 0. \tag{A.40}$$

Proof. Recall that $\beta_-(i) = -c/2 - \sqrt{c^2/4 + 1 - i}$. A computation reveals that

$$\frac{d}{di} \frac{1-i}{|\beta_-(i)|} = -\frac{d}{di} \frac{1-i}{\beta_-(i)} = -\frac{-\beta_- + \frac{1-i}{2\sqrt{c^2/4+1-i}}}{\beta_-^2} < 0 \tag{A.41}$$

□

Now, since $\gamma_r(i)$ is the angle between the two vectors $(-1,0)$ and $-r_+(i)$, the previous Lemma implies

Corollary A.16. *Let $c > 0$ and $i_c \leq i_1 < i_2 < 1$. It holds that $\gamma_r(i_1) > \gamma_r(i_2)$, the angle $\gamma_l(i)$ is increasing in $-i$.*

For the invariance of $T_c(i)$, we need

Lemma A.17. *For any $p > 0$, the Flow (A.30) at the point $(\bar{a}, \bar{b}) = (1 - i, 0) - p \cdot r_+(i)$ points inwards $T_c(i)$.*

Proof. Let $R_{inw} := \big(i-1, -\beta_-(i)\big)$ be orthogonal to $r_+(i)$ and point inwards $T_c(i)$. The claim of the Lemma is now equivalent to

$$\left\langle \begin{pmatrix} \bar{a}' \\ \bar{b}' \end{pmatrix}, R_{inw} \right\rangle > 0. \tag{A.42}$$

Let $p > 0$. We compute the Flow (A.30) at

$$\begin{aligned} \begin{pmatrix} \bar{a} \\ \bar{b} \end{pmatrix} &= \begin{pmatrix} 1 - 0 \\ 0 \end{pmatrix} - p \cdot r_+(i) = \begin{pmatrix} 1 - i + p\beta_- \\ p(i-1) \end{pmatrix} : \\ \begin{pmatrix} \bar{a}' \\ \bar{b}' \end{pmatrix} &= \begin{pmatrix} p(i-1) \\ (1 - i + p\beta_-)(1 - i + p\beta_- + i - 1) - cp(i-1) \end{pmatrix} \\ &= p \begin{pmatrix} i - 1 \\ \beta_-(1 - i + p\beta_-) - c(i-1) \end{pmatrix}. \end{aligned} \tag{A.43}$$

Its part in direction R_{inw} is given by

$$\left\langle \begin{pmatrix} \bar{a}' \\ \bar{b}' \end{pmatrix}, R_{inw} \right\rangle = p\Big[(i-1)^2 - \beta_-\big[\beta_-(1-i) + p\beta_-^2 - c(i-1)\big]\Big]. \tag{A.44}$$

Since $\beta_- < 0$, it follows that $-p^2\beta_-^3 > 0$. Since $p > 0$, the proof is complete if we can show that

$$(1-i)^2 - \beta_-\big[\beta_-(1-i) + c(1-i)\big] \geq 0. \tag{A.45}$$

After dividing by $(1 - i) > 0$ and rearranging, this is equivalent to

$$1 - i - c\beta_- \geq \beta_-^2. \tag{A.46}$$

This is in fact an equality, since $\beta_-(i) = -c/2 + \sqrt{c^2/4 + 1 - i}$. □

Considering the invariance of $T_c(i)$, we conclude the

Proof of Proposition A.10. We need to show that the Flow (A.30) at the boundary of $T_c(i)$ points inwards. The Lemmas A.14 and A.17 treat the left and right edge of $T_c(i)$, see again Figure A.5. For the third edge, we consider points of type $(\bar{a}, 0)$, where $0 < \bar{a} < 1 - i$. The derivative at $(\bar{a}, 0)$ is given by $\big(0, \bar{a} \cdot (\bar{a} + i - 1)\big)$. Its $\bar{b}$-component is negative, hence it points inwards $T_c(i)$. The only points on the boundary of $T_c(i)$ where the flow does not point strictly inwards are the two fixed points $(0, 0)$ and $(1 - i, 0)$. □

Considering the monotonicity of $T_c(i)$, we conclude the

Proof of Proposition A.11. Let $c > 0$. The point $(0, 1-i)$ moves to the right as i decreases. Further, we have shown that the two internal angles $\gamma_l(i), \gamma_r(i)$ increase in $-i$, and so does $T_c(i)$. □

A.6 Attractor of the full system

We now analyze solutions of the full Wave System (A.7) under initial condition $(a, b, i) = (a_0, 0, i_0)$, such that $(a_0, 0) \in T_c(i_0)$ as defined in the previous Section. In Section A.6.1, we apply the results about the two-dimensional subsystem to the full system. Theorem A.18 states that as long as $i(x) \geq i_c$, the (a, b)-components of the full system stay within the triangle $T_c(i_c)$. Thus, it suffices to control $i(x) \geq i_c$, which we do in two steps.

In Section A.6.2, we prove via some rough bounds that $i(x) \geq i_c$ for sufficiently small initial values $0 \leq a_0 \ll 1$. This result is refined in Section A.6.3: the Lyapunov-stability of the limiting point at $x = +\infty$ implies that the entire trajectory including its limit is continuous in initial data. Carefully increasing a_0, we increase the known attractor of the stable set $S_{+\infty}$, resulting in Theorem A.27. This procedure is sketched in Figure A.6.

Assumption: If not explicitly stated otherwise, we will use the following setup over the entire Section A.6: For $c > 0$, let $i_0 \in [i_c, 1)$ and $a_0 \in [0, 1-i_0]$, which implies that $(a_0, 0) \in T_c(i_0)$. Let $a(x), b(x), i(x)|_{z\geq 0}$ be the solution of the Wave Eq. (A.7) under initial values $(a_0, 0, i_0)$.

A.6.1 Invariant region of the full system

Theorem A.18 (Invariant region of the full system)**.** *Assume that $i(x) \geq i_c$ for all $x \in [0, \infty)$. We then can control the two remaining coordinates $a(z), b(z)$ of the wave. It holds that*

$$a(x), b(x) \in T_c(i_c) \qquad \forall x \in [0, \infty). \tag{A.47}$$

Within $T_c(i_c)$, $a \geq 0$ and $b \leq 0$. Notice that while $a, i \geq 0$, it holds that $ci' = -a(a + i + r) \leq 0$. This directly implies the following

Corollary A.19. *Under the assumption that $i(x) \geq i_c$ for all $x \in [0, \infty)$, the trajectory stays non-negative and converges as $x \to +\infty$:*

$$\begin{aligned} a(x) &\to 0, \\ b(x) &\to 0, \\ i(x) &\to i_{+\infty} \in [i_c, 1). \end{aligned} \tag{A.48}$$

Proof of Theorem A.18. In the full System (A.7) with coordinates (a, b, i), neither b nor b' depend on i', but only on a and i. Thus, we can easily compare the full system to the two-dimensional System (A.30) in coordinates $\bar{a}, \bar{b}$. At a phase-time x, the two vector fields (a', b') and $(\bar{a}', \bar{b}')$ for fixed value $i = i(x)$ are equal, compare (A.7) and (A.30).

By Proposition A.11, this implies that (a', b') points strictly inwards $T_c\big(i(x)\big)$. There are two irrelevant exceptions: for $(a, b) = (0, 0)$, the system has already reached its limiting state. The point $(a, b) = (1 - i_0, 0)$ is a fixed point of the reduced, but not of the full system. In this case, since $b = 0, b' = a(a + i - 1) = 0, b'' = ai' < 0$ and $ci' < 0$, a Taylor-expansion reveals that for small times $\epsilon > 0$: $i(\epsilon)$ changes much faster than $a(\epsilon)$ and $a(\epsilon) \in T_c\big(i(\epsilon)\big)$.

Importantly, the set $T_c\big(i(x)\big)$ is not decreasing as a function of x. Hence, at each phase-time $x \geq 0$, the two components $a(x), b(x)$ can not escape $T_c\big(i(x)\big)$. In fact, since $i' \leq 0$ and $T_c(i)$ is increasing in $-i$, the set $T_c\big(i(x)\big)$ is increasing in x, at most up to $T_c(i_c)$. Thus, $a(x), b(x)$ remain within $T_c(i_c)$ for all $x \geq 0$. □

With a similar argument, we can determine the rate of convergence:

Proposition A.20. *Assume that $i(z) \geq i_c$ for all $z \in [0, \infty)$, such that $(a, b, i) \to (0, 0, i_{+\infty})$ as $z \to +\infty$ for some $i_{+\infty} \in [i_c, 1)$. If $i_{+\infty} > c^2/4 - 1$, then convergence is exponentially fast with rate*

$$\mu_{+\infty} = -\frac{c}{2} + \sqrt{\frac{c^2}{4} + i_{+\infty} - 1} < 0. \tag{A.49}$$

Further, if $i_{+\infty} = c^2/4 - 1$, which can only happen if $i_{+\infty} = i_c$, then the system converges sub-exponentially fast. As $z \to +\infty$, the distance to the limit is of order $z \cdot e^{-\frac{c}{2}z}$.

Proof. In the case $i_{+\infty} \in (i_c, 1)$, all eigenvalues of the limit are simple, we refer to Section A.4. The system converges exponentially fast, as shown in Theorem A.6. It remains to determine the rate of convergence. The two candidates are $\lambda_\pm = -\frac{c}{2} \pm \sqrt{\frac{c^2}{4} + i_{+\infty} - 1}$. Corresponding to $\lambda_\pm$, the projections of the eigenvectors into the (a, b)-plane are given by

$$l_\pm := \begin{pmatrix} \lambda_\mp \\ 1 - i_{+\infty} \end{pmatrix}. \tag{A.50}$$

We know that $a(z), b(z) \in T_c(i_{+\infty})$ for all $z \geq 0$. At $(0, 0)$, the triangle $T_c(i_{+\infty})$ is bounded by the line $-l_+$, see Definition A.9 and Figure A.5. Since $0 > \lambda_+ > \lambda_-$, the direction of l_- is steeper than that of l_+, such that the line $\{q \cdot l_- \,|\, q \in \mathbb{R}\}$ lies outside $T_c(i_{+\infty})$ for all $q \neq 0$. Thus, the two components $a(z), b(z)$ cannot converge towards $(0, 0)$ along $-l_-$. But

since they converge exponentially fast, the only possible remaining rate of convergence is λ_+.

We do not have a complete description of the asymptotics around the fixed point for the degenerate case $\lambda_+ = \lambda_- = -c/2$. However, under the assumption that the system stays non-negative and converges, the relation $(a,b,i)' = -\frac{c}{2} \cdot (a,b,i) + o(|(a,b,i)|^2)$ holds asymptotically. This will be proven in Theorem A.27 (which does not rely on the type of convergence). The eigenvalue $-c/2$ has algebraic multiplicity 2, but geometric multiplicity 1. It is well-known that this results in sub-exponential convergence, cf. Chapter 9 in [20]. □

A.6.2 A small attractor

In view of the previous paragraph, convergence and non-negativeness follow if we can show that $i(z) \geq i_c$ for all $z \geq 0$. If we choose a_0 small enough, some rough bounds do the trick. We control the total mass of active particles via

Lemma A.21. *Fix $c > 0$, $i_0 \in (i_c, 1)$ and let $a_0 \in [0, (1-i_0)/2]$. Under the assumption that $i(s) \geq i_c$ is true for all $s \in [0,x]$, there exists a finite constant $L(c, i_0) \geq 0$, such that the following bound holds for all $s \in [0,x]$:*

$$\int_0^s a(t)\,dt \leq \frac{ca_0 - b(x)}{1-(i_0+a_0)} \leq L \cdot a_0. \tag{A.51}$$

Proof. With the help of Theorem A.18, we can use that $a(s), b(s) \in T_c(i_c)$ for all $s \in [0,x]$. We integrate $a(s) \cdot \big[1 - i(s)\big] = a^2(s) - b'(s) - cb(s)$ and use that $b(0) = 0$:

$$\int_0^x a(s) \cdot \big[1-i(s)\big]\,ds = ca_0 - ca(x) - b(x) + \int_0^x a^2(s)\,ds. \tag{A.52}$$

By monotonicity: $1 - i_0 \leq 1 - i(s)$ and $0 \leq a(s) \leq a_0$. It follows that

$$\begin{aligned}(1-i_0-a_0)\int_0^x a(s)\,ds &\leq ca_0 - ca(z) - b(z) \\ &\leq ca_0 - b(z), \\ \Leftrightarrow \int_0^x a(s)\,ds &\leq \frac{ca_0 - b(x)}{1-(i_0+a_0)},\end{aligned} \tag{A.53}$$

where we need $a_0 + i_0 < 1$ to avoid a blow-up, which is true by our choice of a_0. It remains to bound $-b(x)$. Take a look at the flow in the (a,b)-plane in Figure A.5. It holds that $a(x), b(x)$ stay within $T_c(i_c)$. Within the triangle $T_c(i_c)$, it holds for the left inner angle $\gamma_l(i_c)$ that

$$\tan\big(\gamma_l(i_c)\big) \geq \frac{|b|}{|a|}. \tag{A.54}$$

Thus, also $-b(x) \leq \tan\big(\gamma_l(i_c)\big) \cdot a(z) \leq L_1 \cdot a_0$. □

Since we can bound the total mass of active particles, we can also bound the change of $i(z)$:

Proposition A.22 (Small attractor of $S_{+\infty}$)**.** *Fix $c > 0$ and $i_0 \in (i_c, 1)$. There exists a constant $M(c, i_0, r)$, $0 < M \ll 1$, such that for all $0 \leq a_0 \leq M$:*

$$i(x) \geq i_c \qquad \forall x \geq 0. \tag{A.55}$$

Hence, also $a(x), b(x) \in T_c(i_c)$ for all $z \geq 0$. The trajectory is non-negative and converges to $S_{+\infty}$ as $x \to +\infty$.

Proof. As long as $i(x) \geq i_c$, it must be that $a(x), b(x) \in T_c(i_c)$ by Theorem A.18. Assume there exists finite phase-time $\tau := \inf_{z \geq 0}\{i(z) < i_c\}$:

$$\begin{aligned} i(\tau) = i_0 + \int_0^\tau i'(z)\,dz \quad &= i_0 - \frac{1}{c}\int_0^\tau a(s)\big[a(s) + i(s) + r\big]\,ds \\ &\geq i_0 - \frac{1}{c}\int_0^\tau a(s)\big[1 + r\big]\,ds, \end{aligned} \tag{A.56}$$

where we used $a(s) + i(s) \leq 1$. For $z \leq \tau$ and a_0 sufficiently small, we can apply Lemma A.21. This implies that there is a finite constant L, which does not depend on a_0, such that

$$i(\tau) \geq i_0 - \frac{L}{c}(1 + r) \cdot a_0. \tag{A.57}$$

The right-hand side is strictly larger than i_c for sufficiently small a_0, say $a_0 \leq M$, and the bound is independent of the phase-time. Thus, there is no such τ for $a_0 \leq M$. □

A.6.3 Extending the attractor

The previous section ended with a condition of type $a_0 \ll 1$, under which the system stays non-negative and converges. However, given a_0 and i_0 and under the assumption that the system converges, we can explicitly calculate its limit $i_{+\infty}$. Then, for fixed i_0, we continuously deform the trajectory while increasing a_0 up to some upper bound $a^*(i_0)$, as sketched in Figure A.6. This results in Theorem A.27.

We apply Proposition A.3 to interrelate the limit $(0, 0, i_{+\infty})$ of the trajectory to its initial data $(a_0, 0, i_0)$:

Lemma A.23. *If $i(z) \geq i_c$, such that the system stays non-negative and converges to $(0, 0, i_{+\infty})$ as $x \to +\infty$, then $i_{+\infty}$ can be written as a function of a_0 and i_0:*

$$i_{+\infty}(a_0, i_0) = 1 - \sqrt{(i_0 + a_0 - 1)^2 + \frac{1 + r}{c^2}(a_0^2 + 2c^2 a_0)}. \tag{A.58}$$

The function $i_{+\infty}(a_0, i_0)$ is decreasing in a_0, for $a_0 \in [0, 1 - i_0]$.

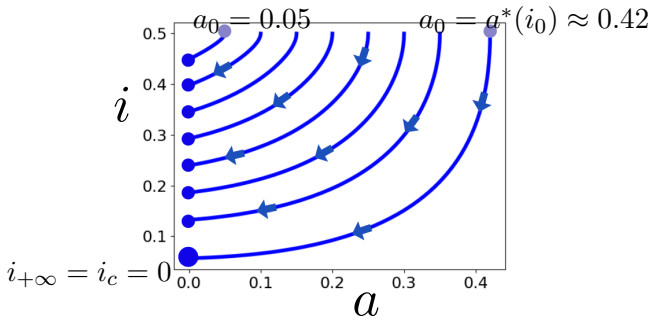

Figure A.6: Trajectories of $a(x), i(x)$ of the Wave System (A.7) for $c = 2, r = 0$. Initial values are $b(0) = 0, i_0 = 0.5$, and a_0 such that $a_0 \in [0, a^*(i_0) \approx 0.42]$. The upper bound a^* is given in Definition A.25. Trajectories with such initial data converge and stay non-negative, since $i(z) \geq i_c$.

Proof. We apply Proposition A.3, and solve the resulting system for $i_{+\infty}$. In the present case, since $a_0 \neq 0$, this results in a quadratic equation with two possible solutions. Since $i(x)$ is decreasing, it must be that $i_{+\infty} < 1$, which uniquely determines (A.58). A short computations proves that $\frac{\partial}{\partial a_0} i_{+\infty}(a_0, i_0) \leq 0$. □

We look for values of a_0 that ensure $i_{+\infty} \geq i_c$. Thus, we rearrange (A.58) for a_0, set $i_{+\infty} = i_c$, and choose the only possible positive solution of the resulting quadratic equation:

Lemma A.24. *Given i_0 and under the assumption that $i_{+\infty} = i_c$, the value of a_0 is uniquely determined by*

$$\alpha(i_0) := \frac{c^2}{1 + c^2 + r} \Bigg\{ -(i_0 + r) + \sqrt{(i_0 + r)^2 + \frac{c^2 + 1 + r}{c^2}\Big((1 - i_c)^2 - (1 - i_0)^2\Big)} \Bigg\}. \tag{A.59}$$

Equation (A.59) can be restated as $i_{+\infty}\big(\alpha(i_0), i_0\big) = i_c$, but keep in mind that still have to prove convergence. It can easily be seen that $\alpha(i_c) = 0$. Since we require that $a_0 \in [0, 1 - i_0]$, such that $a_0 \in T_c(i_0)$, this leads to our

Definition A.25 (Upper bound for a_0)**.** For fixed $c > 0$ and, we define

$$a^*(i_0) := \min\Big\{\alpha(i_0), 1 - i_0\Big\}, \quad \text{for } i_0 \in [i_c, 1). \tag{A.60}$$

This will hold as sharp upper bound for a_0, such that the trajectory stays non-negative and converges. Before we state the corresponding theorem, we perform a last check that we are in the correct setup:

Lemma A.26. *Let $i_0 \in [i_c, 1)$ and $a_0 \in [0, a^*(i_0)]$. If the system stays non-negative and converges to $(0, 0, i_{+\infty})$, then*

$$i_{+\infty}(a_0, i_0) \in [i_c, i_0], \tag{A.61}$$

where $i_{+\infty}(a_0, i_0)$ is given as in Lemma A.23.

Proof. It holds that $i_{+\infty}(0, i_0) = i_0$. The claim follows since $i_{+\infty}(a_0, i_0)$ is decreasing in a_0 and since $a^*(i_0) \leq \alpha(i_0)$, where $i_{+\infty}\big(\alpha(i_0), i_0\big) = i_c$. □

After all these preparations, we are now ready to prove that the system converges and stays non-negative. We state

Theorem A.27 (Attractor of $S_{+\infty}$)**.** *For $r \geq 0, c > 0$, let $i_0 \in [i_c, 1)$ and $a_0 \in \big[0, a^*(i_0)\big]$. Let $a(x), b(x), i(x)$ be the solution of Eq. (A.7) with initial data $(a_0, 0, i_0)$.*

It holds that $a(x), i(x) \geq 0$ and $i'(x), b(x) \leq 0$ for all $x \geq 0$. As $x \to +\infty$, $a(x)$ and $b(x)$ converge to 0, and $i(x)$ converges to

$$i_{+\infty}(a_0, i_0) = 1 - \sqrt{(i_0 + a_0 - 1)^2 + \frac{1+r}{c^2}(a_0^2 + 2c^2 a_0)} \quad \in [i_c, 1). \tag{A.62}$$

The type of convergence depends on $i_{+\infty}$ and is given in Proposition A.20.

Proof. **Notation**: We fix $i_0 \in (i_c, 1)$ and change only a_0. If $i_0 = i_c$, we must choose $a_0 = 0$. For a compact notation, $\Phi_x(x)$ is the state of the system at phase-time x, starting in $x = (a, b, i)$. If the limit of a trajectory exists, we denote

$$\Phi_{+\infty}(a_0, 0, i_0) := \lim_{x \to +\infty} \Phi_x(a_0, 0, i_0) = (0, 0, i_{+\infty}). \tag{A.63}$$

Step 1: starting interval
For a_0 positive but small enough, Proposition A.22 grants that for all $x \geq 0$:

$$i(x) \geq i_c \quad \text{and} \quad a(x), b(x) \in T_c(i_c), \tag{A.64}$$

where $T_c(i_c)$ is a bounded invariant region that contains only points such that $a \geq 0, b \leq 0$. Thus, $a(x), i(x) \to (0, i_{+\infty})$ monotone. With the help of Lemma A.23, we can explicitly calculate $i_{+\infty}$ as stated in Eq. A.62, and our claim holds on some small non-empty interval $a_0 \in [0, a_u)$.

Step 2: neighborhood of existing trajectories
Pick some $a_0 < a^*(i_0)$ for which the statement is already proven. By choice of a_0, it holds that $i_{+\infty} > i_c$. Thus, the limit $\Phi_{+\infty}(a_0, 0, i_0)$ is Lyapunov stable by our previous analysis of the asymptotics, see Theorem A.6: for every $\epsilon_\infty > 0$, there exists a $\delta_\infty > 0$, such that

$$||x - \Phi_{+\infty}(a_0, 0, i_0)|| < \delta_\infty \;\Rightarrow\; ||\Phi_x(x) - \Phi_{+\infty}(a_0, 0, i_0)|| < \epsilon_\infty \tag{A.65}$$

for all $x \in [0, \infty)$. Choose $\epsilon_\infty \leq i_{+\infty}(a_0, i_0) - i_c$ and assure that $0 < \delta_\infty \leq \epsilon_\infty$. This grants $i(x) \geq i_c$ after entering the δ_∞-neighborhood. Within this attractor, also $a(x) \geq 0$ in view of Theorem A.18, since $i(x) \geq i_c$.

Starting in $(a_0, 0, i_0)$, we follow the trajectory up to some finite time τ, where it has entered the δ_∞-neighborhood:

$$||\Phi_\tau(a_0, 0, i_0) - \Phi_{+\infty}(a_0, 0, i_0)|| \leq \frac{\delta_\infty}{2}. \tag{A.66}$$

The derivative of the system is locally Lipschitz and all trajectories are within a bounded domain. Thus, the trajectories $\Phi_x(x_0)$ are uniformly continuous in initial data x_0 on any finite time interval $[0, T]$, with respect to the maximum norm $||.||_{[0,T]}$. This is a classic result and can easily be proven via a Grönwall's inequality, we refer to Chapter 2 of the textbook of Hsieh and Yasutaka [79]. There exists some $\delta_0 > 0$, s.t. for all $x \in \mathbb{R}^3$ with $||x - (a_0, 0, i_0)|| < \delta_0$:

$$||\Phi_x(x) - \Phi_x(a_0, 0, i_0)||_{[0,\tau]} < \frac{\delta_\infty}{2}. \tag{A.67}$$

This implies for all such trajectories Φ_x:

$$1)\ ||\Phi_\tau(x) - \Phi_{+\infty}(a_0, 0, i_0)|| < \delta_\infty, \text{ and} \tag{A.68}$$

$$2)\ i(x) \geq i_c \qquad \forall x \in [0, \tau]. \tag{A.69}$$

In particular, $\Phi_\tau(x)$ lies within the δ_∞-neighborhood, so ultimately

$$3)\ i(x) \geq i_c \qquad \forall x \geq 0. \tag{A.70}$$

Again, Theorem A.18 implies $a(x), i(x) \in T_c(i_c)$ for all $x \geq 0$. As before, the system is integrable and converges as $x \to +\infty$, so we can explicitly calculate $i_{+\infty}(a_0, i_0)$. Thus, our claim holds for all starting points a small open neighborhood of $(a_0, 0, i_0)$.

Step 3: limits of trajectories

Assume that the claim holds for all $a_0 \in [0, a_u)$. For all trajectories starting in $(a_0, 0, i_0)$, where $a_0 \in [0, a_u)$, it holds that $i(x)$ is monotone and bounded from below by i_c, such that $a(x), b(x)$ stay within $T_c(i_c)$. Fix any finite time-horizon $[0, T]$. As mentioned before, the trajectories $\Phi_x(a_0, 0, i_0)$ are uniformly continuous in initial data on finite time-intervals, and thus form a Cauchy-sequence on $||.||_{[0,T]}$ as $a_0 \to a_u$. Since T can be chosen arbitrarily large and since the limits $\Phi_{+\infty}(a_0, 0, i_0)$ are also continuous in a_0, our claim holds for the trajectory that starts in a_u.

Step 4: conclusion

By step 1, the claim holds for a_0 in some small interval $[0, a_u)$. By step 3, it then also holds for $a_0 = a_u$. If now $a_u < a^*$, the claim holds for $a_0 \in [0, a_u + \epsilon)$ by step 2 for some $\epsilon > 0$. Iterating these two steps, the claim ultimately holds for all $a_0 \in \big[0, a^*(i_0)\big]$. In particular, we have proven that the trajectories $\Phi_z(a_0, 0, i_0)$ are uniformly continuous with respect to

initial data on $z \in [0, +\infty]$. This continuity allows us to finish the proof of Proposition A.20. In the non-critical cases where $c^2/4 + i_{+\infty} - 1 > 0$, the trajectories converge along a stable manifold with rate of convergence $-c/2 + \sqrt{c^2/4 + i_{+\infty} - 1}$. As $c^2/4 + i_{+\infty} - 1 \to 0$, the critical trajectory must converge along the limit of these manifolds. □

A.7 The complete trajectory

We track the non-negative branch of the unstable manifold of $S_{-\infty}$, see (A.14), and show that it stays positive and enters the attractor of $S_{+\infty}$ from the previous section, cf. Theorem A.27.

Assumption: We will use the following setup over the entire Section A.7: Let $i_{-\infty} > 1$ and let $a(z), b(z), i(z)$ be the unique solution of the ODE-System (A.7) that emerges from $(0, 0, i_{-\infty})$ as $z \to -\infty$ and where $a(x) > 0$ asymptotically as $x \to -\infty$.

For all $i_{-\infty} > 1$, existence and uniqueness of these trajectories have been proven in Section A.4. Moreover, we know their asymptotic behavior:

Lemma A.28. *The following holds as $x \to -\infty$:*

$$a(x) > 0, \qquad b(x) > 0, \qquad (a + i)' < 0. \tag{A.71}$$

Proof. The first two inequalities are given by Theorem A.5, which also yields $b'(x) > 0$ asymptotically. Noticing that $c(a + i)' = -a(1 + r) - b' < 0$ completes the proof. □

A.7.1 The maximum of active particles

For connecting these trajectories with the attractor of $S_{+\infty}$, we will prove

Proposition A.29 (The maximum of active particles)**.** *There exists a finite phase-time z_0, such that $b(z_0) = 0$ for the first time.*

We will prove that the sum $a(z) + i(z)$ decreases below 1. Given this, the term $cb(z) + b'(z) = a(z) \cdot [a(z) + i(z) - 1]$ becomes negative, so b must eventually reach 0.

Lemma A.30. *As long as $b(s) > 0$ for all $s \in (-\infty, z]$, it holds that*

$$b(x) + i'(x) < 0. \tag{A.72}$$

Proof. In view of the asymptotic behavior of the trajectory, described in Lemma A.28, assume that there exists a finite time x^*, such that for the

first time $b(x^*) + i'(x^*) = 0$, but still $b(x^*) > 0$. The wave-equations $0 = b' + cb + a - a(a+i)$ and $0 = ci' + a(a+i) + ra$ imply that

$$\begin{aligned} 0 &= cb(x^*) + ci'(x^*) && \text{(A.73)}\\ &= -a(x^*) \cdot (1+r) - b'(x^*) && \text{(A.74)}\\ &= c \cdot b(x^*) - a(x^*) \cdot \big[a(x^*) + i(x^*) + r\big]. && \text{(A.75)} \end{aligned}$$

Rearranging the third line yields $cb(x^*) = a(x^*) \cdot \big[a(x^*) + i(x^*) + r\big]$. As long as $x < x^*$, it holds that $b(x) + i'(x) < 0$, hence also

$$cb(x) < a(x) \cdot \big[a(x) + i(x) + r\big]. \tag{A.76}$$

However, equality at $x = x^*$ implies that

$$\frac{d}{dx} cb(x)\Big|_{x^*} \geq \frac{d}{dx} a(x) \cdot \big[a(x) + i(x) + r\big]\Big|_{x^*}, \tag{A.77}$$

which we can rewrite, using both (A.74) and (A.75) :

$$\begin{aligned} c \cdot b'(x^*) &\geq b(x^*) \cdot \big[a(x^*) + i(x^*) + r\big] + a(x^*) \cdot \big[b(x^*) + i'(x^*)\big] \\ &= \frac{a(x^*)}{c} \cdot \big[a(x^*) + i(x^*) + r\big]^2 + 0 \geq 0. \end{aligned} \tag{A.78}$$

But $a(x^*) > 0$, so Eq. (A.74) implies that $b'(x^*) = -(1+r)a(x^*) < 0$. This contradicts (A.78). □

Lemma A.31. *As long as $b(s) > 0$ for all $s \in (-\infty, z]$, it can not happen that $a(x) + i(x)$ converges to some finite $L > 0$.*

Proof. By the previous lemma: $(a+i)' < 0$ while $b > 0$. Assume that $a(x) + i(x)$ converges to a finite value $L > 0$ from above, which we denote as $a(x) + i(x) \searrow L$. This implies that also $b + i' \nearrow 0$. By the Wave Equations (A.2), these two expressions are equivalent to

$$\begin{aligned} -a(1+r) - b' &\nearrow 0 \quad \text{and} && \text{(A.79)}\\ cb - a(a+i+r) &\nearrow 0. && \text{(A.80)} \end{aligned}$$

The first convergence indicates that $b' \leq \delta < 0$ after some time x_δ, since a is strictly increasing and hence positive. The second statement is equivalent to $cb - a \cdot (L + r) \nearrow 0$. Thus, also b is increasing. But $b'(x) < 0$ for all $x \geq x_\delta$ and while $b > 0$, a contradiction. □

We can now show that there exists a finite phase-time x_0 such that $b(x_0) = 0$, finishing the

Proof of Proposition A.29. By the previous lemma, $a(x)+i(x)$ decreases below every positive value as long as $b(x) > 0$. In particular, for some $\epsilon > 0$: $a(\tau) + i(\tau) \leq 1 - \epsilon$ after some phase-time τ. Then for all $x \geq \tau$, since $a > 0$:

$$\begin{aligned} cb(x) + b'(x) &= a(x) \cdot \big[a(x) + i(x) - 1\big] \\ &\leq a(x) \cdot (1 - \epsilon - 1) = -a(x)\epsilon < 0. \end{aligned} \tag{A.81}$$

Either $cb(x) < 0$ and the system has already passed a first local maximum of $a(x)$, or we may assume that $b'(x) \leq -a(\tau)\epsilon = -\delta < 0$. If now $b'(x) \leq -\delta$, then $b(x)$ reaches zero after a finite time z_0, which can not be larger than $\tau + \frac{b(\tau)}{\delta}$. □

A.7.2 Reaching the attractor of $S_{+\infty}$

We now prove that $(a_{x_0}, 0, i_{x_0})$ lies in the attractor of the stable set $S_{+\infty}$. Therefore, we show that $a_{x_0} \leq a^*(i_{x_0})$, then Theorem A.27 ensures non-negativity and convergence as $z \to +\infty$. We again use Proposition A.3, now to interrelate $(0, 0, i_{-\infty})$ and $(a_{z_0}, 0, i_{z_0})$:

Lemma A.32. *The following holds at phase-time x_0:*

$$a_{x_0} > 0, \quad a_{x_0} + i_{x_0} \leq 1, \tag{A.82}$$

$$\begin{aligned} a_{x_0} = \frac{c^2}{c^2 + 1 + r} \Bigg\{ &- (i_{x_0} + r) \\ &+ \sqrt{(i_{x_0} + r)^2 + \frac{c^2 + 1 + r}{c^2}\Big((i_{-\infty} - 1)^2 - (1 - i_{x_0})^2\Big)} \Bigg\}. \end{aligned} \tag{A.83}$$

In the case $i_{-\infty} \in (1, 2 - i_c]$, then additionally

$$i_{x_0} \in (i_c, 1), \qquad a_{x_0} \in (0, 1), \tag{A.84}$$

and the trajectory is non-negative on the interval $(-\infty, x_0]$.

Proof. As $x \to -\infty$, all $a(x), b(x), b'(x), i'(x)$ have exponential and hence integrable tails, cf. Theorem A.5. We thus can apply Proposition A.3 on the interval $(-\infty, x_0]$, for finite x_0. This results in Eq. (A.83), we omit the intermediate steps. It holds that $a_{x_0} > 0$ because $b(x) > 0$ for all $x < x_0$.

In particular, $a_{x_0} > 0$ implies that the second summand under the root in (A.83) must be strictly positive, which yields $(i_{-\infty} - 1)^2 > (1 - i_{x_0})^2$. Since $b(x_0) = 0$ for the first time, it must hold that $b'(x_0) \leq 0$. Given this, we use $b'(x_0) + cb(x_0) = a_{x_0}(a_{x_0} + i_{x_0} - 1)$ to bound $0 \geq a_{x_0}(a_{x_0} + i_{x_0} - 1)$. Since $a_{x_0} > 0$, this shows that $i_{x_0} \leq 1 - a_{x_0} < 1$.

If we assume additionally that $i_{-\infty} \in (1, 2 - i_c]$, then $(i_{-\infty} - 1)^2 > (1 - i_{x_0})^2$ implies that $i_{x_0} > 2 - i_{-\infty} \geq i_c$. Up to x_0, $a(z) + i(z)$ is decreasing, which was proven in Lemma A.30. Since $a(z)$ is strictly increasing up to

x_0, $i(z)$ must be strictly decreasing, but not below $i(z_0) > 0$. Hence, the trajectory stays positive. The inequality $a_{z_0} + i_{z_0} \leq 1$ implies that $a_{z_0} < 1$. □

This allows us to connect the unstable manifold of $(0, 0, i_{-\infty})$ with the attractor of $S_{+\infty}$:

Proposition A.33 (Reaching the attractor of $S_{+\infty}$)**.** *Let $i_{-\infty} \in (1, 2 - i_c]$. The non-negative branch of the unstable manifold of $(0, 0, i_{-\infty})$ reaches the point $(a_{x_0}, 0, i_{x_0})$, where $a_{x_0} \in (0, 1)$ and $i_{x_0} \in (i_c, 1)$. It then holds that*

$$0 < a_{x_0} \leq a^*(i_{x_0}), \tag{A.85}$$

for a^* like in Definition A.25. In view of Theorem A.27, the trajectory that starts/continues in such a point $(a_{x_0}, 0, i_{x_0})$ converges to $S_{+\infty}$ and stays non-negative.

Proof. We have just shown that $i_{x_0}, a_{x_0} > 0$ and that $a_{x_0} + i_{x_0} \leq 1$. Recall Definition A.25: $a^*(i_0) = \min\{\alpha(i_0), 1 - i_0\}$, where $\alpha(i_0)$ is given by

$$\begin{aligned}\alpha(i_0) = \frac{c^2}{1 + c^2 + r}\Bigg\{ &- (i_0 + r) \\ &+ \sqrt{(i_0 + r)^2 + \frac{c^2 + 1 + r}{c^2}\Big((1 - i_c)^2 - (1 - i_0)^2\Big)}\Bigg\}.\end{aligned} \tag{A.86}$$

We have already verified that $a_{x_0} \leq 1 - i_{x_0}$, so proving $a_{x_0} \leq \alpha(i_{x_0})$ suffices for proving $a_{x_0} \leq a^*(i_{x_0})$. By (A.83), we know that

$$\begin{aligned}a_{x_0} = \frac{c^2}{c^2 + 1 + r}\Bigg\{ &- (i_{x_0} + r) \\ &+ \sqrt{(i_{x_0} + r)^2 + \frac{c^2 + 1 + r}{c^2}\Big((i_{-\infty} - 1)^2 - (1 - i_{x_0})^2\Big)}\Bigg\}.\end{aligned} \tag{A.87}$$

The two expressions (A.86) and (A.87) are very similar. After some elementary steps, the claim $a_{x_0} \leq \alpha(i_{x_0})$ is equivalent to

$$(i_{-\infty} - 1)^2 \leq (1 - i_c)^2. \tag{A.88}$$

This is equivalent to $i_{-\infty} \leq 2 - i_c$, since $i_{-\infty} > 1$ and $i_c \leq 1$. But that is just how we have chosen $i_{-\infty}$. □

A.8 Concluding the proof of the main result

With the results from the previous sections, we complete the

Proof of Theorem A.1. Consider the ODE System (A.7) in coordinates a, b, i and let $i_{-\infty} \in (1, 2 - i_c]$. The unstable manifold of the fixed point $(a, b, i) = (0, 0, i_{-\infty})$ has dimension one. Its two branches are the only trajectories that leave the fixed point, which is stated in Theorem A.5. There is one branch of the unstable manifold such that $a(x) > 0$ as $x \to -\infty$, we follow this trajectory in positive direction of x. There is a finite phase-time x_0, such that for the first time $b(x_0) = 0$, see Proposition A.29. For all $z < x_0$, it holds that $a(x), b(x), i(x) > 0$. Denote the state of the system at x_0 as $(a_{x_0}, 0, i_{x_0})$. Lemma A.32 states that $i_{x_0} \in (i_c, 1)$, Proposition A.33 states that $a_{x_0} \in (0, a^*(i_{x_0})]$, for a^* as in Definition A.25. By Theorem A.27, we then know that $(a_{x_0}, 0, i_{x_0})$ lies in a non-negative attractor of the set $S_{+\infty}$. Thus, $a(x), b(x), i(x) \to (0, 0, i_{+\infty})$ as $x \to +\infty$, where $i_{+\infty} \in [i_c, 1)$, and ultimately $a(x), i(x) \geq 0$ for all $x \in \mathbb{R}$.

For any non-negative and bounded solution, the identity $i_{-\infty} + i_{+\infty} = 2$ holds by Proposition A.4. For $c > 0$ and $i_{-\infty} \in (1, 2 - i_c]$, the previous paragraph proves existence and uniqueness of the claimed wave. For $i_{-\infty} = 1$, the constant solution can be the only non-negative and bounded one.

We then consider an arbitrary non-constant, bounded and non-negative solution. By monotonicity of $i(z)$, it must converge as $z \to \pm\infty$. If we assume that $i_{-\infty} \in (1, 2 - i_c]$, it is one of the above solutions. If we assume that $i_{-\infty} > 2 - i_c$, then $i_{+\infty} < i_c$. In this case, the trajectory can not stay non-negative as $z \to +\infty$, which is stated by Proposition A.7, contradicting the assumption. □

A.9 Discussion and outlook at stability

A.9.1 FKPP-waves

We have given a description of all bounded and non-negative traveling waves of the Reaction-Diffusion System (A.1). For the most related systems, the FKPP-equation [91, 50], the FitzHugh-Nagumo-equation [51, 112] and combustion equations [15], no such continuum of traveling waves has yet been constructed.

Still, the non-negative traveling waves of System (A.1) are closely related to pulled FKPP-waves with only a single type of particles [50, 91]. The equation for such a wave $w(z)$ reads $0 = cw' + w'' + F(w)$. For the purpose of a simple comparison, we let $F(w) = gw - w^2$, where $g > 0$ is the initial growth rate of the particles. In this case, Theorem A.1 states that the convergence of System (A.1) as $z \to +\infty$ is identical to that of w, if $g = 1 - i_{+\infty}$, see e.g. [148]. In words, the asymptotic growth speed of traveling waves of System (A.1) coincides with that of simple FKPP-waves in presence of a constant

density $i_{+\infty}$ of inhibiting particles. Moreover, Theorem A.1 implies that $i_c = 0$ for all $c \geq 2$. Thus, the minimal speed of an invasive front, where $i_{+\infty} = 0$, is given by $c_{\min} = 2$. Again, this coincides with the minimal wave speed of the associated FKPP-equation, *i.e.* in the absence of inactive particles. It is this critical front which can be interpreted as the most natural one, our simulations indicate that it always arises under compact initial data. If we assume convergence, a technique of Berestycki, Brunet & Derrida [16] yields an upper bound for the speed of the traveling front, just by ignoring the dampening influence of the inactive particles. For compact initial data, the system always chooses the smallest possible wave speed, as suggested.

The emergence of traveling fronts is known for many reaction-diffusion systems. We suggest the literature [24, 156, 114] for more examples with a biological motivation. Rigorous proofs of these phenomena are rare. Often, only the form of the traveling waves is analyzed analytically. The FKPP-equation is one of the cases, where the convergence of the front of the PDE towards a traveling wave solution can be proved. The first rigorous proof was done by Kolmogorov, Petrovski & Piscunov in 1937 [91]. Extensions of this result to more general initial data and a more precise description of the speed of the front have been provided by Uchiyama [148] and M. Bramson [22]. The approach of Kolmogorov et al. and Uchiyama seems to be restricted to systems with only a single type of particles, as it relies on a maximum principle and monotonicity of the front. The approach of Bramson relies on a relationship between the FKPP-equation and branched Brownian motion, which can not be applied in the present case since the inactive particles do not diffuse. A singular perturbation of System (A.1), which again introduces a small diffusion to the inactive particles will be subject to future investigations. Despite the fact that this system would be biologically interesting, since no tissue or population is entirely static, this would also rule out some difficulties when analyzing the stability of the traveling waves against perturbations.

A.9.2 Stability of the traveling waves

We give a brief introduction to the stability of traveling waves against small perturbations, in the spirit of the introduction in [63]. A good overview, where the following concepts are presented in greater depth, has been written by Sandstede [130].

Consider a reaction-diffusion system

$$Y_t = D \cdot Y_{xx} + R(Y), \tag{A.89}$$

where $Y \in \mathbb{R}^n, x \in \mathbb{R}, t \geq 0, D = \operatorname{diag}(d_1, \ldots, d_n)$ with $d_i \geq 0$, and R a smooth reaction. In the moving frame $z = x - ct$, the System reads

$$Y_t = D \cdot Y_{zz} + cY_z + R(Y). \tag{A.90}$$

A traveling wave $w(z)$ with speed c is a constant solution of Eq. (A.90). The wave w is called *nonlinearly stable* in a space $\mathcal{X}$, if any solution of the PDE (A.90) which starts in $Y_0 = w + \tilde{Y}$, where $\tilde{Y} \in \mathcal{X}$ is a sufficiently small perturbation, converges to a shift of w. This type of stability is often encoded in the spectrum of the operator $\mathcal{L}$, that is obtained by linearizing the equation for the perturbation $\tilde{Y}$ in (A.90) around to the constant part w:

$$\tilde{Y}_t = D \cdot \tilde{Y}_{zz} + c\tilde{Y}_z + JR(w) \cdot \tilde{Y} := L\tilde{Y}, \tag{A.91}$$

where JR is the Jacobian of the reaction R. Let $\mathcal{L} : \mathcal{X} \to \mathcal{X}$ be the operator given by $\tilde{Y} \to L\tilde{Y}$. We say that the wave w is *spectrally stable* in $\mathcal{X}$ if the spectrum of $\mathcal{L}$ is contained in the half-plane $\mathfrak{Re}(\gamma) < 0$, except maybe a simple a simple eigenvalue at 0 (that corresponds to the traveling wave itself, if $w' \in \mathcal{X}$). For diffusive systems, where $\det(D) > 0$, a quite general theory has been developed. If $\mathcal{X}$ is appropriately chosen, spectral stability implies nonlinear stability, we refer to the literature [130, 63]. Classical results are e.g. given for subspaces of $\mathcal{X} = H^1$, the L^2-Sobolev space.

As explained in the next paragraphs, we are not aware of any rigorous framework for studying the nonlinear stability of System (A.1). Several technical problems arise, that so far have been treated only separately [63, 89].

Most importantly, the traveling waves of System (A.1) can not be stable against perturbations in the classical sense, since the inactive particles neither react nor diffuse. Any initial deviation remains for all times, as shown in Figure A.1. However, the actual front of the system does converge to a traveling wave. For capturing this idea, we introduce the weighted space $\mathcal{X} = H^1_\alpha$ with norm $||f||_{H^1_\alpha} = ||f \cdot e^{\alpha z}||_{H^1}$ for some $\alpha > 0$. Nonlinear stability in H^α_1 is referred to as *convective stability*. Convergence of the PDE in the moving frame (A.90) in H^1_α means that the front of the system approaches the traveling wave, whereas any initial finite and local deviation is convected towards $z = -\infty$ and vanishes due to the weighting. A first rigorous result regarding convective stability was obtained by Ghazaryan et al. [63]. They could show that in some cases, spectral stability in H^1_α implies convective stability against small perturbations in $H^1_\alpha \cap H^1$. For their approach, the authors require that the weight α can be chosen such that all eigenvalues γ of $\mathcal{L}$ except zero fulfill $\mathfrak{Re}(\gamma) \leq \nu < 0$ and such that the derivative $w' \in H^1_\alpha$ of the traveling wave is an eigenfunction that corresponds to a simple eigenvalue at zero. Unfortunately, this setting is not suited for studying pulled FKPP-fronts: the assumption $w' \in H^1_\alpha$ implies that the continuous spectrum of $\mathcal{L}$ touches the origin, see e.g. Chapter 6 in the work of Sattinger [132].

Another difficulty arises when studying critical pulled fronts (with minimal possible speed) whose tail as $z \to +\infty$ converges sub-exponentially, as in Theorem A.1. In this case, the requirement $w' \in H^1_\alpha$ is only fulfilled for

rather small values of α, which do not suffice for shifting the continuous spectrum of $\mathcal{L}$ to the left half-plane. For diffusive systems, nonlinear stability of this more delicate case was first treated rigorously by Kirchgässner [89], a recent overview is given in [47]. After introducing a small diffusion to the inactive particles, we could apply this theory to the critical front.

For the most natural traveling wave solution, the critical one with speed $c = 2$ and $i_{+\infty} = i_c = 0$, we performed a numerical analysis that strongly indicates that this wave is spectrally stable in H^1_α, when we choose $\alpha = -\mu_{+\infty} = c/2$. The details are presented in Appendix A.10.2. Thus, based on the work of Ghazaryan et al. regarding convective stability [63] and the work of Kirchgässner regarding critical fronts [89], we dare to make an educated guess: we expect that this traveling wave is convectively stable against small perturbations in $H^1_{c/2} \cap H^1$.

Acknowledgment: The author would like to thank Anton Bovier and Muhittin Mungan for their support and the fruitful discussions. He also would like to thank the anonymous referees who provided very useful and detailed comments on a previous version of the manuscript.

Numerical analysis: The spectral analysis was performed numerically via STABLAB [13], which is a MATLAB-library exactly for this purpose. The simulations of the Reaction-Diffusion System (A.1) were performed via Wolfram Mathematica. The code can be accessed upon request.

Funding: This work was partly funded by the Deutsche Forschungsgemeinschaft (DFG, German Research Foundation) under Germany's Excellence Strategy - GZ 2047/1, Projekt-ID 390685813 and by the Deutsche Forschungsgemeinschaft (DFG, German Research Foundation) - Projektnummer 211504053 - SFB 1060.

A.10 Appendices of this publication

A.10.1 Center manifold calculations

A.10.1.1 Review of center manifold theory

Definition A.34 (Normal form)**.** Given a dynamical system $dx/dt = f(x), x \in \mathbb{R}^n$ around its fixed point $0 \in \mathbb{R}^n$, write $x = (y, z)$ where $y \in \mathbb{R}^k, z \in \mathbb{R}^l$ and $k + l = n$, such that $dx/dt = f(x)$ is equivalent to:

$$\begin{aligned} \frac{dy}{dt} &= A \cdot y + g(y, z), \\ \frac{dz}{dt} &= B \cdot z + h(y, z). \end{aligned} \tag{A.92}$$

We require that the eigenvalues of $A \in \mathbb{R}^{k\times k}$ have zero real parts and those of $B \in \mathbb{R}^{l\times l}$ have nonzero real parts. Further, both functions $g : \mathbb{R}^n \to \mathbb{R}^k$ and $h : \mathbb{R}^n \to \mathbb{R}^l$ are smooth and vanish together with their first-order partial

derivatives at the origin. Then, System (A.92) is called the *normal form* of the system.

Proposition A.35. *Let $f : \mathbb{R}^n \to \mathbb{R}^n$ be smooth. Let a dynamical system $dx/dt = f(x), x \in \mathbb{R}^n$ have a fixed point $x_0 \in \mathbb{R}^n$, such that the eigenvectors of the Jacobian $Df(x_0)$ span the entire $\mathbb{R}^n$. The system can be written in normal form as in Definition A.34.*

The proof includes a change of coordinates into the system of eigenvectors of the Jacobian $Df(x_0)$. This will be done explicitly in Section A.10.1.2. For the underlying theory and the more general case, we refer to the monograph of U. Kirchgraber & K.J. Palmer [90].

Definition A.36 (Center manifold)**.** Consider a dynamical system in normal form (A.92). Let $\phi : \mathbb{R}^k \to \mathbb{R}^l$ be a smooth function such that $\phi(0) = 0$ and also its derivative $D\phi(0) = 0$. Assume that the set

$$\mathcal{CM} = \Big\{ y \in \mathbb{R}^k, z \in \mathbb{R}^l : \, z = \phi(y) \Big\} \tag{A.93}$$

is invariant under Dynamics (A.92). The set $\mathcal{CM}$ is called a *center manifold* of the fixed point (due to its vanishing derivative at 0).

We will use a local version of the center manifold, which can be shown to exist in a neighborhood of the fixed point:

Theorem A.37 (Local center manifold, cf. Theorem 4.1. in [90])**.** *Consider a smooth dynamical system in normal-form* (A.92)*, where* $\dim(y) = k \geq 1$*, such that the Jacobian at the fixed point has k eigenvalues with zero real part. Let $c_1 + c_2 = \dim(z)$, where the matrix B has c_1 eigenvalues with positive real part and c_2 eigenvalues with negative real part. Then locally, there exist a unique center manifold of dimension k, a unique unstable manifold of dimension c_1 and a unique stable manifold of dimension c_2.*

The center manifold can be written as $\big\{(y, z) : \, z = \phi(y)\big\}$ *like in* (A.93)*. There exists a homeomorphism defined in an open neighborhood of the origin which takes solutions of $dx/dt = f(x)$ onto solutions of*

$$\begin{aligned} \frac{dy}{dt} &= A \cdot y + g\big(y, \phi(y)\big), \\ \frac{dz}{dt} &= B \cdot z. \end{aligned} \tag{A.94}$$

Definition A.38 (Error of approximation of the center manifold)**.** Consider a smooth dynamical system in normal-form (A.92). For a smooth function $T : \mathbb{R}^k \to \mathbb{R}^l$ define the error of approximation of the normal form by

$$(HT)(y) := DT(y) \cdot \big[Ay + g\big(y, T(y)\big)\big] - B \cdot T(y) - h\big(y, T(y)\big). \tag{A.95}$$

Theorem A.39 (Approximating the center manifold, cf. Theorem 3 in [30]). *Consider a smooth dynamical system in normal form* (A.92) *with local center manifold* $\{(y,z) : z = \phi(y)\}$ *as in* (A.93). *Let* $T : \mathbb{R}^k \to \mathbb{R}^l$ *be smooth with* $T(0) = 0$ *and* $DT(0) = 0$. *Suppose that as* $y \to 0$, *for some* $q > 1$:

$$(HT)(y) = \mathcal{O}(|y|^q). \tag{A.96}$$

Then, as $y \to 0$, *also*

$$|T(y) - \phi(y)| = \mathcal{O}(|y|^q). \tag{A.97}$$

A.10.1.2 Calculating the normal form and the center manifold

We analyze the flow of the ODE System (A.7) around its fixed points by applying the theory from the previous section. We therefore write the system into normal form, see Def. A.34. For a fixed point $(a, b, i) = (0, 0, K)$, we begin with the affine transformation

$$j = i - K, \tag{A.98}$$

and then decompose the resulting system into a linear part M and a nonlinear part G. To be concise with the notation from the previous section, which is adopted from the existing literature, we use a vectorial notation in coordinates (j, a, b), such that the center manifold can be written as $\big\{(j, a, b) : (a, b) = \phi(j)\big\}$.

Definition A.40. Given $c > 0, K \in \mathbb{R}$, introduce the matrix M as

$$M := \begin{pmatrix} 0 & -\frac{K+r}{c} & 0 \\ 0 & 0 & 1 \\ 0 & K-1 & -c \end{pmatrix}. \tag{A.99}$$

Further, define the nonlinear functions $g(j, a) := a^2 + aj$ and $G : \mathbb{R}^3 \to \mathbb{R}^3$:

$$G \begin{pmatrix} j \\ a \\ b \end{pmatrix} := g(j,a) \cdot \begin{pmatrix} -\frac{1}{c} \\ 0 \\ 1 \end{pmatrix}. \tag{A.100}$$

Lemma A.41 (Linear and nonlinear part). *For* $c > 0, K \in \mathbb{R}$, *the ODE System* (A.7) *can be decomposed in its linear and nonlinear part. In coordinates* (j, a, b), *where* $j = i - K$, *and using Def. A.40, this reads as*

$$\begin{pmatrix} j' \\ a' \\ b' \end{pmatrix} = M \cdot \begin{pmatrix} j \\ a \\ b \end{pmatrix} + G \begin{pmatrix} j \\ a \\ b \end{pmatrix}. \tag{A.101}$$

Definition A.42. For given $c > 0, K \in \mathbb{R}$, we define the discriminant

$$\Delta := \sqrt{\frac{c^2}{4} + K - 1}. \tag{A.102}$$

The eigenvalues and eigenvectors of M are then given by (cf. (A.11))

$$\lambda_0 = 0, \quad \lambda_\pm = -\frac{c}{2} \pm \Delta, \tag{A.103}$$

$$e_0 = \begin{pmatrix} 1 \\ 0 \\ 0 \end{pmatrix}, e_\pm = \begin{pmatrix} \frac{K+r}{c} \cdot \frac{\lambda_\mp}{\lambda_\pm} \\ -\lambda_\mp \\ K-1 \end{pmatrix}. \tag{A.104}$$

Technical difficulties arise when the eigenvectors no longer span the entire $\mathbb{R}^3$. We require $K \neq 1$ in view of (A.104), which also eliminates the case $\lambda_+ = 0$. For similar reasons, we also exclude the case that $\lambda_+ = \lambda_-$, so we require that $\Delta \neq 0$. This is given if $K \neq 1 - c^2/4$.

Lemma A.43. *Let $c > 0$ and $K \notin \{1, 1 - c^2/4\}$. The matrix M can be written in diagonal form, such that $M = EDE^{-1}$. The matrices D, E, E^{-1} are given by:*

$$D = \operatorname{diag}(\lambda_0, \lambda_+, \lambda_-), \tag{A.105}$$

$$E = \begin{pmatrix} e_0 & e_+ & e_- \end{pmatrix} = \begin{pmatrix} 1 & \frac{K+r}{c} \cdot \frac{\lambda_-}{\lambda_+} & \frac{K+r}{c} \cdot \frac{\lambda_+}{\lambda_-} \\ 0 & -\lambda_- & -\lambda_+ \\ 0 & K-1 & K-1 \end{pmatrix}, \tag{A.106}$$

$$E^{-1} = \begin{pmatrix} 1 & -\frac{K+r}{(1-K)} & -\frac{K+r}{c(1-K)} \\ 0 & \frac{1}{2\Delta} & -\frac{\lambda_+}{2\Delta(1-K)} \\ 0 & -\frac{1}{2\Delta} & \frac{\lambda_-}{2\Delta(1-K)} \end{pmatrix}. \tag{A.107}$$

Lemma A.44 (Dynamics in normal form)**.** *Let $c > 0$ and $K \notin \{1, 1 - c^2/4\}$. The eigenvectors e_0, e_+, e_- of M form a basis of $\mathbb{R}^3$. We introduce the coordinates (u, v, w), such that any $x \in \mathbb{R}^3$ can be written as $x = u \cdot e_0 + v \cdot e_+ + w \cdot e_-$. The System (A.7) in coordinates (u, v, w) follows dynamics*

$$\begin{pmatrix} u' \\ v' \\ w' \end{pmatrix} = \begin{pmatrix} 0 \\ \lambda_+ v \\ \lambda_- w \end{pmatrix} + P(u, v, w) \cdot \begin{pmatrix} -\frac{1}{c}(1 + \frac{K+r}{1-K}) \\ -\frac{\lambda_+}{2\Delta(1-K)} \\ \frac{\lambda_-}{2\Delta(1-K)} \end{pmatrix}, \tag{A.108}$$

where P is a polynomial such that $P(u, 0, 0) = 0$:

$$P(u, v, w) := -\Big(\lambda_- v + \lambda_+ w\Big) \cdot \Big(-\lambda_- v - \lambda_+ w + u + \frac{K+r}{c}\big[\frac{\lambda_-}{\lambda_+} v + \frac{\lambda_+}{\lambda_-} w\big]\Big). \tag{A.109}$$

Proof. We change coordinates from u, v, w to j, a, b and back:

$$\begin{pmatrix} u' \\ v' \\ w' \end{pmatrix} = \begin{pmatrix} 0 \\ \lambda_+ v \\ \lambda_- w \end{pmatrix} + E^{-1} \cdot G(E \cdot \begin{pmatrix} u \\ v \\ w \end{pmatrix}). \tag{A.110}$$

Now recall the functions G and g, see (A.100). Explicitely calculating the nonlinear part $E^{-1}GE$ results in

$$\begin{aligned} E^{-1} \cdot G(E \cdot \begin{pmatrix} u \\ v \\ w \end{pmatrix}) &= E^{-1} \cdot \begin{pmatrix} -\frac{1}{c} \\ 0 \\ 1 \end{pmatrix} \cdot g(E \cdot \begin{pmatrix} u \\ v \\ w \end{pmatrix}) \\ &= \begin{pmatrix} -\frac{1}{c}(1 + \frac{K+r}{1-K}) \\ -\frac{\lambda_+}{2\Delta(1-K)} \\ \frac{\lambda_-}{2\Delta(1-K)} \end{pmatrix} \cdot g \begin{pmatrix} u + \frac{K+r}{c}(\frac{\lambda_-}{\lambda_+} v + \frac{\lambda_+}{\lambda_-} w) \\ -\lambda_- v - \lambda_+ w \\ b\big(u, v, w\big) \end{pmatrix} \\ &= P(u, v, w) \cdot \begin{pmatrix} -\frac{1}{c}(1 + \frac{K+r}{1-K}) \\ -\frac{\lambda_+}{2\Delta(1-K)} \\ \frac{\lambda_-}{2\Delta(1-K)} \end{pmatrix}. \end{aligned} \tag{A.111}$$

Luckily, for evaluating $g(j, a)$, we do not have to calculate the coordinate $b(u, v, w)$. □

Now we have all ingredients for computing the center manifold. We use the approximation argument from Theorem A.39:

Theorem A.45 (Asymptotic behavior)**.** *Let $c > 0$ and $K \notin \{1, 1 - c^2/4\}$, and let $(a, b, i) = (0, 0, K)$ be a fixed point of the System* (A.7)*. Locally around $(0, 0, K)$, the center manifold of the fixed point coincides with the set*

$$\{a = b = 0\}. \tag{A.112}$$

In a non-empty open neighborhood around $(0, 0, K)$, the flow of the System (A.7) *is equivalent to*

$$\begin{pmatrix} u' \\ v' \\ w' \end{pmatrix} = \begin{pmatrix} 0 \\ \lambda_+ v \\ \lambda_- w \end{pmatrix}, \tag{A.113}$$

where u, v, w are the coordinates in the system of eigenvectors e_0, e_+, e_- of the matrix M, see (A.104)*.*

Proof. In the normal form from Lemma A.44, the center manifold can be calculated as a function $\phi(u) : \mathbb{R} \to \mathbb{R}^2$. As $u \to 0, \phi(u) \in \mathcal{O}(u^2)$, and $\phi(u)$ can be approximated to any degree by some polynomial without linear and constant parts. For some arbitrary approximation $T : \mathbb{R} \to \mathbb{R}^2$ with

components T_v, T_w, we can estimate the error of the approximation $(HT)(u)$ by Theorem A.39. Inserting the normal form from Lemma A.44 results in

$$\begin{aligned}(HT)(u) = &- DT(u) \cdot P\big(u, T(u)\big) \cdot \frac{1}{c}(1 + \frac{K-r}{1-K}) - \begin{pmatrix} \lambda_+ \cdot T_v(u) \\ \lambda_- \cdot T_w(u) \end{pmatrix} \\ &- P\big(u, T(u)\big) \cdot \begin{pmatrix} -\frac{\lambda_+}{2\Delta(1-K)} \\ \frac{\lambda_-}{2\Delta(1-K)} \end{pmatrix}.\end{aligned} \tag{A.114}$$

For the center manifold, $(H\phi)(u) = 0$. From Eq. (A.114), we can extract the coefficients of the Taylor Expansion of $\phi(u)$ around the fixed point iteratively, by choosing better and better approximating polynomials T_n. For the start, take some polynomial $T_2(u) : \mathbb{R} \to \mathbb{R}^2$ of order 2. Let $\alpha, \beta \in \mathbb{R}$ and define

$$T_2(u) := (\alpha u^2, \beta u^2). \tag{A.115}$$

Note that $P\big(u, T_2(u)\big) = \mathcal{O}(u^3)$, for P as defined in (A.109). Thus

$$(HT_2)(u) = \mathcal{O}(u^3) - \begin{pmatrix} \lambda_+ \, \alpha u^2 \\ \lambda_- \, \beta u^2 \end{pmatrix}. \tag{A.116}$$

We see that for any approximation of type $T_2(u) = (\alpha u^2, \beta u^2)$, the leading error term is of order $\mathcal{O}(u^3)$ if and only if $T_2(u) \equiv (0,0)$. We conclude that the second order approximation of ϕ is given by $T_2(u) \equiv (0,0)$. By an easy induction, it follows that $T_n(u) = (0,0)$ for all $n \geq 2$, and so the local center manifold is given by $\phi(u) = (0,0)$. In the original system, this corresponds to $\{a = b = 0\}$, which are the fixed points of the ODE (A.7). We can now calculate the asymptotic flow in the normal form, given by (A.94). This results in the claimed asymptotics (A.113), when we use that the nonlinear part vanishes: $P\big(u, \phi(u)\big) = P(u, 0, 0) = 0$. □

A.10.2 Numerical evaluation of the spectrum of $\mathcal{L}$

As announced in our discussion in Section A.9, we analyze the spectral stabilty of the critical traveling wave. The theoretical background is presented in [130, 63], the details about the computational approach are presented by Barker et al. [12].

Here and from now on, $c = 2$ and we denote as $a(z), i(z)$ the critical traveling wave with speed $c = 2$ and $i_{+\infty} = 0$. We denote the exponent of the weight-function as $\alpha > 0$ and analyze the spectral stability of the critical traveling wave in the weighted L^2-Sobolev space H^1_α, with norm $||f||_{H^1_\alpha} = ||f \cdot e^{\alpha z}||_{H^1}$.

We linearize the PDE around $a(z), i(z)$ and analyze the non-negative spectrum of the resulting linear operator $\mathcal{L}$, as defined in (A.91). For System (A.1), this operator $\mathcal{L} : H^2_\alpha(\mathbb{R}) \times H^1_\alpha(\mathbb{R}) \to H^2_\alpha(\mathbb{R}) \times H^1_\alpha(\mathbb{R})$ acts on a pair

of functions $u \in H^2_\alpha, v \in H^1_\alpha$, which correspond to perturbations of a and i, respectively:

$$\begin{aligned} u &\mapsto u'' + cu' + u(1 - (2a + i)) - va, \\ v &\mapsto cv' + u(2a + i + r) + va. \end{aligned} \tag{A.117}$$

The operator $\mathcal{L}$ is equivalent to a first-order operator $\tilde{\mathcal{L}} : H^1_\alpha(\mathbb{R}^3) \to H^1_\alpha(\mathbb{R}^3)$, when we introduce an auxiliary variable for u'. We will omit the tilde.

As will see in a moment, we only need to consider the point-spectrum of $\mathcal{L}$. Thus, for $\gamma \in \mathbb{C}$ with $\mathfrak{Re}(\gamma) \geq 0$, we look for a function $U \in H^1_\alpha$ that solves $\mathcal{L}U = \gamma \cdot U$. Now, $\gamma \in \mathbb{C}$ lies in the point spectrum of $\mathcal{L}$ if and only if there exists a function $U : \mathbb{R} \to \mathbb{C}^3, U \in H^1_\alpha$, which solves

$$\frac{d}{dz}U = M(z,\gamma) \cdot U, \quad M(z,\gamma) := \begin{pmatrix} 0 & 1 & 0 \\ \gamma + 2a(z) + i(z) - 1 & -c & a(z) \\ -\frac{2a(z)+i(z)+r}{c} & 0 & \frac{\gamma - a(z)}{c} \end{pmatrix}. \tag{A.118}$$

It can easily be seen that the matrix $M(+\infty, \gamma)$ has eigenvalues

$$\beta_1 = \frac{\gamma}{c}, \qquad \beta_2 = -\frac{c}{2} + \sqrt{\gamma}, \qquad \beta_3 = -\frac{c}{2} - \sqrt{\gamma}, \tag{A.119}$$

whereas the matrix $M(-\infty, \gamma)$ has eigenvalues

$$\beta_1 = \frac{\gamma}{c}, \qquad \beta_2 = -\frac{c}{2} + \sqrt{2 + \gamma}, \qquad \beta_3 = -\frac{c}{2} - \sqrt{2 + \gamma}. \tag{A.120}$$

If $U \in H^1_\alpha$, then $W(z) := U(z) \cdot e^{\alpha z}$ is bounded and vanishes. The function $W(z)$ fulfills

$$W'(z) = \big(M(z,\gamma) + \alpha \cdot \mathbb{1}\big) \cdot W(z). \tag{A.121}$$

Remark that the matrix $M + \alpha\mathbb{1}$ has the same eigenvectors as M, and that its eigenvalues are shifted by α when compared to M. If $M(\pm\infty) + \alpha\mathbb{1}$ has no eigenvalues with zero real-part, the theory of *exponential dichotomies* implies that any bounded solution $W(z)$ must vanish exponentially fast as $z \to \pm\infty$, and that it asymptotically approaches the unstable (resp. stable) manifold of the constant matrix $M(-\infty, \gamma)$ as $z \to -\infty$ (resp. $M(+\infty, \gamma)$ as $z \to +\infty$) [130]. Therefore, a bounded solution exists if and only if the trajectories that emerge from these manifolds intersect. This allows us to compute the Evans-function: it is a determinant that evaluates to zero if and only if the solutions that decay at $-\infty$ and those that decay at $+\infty$ are somehow linearly dependent.

We investigate the case $\alpha = \frac{c}{2}$, which is equal to the rate of convergence of the wave as $z \to +\infty$, up to a sub-exponential term, see Theorem A.1. For $\alpha = \frac{c}{2}$, then within the region $\{\mathfrak{Re}(\gamma) \geq 0, \gamma \neq 0\}$ the following holds: the

dimension of the unstable space of $M(-\infty,\gamma)+\frac{c}{2}\cdot\mathbb{1}$ is given by $k_-=2$, and the dimension of the stable space of $M(+\infty,\gamma)+\frac{c}{2}\cdot\mathbb{1}$ is given by $k_+=1$. This can easily be deduced from the corresponding Eigenvalues (A.119), (A.120), which do not cross the imaginary axis. The values k_- and k_+ add up to the dimension of the ODE (A.118). We say that $\{\mathfrak{Re}(\gamma)\geq 0, \gamma\neq 0\}$ is contained in the *region of consistent splitting* of the operator $\mathcal{L}$. This implies that the non-negative part of the spectrum of $\mathcal{L}$ is contained in the point spectrum of the operator, which is a standard result [130, 132]. Within the region of consistent splitting, we can define the Evans-function $E(\gamma)$.

Given γ with $\mathfrak{Re}(\gamma)\geq 0, \gamma\neq 0$, we let $X(z)$ be the unique (up to a shift) solution of Eq. (A.121) that vanishes at $z=+\infty$, and let $Y_1(z), Y_2(z)$ span the two-dimensional space of solutions of Eq. (A.121) that vanish at $z=-\infty$. The Evans-function is defined as

$$E(\gamma) := \det\big(Y_1(z)\big|Y_2(z)\big|X(z)\big)\Big|_{z=0}. \tag{A.122}$$

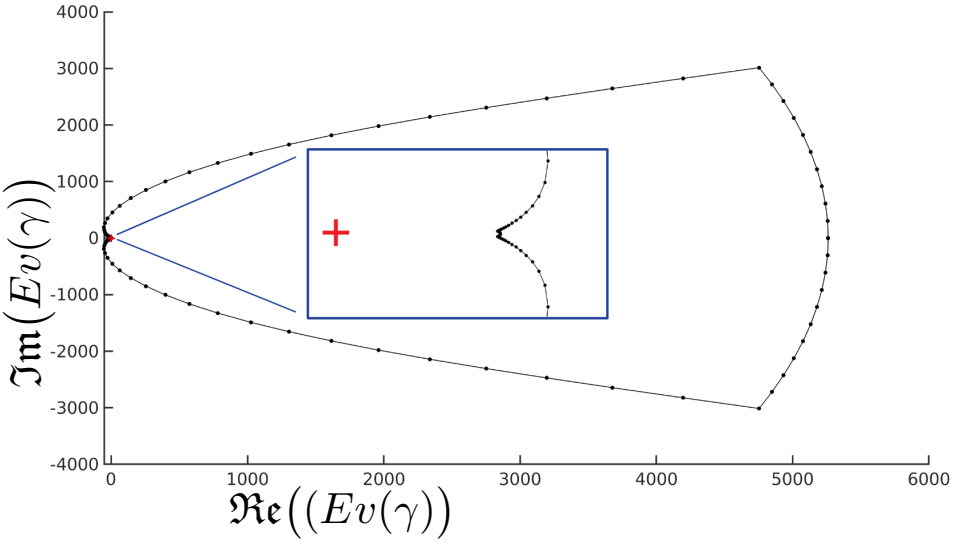

Figure A.7: Numerical evaluation of the Evans-function (A.122) $Ev(\gamma)$ *for* $r=0$ *and* γ *on the boundary of the Domain* S*, defined in* (A.123)*. The Evans-function for* $r=1$ *is very similar. The origin is marked with a small red cross. The graph does not enclose the origin and it can visually be seen that its winding number is equal to zero. We conclude that the Region* S *contains no zeros of* $Ev(\gamma)$*.*

The Evans-function is not unique, but it holds that $E(\gamma)=0$ if and only if γ lies in the point spectrum of $\mathcal{L}$. Moreover, $E(\gamma)$ is analytic if X, Y_1, Y_2 are chosen such that they are analytic in γ [130]. Thus it suffices to calculate $E(\gamma)$ along the boundary of a domain: the winding number along this contour then corresponds to the number of zeros inside the domain.

We use this to verify that there are no zeros of $E(\gamma)$ within the set

$$S := \Big\{\gamma\in\mathbb{C}\,\Big|\,\mathfrak{Re}(\gamma)\geq 0,\ 10^{-3}\leq|\gamma|\leq 1000\Big\}, \tag{A.123}$$

where we keep a small distance from the origin to prevent that the eigenvalues of the matrices $M(\pm\infty, \gamma) + \frac{c}{2} \cdot \mathbb{1}$ touch the imaginary axis, and hope that there are no unexpectedly large eigenvalues. We want to remark that for systems with a degenerate diffusion, no general a-priori upper bound for the size of the eigenvalues with non-negative real-part has been found yet, which would allow for a numerical proof of spectral stability. It may be possible to generalize the approach in [97]. Simple energy estimates exist for traveling waves of diffusive systems, see e.g. Chapter 6 in [115].

The various numerical challenges that arise when computing the Evans-function, as well as their solutions, are described in detail by Barker et al. [12], who also suggest using their library STABLAB [13]. We gratefully followed this suggestion, and computed the left-adjoint Evans-function, a slight modification which is numerically advantageous in the present setting [12]. The result is presented in Figure A.7 and yields a strong evidence that the critical wave is spectrally stable in $H^1_{c/2}$.

A.10.3 Rescaling the general system

Let $r_S, r_A, D > 0$ and $r_I \geq 0$, and consider the reaction-diffusion system

$$\begin{aligned} A_t &= D \cdot A_{xx} + r_A A - r_S A(A + I), \\ I_t &= r_I A + r_S A(A + I), \end{aligned} \tag{A.124}$$

which is the general form of System (A.1). There exists a linear one-to-one correspondence to the normalized form. Therefore, we rescale time and space, $s := r_A \cdot t$, $y := \sqrt{D/r_A} \cdot x$, and the densities of the particles, $\bar{A} := A \cdot r_S/r_A$, $\bar{I} := I \cdot r_S/r_A$. The rescaled dynamics of System (A.124) follow

$$\begin{aligned} \bar{A}_s &= \bar{A}_{yy} + \bar{A} - \bar{A}(\bar{A} + \bar{I}), \\ \bar{I}_s &= \frac{r_I}{r_A}\bar{I} + \bar{A}(\bar{A} + \bar{I}), \end{aligned} \tag{A.125}$$

which is equivalent to System (A.1) with $r = \frac{r_I}{r_A}$. In view of this, we can formulate a parameter-dependent version of Theorem A.1:

Theorem A.46. *Let $r_S, r_A, D > 0$ and $r_I \geq 0$, and consider the System (A.124) and a wave-speed $c > 0$. Set*

$$i_c := \max\{0, \frac{1}{r_S}\big(r_A - \frac{c^2}{4D}\big)\}. \tag{A.126}$$

For each pair $i_{-\infty}, i_{+\infty} \in \mathbb{R}^+$ such that

$$i_{+\infty} \in [i_c, \frac{r_A}{r_S}), \qquad i_{-\infty} = \frac{2 \cdot r_A}{r_S} - i_{+\infty}, \tag{A.127}$$

there exists a unique bounded and positive traveling wave a, i with speed c such that

$$\lim_{x\to\pm\infty} a(z) = 0, \qquad \lim_{x\to\pm\infty} i(z) = i_{\pm\infty}. \tag{A.128}$$

If $\frac{c^2}{4D} + r_S \cdot i_{+\infty} - r_A = 0$, convergence as $z \to +\infty$ is sub-exponentially fast and of order $z \cdot e^{-\frac{c}{2D}z}$. If $\frac{c^2}{4D} + r_S \cdot i_{+\infty} - r_A > 0$, convergence as $z \to +\infty$ is exponentially fast. Convergence as $z \to -\infty$ is exponentially fast in all cases. The corresponding rates are

$$\mu_{\pm\infty} = -\frac{c}{2D} + \sqrt{\frac{c^2}{4D^2} + \frac{r_S \cdot i_{\pm\infty} - r_A}{D}}. \tag{A.129}$$

In particular, for any invading front, where $i(z) \to 0$ as $z \to +\infty$, the remaining density of particles at the back of the wave is given by $i_{-\infty} = 2 \cdot \frac{r_A}{r_S}$.

B Preprint:
Convective stability of the critical waves of an FKPP growth process

This appendix reproduces exactly the content of the paper [93] with the title "Convective stability of the critical waves of an FKPP growth process", written by the author of this thesis. The preprint is publicly available under https://arxiv.org/abs/2305.10228, *[math.AP], 2023*, it has not been peer-reviewed yet. This preprint was summarized in Chapter 4.

B.1 Introduction and results

We analyze an FKPP-system [50, 91] that models a self-organized growth process. Considering the one-dimensional case $z \in \mathbb{R}, t \in \mathbb{R}_0^+$, the densities $A(t,z), I(t,z) \geq 0$ of active and inactive particles follow dynamics

$$\begin{aligned} \frac{\partial}{\partial t} A &= \frac{\partial^2}{\partial z^2} A + A - A(A+I), \\ \frac{\partial}{\partial t} I &= d\frac{\partial^2}{\partial z^2} I + rA + A(A+I), \qquad r, d \geq 0. \end{aligned} \tag{B.1}$$

This system was introduced by Hannezo et al. in the context of branching morphogenesis [73]. The authors used a stochastic branching particle system to model the morphogenesis of branched glandular structures. The PDE (B.1) for $d = 0$ is the heuristic hydrodynamic limit of their stochastic system. Existence and uniqueness of non-negative solutions of (B.1) follow by classical fixed-point theory, see e.g. Chapter 14 in [138]. Given the normalized System (B.1), the general case can be obtained by rescaling [92].

We construct the traveling waves of System (B.1) and prove that for $d > 0$, those with minimal speed are locally stable against perturbations. The difficulty when analyzing this system is that the inactive particles I do not react, only the active particles A branch and become inactive upon collision. Thus, the system features a continuum of steady states

$$P_I = \{A = 0, I = K \,|\, K \in \mathbb{R}\}, \tag{B.2}$$

and a-priori, we do not know which of these steady states are relevant.

Simulations show that the system forms traveling wave solutions, which select for particular steady states among all possible ones, see Figure B.1. FKPP-systems are well-known to form heteroclinic traveling wave solutions,

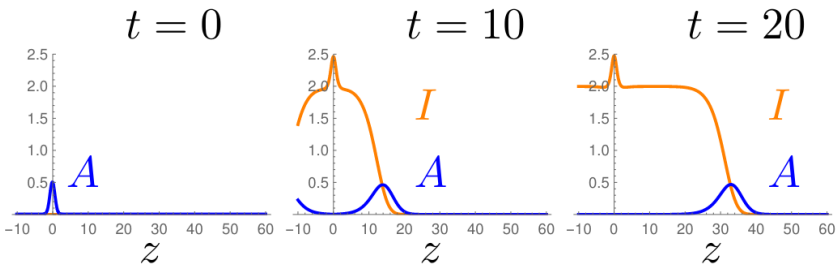

Figure B.1: Simulation of System (B.1) *for* $r, d = 0$. *Given an initial heap of active particles* $A(z,0) = 1/2\exp(-z^2)$, *and* $I(z,0) = 0$, *two identical traveling fronts arise, the right one is shown. After the separation of the two fronts away from the origin, the density of the remaining inactive particles is given by* $I = 2$ *and the front moves asymptotically with speed* $c = 2$.

that connect two different steady states [22, 50, 91, 48, 41]. A (right-) traveling wave solution is constant in the moving frame $x = z - ct$, for a wave-speed $c > 0$. Thereby, we refer to a traveling wave as a non-constant and bounded solution of the system of ODEs

$$\begin{aligned} 0 &= c\frac{\partial}{\partial x}a + \frac{\partial^2}{\partial x^2}a + a - a(a+i), \\ 0 &= c\frac{\partial}{\partial x}i + d\frac{\partial^2}{\partial x^2}i + ra + a(a+i). \end{aligned} \tag{B.3}$$

We call a solution of System (B.3) non-negative if $a, i \geq 0$. Moreover, an *invading front* is a non-negative traveling wave where both $a(x)$ and $i(x)$ vanish as $x \to +\infty$.

For the case $d = 0$, we constructed the traveling waves of the system, but could not analyze their stability [92]. Since the inactive particles neither react nor diffuse, any deviation from the traveling wave remains in the system for all times (see Fig. B.1). Therefore, we introduce the diffusion to the inactive particles. The present article is divided into two parts:

1) In Section B.3, given the traveling waves for $d = 0$ as our starting point, we apply perturbation techniques to construct the traveling waves for $d \neq 0$. These waves are continuous in $d \geq 0$, so we recover the original dynamics as $d \to 0$. We prove the existence of a continuum of traveling wave solutions, that correspond to the continuum of steady states (B.2), check Theorems 3.1 and B.24. For this introduction, we restrict to the invading fronts. In particular, there exists an invading front with minimal possible speed $c = 2$, referred to as *critical front*:

Theorem B.1. *For* $r \geq 0, c > 0$, *consider the Wave System* (B.3) *with*

$$0 < d < \min\left\{1, \frac{3c}{2}, \frac{c^2}{2(r+1)}\right\}. \tag{B.4}$$

If and only if $c \geq 2$, there exists an invading front. The function $i(x)$ is decreasing, and $a(x)$ has a unique local and global maximum. As $x \to -\infty$, the front converges exponentially fast to a fixed point $(a, i) = (0, i_{-\infty})$, where

$$1 < 2 - d \cdot \frac{2(r+1)}{c} < i_{-\infty} < 2. \tag{B.5}$$

The rate of convergence is a function of $i_{-\infty}$, given by

$$\mu_{-\infty} = -\frac{c}{2} + \sqrt{\frac{c^2}{4} + i_{-\infty} - 1} > 0. \tag{B.6}$$

There are two possibilities for the speed of convergence as $x \to +\infty$. In the critical case $c = 2$, the front behaves as $x \cdot e^{-x}$. If $c > 2$, convergence is purely exponential, with rate

$$\mu_{+\infty} = \frac{c}{2} - \sqrt{\frac{c^2}{4} - 1} > 0. \tag{B.7}$$

Such an invading front arises in the simulation depicted in Figure B.1: a pulse of active particles is accompanied by a monotone wave of inactive particles.

2) In Section B.2, we analyze the stability of the critical invading front. In the moving frame $x = z - 2t$, we write a solution of the PDE (B.1) as the sum of the front $a(x), i(x)$ and the perturbations $\tilde{A}(t, x), \tilde{I}(t, x)$:

$$A(t, x) = a(x) + \tilde{A}(t, x), \quad I(t, x) = i(x) + \tilde{I}(t, x). \tag{B.8}$$

The system is not attracted towards a particular limit, as none of the Steady States (B.2) is stable in the classical sense. To overcome this, we operate in a space where we allow the perturbations to grow exponentially as $x \to -\infty$. This type of stability is referred to as *convective stability* [63], since we more or less ignore what happens to perturbations that are convected to the back of the invading front. To stabilize the front as $x \to +\infty$, perturbations must vanish exponentially fast, which is typical for FKPP-fronts [132, 130]. Given a smooth weight $w(x) > 0$, subject to

$$w(x) = \begin{cases} e^{-x} & x \geq 1, \\ e^{-\alpha x} & x \leq -1, \\ 1 & x = 0, \end{cases} \quad \text{with fixed } \alpha \in (0, 1), \tag{B.9}$$

we prove that if the weighted perturbations

$$\frac{\tilde{A}(t, x)}{w(x)}, \quad \frac{\tilde{I}(t, x)}{w(x)} \tag{B.10}$$

are initially small, they vanish pointwise with algebraic decay $t^{-3/2}$. In order to deal with the unbounded weight, we need some a-priori control of the left tail of the PDE. The novelty of the present work is that we use a Feynman-Kac formula to prove exponential decay of the left tail of the perturbations, under the assumption that also the unweighted perturbations are initially small.

We have to assume that the discrete spectrum of the linearized perturbation equation contains no elements with non-negative real-part, check Section B.2.3 for the precise statement. We verify this numerically, the technique is presented in Appendix B.4.2, an analytic proof remains an open problem.

Theorem B.2. *For a pair $d > 0, r \geq 0$ as in Theorem B.1, consider the critical invading front with speed $c = 2$. If we assume that the discrete spectrum of the weighted linearized perturbation equation contains no elements with non-negative real-part (see* (B.44)*), then the critical invading front is locally stable in a space with weight $w(x)$ as above* (B.9)*:*

Fix a pair of constants $C, \mu_0 > 0$. For all $\epsilon > 0$, there exists a $\delta > 0$, such that if the unweighted perturbations fulfill

$$(i) \qquad \forall x \leq 0: \quad |\tilde{A}(0,x)| \leq Ce^{\mu_0 x}, \quad |\tilde{I}(0,x)| \leq \delta, \tag{B.11}$$

and if the weighted perturbations $\tilde{A}(0,x)/w(x), \tilde{I}(0,x)/w(x)$ are elements of $H^2(\mathbb{R})$, and

$$(ii) \qquad \int_{\mathbb{R}} (1+|x|)\Big[\big|\frac{\tilde{A}(0,x)}{w(x)}\big| + \big|\frac{\tilde{I}(0,x)}{w(x)}\big|\Big]\, dx \leq \delta, \tag{B.12}$$

$$(iii) \qquad \big|\big|\frac{\tilde{A}(0,x)}{w(x)}\big|\big|_\infty + \big|\big|\frac{\tilde{I}(0,x)}{w(x)}\big|\big|_\infty \leq \delta, \tag{B.13}$$

then the weighted perturbations decay pointwise with algebraic speed $t^{-3/2}$:

$$\sup_{t\geq 0}\sup_{x\in\mathbb{R}} \frac{(1+t)^{3/2}}{w(x)(1+|x|)}\Big(|\tilde{A}(t,x)| + |\tilde{I}(t,x)|\Big) \leq \epsilon. \tag{B.14}$$

B.1.1 Background

One of the central questions regarding tissue growth is how individual cells react to their microscopic environment, and how this gives rise to distinct macroscopic structures. Mathematical models help to understand these processes, there exists a huge literature of works regarding organ formation, wound healing or tumor growth [37, 46, 83, 99, 106]. While most of the clinically relevant results are numerical, simplified reaction-diffusion systems provide a framework for rigorously analyzing the arising spatiotemporal patterns. The first study of this kind was the seminal analysis of the FKPP-equation in the 1930s [50, 91], describing the spreading of a fitter population,

or "The Wave of Advance of Advantageous Genes" [50]. Given System (B.1), one obtains the original FKPP-equation when substituting $I \equiv 0$.

Hannezo et al. modeled the branching morphogenesi of glandular structures in organs via a stochastic system that is based on branching and annihilating random walks [73, 29]. Their numerical results suggest that this system self-organizes into spatially homogeneous structures, despite the fact that it is based on local mechanisms alone (i.e. there are no global guiding gradients). The authors also suggested the PDE (B.1) with $d = 0$ to study the mean-field behavior of the stochastic system. Since all mechanisms in System (B.1) are purely local, it can be seen as a degenerate Keller-Segel system [88, 116, 120]. For such systems, various organization phenomena are known, and can be proven in some cases [6].

Simulations indicate that System (B.1) forms traveling solutions for a wide range of initial data, an example is depicted in Figure A.1. However, a global convergence result seems difficult to prove since the active particles form a non-monotone pulse, being accompanied by a monotone front of inactive particles of the very same speed. Thereby, the system evades any classical comparison principles. For a Lokta-Volterra system where each consecutive species spreads with a different speed, Ducrot et al. [41] could prove a global convergence result: since the fronts separate, each single one satisfies a comparison principle.

For systems without a comparison principle, typically only the stability against small perturbations can be proven. For noncritical fronts (those with a spectral gap of the linearized perturbation) and for bounded weights, Sattinger [132] proved a general result in 1976. More recently, Ghazaryan et al. [63] proved several general results in the case of unbounded weights, even for mixed ODE-PDE models, but also under the assumption of a spectral gap. They also prefer the notion of *convective stability* [63], to emphasize the pointwise stability (whereas some physicists or biologists prefer to call the same phenomenon *convective instability*, emphasizing the fact that the overall perturbation does not vanish or might even increase [136]). For an a-priori control of the unbounded nonlinearity, Ghazaryan et al. use an energy estimate in H^2, which is not compatible with our pointwise result [61].

The critical case – where the essential spectrum is only marginally stable – requires a different approach. Only for the case of a single reactant, the stability of critical FKPP-fronts has been proven for quite general reaction-terms, by Gallay in 1994 [53]. The author proved that the algebraic speed of decay $t^{-3/2}$ is indeed optimal, we expect this also to be true in the present case. For more than one reactant, rigorous proofs are sparse.

Fayé and Holzer [48] could prove the local stability of the critical waves of a Lokta-Volterra system of two species. They generalize a technique for dealing with marginally stable spectra, which they introduced in 2018 for a system with a single reactant [47], to systems of two reactants. The underlying technique goes back to Zumbrun and Howard [167], in principle it

should be possible to generalize this result to systems of $n > 2$ reactants, but the notation becomes quite tedious. The computations are quite demanding: a precise analysis of the Evans-function in the neighborhood of the essential spectrum is required, making use of the Gap Lemma that goes back to Gardner and Zumbrun [56] – involving several changes of coordinates while keeping track of the resulting error terms. We are in the lucky situation that the linearized perturbation falls into the marginally stable category analyzed in [48], at least if we use an unbounded weight as in Theorem B.2. I want to thank the authors for remarking that their proof is largely independent of the actual weight, which initiated the idea for this project.

We adapt the resulting semi-group estimates to the case where the weight is not integrable. This is why we need an a-priori bound on the tail of the PDE (B.1) in the moving frame. We can then estimate the decay of a linear super-solution via a Feynman-Kac formula, where we can stop the driving Brownian motion at an arbitrarily chosen point, e.g. $x = 0$. As long as the perturbation at this specific point remains small, the super-solution decays exponentially. Our approach of dealing with the unbounded weight can be adapted to other systems with non-negative solutions, given that they are asymptotically monotone and that the nonlinearity essentially depends on a single reactant (which is the reason why we need the unbounded weight at all), check the introduction to Section B.2.

B.1.2 Structure of the paper

In Section B.2, we prove the local stability of the critical invading front. After introducing the necessary objects in Section B.2.1, we present the central steps of the proof in Section B.2.2. The technical details are then given in Section B.2.3 and Section B.2.4. The Feynman-Kac formula, which controls the left tail of the PDE, is proven in Appendix B.4.1. In Appendix B.4.2, we present a numerical evaluation of the non-negative discrete spectrum of the linearized perturbation.

In Section B.3, we construct the traveling waves. Given the traveling waves for $d = 0$ (see Theorem 3.1), we apply perturbation techniques to track any finite segment of the waves for $d \neq 0$, see Section B.3.2. The singular perturbation (for passing continuously from $d = 0$ to $d \sim 0$) is explained in Appendix B.4.3. In Section B.3.3, we analyze the phase space of the non-negative waves. We then extend the previous perturbation result and prove that a traveling wave persists locally under perturbation in d, up to its limit as $x \to +\infty$. Given any traveling wave, we prove an estimate of type $i_{-\infty} + i_{+\infty} = 2 + \mathcal{O}(d)$ regarding the limits in Section B.3.4. We then prove the existence of non-negative traveling waves and invading fronts up to $d \sim 1$, in Section B.3.5.

B.2 The stability of the critical invading front

B.2.1 Notation

In the following, we assume without further mentioning that $a(x), i(x)$ is a non-negative critical invading front as in Theorem B.1. To begin with, we decompose any solution of the PDE (B.1) in the moving frame $x = z - ct$ into

$$A(t,x) = a(x) + \tilde{A}(t,x), \quad I(t,x) = i(x) + \tilde{I}(t,x). \tag{B.15}$$

Then, the perturbations $\tilde{A}(t,x)$ and $\tilde{I}(t,x)$ follow

$$\begin{aligned} \frac{\partial}{\partial t}\tilde{A} &= \frac{\partial^2}{\partial x^2}\tilde{A} + c\frac{\partial}{\partial x}\tilde{A} + \tilde{A}(1-2a-i) - \tilde{I}a - \tilde{A}(\tilde{A}+\tilde{I}), \\ \frac{\partial}{\partial t}\tilde{I} &= d\frac{\partial^2}{\partial x^2}\tilde{I} + c\frac{\partial}{\partial x}\tilde{I} + \tilde{A}(2a+i+r) + \tilde{I}a + \tilde{A}(\tilde{A}+\tilde{I}). \end{aligned} \tag{B.16}$$

For $\tilde{A}, \tilde{I}$ that solve the perturbation Eq. (B.16) and given a strictly positive weight $w(x)$, we define the weighted perturbations $u := \tilde{A}/w, v := \tilde{I}/w$. If w is twice differentiable with derivatives w', w'', they solve

$$\begin{aligned} \frac{\partial}{\partial t}u = \frac{\partial^2}{\partial x^2}u + \frac{\partial}{\partial x}u \cdot \big(c + 2\frac{w'}{w}\big) + u \cdot \big(c\frac{w'}{w} + \frac{w''}{w}\big) \\ + u(1-2a-i) - va - wu(u+v), \\ \frac{\partial}{\partial t}v = d\frac{\partial^2}{\partial x^2}v + \frac{\partial}{\partial x}v \cdot \big(c + 2d\frac{w'}{w}\big) + v \cdot \big(c\frac{w'}{w} + d\frac{w''}{w}\big) \\ + u(2a+i+r) + va + wu(u+v). \end{aligned} \tag{B.17}$$

We summarize this as

$$\frac{\partial}{\partial t}(u,v) = \mathcal{L}(u,v) + N(u,v), \tag{B.18}$$

with the linear part

$$\begin{aligned} \mathcal{L}u := \frac{\partial^2}{\partial x^2}u + \frac{\partial}{\partial x}u \cdot \big(c + 2\frac{w'}{w}\big) + u \cdot \big(c\frac{w'}{w} + \frac{w''}{w}\big) \\ + u(1-2a-i) - va, \\ \mathcal{L}v := d\frac{\partial^2}{\partial x^2}v + \frac{\partial}{\partial x}v \cdot \big(c + 2d\frac{w'}{w}\big) + v \cdot \big(c\frac{w'}{w} + d\frac{w''}{w}\big) \\ + u(2a+i+r) + va, \end{aligned} \tag{B.19}$$

and the nonlinear part

$$Nu := -wu(u+v), \qquad Nv := wu(u+v). \tag{B.20}$$

For compactness of presentation, we introduce the vectorial notation

$$p(t,x) := \begin{pmatrix} u(t,x) \\ v(t,x) \end{pmatrix}, \; N(p)(t,x) := w(x)u(t,x) \cdot \begin{pmatrix} -u(t,x) - v(t,x) \\ u(t,x) + v(t,x) \end{pmatrix}. \tag{B.21}$$

Lastly, we define as $\mathcal{G}(t,x,y)$ the Kernel of the linear Eq. (B.19):

$$\mathcal{G}(t,x,y) := \begin{pmatrix} \mathcal{G}_{11}(t,x,y) & \mathcal{G}_{12}(t,x,y) \\ \mathcal{G}_{21}(t,x,y) & \mathcal{G}_{22}(t,x,y) \end{pmatrix}, \tag{B.22}$$

acting on a space to be defined later. In this compact notation, we will estimate the evolution of the weighted perturbations with a Duhamel principle:

$$p(t,x) = \int_{\mathbb{R}} \mathcal{G}(t,x,y)p(0,y)\,dy + \int_0^t ds \int_{\mathbb{R}} \mathcal{G}(t-s,x,y)N(p)(s,y)\,dy. \tag{B.23}$$

Eq. (B.23) holds if the nonlinearity is locally Lipschitz, see e.g. Pazy p. 185 ff [117].

B.2.2 Central steps

For $d > 0$ and in a function space where the weight grows exponentially as $x \to -\infty$, the operator $\mathcal{L}$ is sectorial [76, 3, 56], see Section B.2.3 for an analysis of its spectrum: the spectrum is contained in the strictly negative half-plane, with the exception of a single half-line that touches the origin. In this setting, we can use a result of Fayé and Holzer [48] to estimate the long-time behavior of $\mathcal{G}$, check Section B.2.4. Roughly, this result states that $\mathcal{G}$ decays like $t^{-3/2}$ for large t. Then, for estimating the evolution of the full nonlinear system via Eq. (B.23), it is crucial to control the nonlinear integral

$$\int_{\mathbb{R}} w(x)u(t,x) \cdot \big(u(t,x) + v(t,x)\big)\,dx. \tag{B.24}$$

We treat the cases $x \leq 0$ and $x \geq 0$ separately. Assuming that $w(x)$ vanishes exponentially fast as $z \to +\infty$, the front satisfies the classical estimate

$$\begin{aligned} &\Big| \int_0^\infty w(x)u(t,x) \cdot \big(u(t,x) + v(t,x)\big)\,dx \Big| \\ &\leq \sup_{x\geq 0} \Big\{ \big(|u(t,x)| + |v(t,x)|\big)^2 \Big\} \cdot \int_0^\infty w(x)\,dx \\ &\leq C \cdot \sup_{x\geq 0} \big\{ ||p(t,x)||_1^2 \big\}. \end{aligned} \tag{B.25}$$

Since $w(x)$ grows exponentially as $x \to -\infty$, we take a different approach for $x \leq 0$. This is where we need the a-priori estimate:

Proposition B.3. *Let $A(t,x), I(t,x)$ be a non-negative solution of the PDE (B.1) in the moving frame $x = z - ct$, for a speed $c > 0$. Assume that there exist constants $K, \delta, \mu_0 > 0$, such that the initial data fulfill*

$$\begin{aligned} I(0,x) &\geq 1+\delta && \forall x \leq 0, \\ A(0,x) &\leq K e^{\mu_0 x} && \forall x \leq 0, \\ A(0,x) + I(0,x) &\leq K && \forall x \in \mathbb{R}. \end{aligned} \tag{B.26}$$

Moreover, assume that for some time $t \in (0,\infty]$, it holds that

$$I(s, x=0) \geq 1+\delta > 1 \qquad \forall s \in [0,t). \tag{B.27}$$

Then, there exist $C, \zeta > 0$ that are independent of t, such that:

$$\forall s \in [0,t),\ x \leq 0: \quad i) \qquad I(s,x) \geq 1+\delta, \tag{B.28}$$

$$ii) \qquad A(s,x) \leq C e^{\zeta x}. \tag{B.29}$$

The proof and the used Feynman-Kac formula are standard, given in Appendix B.4.1. The way we apply this result for controlling the perturbations is new. For the wave it holds that $\lim_{x\to-\infty} i(x) > 1$, where $i(x)$ is monotone. We first shift the wave such that $i(0) = 1 + 2\delta > 1$. Then, it suffices to control

$$|\tilde{I}(t, x=0)| \leq \delta \qquad \forall t \geq 0, \tag{B.30}$$

and in view of Proposition B.3, there exist constants $C, \zeta > 0$ such that

$$|\tilde{A}(t,x)| \leq A(t,x) \leq C e^{\zeta x} \qquad \forall x \leq 0,\ t \geq 0, \tag{B.31}$$

since $A \geq 0$. We re-substitute $wu = \tilde{A}$ to estimate

$$\begin{aligned} &\Big| \int_{-\infty}^{0} w(x) u(t,x) \cdot \big(u(t,x) + v(t,x)\big) \Big| \, dx \\ &\leq \int_{-\infty}^{0} |\tilde{A}(t,x)| \cdot |u(t,x) + v(t,x)| \, dx \\ &\leq \sup_{x\leq 0} \Big\{ |u(t,x)| + |v(t,x)| \Big\} \cdot \int_{-\infty}^{0} |\tilde{A}(t,x)| \, dx \\ &\leq C \cdot \sup_{x\leq 0} \big\{ ||p(t,x)||_1 \big\}. \end{aligned} \tag{B.32}$$

Given both Estimates (B.25) and (B.32), the resulting semi-group estimates are quite standard, though a bit lengthy due to the different cases that need to be dealt with, presented in Section B.2.4.

B.2.3 An appropriate function space

Here and in the following, let $\mathcal{L}$ (B.19) be a densely defined operator

$$\mathcal{L} : H^2(\mathbb{R}) \times H^2(\mathbb{R}) \to L^2(\mathbb{R}) \times L^2(\mathbb{R}), \tag{B.33}$$

where H^2 is the L^2 Sobolev space. For $\lambda \in \mathbb{C}$, consider the Eigenvalue problem $\lambda \cdot (u, v) = \mathcal{L}(u, v)$. With the help of the auxiliary variables

$$U := \begin{pmatrix} u \\ u' \\ v \\ v' \end{pmatrix}, \tag{B.34}$$

the equation $\lambda \cdot (u, v) = \mathcal{L}(u, v)$ can be rewritten as an equivalent linear system of ODEs:

$$U' = M(x, \lambda) \cdot U, \tag{B.35}$$

for a matrix $M(x, \lambda)$ given by

$$M(x,\lambda) := \begin{pmatrix} 0 & 1 & 0 & 0 \\ \lambda + \xi_u(x) & -(c + 2\frac{w'(x)}{w(x)}) & a(x) & 0 \\ 0 & 0 & 0 & 1 \\ -\frac{2a(x)+i(x)+r}{d} & 0 & \frac{\lambda+\xi_v(x)}{d} & -\frac{c+2d\frac{w'(x)}{w(x)}}{d} \end{pmatrix}, \tag{B.36}$$

$$\xi_u(x) := 2a(x) + i(x) - 1 - c\frac{w'(x)}{w} - \frac{w''(x)}{w(x)}, \tag{B.37}$$

$$\xi_v(x) := -a(x) - c\frac{w'(x)}{w(x)} - d\frac{w''(x)}{w(x)}. \tag{B.38}$$

Given a pair of exponents $\alpha_\pm > 0$, we fix a smooth weight $w(x) > 0$, subject to the conditions

$$w(x) := \begin{cases} e^{-\alpha_+ x} & x \geq 1, \\ e^{-\alpha_- x} & x \leq -1, \\ 1 & x = 0. \end{cases} \tag{B.39}$$

Note that this weight is bounded for $x \geq 0$, and unbounded for $x \leq 0$.

Proposition B.4. *For $d \in (0, 1)$ and exponents*

$$\alpha_- \in (0, 1), \quad \alpha_+ = 1, \tag{B.40}$$

consider an exponential weight $w(x)$ as in (B.39)*. Then, for a critical invading front, the essential spectrum of the linear operator $\mathcal{L}$* (B.35)*,*

$$\mathcal{L} : H^2(\mathbb{R}) \times H^2(\mathbb{R}) \to L^2(\mathbb{R}) \times L^2(\mathbb{R}), \tag{B.41}$$

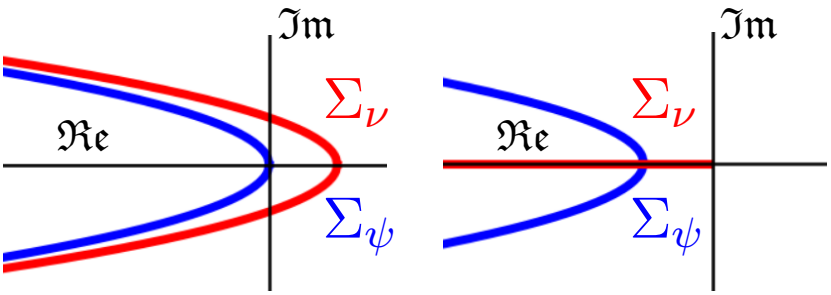

Figure B.2: The two critical parts of the essential spectrum of $\mathcal{L}$ as in Proposition B.4, defined in (B.49) *and* (B.57)*. On the left, the essential spectrum is unstable in an unweighted space. On the right, the essential spectrum is stabilized via an exponential weight, with Exponents* (B.40)*.*

is bounded to the right by the union of three parabolas (B.53)*,* (B.57) *and* (B.58)*, that lie in the strict negative half-plane, except for the half-line*

$$\Sigma_\nu = \left\{\lambda \in \mathbb{C} \middle| \, \mathfrak{Re}\lambda \leq 0, \mathfrak{Im}\lambda = 0\right\}. \tag{B.42}$$

The proof of Proposition B.4 will be given below. The parabola which we need to stabilize with an appropriate weight and the set Σ_η are depicted in Figure B.2. Precisely this type of essential spectrum is considered in [48], and we can use their estimates regarding the long-time behavior of $\mathcal{L}$. So far, we could not analyze the discrete spectrum of $\mathcal{L}$ analytically, and need to make the following critical

Assumption on the discrete spectrum: In the Setting of the above Proposition B.4, let Σ_d be the discrete spectrum of $\mathcal{L}$. Assume that there exist $\delta_0, \delta_1 > 0$, such that for the region

$$\Omega := \left\{\lambda \in \mathbb{C} \middle| \, \mathfrak{Re}\lambda \geq -\delta_0 - \delta_1 \cdot |\mathfrak{Im}\lambda|\right\} \tag{B.43}$$

it holds that

$$\Omega \cap \Sigma_d = \emptyset. \tag{B.44}$$

We verify this assumption numerically, presented in Appendix B.4.2. Note that we require $0 \notin \Sigma_d$. For an invading front $a(x), i(x)$, it is easy to see that the symbolic equation $\mathcal{L}(a', i') = 0$ holds. However, the critical front behaves like xe^{-x} as $x \to +\infty$, so its derivative is not an element of the considered weighted space.

Proof of Proposition B.4. For any non-negative traveling wave, $a(x)$ vanishes as $x \to \pm\infty$, and $i(x)$ converges. Moreover, both converge exponentially fast at both ends. The same applies to the matrices $M(x, \lambda)$, which we

call exponentially localized. In this setting it is a well-known result [130, 56] that the essential spectrum of $\mathcal{L} : H^2 \to L^2$ is bounded to the right by the spectrum of the limit matrices $M(\pm\infty, \lambda)$: those values of $\lambda \in \mathbb{C}$, for which one of $M(\pm\infty, \lambda)$ is defect. Denoting as $\mathcal{E}(M)$ the Eigenvalues of a matrix M, the essential spectrum of $\mathcal{L}$ is thus bounded by the set

$$\begin{aligned} M_{Ess} = &\Big\{\lambda \in \mathbb{C}\Big| \exists\, \mu \in \mathcal{E}\big(M(+\infty, \lambda)\big) : \mathfrak{Re}(\mu) = 0\Big\} \\ &\cup \Big\{\lambda \in \mathbb{C}\Big| \exists\, \mu \in \mathcal{E}\big(M(-\infty, \lambda)\big) : \mathfrak{Re}(\mu) = 0\Big\}. \end{aligned} \tag{B.45}$$

The region to the right of this set is referred to as *region of consistent splitting*, since the dimension of the unstable spectrum of $M(-\infty, \lambda)$ and the dimension of the stable spectrum of $M(+\infty, \lambda)$ add up to the full dimension of the system. In the following, we focus on the critical invading fronts, but in principle, technique and result can be applied to the other critical traveling waves of the system (with minimal speed depending on the chosen limits).

For $d \in (0, 1)$, consider now an invading front $a(x), i(x)$ with speed $c = 2$. We first analyze the matrix $M(+\infty, \lambda)$. Given that $i_{+\infty} = 0$ and with Weight (B.39), the limit of $M(x, \lambda)$ (B.36) at $x = +\infty$ is given by

$$\begin{pmatrix} 0 & 1 & 0 & 0 \\ \lambda - 1 + 2\alpha_+ - \alpha_+^2 & -2 + 2\alpha_+ & 0 & 0 \\ 0 & 0 & 0 & 1 \\ -\frac{r}{d} & 0 & \frac{\lambda + 2\alpha_+ - d\alpha_+^2}{d} & -\frac{2 - 2d\alpha_+}{d} \end{pmatrix}. \tag{B.46}$$

This matrix has two pairs of Eigenvalues:

$$\nu_\pm(\lambda, \alpha_+) = -1 \pm \sqrt{i_{+\infty} + \lambda} + \alpha_+, \tag{B.47}$$

$$\eta_\pm(\lambda, \alpha_+) = \frac{1}{d}\big(-1 \pm \sqrt{d\lambda + 1}\big) + \alpha_+. \tag{B.48}$$

We define the set

$$\Sigma_\nu := \big\{\lambda \in \mathbb{C}\big| \mathfrak{Re}\big(\nu_+(\lambda)\big) = 0\big\}. \tag{B.49}$$

For $w \equiv 1$ (if $\alpha_+ = 0$), the set Σ_ν is a parabola that goes into the right half-plane, as depicted in Figure B.2. In order to stabilize it, we need to operate in a space with weight

$$w(x) = e^{-\frac{c}{2}x} = e^{-x}, \qquad \forall x \geq 1. \tag{B.50}$$

This is the only possible choice for stabilizing the front of a critical FKPP-wave, a classical result, check [132, 47]. For $\alpha_+ = 1$, the Eigenvalues of $M(+\infty, \lambda)$ are then given by

$$\nu_\pm(\lambda, 1) = \pm\sqrt{\lambda}, \quad \eta_\pm(\lambda, 1) = \frac{1}{d}\Big(d - 1 \pm \sqrt{d\lambda + 1}\Big). \tag{B.51}$$

The pair $\nu_\pm$ creates an essential spectrum that lies on the negative real axis and goes up to the origin:

$$\Sigma_\nu = \Big\{ \lambda \in \mathbb{C} \big| \, \mathfrak{Re}\lambda \leq 0, \mathfrak{Im}\lambda = 0 \Big\}. \tag{B.52}$$

Since $d \in (0,1)$, the Eigenvalue $\eta_-(\lambda)$ does not touch the imaginary axis, only the Eigenvalue $\eta_+(\lambda)$ crosses the imaginary axis along a parabola that lies in the strict negative half-plane:

$$\Sigma_\eta = \Big\{ \lambda \in \mathbb{C} \big| \, \mathfrak{Re}\lambda = \frac{1}{d}\big(2(1-d)^2 - 1 - |d\lambda + 1|^2\big) \Big\}. \tag{B.53}$$

We now consider the other limit, $M(-\infty, \lambda)$, given by

$$\begin{pmatrix} 0 & 1 & 0 & 0 \\ \lambda + i_{-\infty} - 1 + 2\alpha_- - \alpha_-^2 & -2 + 2\alpha_- & 0 & 0 \\ 0 & 0 & 0 & 1 \\ -\frac{r + i_{-\infty}}{d} & 0 & \frac{\lambda + 2\alpha_- - d\alpha_-^2}{d} & -\frac{2 - 2d\alpha_-}{d} \end{pmatrix}, \tag{B.54}$$

for some $i_{-\infty} \in (1,2)$, and Eigenvalues

$$\sigma_\pm(\lambda, \alpha_-) = -1 \pm \sqrt{i_{-\infty} + \lambda} + \alpha_-, \tag{B.55}$$

$$\psi_\pm(\lambda, \alpha_-) = \frac{1}{d}\big(-1 \pm \sqrt{d\lambda + 1}\big) + \alpha_-. \tag{B.56}$$

In order to stabilize ψ_+ away from the origin, we can pick any $\alpha_- > 0$, leading to the parabola

$$\Sigma_\psi := \Big\{ \lambda \in \mathbb{C} \big| \, \mathfrak{Re}\lambda = \frac{1}{d}\big(2(1 - d\alpha_-)^2 - 1 - |\lambda + 1|\big) \Big\}. \tag{B.57}$$

As long as $\alpha_- < 2/d$, the Eigenvalue ψ_- does not touch the imaginary axis. The Eigenvalue σ_+ crosses the imaginary axis along a parabola that lies in the strict negative half-plane:

$$\Sigma_\sigma := \Big\{ \lambda \in \mathbb{C} \big| \, \mathfrak{Re}\lambda = -i_{-\infty} - 2(1 - \alpha_-)^2 - |i_{-\infty} + \lambda| \Big\}. \tag{B.58}$$

Lastly, we check that we do not overstabilize σ_-. It holds that

$$\mathfrak{Re}\big(\sigma_-(\lambda)\big) = 0 \;\Leftrightarrow\; \alpha_- - 1 = \mathfrak{Re}\big(+ \sqrt{i_{-\infty} + \lambda}\big). \tag{B.59}$$

The set $\{\mathfrak{Re}\big(\sigma_-(\lambda)\big) = 0\}$ is obviously empty as long as

$$\alpha_- < 1. \tag{B.60}$$

□

B.2.4 Estimating the long-time behavior

We prove the stability of the critical invading front using estimates by Fayé and Holzer [48]. By controlling the behavior of the Evans function (and thereby of the pointwise Green's function) in the neighborhood of the essential spectrum, they prove the following decay of the temporal Green's function:

Theorem B.5 (cf. Prop. 4.1 and Lemma 5.1 in [48]). *For $\mathcal{L}$ with essential spectrum as in Proposition B.4, and given that the discrete spectrum of $\mathcal{L}$ fulfills Assumption* (B.44)*, the temporal Green's function $\mathcal{G}(t,x,y)$ for $\partial_t(u,v) = \mathcal{L}(u,v)$ satisfies the following estimates: there exists constants $C,\kappa > 0$, such that for all pairs of indices $i,j \in \{1,2\}$ and for all $x,y \in \mathbb{R}$:*

$$\left|\mathcal{G}_{ij}(t,x,y)\right| \leq C\frac{1}{t^{1/2}}e^{-\frac{|x-y|^2}{\kappa t}} \qquad \forall t<1, \tag{B.61}$$

$$\int_{\mathbb{R}} \left|\mathcal{G}_{ij}(t,x,y)\right| \cdot |h(y)|\, dy \leq C \cdot ||h||_\infty \qquad \forall t<1. \tag{B.62}$$

Moreover, for all $t \geq 1$ and $x \in \mathbb{R}$:

$$\int_{\mathbb{R}} \left|\mathcal{G}_{i,j}(t,x,y)\right| \cdot |h(y)|\, dy \leq C \cdot \frac{1+|x|}{(1+t)^{3/2}} \int_{\mathbb{R}} (1+|y|)\cdot |h(y)|\, dy. \tag{B.63}$$

In [48], the authors prove a local stability result for the critical traveling waves of a Lotka-Volterra model with two species. They consider an integrable weight $w(x)$ and follow the reasoning behind Inequality (B.25). We extend their proof by using the a-priori bounds that we have for the left tail of the system, see (B.32). The following Lemma gives control of the resulting integrals over time:

Lemma B.6 (Lemma 2.3 in [166]). *Let $\alpha,\beta,\gamma,t > 0$ with $\alpha \leq \beta+\gamma-1$. If either $\alpha \leq \beta, \gamma \neq 1$, or $\alpha < \beta, \gamma = 1$, then there exists a constant C such that*

$$\int_0^{\frac{t}{2}} \frac{1}{(1+t-s)^\beta}\frac{1}{(1+s)^\gamma}\, ds \leq C\frac{1}{(1+t)^\alpha}. \tag{B.64}$$

Similarly, if either $\alpha \leq \gamma, \beta \neq 1$, or $\alpha < \gamma, \beta = 1$, then

$$\int_{\frac{t}{2}}^t \frac{1}{(1+t-s)^\beta}\frac{1}{(1+s)^\gamma}\, ds \leq C\frac{1}{(1+t)^\alpha}. \tag{B.65}$$

We can now prove the stability of the critical front:

Proof of Theorem B.2. We adopt the notation introduced in Section B.2.1. That is, we consider the vector $p = (u,v)$, and write $|p(t,x)| = ||p(t,x)||_1$. Note that since $|wu| = |\tilde{A}| \leq 1$, all reaction-terms of the perturbation System (B.17) are at most linear in $|p|$. Thus, by a standard Gronwall estimate and

a fixed-point argument, a unique smooth solution (that can grow at most exponentially over time) of System (B.17) exists for arbitrarily long times, check e.g. [138, Ch. 14], and [135, Thm. 46.4 ff.].

We will prove that

$$\Theta(t) := \sup_{s\le t}\sup_{x\in\mathbb{R}} \frac{(1+s)^{3/2}}{1+|x|}|p(s,x)| \tag{B.66}$$

is bounded uniformly in $t \geq 0$, if the initial data is small enough. We introduce a border $B \leq 0$ to be specified later, and split the Duhamel Formula (B.23):

$$|p(t,x)| \leq \Big| \int_{\mathbb{R}} \mathcal{G}(t,x,y)p(0,y)\,dy\Big| \tag{B.67}$$

$$+ \Big| \int_0^t ds \int_{-\infty}^{B} \mathcal{G}(t-s,x,y)N(p)(s,y)\,dy\Big| \tag{B.68}$$

$$+ \Big| \int_0^t ds \int_{B}^{+\infty} \mathcal{G}(t-s,x,y)N\big(p\big)(s,y)\,dy\Big|. \tag{B.69}$$

For $y \geq B$, we use the exponential decay of $w(y)$, whereas for $y \leq B$, we use the exponential decay of $A(t,y)$, see (B.32). Theorem B.5 yields different results for $\mathcal{G}$ for $t \leq 1$ and $t \geq 1$, thus we also differentiate the above terms for $t-s \leq 1$ and $t-s \geq 1$. In the following, we let C be a universal constant that does not depend on B, whereas C_B will be a universal constant that does.

We shift the given traveling wave $a(x), i(x)$, such that there exists a $\delta_I > 0$ with

$$i(x) \geq 1 + 2\delta_I \qquad \forall x \leq 0. \tag{B.70}$$

We assume that $||\tilde{I}(0,x)||_\infty \leq \delta_I$, then

$$I(0,x) = i(x) + \tilde{I}(0,x) \geq 1 + \delta_I \qquad \forall x \leq 0. \tag{B.71}$$

For the moment, we also assume that

$$|\tilde{I}(t,x=0)| = |v(t,x=0)| \leq \delta_I \qquad \forall t \geq 0, \tag{B.72}$$

which in particular implies that

$$I(t,x=0) \geq 1 + \delta_I \qquad \forall t \geq 0. \tag{B.73}$$

We will verify (B.72) a posteriori, by proving that the perturbations stay small. Given (B.71) and (B.72), we can apply Proposition B.3, the Feynman-Kac formula. As a result, there exists an exponent $\zeta > 0$, such that

$$|N(p)(t,x)| = \big|w(x)u(t,x)\cdot\big(u(t,x)+v(t,x)\big)\big|$$

$$\begin{aligned} &\leq A(t,x)\cdot\big|p(t,x)\big| && (B.74)\\ &\leq Ce^{\zeta x}\cdot\big|p(t,x)\big| && \forall x\leq B\leq 0. \end{aligned}$$

In contrast, for $x \geq B$, we will use the general bound

$$|N(p)(s,x)| \leq w(x)\cdot|p(t,x)|^2 \qquad \forall x\in\mathbb{R}. \qquad (B.75)$$

Now choose any $\epsilon \leq \delta_I$. We estimate (B.67), (B.68) and (B.69) separately, starting with

1) The long-time case $t \geq 1$

By Estimate (B.63) of Theorem B.5, the linear Part (B.67) is bounded by

$$\Big|\int_{\mathbb{R}} G(t,x,y)p(0,y)dy\Big| \leq C\frac{1+|x|}{(1+t)^{3/2}}\int_{\mathbb{R}}(1+|y|)\cdot|p(0,y)|dy. \qquad (B.76)$$

For the moment, we only require that

$$P(0) := ||p(0,x)\cdot(1+|x|)||_{L^1(\mathbb{R})} \leq 1, \qquad (B.77)$$

then the above expression is of order $(1+|x|)/(1+t)^{3/2}$.

Regarding the nonlinear part, we first consider the case $t-s\leq 1$. For the back of the wave, we use the exponential Decay (B.75) and Estimate (B.62) of Theorem B.5:

$$\begin{aligned} &\int_{t-1}^{t} ds\int_{-\infty}^{B}\big|\mathcal{G}(t-s,x,y)\big|\cdot|N(p)(s,y)|dy\\ &\leq C\int_{t-1}^{t} ds\int_{-\infty}^{B}\big|\mathcal{G}(t-s,x,y)\big|\cdot e^{\zeta y}|p(t,y)|\,dy\\ &\leq C\int_{t-1}^{t} ds\int_{-\infty}^{B}\big|\mathcal{G}(t-s,x,y)\big|\cdot e^{\zeta y}\Theta(s)\frac{1+|y|}{(1+s)^{3/2}}\,dy \qquad (B.78)\\ &\leq C\Theta(t)\frac{1}{(1+t)^{3/2}}\int_{-\infty}^{B}\big|\mathcal{G}(t-s,x,y)\big|\cdot e^{\zeta y}(1+|y|)\,dy\\ &\leq C\Theta(t)\frac{1}{(1+t)^{3/2}}\cdot\sup_{y\leq B}\big\{e^{\zeta y}(1+|y|)\big\}. \end{aligned}$$

Note that by choosing $B \leq 0$ sufficiently small, the supremum in the last term can be made arbitrarily small.

For $x \geq B$, we use the fact $w(x)\cdot(1+|x|)^2$ is bounded in $||.||_\infty$. We apply Estimate (B.62) of Theorem B.5:

$$\begin{aligned} &\int_{t-1}^{t} ds\int_{B}^{\infty}\big|\mathcal{G}(t-s,x,y)\big|\cdot|N(p)(s,y)|\,dy\\ &\leq\int_{t-1}^{t} ds\int_{B}^{\infty}\big|\mathcal{G}(t-s,x,y)\big|\cdot\Theta(s)^2\frac{(1+|y|)^2}{(1+s)^3}w(y)\,dy \end{aligned}$$

$$\leq C\Theta(t)^2 \frac{1}{(1+t)^3} \int_{t-1}^{t} ds \int_{B}^{\infty} \left|\mathcal{G}(t-s,x,y)\right| \cdot (1+|y|)^2 w(y)\, dy \tag{B.79}$$
$$\leq C_B \Theta(t)^2 \frac{1}{(1+t)^3}.$$

Now consider $t - s \geq 1$. Regarding $y \leq B$, we again use Bound (B.75), and Estimate (B.63) of Theorem B.5:

$$\begin{aligned}
&\int_0^{t-1} ds \int_{-\infty}^{B} \left|\mathcal{G}(t-s,x,y)\right| \cdot |N(p)(s,y)|\, dy \\
&\leq C \int_0^{t-1} ds \int_{-\infty}^{B} \left|\mathcal{G}(t-s,x,y)\right| \cdot e^{\zeta y} |p(t,y)|\, dy \\
&\leq C \int_0^{t-1} ds \int_{-\infty}^{B} \left|\mathcal{G}(t-s,x,y)\right| \cdot e^{\zeta y} \Theta(s) \frac{1+|y|}{(1+s)^{3/2}}\, dy \qquad \text{(B.80)} \\
&\leq C\Theta(t) \cdot (1+|x|) \int_0^t \frac{1}{(1+t-s)^{3/2}} \frac{1}{(1+s)^{3/2}}\, ds \int_{-\infty}^{B} e^{\zeta y} (1+|y|)^2\, dy
\end{aligned}$$

We apply Lemma B.6 to bound the integral over time:

$$\leq C\Theta(t) \frac{1+|x|}{(1+t)^{3/2}} \int_{-\infty}^{B} e^{\zeta y} (1+|y|)^2\, dy. \tag{B.81}$$

Again, note that we can make the last integral as small as we want if we shift B appropriately.

Regarding $y \geq B$, by Estimate (B.63) of Theorem B.5:

$$\begin{aligned}
&\int_0^{t-1} ds \int_{B}^{+\infty} \left|\mathcal{G}(t-s,x,y)\right| \cdot |N(p)(s,y)|\, dy \\
&\leq \int_0^{t-1} ds \int_{B}^{\infty} \left|\mathcal{G}(t-s,x,y)\right| \cdot \Theta(s)^2 \frac{(1+|y|)^2}{(1+s)^3} w(y)\, dy \\
&\leq C\Theta(t)^2 (1+|x|) \int_0^t \frac{1}{(1+t-s)^{3/2}} \frac{1}{(1+s)^3}\, ds \int_{B}^{\infty} (1+|y|)^3 w(y)\, dy \\
&\leq C_B \Theta(t)^2 (1+|x|) \int_0^t \frac{1}{(1+t-s)^{3/2}} \frac{1}{(1+s)^3}\, ds \qquad \text{(B.82)}
\end{aligned}$$

We apply Lemma B.6 to bound the integral over time, yielding

$$\leq C_B \Theta(t)^2 \frac{1+|x|}{(1+t)^{3/2}}. \tag{B.83}$$

Now, for all $t \geq 1$, combining our estimates (B.76), (B.79), (B.80), (B.81), (B.83) results in

$$|p(t,x)| \leq CP(0) \frac{1+|x|}{(1+t)^{3/2}} \tag{B.84}$$

$$+ C\Theta(t)\frac{1}{(1+t)^{3/2}} \cdot \sup_{y\le B}\left\{e^{\zeta y}(1+|y|)\right\} \tag{B.85}$$

$$+ C_B\Theta(t)^2\frac{1}{(1+t)^{3/2}} \tag{B.86}$$

$$+ C\Theta(t)\frac{1+|x|}{(1+t)^{3/2}}\int_{-\infty}^{B} e^{\zeta y}(1+|y|)^2\,dy \tag{B.87}$$

$$+ C_B\Theta(t)^2\frac{1+|x|}{(1+t)^{3/2}}. \tag{B.88}$$

Next, choose B sufficiently small such that the constants in (B.85) and (B.87), the terms that are linear in Θ, are both bounded by $1/8$. Then, we can simplify the above to

$$|p(t,x)| \le CP(0)\frac{1+|x|}{(1+t)^{3/2}} + \frac{1}{4}\Theta(t)\frac{1+|x|}{(1+t)^{3/2}} + C_B\Theta(t)^2\frac{1+|x|}{(1+t)^{3/2}}. \tag{B.89}$$

Inserting our definition of Θ, see (B.66), we get

$$\Theta(t) \le CP(0) + \frac{1}{4}\Theta(t) + C_B\Theta(t)^2 \qquad \forall t \ge 1. \tag{B.90}$$

2) The short-time case $t < 1$

Estimate (B.62) of Theorem B.5 yields the following bound for the linear Part (B.67):

$$\int_{\mathbb{R}} \left|\mathcal{G}(t,x,y)\right| \cdot |p(0,y)|\,dy \le C \cdot ||p(0,x)||_\infty. \tag{B.91}$$

For the nonlinear part, we again split the expression into two parts. This time, we use the pointwise Estimate (B.61) of Theorem B.5, valid for short times:

$$\begin{aligned}
&\int_0^{t-1} ds \int_{-\infty}^{B} \left|\mathcal{G}(t-s,x,y)\right| \cdot |N(p)(s,y)|\,dy \\
&\le \int_0^{t-1} ds \int_{-\infty}^{B} \left|\mathcal{G}(t-s,x,y)\right| \cdot e^{\zeta y}|p(t,y)|\,dy \\
&\le \Theta(t)\frac{1}{(1+t)^{3/2}} \cdot \int_0^{t-1} ds \int_{-\infty}^{B} \left|\mathcal{G}(t-s,x,y)\right| \cdot e^{\zeta y}(1+|y|)\,dy \qquad \text{(B.92)} \\
&\le C\Theta(t)\int_0^{t-1} ds \int_{-\infty}^{B} \frac{1}{t^{1/2}} e^{-\frac{|x-y|^2}{\kappa t}} e^{\zeta y}(1+|y|)\,dy.
\end{aligned}$$

The last integral is a short-time heat kernel applied to the exponentially decaying function $e^{\zeta x}(1+|x|)$. We choose B appropriately such that the entire above expression is bounded by

$$\le \frac{1}{16}\Theta(t). \tag{B.93}$$

Considering $y \geq B$:

$$\begin{aligned}
&\int_0^{t-1} ds \int_B^{+\infty} \left|\mathcal{G}(t-s,x,y)\right| \cdot |N(p)(s,y)|\, dy \\
&\leq \int_0^{t-1} ds \int_B^{+\infty} \left|\mathcal{G}(t-s,x,y)\right| \cdot \Theta(s)^2 \frac{(1+|y|)^2}{(1+s)^3}\, dy \\
&\leq C\Theta(t)^2 \int_0^{t-1} ds \int_B^{+\infty} \frac{1}{t^{1/2}} e^{-\frac{|x-y|^2}{\kappa t}} (1+|y|)^2\, dy \qquad \text{(B.94)} \\
&\leq C_B \Theta(t)^2.
\end{aligned}$$

In view of (B.91), (B.93), (B.94), we see that for all $t < 1$:

$$|p(t,x)| \leq C\, ||p(0,x)||_{L^\infty(\mathbb{R})} + \frac{1}{16}\Theta(t) + C_B\Theta(t)^2. \qquad \text{(B.95)}$$

This implies that for small times, by the Definition of Θ (B.66):

$$\Theta(t) \leq C\, ||p(0,x)||_{L^\infty(\mathbb{R})} + \frac{1}{4}\Theta(t) + C_B\Theta(t)^2 \qquad \forall t < 1. \qquad \text{(B.96)}$$

3) Convergence given small initial data

To control both the short-time Bound (B.96) and the large-time Bound (B.90), we will consider initial data where

$$Q(0) := ||p(0,x)||_{L^\infty(\mathbb{R})} + ||p(0,x)\cdot(1+|x|)||_{L^1(\mathbb{R})} \qquad \text{(B.97)}$$

is sufficiently small. Regarding both the long-time and the short-time case, we first choose a border $B \in \mathbb{R}$ such that both (B.96) and (B.90) are valid, resulting in

$$\Theta(t) \leq CQ(0) + \frac{1}{4}\Theta(t) + C_B\Theta(t)^2 \qquad \forall t \geq 0. \qquad \text{(B.98)}$$

Without loss of generality, we may assume that $C \geq 1$. Consider initial data that are small enough to fulfill

$$2CQ(0) < \epsilon \quad \text{and} \quad 4CC_BQ(0) < \frac{1}{2}, \qquad \text{(B.99)}$$

where $\epsilon \leq \delta_I$, with δ_I chosen in (B.70). Then, at $t = 0$:

$$\Theta(0) = \sup_{x\in\mathbb{R}} \frac{|p(0,x)|}{1+|x|} \leq Q(0) < 2CQ(0) < \epsilon. \qquad \text{(B.100)}$$

For such initial data, our critical Assumption (B.72) holds for small times $t > 0$, since $\Theta(t)$ is continuous in t. Now suppose that there exists a first

time $T \in (0, \infty)$ such that $\Theta(T) = 2CQ(0)$ for the first time. But then, by (B.98):

$$\begin{aligned}\Theta(t) &\leq CQ(0) + \frac{1}{4}\Theta(t) + C_B\Theta(t)^2 \\ &\leq CQ(0) + \frac{1}{4}2CQ(0) + C_B 4C^2 Q(0)^2 \\ &\leq CQ(0) + \frac{1}{2}CQ(0) + CQ(0)\big[4CC_B Q(0)\big] \\ &< 2CQ(0),\end{aligned} \tag{B.101}$$

a contradiction to our assumption. As a result, it holds that

$$\Theta(t) < 2CQ(0) < \epsilon \qquad \forall t \geq 0, \tag{B.102}$$

which not only proves that the perturbation decays, but also shows that the necessary Bound (B.72) holds for all $t \geq 0$. □

B.3 Construction of the traveling waves

B.3.1 Overview and notation

In the following, we refer to the Wave System (B.3) as S_0 if $d = 0$, and to S_d for $d > 0$. We cite the result for the traveling waves of S_0, which was the subject of a previous study:

Theorem B.7 (Thm. 1.1 in [92]). *For $d = 0$ and $r \geq 0, c > 0$, consider System S_0 (B.3). Set $i_c := \max\{0, 1 - c^2/4\}$. For each pair $i_{-\infty}, i_{+\infty} \in \mathbb{R}_0^+$ such that*

$$i_{+\infty} \in [i_c, 1), \qquad i_{-\infty} = 2 - i_{+\infty}, \tag{B.103}$$

there exists a unique non-negative traveling wave $a, i \in C^\infty(\mathbb{R}, \mathbb{R}^2)$ such that

$$\lim_{x\to\pm\infty} a(x) = 0, \qquad \lim_{x\to\pm\infty} i(x) = i_{\pm\infty}. \tag{B.104}$$

The function $i(x)$ is decreasing, whereas $a(x)$ has a unique local and global maximum. If $\frac{c^2}{4} + i_{+\infty} - 1 = 0$, then the distance of the front to its limit behaves like $x \cdot e^{-\frac{c}{2}x}$ asymptotically as $x \to +\infty$. If $\frac{c^2}{4} + i_{+\infty} - 1 > 0$, then convergence as $x \to +\infty$ is purely exponential. Convergence as $x \to -\infty$ is purely exponential in all cases. The rates of convergence are

$$\begin{aligned}\mu_{-\infty} &= -\frac{c}{2} + \sqrt{\frac{c^2}{4} + i_{\pm\infty} - 1} > 0, \\ \mu_{+\infty} &= \frac{c}{2} - \sqrt{\frac{c^2}{4} + i_{\pm\infty} - 1} > 0.\end{aligned} \tag{B.105}$$

Moreover, these are all bounded, non-negative, non-constant and twice differentiable solutions of Eq. (B.3) for $d = 0$.

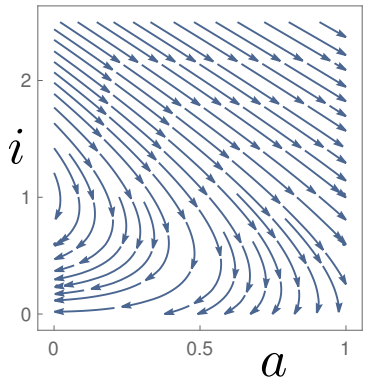

Figure B.3: Two-dimensional representation of the family of traveling waves of S_0 for $c = 2$ and $r = 0$. A unique trajectory emerges from each point where $i_{-\infty} > 1$, and converges to a limit where $i_{+\infty} < 1$, where $i_{-\infty} + i_{+\infty} = 2$. For $i_{-\infty} > 2$, the trajectory eventually becomes negative (even though it still seems to converge).

The bound $i_{+\infty} \geq 1 - c^2/4$ is classical for FKPP-fronts. If it is not fulfilled, the solutions spiral around their limit as $x \to +\infty$, see Section B.3.2.1. Thus, they become negative and are physically irrelevant.

For the entire Section B.3, keep the phase-plot of S_0 in Figure B.3 in mind. Qualitatively, we prove that this portrait remains valid for S_d: there exists a family of solutions, that continuously vary along the limits $i_{\pm\infty}$. The only change is a perturbation estimate of type

$$i_{-\infty} + i_{+\infty} = 2 + \mathcal{O}(d), \tag{B.106}$$

which replaces the precise Statement (B.103) for $d = 0$. Since we focus on the invading fronts, we consider only the case $c \geq 2$, the result is given in Theorem B.24.

We transform the wave Eq. (B.3) into an equivalent System of ODEs. We denote differentiation w.r.t. x by a prime, and introduce two auxiliary variables $b = a'$ and $j = i'$. For $d \neq 0$, this system in coordinates $(a, b, i, j) \in \mathbb{R}^4$ reads

$$\frac{d}{dx}\begin{pmatrix} a \\ b \\ i \\ j \end{pmatrix} = \begin{pmatrix} b \\ a(a+i) - a - cb \\ j \\ -\frac{1}{d}[cj + ra + a(a+i)] \end{pmatrix}. \tag{B.107}$$

By abuse of notation, we will denote $a' = b$ and $i' = j$, since introducing two auxiliary variables only obfuscates the system.

Section B.3 is organized as follows: for $d > 0$ and $K > 1$, we analyze the unstable manifold of the fixed point $(a, a', i, i') = (0, 0, K, 0)$. It is one-dimensional and has one branch that is asymptotically non-negative, which we call $M_d^-(K)$. In Section B.3.2, we will prove that any finite segment

of $M_d^-(K)$ is continuous both in d and K. For $d > 0$, this will follow from standard perturbation theory for dynamical systems. For passing from $d = 0$ to $d \sim 0$, we use geometric singular perturbation theory due to Fénichel [84]. In Section B.3.3, we prove that a traveling wave $M_d^-(K)$ persists under small perturbations in d, up to its limit as $z \to +\infty$. The estimate $i_{-\infty} + i_{+\infty} = 2 + \mathcal{O}(d)$ is proven in Section B.3.4. We use all previous results to prove the existence of a family of non-negative traveling wave solutions in Section B.3.5. Given the existence of these non-negative traveling waves, we conclude that there also must be an invading front among those.

B.3.2 Dynamics around the fixed points

B.3.2.1 A degenerate linearization

At a fixed point $(a, a', i, i') = (0, 0, K, 0)$, the Jacobian of the system has Eigenvalues

$$\begin{aligned} \lambda_1 &= 0, & \lambda_2 &= -\frac{c}{d}, \\ \lambda_3 &= -\frac{c}{2} - \sqrt{\frac{c^2}{4} + K - 1}, & \lambda_4 &= -\frac{c}{2} + \sqrt{\frac{c^2}{4} + K - 1}. \end{aligned} \tag{B.108}$$

The Eigenvalue λ_2 is new compared to the unperturbed system, all other Eigenvalues remain the same. The associated eigenvectors are given by

$$\begin{aligned} e_1 &= \begin{pmatrix} 0 \\ 0 \\ 1 \\ 0 \end{pmatrix}, & e_2 &= \begin{pmatrix} 0 \\ 0 \\ -\frac{d}{c} \\ 1 \end{pmatrix}, \\ e_3 &= \begin{pmatrix} -c\lambda_3 - d \cdot \lambda_3^2 \\ -c \cdot \lambda_3^2 - d \cdot \lambda_3^3 \\ K + r \\ \lambda_3(K + r) \end{pmatrix}, & e_4 &= \begin{pmatrix} -c\lambda_4 - d \cdot \lambda_4^2 \\ -c \cdot \lambda_4^2 - d \cdot \lambda_4^3 \\ K + r \\ \lambda_4(K + r) \end{pmatrix}. \end{aligned} \tag{B.109}$$

For $K \in [0, 1)$, corresponding to a possible limit as $x \to +\infty$, the Eigenvalues are real-valued if $K \geq 1 - c^2/4$. For $K = 0$, which is the limit of an invading front, we require that $c \geq 2$, otherwise converging trajectories can not stay non-negative: the a-component spirals around its limit 0 if λ_3 and λ_4 have an imaginary part.

For fixed $d > 0$, we first analyze the behavior around a fixed point $(a, a', i, i') = (0, 0, K, 0)$ locally. The Jacobian of the system at the fixed point is degenerate due to the continuum of fixed points, we apply center manifold theory to work out the higher moments of the approximation. A practical introduction to this topic has been written by J. Carr [30]. If we ensure that all Eigenvectors (B.109) are distinct, they span the entire $\mathbb{R}^4$. In this case, the Jacobian can be diagonalized and the calculations are standard:

no bifurcaction, neither in d nor K, occurs as long as all the Eigenvalues $\lambda_{2,3,4}$ remain real-valued and unequal zero.

If $K = 1$, then $\lambda_4 = 0$, and if $K = 1 - c^2/4$, then $\lambda_3 = \lambda_4$ and their eigenspaces become colinear. If we exclude these two cases, the result is as intuitive as it is comfortable: the center manifold locally coincides with the set of fixed points, a defect linearization with three hyperbolic directions and one constant direction is the result, see Proposition B.8. For the case $d = 0$, we present the rather standard calculations and the necessary changes of coordinates into the system of Eigenvectors in detail [92]. The following result is completely analogue:

Proposition B.8. *For $d > 0, c > 0$ and $K \in \mathbb{R}$ subject to the conditions*

$$K \neq 1, \quad K \neq 1 - c^2/4, \tag{B.110}$$

consider the fixed point $(0, 0, K, 0)$ of S_d. Then, in a neighborhood of the fixed point, the center manifold of the fixed point coincides with the set of points

$$\{a = a' = i' = 0,\, i \in \mathbb{R}\}. \tag{B.111}$$

Moreover, in this neighborhood, the flow S_d is homeomorphic to

$$\begin{pmatrix} p' \\ u' \\ v' \\ w' \end{pmatrix} = \begin{pmatrix} 0 \\ \lambda_2 \cdot u \\ \lambda_3 \cdot v \\ \lambda_4 \cdot w \end{pmatrix}, \tag{B.112}$$

where p, u, v, w are the coordinates in the system of Eigenvectors (B.109).

Proposition B.8 has two important implications. First, regarding the asymptotics as $x \to +\infty$, we can use Equation (B.112) to deduce

Corollary B.9. *For $c > 0, d > 0$ and $K \in (1 - \frac{c^2}{4}, 1)$, the fixed point $(0, 0, K, 0)$ of S_d is Lyapunov-stable, and trajectories asymptotically converge along $e_{2,3,4}$* (B.109).

Proof. Holds by (B.112), since $\lambda_2, \lambda_3, \lambda_4$ are real-valued and strictly negative. □

B.3.2.2 Continuity with respect to the parameters

Regarding the asymptotics as $x \to -\infty$, we get

Corollary B.10. *For $d > 0, c > 0, K > 1$, the fixed point $(0, 0, K, 0)$ of S_d has a fast unstable manifold of dimension one, associated to the Eigenvalue*

$$\lambda_4 = -\frac{c}{2} + \sqrt{\frac{c^2}{4} + K - 1} > 0. \tag{B.113}$$

This manifold has one branch such that $a, i > 0$ asymptotically, which we denote as $M_d^-(K)$. Outgoing from the fixed point, the asymptotic direction of the unstable manifold in coordinates (a, a', i, i') is given by

$$\begin{pmatrix} c\lambda_4 + d \cdot \lambda_4^2 \\ c \cdot \lambda_4^2 + d \cdot \lambda_4^3 \\ -(K+r) \\ -\lambda_4(K+r) \end{pmatrix}. \tag{B.114}$$

Locally, the manifold $M_d^-(K)$ is continuous in K.

The local continuity of $M_d^-(K)$ w.r.t K can be extended to arbitrarily finite segments:

Corollary B.11. *Let $d > 0, K_0 > 1, c > 0$ and choose any finite time-horizon $T \in \mathbb{R}$. Assume that the manifold $M_d^-(K_0, x)|_{x\in(-\infty,T]}$ exists, is smooth and bounded. Then, for K sufficiently close to K_0, each of the manifolds $M_d^-(K, x)|_{x\in(-\infty,T]}$ is smooth and bounded, and they have a representation that is continuous in K.*

Proof. The proof is a standard gluing argument: Fix some $K_0 > 1$ and a finite time-horizon $T \in \mathbb{R}$. Assume that the manifold $M_d^-(K_0, x)|_{x\in(-\infty,T]}$ exists, is smooth and bounded. Consider a small ball B_δ of radius $\delta > 0$ around the fixed point $(0, 0, K_0, 0)$, such that within B_δ, the flow is equivalent to the linearized Flow (B.112). Define the exit time

$$x_\delta := \sup_{x\in\mathbb{R}} \big\{\forall s \le x : M_d^-(K_0, s) \in B_\delta\big\}, \qquad x^* := \frac{x_\delta}{2}. \tag{B.115}$$

As $K \to K_0$, the trajectories $M_d^-(K, x)|_{x\in(-\infty,x^*]}$ are continuous in K, due to the local statement B.11. In particular, the points $M_d^-(K, x^*)$ converge to $M_d^-(K_0, x^*)$. We can now treat the rest of the trajectories

$$M_d^-(K, x)|_{x\in[x^*,T]} \tag{B.116}$$

as initial value problems with converging initial data. Since $[x^*, T]$ is a finite time-interval, this follows from a Gronwall estimate for locally Lipschitz systems, check for example Theorem II-1-2 and Remark II-1-3 in the textbook of Hsieh and Yasutaka [79]. □

Similarly, continuity of $M_d^-(K_0, x)|_{x\in(-\infty,T]}$ w.r.t. d holds. The result for $d \gg 0$ is standard: local continuity follows from center manifold theory, see e.g. Section 1.5 in the monograph of J. Carr [30]. Is is one of the fundamental tools for analyzing bifurcations, as explained by J. Guckenheimer and P. Holmes, see Sections 3.2 and 3.4 in [67]. The assumptions that the Eigenvectors (B.108) are distinct and that the Eigenvalues $\lambda_{2,3,4}$ are real-valued and non-zero are again crucial: they imply that locally in K and d, no bifurcation occurs. The local statement can easily be extended to arbitrary finite segments as before:

Proposition B.12. *Let $K > 1, d_0 > 0, c > 0$. For a finite time-horizeon $T \in \mathbb{R}$, assume that the manifold $M^-_{d_0}(K,x)|_{x\in(-\infty,T]}$ is smooth and bounded. There exists an open interval $I \subset \mathbb{R}^+_0, d_0 \in I$, such that for all $d \in I$, each of the manifolds $M^-_d(K,x)|_{x\in(-\infty,T]}$ is smooth and bounded, and they have a representation that is continuous in d.*

For passing from $d = 0$ to $d \sim 0$, we use geometric singular perturbation theory. The ODE-system with $d = 0$ is three-dimensional, as it is independent of i', but can be embedded into the $\mathbb{R}^4$, and then be perturbed smoothly when introducing a small diffusion $d > 0$. The resulting statement is analogue to Proposition B.12, the proof is presented in Appendix B.4.3:

Corollary B.13. *Let $K > 1, c > 0, r \geq 0$. First consider the fixed point $(\bar{a}, \bar{a}', \bar{i}) = (0, 0, K)$ of S_0, together with its one-dimensional unstable manifold $M^-_0(K)$. Fix any semi-open interval $x \in (-\infty, T]$, where T is finite, and assume that $M^-_0(K,x)|_{x\in(-\infty,T]}$ is smooth and bounded. Lift it naturally into $\mathbb{R}^4$ via the fourth coordinate $i' = -a(a+i+r)/c$.*

Now consider the perturbed system S_d. There exist some $d^* > 0$ such that for all $d \in (0, d^*)$: the fixed point $(a, a', i, i') = (0, 0, K, 0)$ has an adjacent one-dimensional unstable manifold $M^-_d(K,x)|_{x\in(-\infty,T]}$, that is continuous in d and converges to $M^-_0(K,x)|_{x\in(-\infty,T]}$ as $d \to 0$.

B.3.3 Persistence of traveling waves under perturbation

We will not only prove the existence of non-negative traveling waves of S_d, but also that they all share certain monotonicity properties. We consider only the case $c \geq 2$, since this is regime in which an invading front can exist.

Properties of traveling waves that are not invading fronts (TW): Let $K > 1, d \geq 0, c > 0$. Consider the manifold $M^-_d(K)$, and denote representing functions $a(x), a'(x), i(x), i'(x)|_{x\in\mathbb{R}}$. We say that $M^-_d(K)$ admits the traveling wave properties **(TW)** if the following holds:

1. $i'(x) < 0 \quad \forall x \in \mathbb{R}$,
2. $a(x) > 0 \quad \forall x \in \mathbb{R}$,
3. $i(x) \geq i_{+\infty} > 0 \quad \forall x \in \mathbb{R}$,
4. The function $a(x)$ has a unique local maximum, which is also the global one. At the phase-time of the maximum, it holds that $a + i \leq 1$.
5. The trajectory converges monotonously to its limit as $x \to +\infty$. There exists a finite phase-time x^*, such that for all $x \geq x^*$:

$$a'(x) < 0, \quad i''(x) > 0. \tag{B.117}$$

An invading front fulfills the same properties, with the exception that $\lim_{x\to+\infty} i(x) = 0$. However, the assumption $i(x) \geq \gamma > 0$ allows us to perturb the trajectory in such a way that the perturbed solutions stay non-negative. The properties **TW** have been proven for the non-negative traveling waves of S_0, as part of the proof of Theorem 3.1, see [92]. We prove that a given traveling wave persists under small perturbations in d:

Proposition B.14. *For $c \geq 2, d_0 \in [0, 3c/2)$ and $K \in (1, 2]$, assume that the manifold $M^-_{d_0}(K)$ admits the wave-properties **TW**. Then, there exists an open interval $I \subset \mathbb{R}^+_0, d_0 \in I$, such that for all $d \in I$: the manifold $M^-_d(K)$ also admits **TW**.*

The rest of Section B.3.3 is devoted to the proof of Proposition B.14. The required phase-space analysis is not relevant for the rest of the paper and can be skipped at first reading, we recommend to continue with Section B.3.4.

B.3.3.1 Monotonicity, non-negativeness, and an attractor

Our analysis begins with the fact that $i(x)$ must be monotone as long as the trajectory is non-negative:

Lemma B.15. *Let $K > 1, c > 0$ and $d > 0$. Along the manifold $M^-_d(K, x)$, the inequality*

$$i'(x) < 0 \tag{B.118}$$

holds as long as $a(x) > 0, i(x) \geq 0$.

Proof. By Corollary B.11: $i'(x) < 0$ as $x \to -\infty$. We assume that there exists a finite phase-time x^* such that $i'(x^*) = 0$ for the first time. This implies that $i(x^*)'' \geq 0$, since $i'(x) < 0$ for all $x < x^*$. However, it also holds that $di'' = -ci' - ra - a(a + i)$, which implies that $i''(x^*) < 0$ if $i(x^*) \geq 0$ and $a(x^*) > 0$. Thus, there can not be such a finite time x^*. □

Since we do not change the equation for $a(x)$ in Eq. (B.3), the following result – that traps $a(x)$ within a non-negative region – can be taken over from the unperturbed system. This statement relies on an analysis of the subsystem for $a(x)$ for fixed $i(x) = K$, and on the fact that $i(x)$ is monotone. We consider only wave-speeds $c \geq 2$, to simplify the representation:

Proposition B.16 (c.f. Thm. 6.1 and Prop. 6.4 in [92])**.** *For $c \geq 2, r \geq 0$ and $d \geq 0$, consider a solution of the Wave-Eq.* (B.107)*, that at time $x = 0$ is subject to the conditions*

$$a(0) > 0, \tag{B.119}$$
$$a'(0) = 0, \tag{B.120}$$
$$a(0) + i(0) \leq 1. \tag{B.121}$$

Assume further that there exists some $T \in (0, +\infty]$ *such that*

$$i(x) \geq 0,\ i'(x) \leq 0 \quad \forall x \in [0, T). \tag{B.122}$$

Then, $a(x)$ *is trapped in a non-negative attractor. It holds that*

$$a(x) > 0 \text{ and } a'(x) < 0 \qquad \forall x \in (0, T). \tag{B.123}$$

Moreover, if for some $\kappa \in (0, 1)$ *and* $x_\kappa \in (0, T)$*, it holds that*

$$a(x_\kappa) + i(x_\kappa) = 1 - \kappa, \tag{B.124}$$

then there exists a finite constant $L_\kappa \geq 0$*, that depends only on* κ*, such that*

$$\int_{s_1}^{s_2} a(x)\, dx \leq L_\kappa \cdot a(s_1) \quad \forall\, 0 \leq s_1 \leq s_2 \leq T. \tag{B.125}$$

Lemma B.15 and Proposition B.16 imply that along $M_d^-(K, x)$, we only have prove that $a(x)$ reaches a local maximum, and that $i(x) \geq 0$ for all $x \in \mathbb{R}$, then convergence and non-negativeness follow. As $i'(x)$ essentially depends on $a(x)$, Inequality (B.125) will be handy for proving that $i'(x) \to 0$. For S_0, we did this in Sections 6.3 and 6.4 of [92]. For S_d, the new term di'' needs to be dealt with, see the following Section B.3.3.2. Before, we conclude this section with another simple phase space argument:

Lemma B.17. *Let* $K > 1, c > 0, r \geq 0$ *and* $d > 0$*. Consider the manifold* $M_d^-(K, x)$*. If there exists some* $T \in \mathbb{R}$ *such that*

$$i(x) \geq 0 \quad \forall x \in (-\infty, T], \tag{B.126}$$

then $a(x)$ *has at most one local maximum, say at some phase-time* $x_0 \in (-\infty, T]$*. There, it holds that* $a(x_0) + i(x_0) \leq 1$*. Moreover:*

$$a(x) > 0,\ i'(x) < 0 \quad \forall x \in (-\infty, T]. \tag{B.127}$$

If $T = +\infty$*, then both* $a(x)$ *and* $i(x)$ *converge and stay non-negative.*

Proof. The manifold $M_d^-(K)$ leaves the fixed point in positive direction of a and negative direction of i. We have already proven that $i'(s) < 0$ as long as $a > 0, i \geq 0$. Assume that $a(s)$ has a first local maximum at some $x_0 \in \mathbb{R}$. There, it holds that

$$0 \geq a''(x_0) = a(x_0) \cdot \big(a(x_0) + i(x_0) - 1\big), \tag{B.128}$$

which implies that $a(x_0) + i(x_0) \leq 1$, since $a(x_0) > 0$. But since $i(s) \geq 0$ for all $s \in (-\infty, x]$, we can apply Proposition B.16 to trap $a(s)|_{x \in (x_0, x]}$: along this part of the trajectory, it holds that $a(x) > 0$ and $a'(x) < 0$. □

B.3.3.2 The tail of a perturbed trajectory

For the entire Section B.3.3.2, we work under the assumption that a reference trajectory $M^-_{d_0}(K)$ exists for some $d_0 \geq 0$, which we perturb when changing $d \sim d_0$:

Assumption: Let $K > 1, c \geq 2, r \geq 0$ and $d_0 \geq 0$. Assume that the manifold $M^-_{d_0}(K)$ admits properties **TW**, and choose four representing functions

$$\bar{a}(x), \bar{a}'(x), \bar{i}(x), \bar{i}'(x), \quad x \in \mathbb{R}. \tag{B.129}$$

Given $M^-_{d_0}(K)$, we vary the parameter d and track the perturbed trajectories. Therefore, we denote the representing functions of the manifolds $M^-_d(K)$ as

$$a_d(x), a'_d(x), i_d(x), i'_d(x), \quad x \in \mathbb{R}, \tag{B.130}$$

to emphasize their dependency on d.

The results of Proposition B.12 and Corollary B.13 are structurally similar: they yield continuity of arbitrarily large, but finite time-horizons of $M^-_d(K)$, when varying $d \geq 0$, resulting in the following Proposition B.18. It remains to control the tail as $x \to +\infty$ (for the result, see Prop. B.14: the wave proverties **TW** persist for d close to d_0).

Proposition B.18. *Let the manifold $M^-_{d_0}(K)$ be as above and choose a finite time-horizon $T \in \mathbb{R}$. For all $\epsilon > 0$, there exists an open interval $I \subset \mathbb{R}^+_0, d_0 \in I$, such that for all $d \in I$: the manifold $M^-_d(K,x)|_{x\in(-\infty,T]}$ is of distance at most ϵ to $M^-_{d_0}(K,x)|_{x\in(-\infty,T]}$ and is strictly non-negative.*

Proof. For the reference trajectory, note that there exists a $\gamma > 0$ such that

$$\bar{i}(x) \geq \gamma \quad \forall x \in (-\infty, T]. \tag{B.131}$$

If $d_0 = 0$, apply Corollary B.13, if $d_0 > 0$ apply Proposition B.12, both yield continuity in d: for all $\epsilon > 0$, there exists an open interval $I \subset \mathbb{R}^+_0, d_0 \in I$ such that for all $d \in I$:

$$\left|\left|M^-_d(K,x) - M^-_{d_0}(K,x)\right|\right|_\infty \leq \epsilon \qquad \forall x \in (-\infty, T]. \tag{B.132}$$

In particular, for $\epsilon \leq \gamma/2$:

$$i_d(x) \geq \bar{i}(x) - \epsilon \geq \gamma - \gamma/2 > 0 \qquad \forall x \in (-\infty, T]. \tag{B.133}$$

By Lemma B.17, this implies also positiveness of $a_d(x)|_{x\in(-\infty,T]}$. □

We trap $M^-_d(K)$ in the attractor from Proposition B.16:

Lemma B.19. *Let $M^-_{d_0}(K)$ as before. There exists a constant $\kappa \in (0,1)$, an open interval $I_0 \subset \mathbb{R}^+_0, d_0 \in I_0$, and a finite phase-time x_κ, such that for all $d \in I_0$:*

1. *the unstable manifold $M^-_d(K,x)|_{x\in(-\infty,x_\kappa]}$ is strictly positive and has a unique first local maximum of active particles at a finite phase-time $\tilde{x}_0(d) \in (-\infty, x_\kappa]$.*
2. *It holds that*

$$a'_d(x_\kappa) < 0, \quad a_d(x_\kappa) + i_d(x_\kappa) \leq 1 - \kappa.$$

Proof. On $M^-_{d_0}(K,x)$, there exists a unique sharp global maximum of $\bar{a}(x)$, say at some phase-time x_0. Choose a phase-time $x_\kappa > \tilde{x}$ so large, such that

$$\bar{a}(x_\kappa) + \bar{i}(x_\kappa) \leq 1 - 2\kappa, \quad \text{for some } \kappa \in (0,1), \tag{B.134}$$
$$\bar{a}'(x_\kappa) \leq 2\delta < 0, \quad \text{for some } \delta > 0, \tag{B.135}$$

which must exist since $M^-_{d_0}(K,x)$ admits **TW**.

Apply the previous Proposition B.18 over the interval $(-\infty, x_\kappa]$, such that we can control $M^-_d(K,x)|_{x\in(-\infty,x_\kappa]}$ for d in some open interval $I \subset \mathbb{R}^+_0$. We choose $|d - d_0|$ sufficiently small such that

$$i_d(x) > 0 \quad \forall x \in (-\infty, x_\kappa], \tag{B.136}$$
$$a_d(x_\kappa) + i_d(x_\kappa) \leq 1 - \kappa, \tag{B.137}$$
$$a'_d(x_\kappa) \leq \delta < 0. \tag{B.138}$$

By Corollary B.11: $a'_d(x) > 0$ as $x \to -\infty$. Hence, also $a_d(x)$ must have a local maximum before x_κ. It is unique since $i_d(x)|_{x\in(-\infty,x_\kappa]} > 0$ and by Lemma B.17. □

In view of Proposition B.16, we now have trapped M^-_d in a non-negative monotone attractor, as long as we can control $i_d \geq 0$. We first prove monotonicity of the tail as $x \to +\infty$:

Lemma B.20. *Consider $M^-_{d_0}(K), I_0$ and x_0 as in Lemma B.19. There exists a phase-time $x_{tail} \geq x_\kappa$, such that for all $x^* \in (x_{tail}, \infty)$:*

There exists an open interval $I_1 \subset I_0, d_0 \in I_1$, such that for all $d \in I_1$:

$$\begin{aligned} &a_d(x^*), i_d(x^*) > 0, \\ &a'_d(x^*), i'_d(x^*) < 0, \\ &i''_d(x^*) > 0. \end{aligned} \tag{B.139}$$

Moreover, given the existence of such an x^*, it holds for all $x \geq x^*$, and as long as $i_d(x) \geq 0$:

$$i''_d(x) > 0, \tag{B.140}$$

and thus all a_d, a'_d, i_d, i'_d converge monotonously to zero.

Proof. The Inequalities (B.139) are true on the tail of $M^-_{d_0}$, say for all $x \geq x_1$, where we let $x_1 \geq x_\kappa$ without loss of generality. Now pick some $x_2 > x_1$. There exists an open interval $I_1 \subset I_0, d_0 \in I_1$, such that for all $d \in I_1$:

The manifold $M^-_d(K,x)|_{x\in(-\infty,x_2]}$ exists, is non-negative and converges to $M^-_0(K,x)|_{x\in(-\infty,x_2]}$ as $d \to d_0$. By continuity: for $|d-d_0|$ sufficiently small and for all $x \in [x_1, x_2]$:

$$a_d(x), i_d(x) > 0, a'_d(x) < 0, i'_d(x) < 0. \tag{B.141}$$

On $[x_1,x_2]$: $\bar{i}''(x) > 0$, so $\bar{i}'(x_1) < \bar{i}'(x_2)$. Since $i'_d \to \bar{i}'$, there must also be some $x^*_d \in [x_1,x_2]$, such that $i''_d(x^*_d) > 0$, for all d such that $|d-d_0|$ is sufficiently small.

We assume that there exists a finite time $x_3 \geq x^*_d$ such that $i''_d(x_3) = 0$ for the first time after x^*. This implies that $i'''_d(x_3) \leq 0$. On the other hand, deriving the equation for i in (B.3) once yields

$$\begin{aligned} d \cdot i''' &= -(ci' + ra + a(a+i))' \\ &= -\big(ci'' + ra' + a'(a+i) + a(a'+i')\big) \\ &= -ra' - a'(a+i) - a(a'+i'). \end{aligned} \tag{B.142}$$

As long as $i_d \geq 0$, we can apply Lemmas B.17 and B.15. Then, all three terms in the last line are strictly positive, resulting in $i'''_d(x_3) > 0$, contradicting our assumption. This allows to fix $x_{tail} = x_2$, independent of d. □

Remark: Note that we can choose x^* from Lemma B.20 as large as we want, the price is a stronger restriction regarding $d \sim d_0$. This will be helpful if we assume that $M^-_{d_0}(K)$ converges: also the perturbed trajectories get as close to the limit as we need.

Given monotonicity of the tail, we can control $i_d(x)$ for $x \in [x^*, \infty)$:

Corollary B.21. *Consider $M^-_{d_0}(K)$ and I_1, x^* as in Lemma B.20. There exists a finite constant $J \geq 0$, such that for all $d \in I_1$ and all phase-times $x_2 \geq x_1 \geq x^*$, the bound*

$$c \cdot \big|\big(i_d(x_1) - i_d(x_2)\big)\big| \leq d \cdot |i'_d(x_1)| + J \cdot a_d(x_1) \tag{B.143}$$

holds as long as $i_d(x) \geq 0$ for all $x \in (-\infty, x_2]$.

Proof. Choose x^* as in the previous Lemma B.20. For $x_2 \geq x_1 \geq x^*$, integrate $0 = di''_d + ci'_d + a_d(a_d + i_d + r)$:

$$c \cdot \big|i_d(x_2) - i_d(x_1)\big| = \Big|d \cdot \big(i'_d(x_2) - i'_d(x_1)\big) + \int_{x_1}^{x_2} a_d(a_d + i_d + r)\, ds\Big|. \tag{B.144}$$

As long as $i_d \geq 0$, Proposition B.16 and the previous Lemmas B.17, B.15 and B.20 imply $a_d \geq 0, a_d' \leq 0, i_d' \leq 0$ and $i_d'' \leq 0$. Thus, since $a_d + i_d + r \leq 1 + r$:

$$c \cdot \left| i_d(x_2) - i_d(x_1) \right| \leq d \cdot \left| i_d'(x_1) \right| + (1 + r) \cdot \int_{x_1}^{x_2} a_d(x)\, dx. \tag{B.145}$$

By our bound $a_d(x_\kappa) + i_d(x_\kappa) \leq 1 - \kappa$, for some $x_\kappa \leq x^*$, Proposition B.16 implies that there exists a constant $L_\kappa \geq 0$ such that

$$\int_{x_1}^{x_2} a(s)\, ds \leq L_\kappa \cdot a_d(x_1) \qquad \forall x_2 \geq x_1 \geq x_0, \tag{B.146}$$

as long as $i_d(x) \geq 0$ for all $x \in (-\infty, x_2]$. □

We now prove the existence of a non-negative traveling wave for $d \sim d_0$, all that is left to be done is to prove convergence as $x \to +\infty$:

Proof of Proposition B.14. Consider a manifold $M_{d_0}^-(K)$ that fulfills **TW**. Then, there exists a constant $\gamma > 0$, such that $\bar{i}(x) \geq \gamma$ for all $x \in \mathbb{R}$. We prove that for all d sufficiently close to d_0:

$$|i_d(x) - \bar{i}(x)| \leq \frac{\gamma}{2} \qquad \forall x \in \mathbb{R}. \tag{B.147}$$

This implies that $i_d(x) \geq \frac{\gamma}{2} > 0$, and Lemma B.15 yields positiveness and convergence of $M_d^-(K)$. The rest of the wave properties **TW** then follows by Lemma B.15.

Let x^* as in Corollary B.21: there exists an open interval $I_1 \subset \mathbb{R}_0^+$ such that for all $d \in I_1$: the trajectory $M_d^-(K, x)|_{x \in (-\infty, x^*]}$ is non-negative, and there exists some $J \geq 0$ such that for all $x_2 \geq x_1 \geq x^*$:

$$i_d(x_2) \geq i_d(x_1) - \frac{d}{c} |i_d'(x_1)| - \frac{J}{c} \cdot a_d(x_1), \tag{B.148}$$

as long as $i_d \geq 0$. Now, choose $x_1 \geq x^*$ large enough such that both

$$\frac{J}{c} \cdot \bar{a}(x_1) \leq \delta := \frac{\gamma}{7}, \tag{B.149}$$

$$|\bar{a}(x_1)| + |\bar{a}'(x_1)| + |\bar{i}'(x_1)| + |\bar{i}(x_1) - \gamma| \leq \delta := \frac{\gamma}{7}, \tag{B.150}$$

which is possible since $M_{d_0}^-(K)$ converges. Then choose an even smaller open interval $I_2 \subset I_1, d_0 \in I_2$, such that by continuity: for all $d \in I_2$, $M_d^-(K, x)|_{x \in (-\infty, x_1]}$ is non-negative and of distance at most

$$\epsilon = \frac{\gamma}{7(1 + \frac{J}{C})} \tag{B.151}$$

to $M_{d_0}^-(K, x)|_{x \in (-\infty, x_1]}$. Then, in view of Eq. (B.149) and (B.150), also

$$\frac{J}{c} \cdot a_d(x_1) \leq \frac{2\gamma}{7} = 2\delta, \tag{B.152}$$

$$|a_d(x_1)| + |a_d'(x_1)| + |i_d'(x_1)| \leq \frac{2\gamma}{7} = 2\delta. \tag{B.153}$$

This implies that for all $d \in I_2$ and $x_2 \geq x_1$, and by Eq. (B.148):

$$\begin{aligned} i_d(x_2) &\geq i_d(x_1) - \frac{d}{c}\left|i_d'(x_1)\right| - \frac{J}{c} \cdot a_d(x_1) \\ &\geq \bar{i}(x_1) - \epsilon - \frac{d}{c}\left|\bar{i}'(x_1) + \epsilon\right| - 2\delta \\ &\geq \gamma - \frac{\gamma}{7} - \frac{d}{c} \cdot \left|\frac{\gamma}{7} + \frac{\gamma}{7}\right| - 2\frac{\gamma}{7} \\ &\geq \frac{4\gamma}{7} - \frac{d}{c} \cdot \frac{2\gamma}{7}. \end{aligned} \tag{B.154}$$

The last line is strictly positive for $d < 3c/2$. Thus, $i_d(x_2) \geq 0$ for all $x_2 \geq x_1$, and the trajectory stays non-negative and converges monotonously to its limit, as claimed. □

B.3.4 The mapping of the limits

In view of the previous Section, the wave properties **TW** persist under small perturbations in d as long as $i_{+\infty} > 0$. However, we can relate the limits of any bounded and non-negative solution up to a term of order $\mathcal{O}(d)$:

Proposition B.22. *For $d > 0$, the two limits $i_{-\infty}$ and $i_{+\infty}$ of any smooth, bounded and non-negative traveling wave (where $a \not\equiv 0$) fulfill*

$$2 - d \cdot \frac{2(r+1)}{c^2} < i_{-\infty} + i_{+\infty} < 2. \tag{B.155}$$

For the proof, we first verify integrability of any non-negative traveling wave:

Lemma B.23. *For $d > 0$, let $a(x), a'(x), i(x), i'(x)|_{x\in\mathbb{R}}$ be a smooth, bounded and non-negative solution of System* (B.107)*, where $a \not\equiv 0$. Then, as $x \to \pm\infty$, $a(x)$ vanishes and $i(x)$ converges, and $a, a', a'', i', i'' \in L^1(\mathbb{R})$. Moreover, $i(x)$ is not constant and $i' \leq 0$. The function $a(x)$ has a unique global and local maximum, and $a(x) > 0$ for all $x \in \mathbb{R}$.*

Proof. Let $a(x), b(x), i(x), i'(x)$ as above. If $i(x)$ does not converge at either $x \to +\infty$ or $x \to -\infty$, it must oscillate: in this setting, we can use the reasoning in the proof of Lemma B.15 to provoke a contradiction. Thus, $i(x)$ is either increasing or decreasing. If $i'(x) \geq 0$ for all $x \in \mathbb{R}$, then

$$-d \cdot i'' \geq i' + a(a + i + r) \geq 0. \tag{B.156}$$

As a consequence, the trajectory can not be bounded, since $i'(x)$ can not vanish at both $x \to \pm\infty$, or $i(x)$ must be constant. However, if $i(x)$ was constant, then

$$0 \equiv di'' + ci' = -a(a + i + r), \tag{B.157}$$

which can not hold since we assumed that $a \not\equiv 0$. It follows that $i(x)$ is decreasing and by boundedness must converge as $x \to \pm\infty$, so $i' \in L^1(\mathbb{R})$. The two limits must be fixed points, we denote them as $(0, 0, i_{-\infty}, 0)$ and $(0, 0, i_{+\infty}, 0)$.

Assume that at some finite phase-time x^*: $a(x^*) = 0$. Since we assumed that $a \geq 0$, this must be a local minimum, so $a'(x^*) = 0$. Then also $-a''(x^*) = ca'(x^*) + a(x^*) - a(x^*)(a(x^*) + i(x^*)) = 0$, and by induction: $a^{(n)}(x^*) = 0$ for all $n \in \mathbb{N}$. But this contradicts the assumption $a \not\equiv 0$.

For $a(x) \not\equiv 0$, there is at least one local maximum of active particles, since the trajectory converges at both ends. We denote this maximum as $(a_0, 0, i_0, i_0')$. At this point, $a'' = a_0(a_0 + i_0 - 1) \leq 0$, so $a_0 + i_0 \leq 1$, since $a_0 > 0$. Assume that there is also a local minimum of $a(x)$, denoted as $(a_m, 0, i_m, i_m')$. Since $a(x)$ vanishes at both ends, we may assume without loss of generality that this be the first local minimum after passing through $(a_0, 0, i_0, i_0')$.

Now, since $a_m(a_m + i_m - 1 - 1) = a_m'' \geq 0$, it must hold that $a_m + i_m \geq 1$. But $i(x)$ is decreasing, so $a(x)$ must have been increasing, a contradiction to the assumption that this is the first local minimum after the maximum $(a_0, 0, i_0, i_0')$. As a consequence, there is only one local maximum of active particles, which is also the global one. Further, this implies $a' \in L^1(\mathbb{R})$.

Given that $i' \in L^1(\mathbb{R})$, we know that the expression

$$\int_{\mathbb{R}} d \cdot i(x)'' + a(x)\big[a(x) + i(x) + r\big]dx = c(i_{-\infty} - i_{+\infty}) \tag{B.158}$$

is finite, however the left side might only exist in a Riemannian sense. Integrating the left-hand side over a finite interval $[-M, M]$, it also holds that

$$\begin{aligned} &\int_{-M}^{M} d \cdot i(x)'' + a(x)\big[a(x) + i(x) + r\big]dx \\ &= d\big[i'(M) - i'(-M)\big] + \int_{-M}^{M} a(x)\big[a(x) + i(x) + r\big]dx. \end{aligned} \tag{B.159}$$

By monotonicity of $i(x)$, it holds that $i'(x) \to 0$ as $x \to \pm\infty$. By (B.158) and (B.159):

$$c(i_{-\infty} - i_{+\infty}) = \int_{\mathbb{R}} a(x)\big[a(x) + i(x) + r\big]dx, \tag{B.160}$$

and the right-hand side is integrable, since all terms are non-negative. In view of (B.159), also $i''(x)$ is integrable, as a sum of integrable terms. We proceed in a similar fashion with the equation $a'' + ca' + a = a(a + i)$. We integrate it over the finite interval $[-M, M]$:

$$\int_{-M}^{M} a''(x) + ca'(x) + a(x)\,dx = \int_{-M}^{M} a(x) \cdot \big[a(x) + i(x)\big]dx. \tag{B.161}$$

We already know that the right-hand is integrable, and that both $a(\pm M)$ and $a'(\pm M)$ vanish as $M \to +\infty$. This implies

$$\begin{aligned}
&\int_{\mathbb{R}} a(x)dx \\
&= \lim_{M\to+\infty} \Big[a'(M) - a'(-M) + c\big[a(M) - a(-M)\big] + \int_{-M}^{M} a(x)dx\Big] \\
&= \int_{\mathbb{R}} a(x)\cdot\big[a(x)+i(x)\big]\,dx.
\end{aligned} \tag{B.162}$$

Hence also $a(x)$ is integrable, since it is non-negative. Finally, as a sum of integrable terms, also $a''(x)$ is integrable. □

Proof of Proposition B.22. Given integrability a non-negative traveling wave, we define

$$A(x) := \int_{-\infty}^{x} a(s), \quad \mathcal{A} := A(+\infty). \tag{B.163}$$

Then, integrating the equation for $a(x)$ in (B.3), it must hold that

$$\begin{aligned}
\mathcal{A} &= \int_{\mathbb{R}} a(x)\big[a(x)+i(x)\big]dx > 0, \\
c\cdot\big(i_{-\infty} - i_{+\infty}\big) &= r\cdot\mathcal{A} + \int_{\mathbb{R}} a(x)\big[a(x)+i(x)\big]dx.
\end{aligned} \tag{B.164}$$

Moreover, by integration by parts:

$$\begin{aligned}
&\int_{\mathbb{R}} a(x)\big[a(x)+i(x)\big]dx \\
&= \mathcal{A}\cdot i_{+\infty} - \int_{\mathbb{R}} A(x)\big[a'(x)+i'(x)\big]dx \\
&= \mathcal{A}\cdot i_{+\infty} + \frac{1}{c}\int_{\mathbb{R}} A(x)\big[(1+r)a(x) + di''(x) + a''(x)\big]dx \\
&= \mathcal{A}\cdot i_{+\infty} + \frac{1+r}{2c}\mathcal{A}^2 + \frac{1}{c}\int_{\mathbb{R}} A(x)\cdot a''(x)\,dx + \frac{d}{c}\int_{\mathbb{R}} A(x)\cdot i''(x)\,dx \\
&= \mathcal{A}\cdot i_{+\infty} + \frac{1+r}{2c}\mathcal{A}^2 - \frac{d}{c}\int_{\mathbb{R}} a(x)\cdot i'(x)\,dx.
\end{aligned} \tag{B.165}$$

Using this and Eq. (B.164), it follows that

$$\mathcal{A} = \frac{c}{1+r}\cdot(i_{-\infty} - i_{+\infty}), \tag{B.166}$$

$$\mathcal{A} = \mathcal{A}\cdot i_{+\infty} + \frac{1+r}{2c}\mathcal{A}^2 - \frac{d}{c}\cdot\int_{\mathbb{R}} a(x)\cdot i'(x)\,dx. \tag{B.167}$$

We know that $\int_{\mathbb{R}} a \cdot i' < 0$. We drop this term in Eq. (B.167), divide by $\mathcal{A} > 0$ and then eliminate the variable $\mathcal{A}$ via (B.166), leading to

$$1 > i_{+\infty} + \frac{1}{2}(i_{-\infty} - i_{+\infty}). \tag{B.168}$$

The first part of the claim follows: $2 > i_{+\infty} + i_{-\infty}$.

At the local maximum of $a(x)$, it holds that $a < a + i \leq 1$, see the proof of Lemma B.17. Thus $-i' \geq -ai' \geq 0$, and we can bound (using (B.166)):

$$-\frac{d}{c}\int_{\mathbb{R}} a(x) \cdot i'(x)\, dx < \frac{d}{c} \cdot (i_{-\infty} - i_{+\infty}) = \frac{d}{c} \cdot \frac{1+r}{c}\mathcal{A}. \tag{B.169}$$

As before, we apply this bound to (B.167), divide by $\mathcal{A}$ and eliminate $\mathcal{A}$ via (B.166), which leads to

$$2 < i_{-\infty} + i_{+\infty} + 2\frac{d(1+r)}{c^2}. \tag{B.170}$$

□

Remark: These estimates seem to be sharp only asymptotically for $d \sim 0$, see the numerical Table B.4 in Appendix B.4.2.

B.3.5 Existence of the traveling waves

The existence of an invading front is proven in two steps: we first prove that for $d > 0$, there exists a traveling wave that is non-negative, but not necessarily a traveling front, as long as we can control the limits via the $\mathcal{O}(d)$-Estimate (B.155). Afterwards, we show that for fixed $d \geq 0$, the existence of an arbitrary non-negative traveling wave also implies the existence of an invading front, by using the continuum of possible limits.

B.3.5.1 Arbitrary bounded non-negative solutions

Theorem B.24 (Existence of a traveling wave solution)**.** *Let $r \geq 0, c \geq 2$ and $i_{-\infty} \in (1, 2)$. Then, for all $d > 0$ that fulfill*

$$d < \frac{3c}{2}, \tag{B.171}$$

$$d\frac{2(r+1)}{c^2} \leq 2 - i_{-\infty}, \tag{B.172}$$

there exists a non-negative traveling wave with limits

$$\lim_{x \to \pm\infty} a(x) = 0, \tag{B.173}$$

$$\lim_{x \to -\infty} i(x) = i_{-\infty}, \tag{B.174}$$

$$\lim_{x\to+\infty} i(x) > 2 - i_{-\infty} - d\frac{2(r+1)}{c^2} \geq 0. \tag{B.175}$$

*All these waves admit the wave properties **TW**. Moreover, for $d \in (0,1)$, the waves converge exponentially fast. The rates of convergence depend on $i_{\pm\infty}$ and are given by* (B.105)*, as in the case $d = 0$.*

Proof. Fix $i_{-\infty} \in (1,2)$, and consider the manifold $M_d^-(i_{-\infty})$ as before. We prove **TW** for all d as claimed. For $d = 0$, this statement is part of the proof of Theorem 3.1. We will use continuity in d, see Proposition B.14, for which we need Bound (B.171). The second Bound (B.172) is the one from Proposition B.22, it will ensure that $\lim_{x\to+\infty} i(x) > 0$. The rates of convergence will be discussed when finishing the proof of Theorem B.1, at the end of Section B.3.5.2.

Since **TW** is true for $d = 0$, it is also true for $d \in [0, d_1)$, for some $d_1 > 0$, by Proposition B.14. Let

$$d^* = \sup_{d_1 \geq 0} \left\{ \forall d \in [0, d_1) : \textbf{TW} \text{ holds for } M_d^-(i_{-\infty}) \right\} > 0. \tag{B.176}$$

Assume that d^* does violate neither (B.171) nor (B.172). The manifold $M_{d^*}^-(i_{-\infty})$ exists locally around the fixed point $(a, a', i, i') = (0, 0, i_{-\infty}, 0)$ due to Corollary B.10. Let $R > 0$. Since the System S_{d^*} is a smooth vector field, also the continuation

$$M_{d^*}^-(i_{-\infty}) \cap \{x \in \mathbb{R}^4 : ||x||_\infty < R\} \tag{B.177}$$

is a smooth and bounded manifold. If it is non-negative, we proceed with the next paragraph. If not, choose a representation

$$M_{d^*}^-(i_{-\infty}, x)|_{x\in(-\infty,T]}$$

for some finite $T \in \mathbb{R}$, such that the manifold has become strictly negative at time T. By Proposition B.12, there exists an open interval $I \subset \mathbb{R}_0^+, d^* \in I$, such that for all $d \in I$: the manifolds $M_d^-(i_{-\infty}, x)|_{x\in(-\infty,T]}$ exists and are continuous in d. However, for all $d < d^*$, these manifolds are also non-negative, by choice of d^*. Thus, also $M_{d^*}^-(i_{-\infty}, x)|_{x\in(-\infty,T]}$ must be non-negative.

Since $R > 0$ was arbitrary, the entire manifold $M_{d^*}^-(i_{-\infty})$ must be non-negative. Since it is not constant, it fulfills the conditions of Proposition B.22, so

$$\lim_{x\to+\infty} i_{d^*}(x) > 2 - i_{-\infty} - d^*\frac{2(r+1)}{c^2} \geq 0, \tag{B.178}$$

in view of Condition (B.172), which was not violated. Now, Lemma B.23 yields some structural results: it holds that $i'_{d^*}(x) < 0, a_{d^*}(x) > 0$, and

$a_{d^*}(x)$ has a unique local and global maximum. Since $a_{d^*}(x), i_{d^*}(x)$ converge as $x \to +\infty$, there exists some x^* as claimed in Lemma B.20, which yields monotonicity of the tail. Thus, we have verified **TW** also for d^*, and can again apply Proposition B.14 to $M^-_{d^*}$. This proves **TW** in a local neighborhood of d^*. Insofar, d^* can not have been chosen as claimed, and either (B.171) or (B.172) must be violated for d^*. □

By choosing $i_{-\infty}$ arbitrarily close to 1, Theorem B.24 has a simple

Corollary B.25. *Let $r \geq 0, c \geq 2$. Then, for all $d \geq 0$ such that*

$$d < \min\{\frac{3c}{2}, \frac{c^2}{2(r+1)}\}, \tag{B.179}$$

there exists some $i_{-\infty} \in (1,2)$ such that the manifold $M^-_d(i_{-\infty})$ is a non-negative traveling wave.

B.3.5.2 The invading front

It remains to show that there exists a wave where $i_{+\infty} = 0$, despite the $\mathcal{O}(d)$-estimate regarding the limits (B.175). We begin with the simple

Lemma B.26. *For all $d > 0, c > 0, r \geq 0$, the manifold*

$$M^-_d(2) \tag{B.180}$$

is not non-negative.

Proof. Asymptotically as $x \to -\infty$: $a(x) > 0$ by Corollary B.10. Assume that $a(x), i(x) \geq 0$ for all $x \in \mathbb{R}$. Then, denoting the other limit of the wave as $i_{+\infty} = \lim_{x\to+\infty} i(x) \geq 0$, Proposition B.22 implies

$$2 + i_{+\infty} < 2, \tag{B.181}$$

a contradiction. □

Given a non-negative and converging trajectory $M^-_d(K_0)$, the following lemma yields continuity and non-negativeness of $M^-_d(K)$ with respect to K in a neighborhood of K_0:

Lemma B.27. *Let $c \geq 2, d > 0, r \geq 0$ and $K_0 \in (1,2)$. Assume that the manifold $M^-_d(K_0)$ is a non-negative traveling wave, and thus converges as $x \to +\infty$, where*

$$\lim_{x\to+\infty} i(x) = i_{+\infty} \in (0,1). \tag{B.182}$$

Then, there exists an open interval $I \subset (1,2), K_0 \in I$ such that for all $K \in I$: the entire manifold $M^-_d(K)|_{x\in\mathbb{R}}$ is continuous in K, and moreover is also a non-negative traveling wave.

Proof. Consider $M_d^-(K_0)$ as proposed, and denote its limit as $i^*_{+\infty}$. We use Corollary B.11 to control $M_d^-(K,x)|_{x\in(-\infty,T]}$ for some $T \in \mathbb{R}$. By Corollary B.9, the fixed point $(0,0,i^*_{+\infty},0)$ is Lyapunov stable, and we can control also the tail as $x \to +\infty$.

Choose some

$$\rho \in (0, i^*_{+\infty}). \tag{B.183}$$

There exists $\epsilon > 0$, such that for all trajectories $a(x), a'(x), i(x), i'(x)$ that start with in range of ϵ to $(0,0,i^*_{+\infty},0)$:

$$\left|\big(a(x),a'(x),i(x),i'(x)\big) - \big(0,0,i^*_{+\infty},0\big)\right| \le \rho, \quad \text{for all } x \ge 0, \tag{B.184}$$

since the fixed point is Lyapunov-stable. Wlog let $\epsilon \le \rho$. There exists a finite phase-time T, such that

$$\left|M_d^-(K_0,T) - \big(0,0,i_{+\infty},0\big)\right| \le \frac{\epsilon}{2}. \tag{B.185}$$

We now use the continuity of $M_d^-(K,x)|_{x\in(-\infty,T]}$ with respect to K, see Corollary B.11: there exists a $\delta > 0$ with $K_0 - \delta > 1$, and such that for all $K \in [K_0-\delta, K_0+\delta]$: the manifold $M_d^-(K,x)|_{x\in(-\infty,T]}$ is of distance at most $\epsilon/2$ to $M_d^-(K_0,x)|_{x\in(-\infty,T]}$.

Then, for all $K \in [K_0-\delta, K_0+\delta]$, the manifold $M_d^-(K_0,x)|_{x\in(-\infty,T]}$ is also strictly non-negative, since $i(x) \ge i^*_{+\infty} - \frac{\rho}{2} > 0$ for all $x \in (-\infty, T]$, by Lemmas B.15 and B.17. Moreover, at time T, any such manifold has entered the ρ-neighborhood of $(0,0,i^*_{+\infty},0)$. Thus, $i(x) \ge 0$ for all $x \in \mathbb{R}$ and we can apply Lemma B.17 to conclude that also $a(x) \ge 0$ for all $x \in \mathbb{R}$. Moreover, all such trajectories have at most distance $\epsilon \le \rho$ from $M_d^-(K_0)$. Since we can choose ρ as small as we want, this also proves continuity of the entire manifold $M_d^-(K,x)|_{x\in\mathbb{R}}$ in K.

□

Continuity of the traveling waves w.r.t. K implies the existence of an invading front:

Theorem B.28. *Let $c \ge 2, r \ge 0, d > 0$ and $K_0 \in (1,2)$ such that $M_d^-(K_0)$ is a non-negative traveling wave. Then, there exists also some $K_1 \in [K_0, 2)$, such that $M_d^-(K_1)$ is an invading front.*

Proof. We proof a sort of intermediate value theorem, increasing K as much as possible. For a manifold $M_d^-(K)$ that is non-negative and converges, we denote $i_{+\infty}(K) := \lim_{x\to+\infty} i(x) \ge 0$.

We are done if $i_{+\infty}(K_0) = 0$, so we assume $i_{+\infty}(K_0) > 0$ in the following. Then, the manifold $K_d^-(K_0)$ fulfills the conditions of Lemma B.27. It follows that there exists a neighborhood $I \subset \mathbb{R}$ with $K_0 \in I$, such that the entire

manifold $M_d^-(K)$ is continuous w.r.t. $K \in I$, including its limit $i_{+\infty}(K)$. We extend this to a non-local statement by defining

$$K_1 := \sup_{L \geq K_0} \Big\{ \forall K \in [K_0, L) \Big| \, M_d^-(K) \text{ is non-negative and converges} \Big\}. \tag{B.186}$$

Recall that for $K = 2$, the manifold $M_d^-(2)$ eventually becomes negative by Lemma B.26, so it must hold that $K_0 < K_1 < 2$. For all $K \in [K_0, K_1)$, the manifold $M_d^-(K)$ is non-negative and converges, by the definition of K_1. By Corollary B.10, the manifold $M_d^-(K_1)$ exists locally around the fixed point. Since S_d is a smooth vector field, also the continuation

$$M_d^-(K_1)|R := M_d^-(K_1) \cap \big\{ x \in \mathbb{R}^5 : ||x||_\infty < R \big\} \tag{B.187}$$

exists and is a smooth manifold, for any $R > 0$. Now, since $M_d^-(K)$ is non-negative and converges for all $K \in [K_0, K_1)$, also $M_d^-(K_1)|R$ must be non-negative, by a continuity argument completely analogue to that in the proof of Theorem B.24. Since R can be chosen arbitrarily large, the entire manifold $M_d^-(K_1)$ is non-negative, and thus also converges.

We are done if $i_{+\infty}(K_1) = 0$. So let us assume that $i_{+\infty}(K_1) > 0$. In this case, we again apply Lemma B.27 to $M_d^-(K_1)$, resulting in the existence of non-negative and converging solutions for in an open neighborhood of K_1, a contradiction. □

We finish the

Proof of Theorem B.1. For d as claimed, Corollary B.25 and Theorem B.28 imply the existence of an invading front. It remains to determine its asymptotic behavior, therefore we consider only $d \in (0, 1)$.

As $x \to -\infty$, the rate of convergence along the instable manifold is given in Corollary B.10 (depending on $i_{-\infty}$). Regarding the behavior as $x \to +\infty$, we take a look at the linear Representation (B.112) and the Eigenvalues (B.109). For $d \in (0, 1)$ and $i_{+\infty} \in [1 - \frac{c^2}{4}, 1)$, we can order the purely real-valued Eigenvalues of the limit:

$$0 > \lambda_4 \geq \lambda_3 > \lambda_2, \tag{B.188}$$

where the inequalities are strict if $i_{+\infty} > 1 - \frac{c^2}{4}$. This ordering is crucial: even though we do not have a complete description of the asymptotics, we can determine the rate of convergence, as some components of the system converge with speed λ_4: we apply the same trapping argument as for S_0, see Proposition 6.3 in [92]. As long as $\lambda_4 \geq \lambda_3$, we know by an analysis of the phase space that the two components $a(x), a'(x)$ converge along the Eigenvector e_4 (B.109), associated to λ_4. We now must differentiate between the critical and the noncritical case.

For the noncritical case, where $i_{+\infty} \neq 1-c^2/4$, the asymptotics are equivalent to the linear System (B.112). This implies that the system approaches its limit exponentially with rate λ_4.

The critical case $i_{+\infty} = 1 - c^2/4$ is a bifurcation point of the system: solutions that converge to $i_{+\infty} < 1 - c^2$ spiral, since the Eigenvalues λ_3 and λ_4 have an imaginary part (B.109), they do not spiral and converge exponentially fast if the limit fulfills $i_{+\infty} > 1 - c^2/4$. Luckily, we do not have to find a complete representation for the behavior around the bifurcation point: we only need to determine the dynamics of a trajectory that converges to the specific limit $i_{+\infty} = 1 - c^2/4$. In this case, we still know that the center manifold of the fixed point $(a, a', i, i') = (0, 0, i_{+\infty}, 0)$ has dimension one, and thereby must coincide with the adjacent line of fixed points. Thus, any trajectory that converges to $i_{+\infty} = 1 - c^2/4$ must be contained in the remaining three-dimensional strictly hyperbolic subsystem. The Eigenvalue $\lambda_3 = \lambda_4$ has algebraic multiplicity 2, but geometric multiplicity 1, see the Eigenvectors (B.109). Along the corresponding manifold, trajectories converge as fast as $x \cdot \exp(-x\lambda_4)$, cf. Chapter 9 in Boyce et al. [20]. □

B.4 Appendices of this preprint

B.4.1 A-priori estimates for the left tail of the PDE

We provide the a-priori bounds in the regime $x \to -\infty$ via a Feynman-Kac formula for shifted Brownian motion, which we stop at the origin. The following Lemma B.29 is standard, check e.g. Chapter 4.4 in [86] for more examples and a profound theoretical treatment. For linear problems (e.g. super-solutions in certain regimes of a PDE), this allows for easy estimates:

Lemma B.29. *For $c, L, M \in \mathbb{R}$, let $u(t,x) : \mathbb{R}_0^+ \times \mathbb{R} \to \mathbb{R}$ be a solution of*

$$u_t = \frac{1}{2}\Delta_x u(t,x) + cu_x(t,x) + Lu(t,x) + M, \tag{B.189}$$

twice differentiable in space and once differentiable in time. For fixed $x_0 < 0$, let $W_t = B_t + ct + x_0$ be a shifted Brownian motion starting in x_0. Denote the hitting time $T_0 := \inf\{t \geq 0 : W_t = 0\}$. Assume that for some $t > 0$:

$$\sup_{x \leq 0} |u(t=0,x)| < \infty \quad \textit{and} \quad \sup_{s \in [0,t]} |u(s, x=0)| < \infty. \tag{B.190}$$

It then holds that

$$\begin{aligned} u(t,x_0) = {} & \mathbb{E}_{x_0}\Big[e^{L\cdot t} \cdot u\big(0, W_t\big);\, T_0 > t\Big] \\ & + \mathbb{E}_{x_0}\Big[e^{L\cdot T_0} \cdot u\big(t - T_0, 0\big);\, T_0 \leq t\Big] \\ & + \frac{M}{L} \cdot \mathbb{E}_{x_0}\Big[e^{L(t \wedge T_0)}\Big]. \end{aligned} \tag{B.191}$$

Proof. The proof is standard: fix x_0 and t and apply Itos formula to the stochastic process

$$X_s := e^{L\cdot s} \cdot u(t-s, W_s), \quad s \in [0,t]. \tag{B.192}$$

It follows that

$$\begin{aligned} dX_s &= Le^{L\cdot s}u(t-s,W_s)ds \\ &\quad + e^{L\cdot s}\cdot\Big[-u_s ds + u_x\, dBs + u_x c\, ds + \frac{1}{2}u_{xx}\, ds\Big] \\ &= e^{Ls}\Big[u_x\, dBs - M ds\Big]. \end{aligned} \tag{B.193}$$

The last expression consists of a local martingale and a drift, thus

$$u(t,x_0) = X_0 = \mathbb{E}_{x_0}[X_0] = \mathbb{E}_{x_0}[X_{t\wedge T_0}] + M\cdot\mathbb{E}_{x_0}\Big[\int_0^{t\wedge T_0} e^{Ls}\, ds\Big], \tag{B.194}$$

since $||u||_\infty$ can grow at most exponentially in time. The claim follows by splitting the cases $t < T_0$ and $t \geq T_0$. □

We will need the distribution of the hitting time T_0 as in Lemma B.29. It can be shown (by a Girsanov transformation and the reflection principle), that for $x_0 < 0$, the distribution of T_0 has density

$$\mathbb{P}_{x_0}[T_0 = dt] = \frac{-x_0}{\sqrt{2\pi t^3}}\cdot e^{-\frac{(-x_0-ct)^2}{2t}}\cdot \mathbb{1}_{t>0}\, dt. \tag{B.195}$$

For any speed $c > 0$, this defines a probability density, so the hitting time is almost surely finite.

We can now estimate the decay of $A(t,x)$ at the back of the wave. In an analogue fashion, we could also prove that $I(t,x)$ grows at most exponentially in x, given that $A(t,x) \leq 1$, but we do not need this result (and in fact hope that we can also prove boundedness of I in the future).

Proposition B.30. *Let $A(t,x), I(t,x)$ be a non-negative solution of the PDE* (B.1) *in the moving frame $x = z - ct$, for a speed $c > 0$. Assume that there exist constants $K, \delta, \mu_0 > 0$, such that the initial data fulfill*

$$\begin{aligned} I(0,x) &\geq 1+\delta && \forall x \leq 0, \\ A(0,x) &\leq Ke^{\mu_0 x} && \forall x \leq 0, \\ A(0,x) + I(0,x) &\leq K && \forall x \in \mathbb{R}. \end{aligned} \tag{B.196}$$

Moreover, assume that for some time $t \in (0,\infty]$, it holds that

$$I(s, x=0) \geq 1+\delta > 1 \qquad \forall s \in [0,t). \tag{B.197}$$

Then, there exist $C, \zeta > 0$ that are independent of t, such that:

$$\forall s \in [0,t),\ x \leq 0: \quad i) \qquad I(s,x) \geq 1+\delta, \tag{B.198}$$

$$ii) \qquad A(s,x) \leq Ce^{\zeta x}. \tag{B.199}$$

Proof. Without loss of generality let $K \geq 1$. By boundedness of the initial data, a solution exists for all times. Since $K \geq 1$, it holds that $A(t,x) \leq K$ for all $t \geq 0$.

For the first Bound (B.198), note that the solution $H(t,x)$ of

$$H_t = d \cdot H_{xx} + c \cdot H_z, \quad H(0,x) = I(0,x), \tag{B.200}$$

is a sub-solution for $I(t,x)$, which is not affected by any negative reaction-term. We rescale space, introducing $x = \frac{1}{\sqrt{2d}} y$, such that H fulfills $H_t = \frac{1}{2} H_{yy} + \frac{c}{\sqrt{2d}} H_y$. We can now apply Lemma B.29 with $L = M = 0$. For all $y_0 \leq 0$ and $t \geq 0$, it holds that

$$H(t,y_0) = \mathbb{E}_{y_0}[H(0,W_t);\, T_0 > t] + \mathbb{E}_{y_0}[H(t-T_0,0);\, T_0 \leq t] \geq 1+\delta, \tag{B.201}$$

which is nothing but a maximum principle for a diffusion subject to a moving boundary condition.

Now, given that $I(t,x) \geq 1+\delta$ for all $x \leq 0$, the solution of

$$J_t = J_{xx} + c \cdot J_x - \delta J \tag{B.202}$$

is a super-solution for A. Again, we rescale $x = \frac{1}{\sqrt{2}} y$, such that J fulfills

$$J_t = \frac{1}{2} J_{yy} + \frac{c}{\sqrt{2}} J_y - \delta J. \tag{B.203}$$

We write $\tilde{c} = c/\sqrt{2}$. It holds that for all $y_0 \leq 0$:

$$J(t,y_0) = \mathbb{E}_{y_0}\Big[e^{-\delta t} \cdot J\big(0,W_t\big);\, T_0 > t\Big] \tag{B.204}$$

$$+ \mathbb{E}_{y_0}\Big[e^{-\delta T_0} \cdot J\big(t-T_0,0\big);\, T_0 \leq t\Big]. \tag{B.205}$$

We first estimate (B.204). Therefore, we fix $y_0 \leq 0$ and differentiate between small and large times. To begin with, we assume that

$$(2\tilde{c} + \mu_0)t \geq -y_0. \tag{B.206}$$

Since $A \leq K$, the term (B.204) is bounded by

$$K e^{-\delta t} \leq K e^{\frac{\delta}{2\tilde{c}+\mu_0} y_0}. \tag{B.207}$$

Next, we consider small times $(2\tilde{c}+\mu_0)t \leq -y_0$. The term (B.204) can be bounded by

$$\begin{aligned} &\mathbb{E}_{y_0}\big[J(0,W_t); T_0 > t\big] \leq \mathbb{E}_{y_0}\big[J(0,W_t)\big] \leq \mathbb{E}_{y_0}\big[K \cdot e^{\mu_0 W_t}\big] \\ &= K \exp\big(\mu_0(y_0 + \tilde{c}t)\big) \cdot \mathbb{E}_0[\exp(\mu_0 B_t)], \end{aligned} \tag{B.208}$$

where B_t is a standard Brownian motion. Using the moment generating function of B_t and inserting our small time estimate, we get

$$= K \exp\big(\mu_0[y_0 + \tilde{c}t + \frac{t\mu_0}{2}]\big) \leq K \exp(\frac{\mu_0}{2} y_0). \tag{B.209}$$

We continue with (B.205). For this, we use the distribution of the hitting time T_0, see (B.195). In the following, let C be a universal constant. We estimate

$$\begin{aligned} &\mathbb{E}_{y_0}\Big[e^{-\delta T_0} \cdot J\big(t - T_0, 0\big);\, T_0 \leq t\Big] \leq C\mathbb{E}_{y_0}[e^{-\delta T_0}] \\ &= \frac{-y_0}{\sqrt{2\pi}} \int_0^\infty \exp(-\delta s) \cdot s^{-3/2} \cdot \exp\big(-\frac{1}{2s}(-y_0 - \tilde{c}s)^2\big)\, ds. \end{aligned} \tag{B.210}$$

Again, we differentiate between small and large times. First, consider

$$\begin{aligned} &\frac{-y_0}{\sqrt{2\pi}} \int_{\frac{-y_0}{2\tilde{c}}}^\infty \exp(-\delta s) \cdot s^{-3/2} \cdot \exp\big(-\frac{1}{2s}(-y_0 - \tilde{c}s)^2\big)\, ds \\ &\leq -Cy_0 \cdot \big(\frac{|y_0|}{2\tilde{c}}\big)^{-3/2} \int_{\frac{-y_0}{2\tilde{c}}}^\infty \exp(-\delta s)\, ds. \end{aligned} \tag{B.211}$$

For $y_0 \leq -1$, this can be bounded by

$$\leq C \exp\big(\frac{\delta}{2\tilde{c}} y_0\big). \tag{B.212}$$

We continue with the small time estimate:

$$\begin{aligned} &\frac{-y_0}{\sqrt{2\pi}} \int_0^{\frac{-y_0}{2\tilde{c}}} \exp(-\delta s) \cdot s^{-3/2} \cdot \exp\big(-\frac{1}{2s}(-y_0 - \tilde{c}s)^2\big)\, ds \\ &\leq -Cy_0 \int_0^{\frac{-y_0}{2\tilde{c}}} s^{-3/2} \cdot \exp\big(-\frac{y_0^2}{4s}\big)\, ds \\ &\leq -Cy_0 \frac{4}{y_0^2} \int_0^{\frac{-y_0}{2\tilde{c}}} \sqrt{s} \cdot \frac{y_0^2}{4s^2} \exp\big(-\frac{y_0^2}{4s}\big)\, ds \\ &\leq -\frac{C}{y_0} \sqrt{\frac{-y_0}{2\tilde{c}}} \cdot \Big|_0^{\frac{-y_0}{2\tilde{c}}} \exp\big(-\frac{y_0^2}{4s}\big)\, ds \end{aligned} \tag{B.213}$$

For $y_0 \leq -1$, this can be bounded by

$$\leq C \exp\big(\frac{\tilde{c}}{2} y_0\big) \tag{B.214}$$

Lastly, remark that for $y \geq -1$, the trivial bound $J(t, y) \leq K$ holds, since $A \leq K$. Considering the Inequalities (B.207), (B.209), (B.212), (B.214), and re-substituting $\tilde{c} = c/\sqrt{2}$, the upper Bound (B.199) for $A(t, x)$ follows. □

B.4.2 Numerical evaluation of the discrete spectrum

We verify Assumption B.44 numerically. That is, we need to find $\delta_0, \delta_1 > 0$ such that the region

$$\Omega = \left\{ \lambda \in \mathbb{C} \middle| \, \mathfrak{Re}\lambda \geq -\delta_0 - \delta_1 \cdot |\mathfrak{Im}\lambda| \right\}, \tag{B.215}$$

contains no elements of the discrete spectrum of $\mathcal{L}$ as in Proposition B.4. In the following, we analyze only the non-negative part of the discrete spectrum.

Given that the non-negative discrete spectrum is empty, a set as above can easily be constructed as follows. For $\mathcal{L}$ as in Prop. B.4 and for a fixed set of type (B.215), it is well-known that there exists a constant $K > 0$ such that

$$\forall \lambda \in \Omega \cap \Sigma_d : \, |\lambda| \leq K. \tag{B.216}$$

This can be proven by rescaling the Eigenvalue-ODE (B.35) for large λ, see e.g. Prop. 2.2 in [3], or Section 2.2 in [56]. Since the Evans function (see Section B.4.2.2) is menomorphic over Ω away from the continuous spectrum (Prop. 4.7 in [167]), the bounded set

$$\Omega_K^- := \Omega \cap \{ \lambda \in \mathbb{C} \big| \, \mathfrak{Re}\lambda < 0, |\lambda| \leq K \} \tag{B.217}$$

can contain at most finitely many elements of the discrete spectrum. Thus, if the non-negative part of Ω contains no element of the discrete spectrum, one finds a set of type (B.215) as claimed by eventually choosing δ_0, δ_1 smaller.

Now, for the numerical analysis of the discrete spectrum, we consider only a single type of weight, namely

$$w(x) = e^{-x}. \tag{B.218}$$

This choice allows for an explicit and rather efficient energy based estimate regarding the maximal possible size of an Eigenvalue with non-negative real-part, presented in Section B.4.2.1. This estimate is much better than the asymptotic Bound (B.216), where an explicit calculation of the constant K is a rather tedious task. However, this approach is restricted to fully diffusive systems. In the subsequent Section B.4.2.2, we briefly review the theory of the Evans function and how it can be used to analyze the discrete spectrum. For the numerical evaluation, we use STABLAB, a tool by Barker et al. [13]. These computations show that $\mathcal{L}$ with the Weight (B.218) is indeed spectrally stable in H^2.

If the non-negative discrete spectrum for the Weight (B.218) is empty, then the same is obviously also true for all

$$w(x)_{|x \leq -1} = e^{-\alpha_- x}, \quad \alpha_- < 1. \tag{B.219}$$

B.4.2.1 An energy bound

The below idea is probably due to J. Humpherys, who also presents a refined version in [75]. A similar bound is found by F. Varas and J. Vega [153], but their calculation turns out to be wrong due to a sign error. Consider the linear problem

$$\lambda \cdot u_i(x) = D_i \cdot u_i''(x) + c_i \cdot u_i'(x) + \sum_{j=1}^{n} f_{i,j}(x) \cdot u_j(x), \qquad i = 1, \dots, n, \tag{B.220}$$

for $\lambda \in \mathbb{C}$, constants $D_i \geq 0, c_i \geq 0$, and functions $f_{i,j} \in L^\infty(\mathbb{R})$.

Now assume that there exists an Eigenvalue $\lambda \in \mathbb{C}$ with $\mathfrak{Re}\gamma \geq 0$, and associated eigenfunctions $u_i \in H^2(\mathbb{R})$. The product structure of H^2 induces an energy estimate on $|\lambda|$:

Theorem B.31 (An a-priori bound for the positive discrete spectrum)**.** *Let $\lambda \in \mathbb{C}$ with $\mathfrak{Re}\lambda \geq 0$ and functions $\big(u_i \in H^2(\mathbb{R})\big)_{i=1\dots n}$ be a solution of the Eigenvalue-problem* (B.220)*. For $i = 1, \dots, n$, define*

$$M_i := \sum_{j=1}^{n} ||f_{i,j}||_\infty. \tag{B.221}$$

Then, the real-part of λ is bounded:

$$\mathfrak{Re}\lambda \leq \max_i \{M_i\}. \tag{B.222}$$

Moreover, if $D_i > 0$ for all $i = 1, \dots, n$, such that the system is with non-degenerate diffusion, it holds that

$$|\mathfrak{Im}\lambda| \leq \max_i \Big\{ c_i \cdot \sqrt{\frac{M_i}{D_i}} + M_i \Big\}. \tag{B.223}$$

Proof. In the following, the norm $||.||_2$ will be the L^2-norm with corresponding scalar product $\langle\, .\, \rangle$. Before proving the above statement, let us note that for any function $u \in H^2(\mathbb{R})$, the product $\langle u', \bar{u} \rangle$ has no real-part, since

$$\begin{aligned} \mathfrak{Re} \int_{\mathbb{R}} u'(x) \cdot \bar{u}(x)\, dx &= \frac{1}{2}\Big(\int_{\mathbb{R}} u'(x) \cdot \bar{u}(x) + \bar{u}' \cdot u(x)\, dz \Big) \\ &= \frac{1}{2} \int_{\mathbb{R}} |u(x)^2|'\, dx = 0. \end{aligned} \tag{B.224}$$

Moreover, it holds by integration by parts that

$$\langle u'', \bar{u} \rangle = -||u'||_2^2 \leq 0. \tag{B.225}$$

Now, assume that there exists an Eigenvalue $\lambda \in \mathbb{C}$ with $\mathfrak{Re}\lambda \geq 0$ and associated eigenfunctions $\big(u_i \in H^2(\mathbb{R})\big)_{i=1\ldots n}$ that solve (B.220). For for each $i \in 1 \ldots n$, multiply (B.220) by $\bar{u}_i$:

$$\begin{aligned}\lambda \cdot ||u_i||_2^2 &= D_i \cdot \langle u_i'', \bar{u}_i\rangle + c_i \cdot \langle u_i', \bar{u}_i\rangle + \sum_{j=1}^{n} \langle f_{i,j} \cdot u_j, \bar{u}_i\rangle \\ &= -D_i ||u_i'||_2^2 + c_i \cdot \langle u_i', \bar{u}_i\rangle + \sum_{j=1}^{n} \langle f_{i,j} \cdot u_j, \bar{u}_i\rangle. \end{aligned} \tag{B.226}$$

Choose $k \in 1 \ldots n$ such that $||u_k||_2 = \max_i ||u_i||_2$. By Eq. (B.226), and since $\langle u_i', \bar{u}_i\rangle$ has no real-part:

$$\begin{aligned} 0 \leq \mathfrak{Re}\lambda \cdot ||u_k||_2^2 &= -D_k \cdot ||u_k'||_2^2 + \sum_{j=1}^{n} \mathfrak{Re}\langle f_{k,j} \cdot u_j, \bar{u}_k\rangle \\ &\leq ||u_k||_2^2 \cdot \sum_{j=1}^{n} ||f_{k,j}||_\infty. \end{aligned} \tag{B.227}$$

The claimed bound for $\mathfrak{Re}\lambda$ follows. We proceed similarly for the imaginary part of Eq. (B.226):

$$\mathfrak{Im}\lambda \cdot ||u_i||_2^2 = c_i \cdot \langle u_i', \bar{u}_i\rangle + \sum_{j=1}^{n} \mathfrak{Im}\langle f_{i,j} \cdot u_j, \bar{u}_i\rangle. \tag{B.228}$$

Again, for $||u_k||_2 = \max_i ||u_i||_2$:

$$|\mathfrak{Im}\lambda| \cdot ||u_k||_2^2 \leq c_k \cdot |\langle u_k', \bar{u}_k\rangle| + \sum_{j=1}^{n} ||f_{k,j}||_\infty \cdot ||u_k||_2^2. \tag{B.229}$$

We are done if we can find a suitable bound for $||u_k'||_2$. This is where we require that $D_i > 0$ for all $i \in 1 \ldots n$. Again take the real-part in Eq. (B.226). The inequality $\mathfrak{Re}\lambda \geq 0$ implies that for all $i = 1, \ldots, n$:

$$D_i \cdot ||u_i'||_2^2 \leq \sum_{j=1}^{n} ||f_{i,j}||_\infty \cdot ||u_i||_2 \cdot ||u_j||_2, \tag{B.230}$$

and thus for k chosen as above: $||u_k'||_2 \leq \sqrt{\frac{M_k}{D_k}} \cdot ||u_k||_2$. We use this in Eq. (B.229) to bound

$$|\mathfrak{Im}\lambda| \leq c \cdot \sqrt{\frac{M_k}{D_k}} + M_k. \tag{B.231}$$

□

We apply Theorem B.31 to the Operator (B.19) that already encodes the transformation into the weighted space. For a traveling wave $a(x), i(x)$ with speed $c = 2$ and the weight $w(x) = e^{-x}$, $\mathcal{L}$ reduces to

$$\begin{aligned} \mathcal{L}u &:= \frac{\partial^2}{\partial x^2}u - u(2a+i) - va, \\ \mathcal{L}v &:= d\frac{\partial^2}{\partial x^2}v + (2-2d)\frac{\partial}{\partial x}v + v\cdot(a+d-2) + u(2a+i+r). \end{aligned} \tag{B.232}$$

Here, it is essential that $w'/w = -1$ is constant, such that we are in the setting of Theorem B.31.

Proposition B.32. *For $d \in (0,1)$, consider $\mathcal{L}$ (B.232) as an operator*

$$H^2(\mathbb{R}) \times H^2(\mathbb{R}) \to L^2(\mathbb{R}) \times L^2(\mathbb{R}). \tag{B.233}$$

For all $\lambda \in \mathbb{C}$ in the discrete spectrum of $\mathcal{L}$ with $\mathfrak{Re}\lambda \geq 0$, it holds that

$$|\lambda| \leq \sqrt{2}\Big[(2-2d)\sqrt{\frac{5+r}{d}} + 5 + r\Big]. \tag{B.234}$$

Proof. This is a direct consequence of Theorem B.31. We can estimate the two constants M_a and M_i, see Eq. (B.221), via the simple bounds $|i| \leq 2, |a| \leq 1$:

$$M_a = |2a - i|_\infty + |a|_\infty \leq 3, \tag{B.235}$$
$$M_i = |a + d - 2|_\infty + |2a + i + r|_\infty \leq 5 + r. \tag{B.236}$$

□

B.4.2.2 The Evans function

The discrete spectrum within the region of consistent splitting of an operator can be evaluated numerically with the help of the Evans function. The following concepts are presented in much more detail by B. Sandstede, who wrote a great overview of the topic [130], a more practical introduction and the numerical tool STABLAB [13] have been written by B. Barker et al. [12].

Recall that for $\mathcal{L}$ as in Proposition B.4, if $\lambda \in \Sigma_d$, this is equivalent to saying that there exists a bounded solution of a linear ODE of type

$$U' = M(x,\lambda)\cdot U, \qquad x \in \mathbb{R}, \tag{B.237}$$

compare (B.35). The matrix $M(x,\lambda)$ is given by (B.36) and encodes the shift of the equation into the weighted space. It is now essential that we consider only $\lambda \in \mathbb{C}$ such that the matrices $M(x,\lambda)$ are analytic in (λ, x) up to $x = \pm\infty$, with strictly hyperbolic limits $M(\pm\infty, \lambda)$.

Since the limiting matrices $M(\pm\infty, \lambda)$ are hyperbolic, the theory of *exponential dichotomies* implies that any bounded solution $U(x)$ must vanish exponentially fast as $x \to \pm\infty$. Moreover, it asymptotically approaches the unstable manifold of the constant matrix $M(-\infty, \lambda)$ as $x \to -\infty$, and the stable manifold of $M(+\infty, \lambda)$ as $x \to +\infty$. Therefore, a bounded solution exists if and only if the trajectories that emerge from these manifolds intersect. This allows us to compute the Evans function: it is a determinant that evaluates to zero if and only if the solutions that decay at $-\infty$ and those that decay at $+\infty$ intersect, and are linearly dependent. The details are given in Section 4.1 in [130].

Definition B.33 (Evans function)**.** Consider the ODE (B.237), with $\lambda \in \mathbb{C}$ such that the matrices $M(x, \lambda)$ are analytic in (λ, x) up to $x = \pm\infty$, with hyperbolic limits $M(\pm\infty, \lambda)$.

Let

$$X_1(x, \lambda), \dots, X_{k_1}(x, \lambda) \tag{B.238}$$

be k_1 linearly independent representatives of those solutions that decay exponentially as $x \to -\infty$, and let

$$Y_1(x, \lambda), \dots, Y_{k_2}(x, \lambda) \tag{B.239}$$

be k_2 linearly independent representatives of those solutions that decay exponentially as $x \to +\infty$, with $k_1, k_2 > 0$ and $k_1 + k_2 = n$. The Evans function $E(\lambda)$ is defined as

$$E(\lambda) := \det\big(X_1(x, \lambda)\big| \dots \big|X_{k_1}(x, \lambda)\big|Y_1(x, \lambda)\big| \dots Y_{k_2,\lambda}\big)\Big|_{x=0}. \tag{B.240}$$

Remark: The Evans function is not unique, since the representatives X_i, Y_i are not unique. However, it holds that $E(\lambda) = 0$ if and only if System (B.237) has a bounded solution. Moreover, $E(\lambda)$ is analytic if the X_i, Y_i are chosen analytically in λ, which can be achieved, see Section 4.1 in [130]. Then, it suffices to calculate $E(\lambda)$ along the boundary of a domain $\mathcal{P} \subset \mathbb{C}$: the winding number of $E(\lambda)$ along $\partial\mathcal{P}$ corresponds to the number of zeros inside the domain.

We first need a numerical solution of a wave-profile, which goes hand in hand with finding the correct value of $i_{-\infty}$ such that the the other limit of the traveling wave fulfills $i_{+\infty} = 0$. Given some $i_{-\infty} > 1$, we solve the forward ODE (B.107) under initial data that approximate the unstable manifold of a fixed point $(a, a', i, i') = (0, 0, i_{-\infty}, 0)$, its asymptotic direction is given in Corollary B.10. The limit as $x \to +\infty$ of this trajectory is Lyapunov-stable, such that the numerical forward solution converges if the initial data are sufficiently close to the unstable manifold of $(0, 0, i_{-\infty}, 0)$. We then change $i_{-\infty}$ until $i_{+\infty} = 0$. This differs from the approach suggested in

[12]: the continuum of fixed points makes the proposed projective boundary value approach invalid. However, since the trajectory converges along the correct stable manifold as $x \to +\infty$, our forward approach is reasonable. This is a consequence of the trapping argument in Proposition B.16, see also Proposition 6.3 in [92]. The numerical evaluation suggests that the value $i_{+\infty}$ is a monotone function of $i_{-\infty}$, such that any root-finding algorithm converges quickly to the (presumably) unique value of $i_{+\infty}$ such that $i_{-\infty} = 0$. The results are depicted in Figure B.4.

	$d = 0.001$	$d = 0.01$	$d = 0.1$	$d = 0.2$	$d = 0.3$	$d = 0.4$
$r = 0$	1.99985	1.99848	1.98489	1.96999	1.95532	1.94091
$r = 1$	1.99984	1.99842	1.98430	1.96897	1.95403	1.93948

Figure B.4: The value of $\lim_{x\to-\infty} i(x)$ *of the invading fronts (where* $i_{+\infty} = 0$*), for different values of* r, d *and for speed* $c = 2$*. The numerical values suggest that the effect of* d *is negligible, and that our bound in Lemma B.22 is not sharp. The root finding was performed with Wolfram Mathematica.*

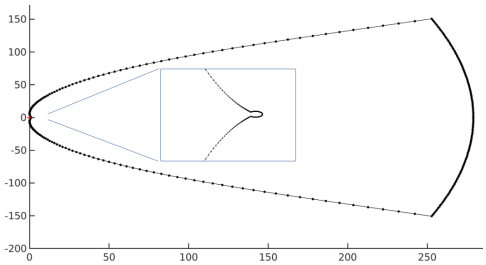

Figure B.5: The Evans function for the weight $w(x) = e^{-x}$*, for* $c = 2.0, d = 0.3$ *and* $r = 1$*, evaluated along the boundary of the domain* $\mathcal{P}$*, see* (B.241)*. The boundary consists of three parts: a semisircle with radius* $\delta = 10^{-3}$ *around the origin, two lines along the imaginary axis, and a semi-circle with radius* R*, see Proposition B.32. The winding number is equal to zero, as a consequence there are no elements of the discrete spectrum of* $\mathcal{L}$ *within* $\mathcal{P}$*. The simulations for all other parameters result in similar pictures.*

The various numerical challenges that arise when computing the Evans function, as well as their solutions, are described in detail by Barker et al. [12], who also suggest using their library STABLAB [13]. Given a numerical solution of the traveling front on an interval $x \in [-L, +L]$ (we choose $L = 50$), centered such that $a'(0) = 0$, STABLAB performs three main steps: first, the unstable and stable spaces of System (B.237) are approximated by the unstable and stable eigenspaces of the constant matrices $M(\pm\infty, \lambda)$. Second, bases of these eigenspaces that are analytic in λ are chosen. Third, the resulting ODEs are solved (forwards on $[-L, 0]$ and backwards on $[0, L]$), in an exponentially weighted space to reduce computation time and increase

numerical stability. We evaluate the Evans function along $\partial\mathcal{P}$, the boundary of the domain

$$\mathcal{P} := \{\gamma \in \mathbb{C} \big| \, \mathfrak{Re}\gamma \geq 0,\, \delta \leq |\gamma| \leq R\}, \tag{B.241}$$

where the radius R is the upper bound for any element of the discrete spectrum with non-negative real-part from Proposition B.32, and a small distance $\delta = 10^{-3}$, since the essential spectrum touches the origin. Note that analytically, the Evans function can be extended up to the origin, see e.g. [48], due to the lack of a discrete eigenvalue zero.

As $d \to 0$, the computation of the Evans function gets numerically unstable. We get reliable results for $d \geq 0.1$, and found no points of the non-negative discrete spectrum for all choices of r, d as in Table B.4. One of the resulting contours is depicted in Figure B.5, all others were very similar.

B.4.3 Geometric singular perturbation theory

For passing continuously from $d = 0$ to $d \ll 1$ in System (B.3), we apply geometric singular perturbation theory for smooth systems, based on work by Fénichel [49, 84]. We present the underlying theory and its application to the present case (briefly, since it is rather standard). Given two C^∞ functions f and g, consider the following smooth field:

$$\begin{aligned} \frac{d}{dt} z &= f(z, y, d), \\ \frac{d}{dt} y &= \epsilon g(z, y, d), \quad \epsilon \sim 0. \end{aligned} \tag{B.242}$$

The variable z is called the *fast variable*, the variable y is called the *slow variable*. Geometric singular perturbation theory leads to a result that describes trajectories that are continuous in ϵ in a neighborhood of $\epsilon = 0$. Introduced by Fénichel in the 70s [49], this approach has been classical for dealing with singularly perturbed systems, check [84]. The central assumption is given as follows, it ensures that the fast variables indeed move along fast stable and unstable manifolds:

Definition B.34. For $z \in \mathbb{R}^n, y \in \mathbb{R}^l$, consider a fixed point $P \in \mathbb{R}^{n+l}$ of a dynamical system as in (B.242). It is called a *normally hyperbolic* critical point, if the linearization of the system around P has exactly l Eigenvalues that lie on the imaginary axis.

For $\epsilon = 0$, the l Eigenvalues with zero real-part of the Jacobian at a normally hyperbolic point must correspond to the slow (constant for $\epsilon = 0$) variables. Only the movement in the fast direction remains. In this setting, a separation of time-scales occurs for $\epsilon \neq 0$ sufficiently small, and one can treat the fast and slow variables separately. The following theorem is a combination of Theorems 1-3 in the monograph of C. Jones [84], this compact form is due to Rottschäfer [125]:

Theorem B.35. *Given a system of type* (B.242)*, such that when* $\epsilon = 0$*, the system of equations has a compact, normally hyperbolic manifold of critical points,* $\mathcal{M}_0$*, where we assume that* $\mathcal{M}_0$ *is given as the graph of a* C^∞ *function* $h^0(y)$*. Then for every* $p \geq 1$*, there exists an* $\epsilon_0 > 0$ *such that for all* $\epsilon \in [0, \epsilon_0)$*, there exists a Manifold* $\mathcal{M}_\epsilon$*:*

1. $\mathcal{M}_\epsilon$ *is locally invariant under the flow defined by* (B.242)*.*
2. $\mathcal{M}_\epsilon = \{(z, y) | z = h^\epsilon(y)\}$*, for a function* h^ϵ *which is* C^p *in both* ϵ *and* y*, and for* y *in some compact set* S*.*
3. *There are locally stable manifolds* $W^s(\mathcal{M}_\epsilon)$ *and unstable ones* $W^u(\mathcal{M}_\epsilon)$*, that lie within* $\mathcal{O}(\epsilon)$ *of and are diffeomorphic to* $W^s(\mathcal{M}_0)$ *and* $W^u(\mathcal{M}_0)$*, respectively. Here,* $W^s(\mathcal{M}_0)$ *and* $W^u(\mathcal{M}_0)$ *are the (fast) stable and unstable manifolds of the unperturbed manifold* $\mathcal{M}_0$*.*

We follow the examples in [84, 125], and analyze the present system for $d \sim 0$. We bring System (B.107) into slow-fast form as in Eq. (B.242), and change the phase-time to the fast phase-time $t := x/d$:

$$\begin{aligned} \frac{d}{dt} i' &= -[ci' + ra + a(a+i)] =: f(a, a', i, i'), \\ \frac{d}{dt} \begin{pmatrix} a \\ a' \\ i \end{pmatrix} &= d \cdot \begin{pmatrix} a' \\ a(a+i) - a - ca' \\ i' \end{pmatrix} =: d \cdot g(a, a', i, i'). \end{aligned} \tag{B.243}$$

Here (a, a', i) are the slow variables and i' is the fast variable. For $d = 0$, there exists a three-dimensional smooth manifold of critical points

$$\mathcal{M}_0 = \left\{ (a, a', i, i') \in \mathbb{R}^4 \,\middle|\, i' = h^0(a, a', i) := -\frac{a(a+i+r)}{c} \right\}. \tag{B.244}$$

We check normal hyperbolicity of $\mathcal{M}_0$. For $d = 0$, we calculate the Jacobian of the system:

$$J_{(a,a',i,i')|M_0} = \begin{pmatrix} 0 & 0 & 0 & 0 \\ 0 & 0 & 0 & 0 \\ 0 & 0 & 0 & 0 \\ r + 2a + i & 0 & a & -c \end{pmatrix}, \tag{B.245}$$

which has a single non-zero Eigenvalue $\lambda = -c$, with fast direction i'. Thus, all points in $\mathcal{M}_0$ have a fast stable manifold of dimension one and no unstable manifold (in fact, $\mathcal{M}_0$ is even a global attractor). In order to apply Theorem B.35, we now choose an arbitrarily large, but bounded subset of $\mathcal{M}_0$. Then, for $d > 0$ sufficiently small, there exists a manifold $\mathcal{M}_d$, that is of distance $\mathcal{O}(d)$ to $\mathcal{M}_0$, together with a local unstable manifold $W^s(\mathcal{M}_d)$ that is of distance $\mathcal{O}(d)$ to $W^s(\mathcal{M}_0)$.

For $d \neq 0$, we can undo our transformation and change back to $x = d \cdot t$. Then, we get that on $\mathcal{M}_d$, the perturbed system is close unperturbed system, in the sense that

$$\frac{d}{dx}\begin{pmatrix} a \\ a' \\ i \end{pmatrix} = \begin{pmatrix} a' \\ a(a+i) - a - ca' \\ i' \end{pmatrix} \tag{B.246}$$

with $i' = h^d(a, a', i)$, subject to the condition

$$ci' = -a(a + i + r) + \mathcal{O}(d), \tag{B.247}$$

which is an $\mathcal{O}(d)$-perturbation of (B.244). Equation (B.247) implies that the restriction of S_d to $\mathcal{M}_d$ is $\mathcal{O}(d)$-close to the unperturbed system S_0. Thus, along $\mathcal{M}_d$, the System S_d can be viewed as a regular perturbation of S_0, which we obtain as a (regular) limit as $d \to 0$:

$$\frac{d}{dx}\begin{pmatrix} a \\ a' \\ i \end{pmatrix} = \begin{pmatrix} a' \\ a(a+i) - a - ca' \\ -\frac{a(a+i+r)}{c} \end{pmatrix}. \tag{B.248}$$

We summarize this in

Corollary B.36. *Fix $p \geq 1$ and choose any smooth bounded set $\bar{\mathcal{M}}_0 \subset \mathcal{M}_0$, for $\mathcal{M}_0$ as defined in* (B.244)*. There exists some $d^* > 0$, such that for all $d \in (0, d^*)$, the System* (B.243) *has a three-dimensional C^p-manifold $\bar{\mathcal{M}}_d$, invariant under S_d and $\mathcal{O}(d)$-close to $\bar{\mathcal{M}}_0$. The flow on this manifold is an $\mathcal{O}(d)$-perturbation of* (B.248)*. Moreover, $\bar{\mathcal{M}}_d$ has no unstable manifold, but only a fast stable manifold $W^s(\bar{\mathcal{M}}_d)$ that is locally diffeomorphic to and within range of $\mathcal{O}(d)$ to $W^s(\bar{\mathcal{M}}_0)$.*

Now let $K > 1$ and consider $d > 0$ sufficiently small. The fixed point $(a, a', i, i') = (0, 0, K, 0)$ has an unstable manifold of dimension one (presumably a traveling wave). With the help Corollary B.36, we can track any finite segment of this manifold:

Corollary B.37 (c.f. Corollary B.13)**.** *Let $K > 1, c > 0, r \geq 0$. First consider the fixed point $(\bar{a}, \bar{a}', \bar{i}) = (0, 0, K)$ of S_0, together with its one-dimensional unstable manifold $M_0^-(K)$. Fix any semi-open interval $x \in (-\infty, T]$, where T is finite, and assume that $M_0^-(K, x)|_{x\in(-\infty,T]}$ is smooth and bounded. Lift it into $\mathbb{R}^4$ via* (B.244)*.*

Now consider the perturbed system S_d. There exist some $d^* > 0$ such that for all $d \in (0, d^*)$: the fixed point $(a, a', i, i') = (0, 0, K, 0)$ has an adjacent one-dimensional unstable manifold $M_d^-(K, x)|_{x\in(-\infty,T]}$, that is continuous in d and converges to $M_0^-(K, x)|_{x\in(-\infty,T]}$ as $d \to 0$.

Proof. Fix a finite time-horizon $T \in \mathbb{R}$ such that $M_0^-(K, x)|_{x\in(-\infty,T]}$ is smooth and bounded. Embed it into $\mathbb{R}^4$ by setting $i' = h^0(a, a', i)$, see

(B.244). Let $\bar{M}_0$ be a smooth bounded subset of M_0, sufficiently large such that

$$M_0^-(K,x)|_{x\in(-\infty,T]} \subset \bar{M}_0. \tag{B.249}$$

There exists an $d^* > 0$, such that for all $d \in [0, d^*)$: there exists a C^p manifold $\bar{M}_d$ that is invariant under S_d, and the restriction of S_d to M_d is a perturbation of S_0 (B.248).

Since $(a, a', i, i') = (0, 0, K, 0)$ is a fixed point, it can not lie on $W^s(\bar{M}_d)$, and therefore must lie within $\bar{M}_d$ itself. Similarly, its unstable manifold, given in Corollary B.10, must lie within $\bar{M}_d$. However, along $\bar{M}_d$, the flow S_d is a regular perturbation of the unperturbed flow S_0, with a perturbation of order $\mathcal{O}(d)$. Thus, the finite segment $M_0^-(K,x)|_{x\in(-\infty,T]}$ is continuous in d, for $d \in (0, d_1)$, with d_1 possibly smaller than d^*, by a regular perturbation analogue to Proposition B.12. □

Numerical analysis: The numerical analysis of the spectrum was performed via STABLAB [13]. The simulations of the Reaction-Diffusion System (B.1) were done with Wolfram Mathematica. The code can be accessed upon request.

C Unpublished:
Tumour architecture and emergence of strong genetic alterations are bottlenecks for clonal evolution in primary prostate cancer

This appendix reproduces exactly the content of the unpublished work "Tumour architecture and emergence of strong genetic alterations are bottlenecks for clonal evolution in primary prostate cancer", authored by Nima Abedpour, Anton Bovier, Reinhard Büttner, Christian Harder, Axel Hillmer, Florian Kreten, Martin Peifer and Yuri Tolkach [94]. At the time of writing, this work is under review, it was summarised in Chapter 5.

C.1 Introduction

Prostate cancer (PCA) is the most prevalent malignant epithelial tumour in male patients [137]. Some of the PCAs are indolent and do not need to be treated, but many tumours are aggressive and need to be diagnosed when the disease is still curable. In these cases, non-diagnosis at an early stage will lead to a metastatic disease, many rounds of therapy, and ultimately, to the patient's death.

PCA, as many other cancers, emerges from accumulation of genomic damage [28]. This means that the consecutive occurrence of genetic alterations in benign epithelial cells in the prostate gland leads to their transformation into a malignant tumour. Depending on how this primary tumour evolves further, it will be either indolent or aggressive [9, 52].

Several major studies provided comprehensive insights into the genetic alterations occurring in primary PCA [2, 5, 18, 52, 158]. More aggressive tumours have a clear tendency to accumulate more genetic alterations [126]. Primary PCAs are highly heterogeneous, both morphologically (appearance under a microscope) and genetically [72, 145]. The former means that different parts of one tumour often show different architectural patterns (the so-called Gleason patterns) that are becoming more complex in aggressive tumours and are related to genomic evolution [42, 126]. The latter means that different parts of a tumour acquire different genetic alterations. There is considerable tumour heterogeneity between individual patients (*interpatient heterogeneity*) and between tumour foci in the case of multifocal PCA in one patient [5, 18, 28, 95, 104, 158]. Importantly, there is also substantial heterogeneity within single tumour foci (*intratumoural heterogeneity*) as a result of

clonal evolution through the whole course of the disease [9, 18, 43, 52, 101]. To date, *interpatient heterogeneity* can be seen as offering a possibility for tailoring therapy to the individual constellation of genetic changes in PCA in single patients. *Intratumoural heterogeneity* (related to clonality), however, is seen as a complex problem. Finding the most relevant tumour clone (e.g. aggressive, metastatic or lethal) within a tumour focus, in order to select the right therapy for a patient, is a very difficult task that has no adequate solution to date [69, 95, 152].

All studies on intratumoural heterogeneity published to date show high levels of intratumoural molecular genetic heterogeneity in primary PCA but seem to touch the problem rather superficially (see Suppl. Table 1 for a review). The studies aimed to provide further relevant insights into intratumoural heterogeneity will warrant systematic investigation of large numbers of spatially separated samples from single tumours (probably $>$ 50–100 samples per tumour are necessary) in large number of cases, using next-generation sequencing approaches. This entails huge financial costs and an enormous amount of bioinformatical and human resources.

In this study, we address the problem of intratumoural heterogeneity and clonal evolution of primary, therapy-naive PCAs from a different perspective. Based on the evidence from recent studies on PCA architecture, biology and evolution, we develop a mathematical model of PCA growth from the time of the formation of the first malignant cell up to its evolution into a full-size PCA, with superimposed genetic evolution and clonal interactions. We characterize in detail the evolutionary processes, resulting clonal architectures, and patterns of spatial interactions between clones. We validate the results of mathematical simulation using deep whole-exome multiregional next generation DNA sequencing of the primary tumours from five patients and demonstrate very close similarities between our predictions of clonal development and real-world data from patient samples.

We fully open-source our model to stimulate further research studies in this area. The code for the simulations, written in Python3, as well as an easy-to-use visual demonstration of the dynamics are available under `https://github.com/floriankreten/Prostate_Cancer_Publication.git`.

C.2 Results

C.2.1 Model development

Three processes are being modelled simultaneously in our virtual PCA models: tumour growth in 3D-space, genetic evolution (acquisition of molecular-genetic alterations), and the competition of arising clones.

Principles of growth of PCA were reconstructed from patient samples earlier and depicted in Figure C.1A. Shortly, prostate cancer grows in hol-

low "channels" lined by epithelial tumour cells (seen as glands in 2D). These channels exhibit a tight spatial intermixing of different branches that are not interconnected, a phenomenon that can be mathematically reproduced using self-avoidance mechanisms. The growth/branching rates and maximal tumour size (number of tumour cells in a clinically relevant PCA is on average 300 mln) were derived from morphometric analysis of patients' tumour samples.

Tumour clone competition stems from the systematic acquisition of driver genetic alterations and occurs on the surface of the "channels" (Figure C.1B). The driver mutations bring *fitness advantage* – basically changing tumour cell birth/death ratio in a positive way, increasing their viability.

To reduce the computational complexity of the model we introduce a model cell (node) which represents a cross-section of the channel (on average 15 tumour cells) and model only driver mutation acquisition while preserving all other relevant principles described above (Figure C.1C). As we are interested in the clonal evolution, we need to define the size of a clinically significant tumour clone that should be at least recognizable morphologically. We estimate this morphometrically (Figure C.1D). A further detailed description of the model, parameters, and biological/morphometric evidence and considerations underlying the parameters and principles is outlined in Sections C.5 and C.7. *For simplicity, in the following we call any type of genetic alteration (including copy-number alterations and any other chromosomal events) a "mutation".*

C.2.2 Tumour architecture: a bottleneck for clonal evolution through the gradual acquisition of driver genetic alterations

We initially aimed to study clonal evolution in our model in the case of gradual acquisition of mutations, selecting 0.04 (4%) found earlier by others [21, 139] to be a reasonable upper bound of the fitness advantage for single mutations. We calculate the effective rate of such mutations that survive the early fluctuations to be $6 \cdot 10^{-6}$ (see Section C.5.5) per cell division. Twenty synthetic tumours were grown to a size of 20 mln nodes (Figure C.2A–D), corresponding to 300 mln real tumour cells. The clonal dynamics were similar in all the tumours (Figure C.2A–D) with 21 independent clones per tumour (clone $=>$ 10.000 model cells in this experiment, s. Figure C.1D) on average (range 14–34), an average fittest-clone fitness of 1.44 (1.32–1.54) and an average maximal number of consecutive mutations in the fittest clone of 9 (7–11). No substantial divergent evolution (formation of subclonal populations with branches) was evident (Figure C.10). The maximal size of the largest clone among all the tumours was only 3.7% (range 0.3–3.7%), with the remaining tumour volume filled with ancestral clone cells and multiple less fit small populations. As for the temporal dynamics (Figure C.2B,C), the substantial fluctuation concerning the time of initial clone emergence

and the maximal number of consecutive mutations shifted to very similar evolutionary trends after the size of eight million cells.

Thus, the gradual acquisition of driver mutations with small fitness advantages does not result in any awaited forms of divergent clonal evolution. The branching tumour architecture with predestined spread vectors and a specific nature of inter-clonal competitive interactions in PCA makes small fitness advantages of little sense for the selection of tumour clones, offering at best only a local advantage.

C.2.3 Single strong mutations: a possibility for clonal expansion depending on the time of appearance and emergence place

In models with gradual acquisition of 'weak' mutations with small fitness advantages, substantial clonal divergence can be achieved only through substantial rises in the mutation rate, which is unrealistic for most tumours. PCA, however, is known for its recurrent genetic alterations in potent genes, which can provide a greater fitness advantage with one hit (e.g. PTEN, TP53, MYC family, copy-number alterations, larger chromosomal events such as chromoplexy/chromotrypsis or whole genome duplication). The functional impact (fitness advantage) of such 'strong' mutations cannot be reliably predicted and may be very different for different genes and in different conditions. The same is true for the mutation rate of strong mutations. We empirically consider a fitness advantage of 0.5 for a single strong mutation to be reasonable and investigate three different "strong" mutation rates based on our initial estimates from available genomic data: $5 \cdot 10^{-10}$ (X10 virtual tumours), $2.5 \cdot 10^{-9}$ (X50 virtual tumours), $5 \cdot 10^{-9}$ (X100 virtual tumours).

To study the influence of architecture on clone development, we simplified the model and placed only one strong mutation in a tumour without other clones (background fitness 1.0) at different fixed tumour sizes, disabling further mutations (Figure C.3). A strong mutation should emerge as early as at 1–3 mln nodes (ca. 10% of the final size) to provide some extent of size dominance in a full-grown tumour. The most advantageous place of emergence is the tumour initiation centre (the root of the tree), allowing quick spread in all directions even with later appearance, but the probability of such an event in the stochastic system is low.

C.2.4 Early consecutive acquisition of strong mutations: a proxy for the formation of aggressive tumours

Next, we performed simulations in full models embracing both types of mutations weak and strong) with three different mutation rates for strong mutations, 50 simulations for each group (X10, X50, X100). Using our previous definition of a clone (hierarchy branch $>$ 10.000 nodes) resulted in substantial

increase of number of clones/tumour (Figure C.4A). Therefore, we revised our clone definition to one that holds greater clinical relevance, classifying it as a branch with a size exceeding 5% of the entire tumour. This choice aligns with the convention cut-off of 5% utilized to identify the tumour portion that could significantly impact the patient's prognosis, commonly known as the tertiary Gleason grade.

Divergent evolution was evident in all the three groups with at least local clonal sweeps (elimination of precursor clones) differing in effect size. In most of the X100 tumours, an ancestor clone was eliminated by clonal sweeps (Figure C.4A). There were several typical patterns of clonal evolution (Figure C.4B, C.5A–B; clonal hierarchies for single tumours in Figures C.11, C.12, C.13). Importantly, even in the case of a high strong mutation rate (X50 and X100), one third of the tumours presented only one dominant clonal branch, compared to 66% of the tumours in group X10 (Figure C.5; Figure C.4B). Branching evolution with both early and late divergence was more typical for groups X50 and X100 ($p < 0.001$). The median numbers of dominant clones (highest fitness) were 1, 2 and 2 in the tumours from groups X10, X50 and X100, respectively (ranges 1–3, 1–4 and 1–5). Importantly, even with a very high strong mutation rate (X100), there was no tendency to formation of a large number of clonal branches (Figure C.5B). At the end of the simulation, X10, X50 and X100, the most advanced clones, had medians of 1, 2 and 3 consecutive strong mutations (ranges 0–3, 1–3 and 1–5), respectively (Figures C.11, C.12, C.13). Most of the tumours (especially X50 and X100) had additional (1–5%) small populations, some of them with a fitness level comparable to that of the dominant clone (Figures C.15, C.16, C.17).

We sought to determine which factors are responsible for certain ways of clonal evolution. Late-arising clonal divergence is mostly influenced by stochastic processes and the local composition of clones, when a new strong mutation emerges. However, early divergence may be influenced by some high-level parameters, such as the timing of the first strong mutations. Statistically, neither the timing of the first nor the second consecutive strong mutation was significantly associated with the number of dominant clones or early versus late clonal divergence patterns (all $p > 0.05$ for pairwise comparison within X-groups, Mann–Whitney U test), leaving the stochastic nature of the clonal interactions and the locations of the emerging mutations primarily responsible for the patterns of clonal divergence.

The clonal-evolution pattern had no influence on the maximal fitness of the dominant clone ($p < 0.05$ in all the X-groups). However, the maximal fitness of the dominant clone(s) at the end of the simulation was clearly correlated with the emergence time of the first and especially the second consecutive mutation, which seems to be a proxy for the development of more aggressive tumours (Figure C.14).

C.2.5 Biopsy extent: crucial for the adequate sampling of relevant clones

Next, we sought to analyse the spatial relationships between clonal populations within synthetic tumours in a clinically relevant context. Approximately 10–12 biopsy cores are usually acquired during systematic multifocal prostate biopsy in patients with PCA suspicion, with (according to our estimation) on average five cores containing a tumour. We set up a virtual biopsy in X10, X50 and X100 tumours with five cores, one taken more centrally and four taken from the peripheral regions (Figure C.6A, C.19), with the penetration depth into the tumour selected randomly for each core. The number of nodes in each core was approximately 30.000-35.000 (see Section C.7.6). We selected a 5% volume threshold for the detection of clones in the biopsy (in clinical practice, 5% is often considered a threshold for reliable detection using next-generation sequencing). In 3/50, 11/50 and 10/50 of the X10, X50 and X100 tumours, respectively, one or more dominant clones were missed by virtual biopsy (total number of missed clones: 3, 14 and 14, respectively) (Figure C.6B). The median sizes of the missed clones were 5.4, 6.1 and 6.6% of the whole tumour size, respectively (range for all the groups 5.2–17.5%). Among the detected dominant clones in groups X10, X50 and X100, 11/62, 27/87 and 27/89 were present in only one biopsy core, implying that they can be missed if the cores are not equidistant or contain less cells (Figure C.6C). In a substantial number of cases in all the groups, there was more than one dominant clone in a single biopsy core (due to prominent spatial intermixing) (Figure C.6D). Larger clones were detected in a higher number of cores, with a higher fraction in single cores (Pearson's correlation > 0.63 in all the groups; $p < 0.0001$) (Figure C.6C). Multiple dominant clones in one core and sampled small populations can make the reconstruction of the clonal architecture from a single core or multiple cores very difficult. A detailed example of such complexity for one tumour is shown in Figures C.7, C.20 and C.21.

C.2.6 Validation of findings: ultra-deep whole-exome sequencing of human tumour samples

In order to validate our theoretic predictions, we performed multi-regional ultra-deep next-generation (NGS) whole-exome sequencing (WES) to study molecular genetic alterations of five primary prostate cancers (Figure C.8, s. Section C.5.8 for a detailed description) with a regional spectrum of morphologies between Gleason scores 3+3 and 4+3 (tumours with branching being a main growth mechanism – therefore following our model's assumptions). WES was performed from at least 5 large, neighboring areas of each tumour with a coverage of up to 400x. Copy number alterations (CNA) were assessed for all tumour samples (Figure C.8B). The somatic point mutations

identified by WES were clustered according to cancer cell fractions (CCF; Figure C.8C). Finally, clonal hierarchies for five tumours were reconstructed based on the results of can analysis and somatic mutation CCFs considering for clonal/subclonal nature of alterations, especially in case of single clone presence in several samples due to intermixing (Figure C.9A).

Among the tumours, we had a clear pre-dominance of larger tumours (otherwise, multiregional sampling with sufficient sample size was not possible). This is mirrored by the substantial number of (stronger) alterations identified than it might be awaited in indolent Gleason Score 3+3 and smaller tumours. As expected, most relevant alterations stem from CNA (Figure C.8B). However, most of the CNAs represent heterozygous alterations, implying that the sampled tumours originate from the intermediate/lower aggressivity spectrum, which aligns with our study's intended focus.

The results of the NGS study and reconstruction of clonal hierarchies (Figure C.9A) validate several important findings from our mathematical simulation. Firstly, we see clear evidence for early, late, and mixed divergence of the clonal branches (Figure C.9A). PCA2 case showed whole-genome duplication as a very early event with other tumours presenting with alterations effecting such genes as TP53, PTEN, RB1, BRCA2, NKX3.1 in their trunks. Secondly, in most tumour leading branch alterations at divergent points embrace known genes which can be considered as strong alterations driving clonal branch formation. Thirdly, the overall number of branches is very similar to our mathematical models with strong mutations, emphasizing their role in PCA development. Fourthly, when we reproduced virtually the samples (number of tumour cells, location and form) taken in patient cases in our virtual tumours, roughly the same number of discernable subclonal populations could be found (Figure C.9B,C; Section C.7.6) implying realistic clonal evolution/intermixing processes derived from mathematical modelling.

In two tumours (PCA4 and PCA5) immediately adjacent to the larger tumour we found a second, genetically completely independent smaller tumour with restricted number of the genetic alterations identified which might imply that growth and development of these tumours was limited due to the presence of more advanced tumours in the neighborhood.

C.3 Discussion

In this study, we addressed the problem of intratumoural heterogeneity in primary PCA. A number of studies (see the detailed review in Suppl. Table 1) have investigated intratumoural heterogeneity in patient samples. These studies showed an enormous extent of heterogeneity with a large number of clonal populations within a tumour. Most of the studies investigated only one sample or a few samples of single tumours. Their results show that the number of samples needed to fully decipher the clonal hierarchy of a single

tumour might be very large (50–100). This implies very high sequencing costs, human resources, and extensive bioinformatical analyses. Our study utilised an *in-silico* approach, which could model PCA development and inform further patient sample studies. Using biological evidence of PCA growth and architecture [146, 150] as well as principles of genetic evolution and clonal competition [71, 144] within a tumour, we created a realistic mathematical model embracing all these processes.

The consecutive acquisition of mutations with small fitness advantages, found to be sufficient in other tumour types and models [21], did not allow for divergent evolution in our PCA models. We attribute this result to the architecture bottleneck and the competitive nature of the process, preventing the formation of clones with relevant sizes or fitness levels, as well as hindering clonal sweeps that lead to the emergence of a dominant clone (Figure C.2). Importantly, the PCA architecture, being a bottleneck and pre-determining the directions of clonal spread, warrants 'strong' genetic events with large fitness advantages to stimulate divergent evolution and formation of aggressive tumours. Such events are presumably known for PCA, such as PTEN and TP53 deletion/mutation (or other CNAs), indirectly alterations of BRCA1/2 and other DNA-repair-related genes (known to have special evolutionary trajectories to advanced cancer), as well as alterations in the MYC gene family and such events as chromoplexy, chromotrypsis, and whole-genome duplication [9, 28, 52, 52, 158].

Importantly, the probability of such strong events is not easy to decipher. A unified rate of 'strong' alterations does presumably not exist, due to the patients different conditions and backgrounds. In our opinion, the groups that we investigated in detail in our study (only weak mutations and weak and strong mutations with strong mutation rates: X10, X50 and X100 virtual tumours) represent a continuum of possible evolutionary processes within PCAs. Thus, indolent tumours (Gleason score 3+3) are probably those mirroring a model setup with only weak mutations. Gleason score 3+4 tumours may be tumours with very low strong mutation rates (or emerging late), and aggressive tumours with higher Gleason scores may follow the evolutionary ways outlined by X50 and X100 groups. Importantly, the results of this study show that tumours with early emergence of a first strong event and rapid consecutive occurrences of further strong events reveal paramount aggressiveness. The first strong event may need to occur as early as at a size of 10–15% of the final average tumour volume at clinical diagnosis or even at a smaller size to fuel the development of an aggressive tumour (Figures C.3, C.4, C.14).

The results of our study concerning the evolutionary trajectories and hierarchies of PCA tumours (Figures C.4, C.5) appear to be even more valuable because they match the results of many studies using patient samples (21 relevant studies summarised in Suppl. Table 1) and our own validation study utilizing multiregional WES of five tumours (Figures C.8, C.9).

Thus, most of these studies showed a small number of clonal branches and patterns of early and late divergence, similar to our results (mathematical modelling and NGS study on patient samples). Moreover, strong alterations are necessary for initiating divergent development with clonal branches in our mathematical study which we could confirm in our NGS study on real patient samples.

Among the studies with a detailed reconstruction of clonal hierarchies, the most prominent, that of Wilkinson et al. [161], showed in 37 patients with a high-risk disease the same patterns of clonal hierarchy we received for the synthetic tumours in our study, including a number of tumours with only one leading clonal branch (see Figure C.18 for the detailed analysis of [161], and Figures C.4, C.5). The disadvantage of this study is that it was performed using biopsy material (limited amount of tissue analyzed).

According to our study, the PCA architecture serves as a bottleneck for the development and fixation of multiple branches and multiple divergent clones. Another landmark study by Espiritu et al. [43] with 293 patients (one tumour sample per patient) showed that 59% of the single-tumour samples in the study contained more than one tumour clone (46% biclonal, 12% triclonal). Espiritu et al., however, did not provide the estimation of dominance of such sampled clones, and the results of our biopsy experiments referred only to the dominant clones with leading fitness levels. However, the monoclonality and biclonality in 66 and 6–16% of the biopsies in this study, respectively, are very close to the results obtained by Espiritu et al. [43] based on the analysis of the patient samples. These and our results imply tight spatial intermixing of different branches and divergent clones in PCA tumours, which is also supported by a number of other studies [4, 33, 40, 78, 152, 164].

Another important finding of our study is that the acquisition of few consecutive strong genetic alterations (appr. 1–5 after the formation of the first malignant clone) is enough for the development of an aggressive tumour. This result is difficult to compare with that of previous studies on patient samples. Normally, dozens of genetic rearrangements (single nucleotide variations, copy number variations) are being identified during tumour exome/genome sequencing [5, 28, 52, 158]. However, it is very difficult to predict the functional impact (driver character) of many of these, especially that of copy number variations (typical for PCA), where many genes are affected simultaneously. However, there is strong evidence (also in other tumour types) that the number of consecutive 'real' driver events that can fuel an aggressive tumour is small. Attempts should be made to identify this kind of driver event for PCA, and to filter out the kinds of events that have no functional significance [123].

Further studies on intratumoural heterogeneity are very important as they will have consequences for therapy selection, prognosis and prediction of such events as metastasis formation and therapy response [36, 52, 95, 100,

152]. These clinical decisions are possible only when the most advanced clone can be reliably identified using prostate biopsy. The evidence from patient-sample-based studies is still scarce. Our study provides a realistic mathematical model based on biological evidence of growth and clonal evolution in PCA. The model that we developed is flexible, and new emergent data of tumour biology and concepts of evolution can be easily integrated in it and tested (e.g. special situations such as DNA-repair-deficient tumours) [52]. It can be applied in further studies using patient samples to avoid large costs linked to extensive multiregional next-generation sequencing. The full code for the model implementation is released with the publication.

Of course, our mathematical model is not devoid of limitations. It is simplified and does not account for issues such as microenvironment influences, spatial growth effects due to the presence of benign tissue and the effects of metabolic and hormonal factors. Tumour growth is restricted to the active growing tips, according to the principles of branching morphogenesis [73]. It also does not consider the nature of the genetic alterations, the pathways in which they arise, their interactions, and the epigenetic mechanisms. The same mutations can bring different effects in different contexts. Some other mutations (e.g. BRCA1/2) might influence baseline mutational processes (mutation rate and type of emergent genetic alterations) rather than directly fitness and require a special model parameter setting to test their effects. Importantly, we did not simulate tumour formation and start with the first ancestor malignant cell and its escape from the host's immune system (already having several genetic alterations necessary for malignant transformation, which can potentially affect evolutionary trajectories). We also chose to fix the branching pattern in all our models. Otherwise, an increasing proportion of branching rate C_b/C_g, for instance, would be necessary, imitating Gleason pattern 4 and 5 tumours with higher branching rates. Therefore, the presented results are applicable to the most frequent type of PCA tumours that are well and moderately differentiated.

C.4 Conclusion

Our simulations provided reasonable predictions of PCA genetic evolution close to the current state of evidence from patient samples. Importantly, we showed that the number of evolutionary trajectories and dominant clones is finite. We outlined different ways of genetic evolution and showed that the formation of an aggressive tumour is possible only in the case of the consecutive and early acquisition of 'strong' genetic alterations. Dominant clones are intermixed in PCA tumours and in biopsy cores, which should be accounted for during molecular genetic characterisation and clinical decision making. Our mathematical model can provide guidance for further targeted clinical research in this area and is flexible for the integration of emerging clinical and experiment data.

C.5 Methods

In this study, we model tumour growth and genetic evolution of PCA starting with the formation of the first invasive malignant cell. We describe the underlying biological processes and their mathematical implementation.

C.5.1 Tumour architecture

PCA is a tumour with a very complicated architecture predictive of tumour aggressiveness. It is measured using the so-called Gleason grading [42]. According to several recent studies that endeavoured to decipher the three-dimensional (3D) architecture and principles of growth in PCA [146, 150], many well and moderately differentiated tumours grow in the form of hollow channels, appearing as glands at the two-dimensional sections. Such PCA tumours form a tree with branches arising through tip bifurcations of single channels–glands (Figure C.1A). These branches are spatially tightly intermixed but not repeatedly interconnected (Figure C.1A). This mirrors a well-studied embryonic branching morphogenesis program typical for many organs [73, 140].

The detailed morphological evaluation from our previous reconstructions [146] showed that: 1) branching always occurs through bifurcation, 2) in tumours that are well and moderately differentiated, bifurcations occur relatively systematically at similar distances. Morphological measurements as bases for the mathematical implementation of growth are provided in Figure C.1C. Tumour size estimates (number of cells) were derived morphologically in ten prostatectomy cases (Figure C.1D, Section C.7.1) with clinically relevant PCA tumours containing on average 300 million (mln) cells. For simplicity, we model PCA tumours that are well and moderately differentiated and that grow by branching (as a subset of the most aggressive tumours show very irregular or no branching patterns).

C.5.2 Mathematical model

We model PCA tumour as a network consisting of nodes (or vertices) that are connected to each other through edges. Every node of the network represents a transversal section (Figure C.1C) of a hollow channel of 15 cells at a fixed position in $\mathbb{R}^3$. The 15 cells of a node are assumed to have the same genotype and are the base entities of our model. In this way, we reduce the cellular movements by one dimension and simplify the hollow nature of the tumour channels–glands (the reconstruction of channels as hollow structures with interactions of the cells on the luminal surface is extremely complex). This simplification preserves the biological sense of cell interactions: any clonal propagation within the channels must occur in the axial direction, along the edges of the network (Figure C.1B,C).

We make the assumption that the aforementioned network is static away from its active growth tips. The growth dynamics can be summarised as a *self-avoiding branching process*. Up to small modifications, we adopt an existing model that was used by Hannezo et al. to study the growth of mammary glands [73]. Together with the clonal dynamics, the evolution of the system is formulated as a time-continuous stochastic jump process [44] that can be simulated using a Gillespie algorithm [65]. At each node, we differentiate four types of possible events: *growth, branching, mutation and competition* (Figure C.1C). Each event is triggered at exponential rates denoted as R_g, R_B, R_μ, R_c. The first occurring event is executed, then the rates are adjusted to the new situation. All the rates depend on the rate of cell division, which effectively acts as fitness in this model and as such is denoted as $f(v,t)$, the fitness of the genotype present at node v at current time t.

We concentrate on driver mutations and ignore neutral or deleterious (yielding a disadvantage in fitness) mutations. In the following, we refer to a *mutation* as any type of genetic alteration that brings fitness advantage to a cell by increasing its rate of cell division. Moreover, we assume that mutations are unique, ignoring the possibility of parallel evolution of independent subpopulations. A *genotype* has a unique combination of consecutive mutations. Over the entire tumour, such mutations occur with a certain probability P_μ per cell division. The resulting fitter genotype spreads along the edges of the network at competition speed depending on its local fitness advantage. The parameters that we chose for the simulations are discussed in Section C.7, but we want to emphasize that qualitatively, our theoretical predictions are a result of the structure of the model.

Remarks on the implementation: Since the process is a stochastic jump process with finite rates, it can be simulated by a Gillespie-algorithm [65]. Each step of the presented algorithm can be computed in $\mathcal{O}(1)$, independent of the current size of the system. This is possible since on the one hand all rates depend only on some local information and on the other hand each event effects the system only locally. The implementation is done in Python 3 and as such is not optimal computation-wise but user-friendly, its different modules can easily be modified independently. Fishplots were made using the corresponding R-package [108].

C.5.3 Growth dynamics

Each growing branch acts independently of the others. At its foremost node (vertex) v, either a growth or a branching event occurs randomly, with exponential rates $R_g(v,t) = f(v,t) \cdot C_g$ and $R_b(v,t) = f(v,t) \cdot C_b$, respectively.

During a growth event, a new random coordinate in front of v is checked, the chosen direction can slightly deviate from the previous one. If the sam-

pled position is not too close to the other branches of the network (Section C.7.1), a new node w is placed there and is connected to v via an edge. If the chosen coordinate is blocked, a new one is sampled independently. After $N_g = 5$ unsuccessful trials, the growth event is considered to have failed due to spatial restrictions. A similar mechanism is used during a branching event, where the two new branches point at opposing directions and have a fixed degree of $\beta = 60°$ to the previous growth direction (Section C.7.1). Both the growth and branching events can occur only once; as such, growth ultimately stops in dense regions.

The two constants $C_g = 0.08$ and $C_b = 0.02$ are defined via the two equations $C_g + C_b = 0.1$ and $C_b/G_g = 0.25$. The former equation regulates the total speed of growth at a single active tip: after the time that it takes a single cell to divide ten times, an active tip grows or branches out (Section C.7.1). The latter equation regulates the resulting architecture.

Without the spatial restrictions, the process would be a well-understood, time-continuous Galton–Watson process [7]. Branching annihilating systems (where particles are removed upon collision) are well-studied [8, 23, 29], but self-avoiding mechanics are intricate to study [105, 149]. We refer to [73] for both an in-depth introduction to the model, different mathematical approaches and applications in biology are also presented by Lang et al. [96]. The simulations show that growth is asymptotically of cubic order as the graph takes the form of a ball whose radius grows with constant speed, whereas exponential growth is assumed in most cancer models. This assumption has already been verified for several types of carcinoma and also for PCA [103]. However, it was also shown that spatial pressure of the surrounding tissue can play a crucial role in the growth of PCA [102]. The tumours that we model are well and moderately differentiated and mimic the morphological aspects of healthy tissue, and grow in cell dense regions. The exponential growth reported for aggressive PCA thereby does not contradict our model. We model the influence of the surrounding tissue indirectly by adjusting the growth rates (Section C.7.1).

C.5.4 Cell of origin

The development of PCA involves the systematic acquisition of genetic alterations (chromosomal aberrations more important than somatic point mutations) by the cells within a tumour, which are primarily related to advantages in terms of the birth-death ratio of tumour cells [59]. No studies definitively clarify the presence and location of cancer stem cells with regard to PCA. All the cells within the tumour seem to have stem cell properties to some extent, or at least the higher-potency stem cells are dispersed over the entire tumour [128]. PCA cells can also conditionally modulate their functionality and cell division rate [128]. In view of this, we assume that mutations can occur at any cell within the tumour. However, even if mutations should be

restricted to stem cells only, they would be supposed to occur in all nodes, as one node in our simulations represents 15 real tumour cells and solid tumours have on average a fraction of cells with stemness properties of up to 5–10% [155]. Therefore, under the assumption of a well-mixed population, roughly every node contains at least one stem cell.

C.5.5 Weak driver mutations

We model two different types of driver mutations. Weak mutations (somatic mutations and copy number alterations) yield a more conservative fitness advantage of $\Delta_f = 4\%$. We set the probability for a weak mutation to per cell division, the same order of magnitude estimated by Bozic et al. [21] and Sun et al. [139]. Under these assumptions, the divergent genetic evolution in tumours through gradual mutation could be shown [21, 139]. This might well represent the processes of evolution in less aggressive PCA tumours (with Gleason scores $3+3=6$ and $3+4=7$), which are indolent and slow growing and virtually never metastasise. As one node represents 15 tumour cells, the mutation rate for weak mutations is given by

$$R_\mu(v,t) = 1.5 \cdot 10^{-4} \cdot f(v,t) \tag{C.1}$$

per node. We do not model genetic drift processes and investigate only mutations that survive the early fluctuations and become fixated in the population. This results in an *effective rate of weak driver mutations* of

$$R_{\mu,eff}(v,t) = R_\mu \cdot \Delta_f = 1.5 \cdot 10^{-4} \cdot f(v,t) \cdot \Delta_f, \tag{C.2}$$

see e.g. Méléard et al. [11], details in Section C.7.2.

C.5.6 Strong driver mutations

We hypothesise (see Section C.2.2) the necessary existence of strong drivers in PCA. Alterations in potent genes such as PTEN, TP53, RB1 or genes of the MYC family and complex driver events of chomotrypsis/chromoplexy (believed to substantially increase the tumour aggressiveness with one hit) are typical for PCA, especially in aggressive tumours [9, 28].

We propose an increase in fitness of $\Delta_f^s = 50\%$ and initially define their rate of occurrence as

$$R^s_{\mu,eff}(v,t) = 5 \cdot 10^{-11} \cdot f(v,t), \tag{C.3}$$

on the basis of our estimation of potentially strong events in primary PCA at or close to the clinically significant stage (Section C.7.4) [28, 52]. The proposed estimate, however, seems to be low as we obviously consider only a limited number of known strong alterations. In further simulations, we increase the corresponding rate to

$$R^s_{\mu,eff}(v,t) = 5 \cdot 10^{-9} \cdot f(v,t), \tag{C.4}$$

a hundredfold increase of our original estimate but still far below the rate of weak driver mutations. As the increased rates might result in extremely high fitness values at the time of evaluation, we set a saturation mechanism using an upper bound of $f_{max} = 10.0$ (Section C.7.5). Given a mutation with either $\Delta = \Delta_f$ or $\Delta = \Delta_f^s$, the new genotype had fitness

$$f_{new}(v,t) := f_{old}(v,t) \cdot \Big[1 + \Delta \cdot \Big(1 - \frac{f_{old}(v,t)}{f_{max}}\Big)\Big], \tag{C.5}$$

where all the simulations start with a single node with $f(v_0, t_0) = 1.0$.

C.5.7 Tumour cell interactions/clonal competition

Given the architecture of PCA, the interactions between the tumour cells and the clonal competition follow different principles compared to tumours with more well-mixed cell populations. The PCA cells in most tumours are arranged in one cell layer on the luminal surface of tumour channels–glands (Figure C.1B), where clonal competition occurs mainly in two dimensions (with similarities to the competition processes on the surfaces of colonic mucosa/adenomas). The channel–gland tree-like architecture of PCA tumours makes the nature and direction of clonal sweeps deterministic to some extent as these should follow the pre-formed tumour branches, otherwise the regular spatial structure would loosen up. Evidence for competition on the surface of the glands is well documented pathologically [71, 144].

Under the assumption of a static interior of the tumour concerning its architecture, each cell division must induce a local competition process. Similar to the effective rate of mutation, we model only the *effective competition*. We take into account the extinction of a new genotype due to early fluctuations by resorting to the effective rate of mutation. In the case of a mutation, we assume that the fitter genotype at node v spreads to its neighbour w (along the edge of the network that connects the two) with speed $R_c(v,w,t)$ (Figure C.1B,C). The resulting competition process is a contact process, resulting in a relabelling of the nodes. The growth behaviour is affected only if a fitter genotype reaches an active node. The rate of competition is defined as

$$R_c(v,w,t) = \frac{f(v,t) - f(w,t)}{N(v,t)}, \tag{C.6}$$

where $N(v,t)$ is the number of edges adjacent to v. Only the advance of the fitter genotype is represented. On a cellular level, this corresponds to the idea that when a cell divides (with either rate $f(v,t) = k + \Delta$ or $f(w,t) = k$), a neighbouring site is chosen, and the resident cell is replaced (Section C.7.3). If node v has only two adjacent edges, the resulting advance of the fitter genotype occurs with speed $R_c(v,w,t) = \Delta/2$. This slow replacement process dictates the rules for evolution.

C.5.8 Next generation sequencing and reconstruction of clonal hierarchies

Fresh frozen tumour samples from five patient cases were cut and stained with Hematoxylin&Eosin to identify tumour tissue. Ten consecutive 14 µm tissue sections were made and tumour tissue areas and benign tissue areas were macrodissected. DNA extraction was performed using Qiagen QIAamp Fast DNA kit (Qiagen, Venlo, The Netherlands) according to manufacturer instructions with a target of at least 250 ng of DNA. All samples passed DNA quality check. Library preparation was performed using Twist Human Core + RefSeq + Mitochondrial Panel (Twist Bioscience, San Francisco, CA, USA). Next generation whole exome sequencing was performed using NovaSeq6000 (2x100 bp; Illumina, San Diego, CA, USA) with a target output of 60 Gb for tumour and 30 Gb for benign tissue samples (sequencing depth 400x/200x, correspondingly). Demultiplexing of sequenced reads was performed using Illumina bcl2fastq (2.20). Adapter trimming was performed using Skewer (0.2.2).

The raw sequencing data were processed as previously described [35, 58, 77, 119]. Sequencing reads were aligned to the human reference genome GRCh37/hg19. Read-pairs with similar coordinates were assumed to be potential PCR duplicates and were subsequently masked out from the read statistics. Aligned Sequencing reads statistics were used to estimate tumour purity, tumour ploidy, and call somatic mutations and copy number alterations [58, 119]. In brief, to determine somatic mutations, variant counts were assessed in tumour and matching normal samples and corrected for sequencing noise and compared to a database of 300 whole exome sequenced normal samples to thus call the somatic mutations [119]. Variants at low allelic fractions are often prone to be resulted from sequencing artifacts, which occur as a consequence of sequencing noise due to low coverage WES or due to fragmented DNA as part of FFPE material. We implemented a filtering criterion for mutations which occur at low allelic fractions of less than 0.2. These mutations were filtered out if 1) the forward-reverse bias ratio was below a threshold (default value 0.2), and 2) if the allelic fraction of the mutation times the minimal coverage of the normal or matching tumour sample at the position in consideration did not exceed a (read count) threshold (default value 10). Thus, the mutations at relatively low allelic fractions and low sequencing coverage are filtered out as potential sequencing noise and false-positive mutation calls. The tumour clones and tumour phylogenies are identified based on somatic mutation calls [35, 77] and assessment of copy-number alterations. In multi-sample studies, a sub-clonal mutation at very low allele fractions in one tumour can be more abundant at another tumour. In this case, a mutation at a low allelic fraction which were filtered out in one sample, were re-introduced as a somatic mutation, if the same mutation passed all filtering criteria in another matched tumour sample.

To identify individual clones from tumour sequencing data, an expected allelic fraction was assigned to each mutation based on a model that considers the tumour purity, average tumour ploidy, the copy number state, and the number of mutation copies at the respective genomic coordinate of the mutation, under the assumption of clonality [35, 119]. Relative observed allelic fraction to the expected allelic fraction estimates a *Cancer Cell Fraction* (CCF) for each mutation. By a subsequent clustering of the mutation CCFs, we identify cell clones represented by subsets of individual mutations [35]. The average CCFs of the mutations in each associated clone in a given tumour represent the clonal fractions of the clones and thus define the overall clonal composition of the tumour at the time point of sampling. Our method is benchmarked in pan-cancer studies [39, 60].

C.5.9 Analysis of clonal architecture from multi-regional tumour samples

In order to study tumour evolution from multi-regional samples of a given patient, we used a 2-dimensional clustering approach to analyze the clonal dynamics in pairs of samples of the same patient [77]. As the first step, we performed adjustments to the mutation calls and copy number state calls assessed individually for each tumour sample, considering all samples of a given patient simultaneously. For this purpose, a unified copy number segmentation for all samples of a patient is generated and the copy numbers were re-called for these unified segments. This step is critical for the comparison of the allele-specific copy number calls and the mutation CCFs across the samples of the same patient. We also created a unified list of *somatic single nucleotide mutations* (SNMs) for all samples of each patient, and re-called the somatic mutation of the unified list in all samples with relaxed filter criteria. This allowed us to detect the high-confidence mutation calls from one sample with lower allelic fractions in other patient-matched samples. Subsequently, the 2-dimensional clustering analyses were performed on the recalculated CCFs of the re-called set of mutations for each sample pairs. Moreover, we set a minimum threshold of four mutations per cluster. Considering the CCF of the cluster center as the representative CCF of the corresponding cell clone, we considered the infinite sites hypothesis, assuming that mutations appear just once in the evolutionary history of a tumour, and the CCF sum rule [134, 141] to infer the phylogenetic tree and the clonal composition per sample. In the rare event in which these assumptions allowed for multiple tumour phylogenies, we considered the maximum parsimony assumption and preferred linear evolution over branched evolution. Since the copy number segments with poly-ploidy allow for ambiguous solutions for the absolute numbers of mutated copies, in the case that mutation clusters conflicted with phylogenetic rules, we re-assess the mutation copy values of the somatic mutations for an alternative possible solution

that resolves the phylogenetic rule conflicts. All copy-number alterations were evaluated with regard to the affected genes and were considered during phylogenetic reconstruction of clonal hierarchy in single tumours together with analysis of somatic point mutations.

Declarations

Ethical considerations

The usage of tumour samples from patients was approved by the ethical committee of the medical faculty of the University Cologne (vote 13-091).

Acknowledgments

We thank Barbara Holz and Vanessa Richartz for their help with processing of tissue samples.

Data availability statement

All mathematical modelling data generated in course of this study is freely available on reasonable request from corresponding authors. The code used for the mathematical simulations is publicly available, see `https://github.com/floriankreten/Prostate_Cancer_Publication.git`. Sequencing data is available from corresponding authors on reasonable request.

Acknowledgments

FK and AB are partially supported by the Deutsche Forschungsgemeinschaft (DFG, German Research Foundation) - Projektnummer 211504053 - SFB 1060 and by Germany's Excellence Strategy - GZ 2047/1, Project ID: 390685813 „Hausdorff Center for Mathematics" at Bonn University. YT, RB, CH are funded by the Wilhelm Sander Foundation, Munich, Germany: Grant 2022.040.1 (YT, CH) and the Federal Ministry of Education and Research of Germany: Project FED-PATH (YT, RB).

Authors' contributions

Study concept: YT. Model design: YT, FK, AB. Mathematical implementation / simulations: FK. Data analysis, statistics: YT, FK, NA. Data interpretation: all authors. Manuscript drafting: YT, FK. Patient samples acquisition and processing: YT, AH. NGS analysis: NA, YT. Supervision, administrative support: RB, MF, AH. Manuscript editing, critical revision for important intellectual context: all authors.

Declaration of interest

The authors declare no conflict of interest.

C.6 Figures

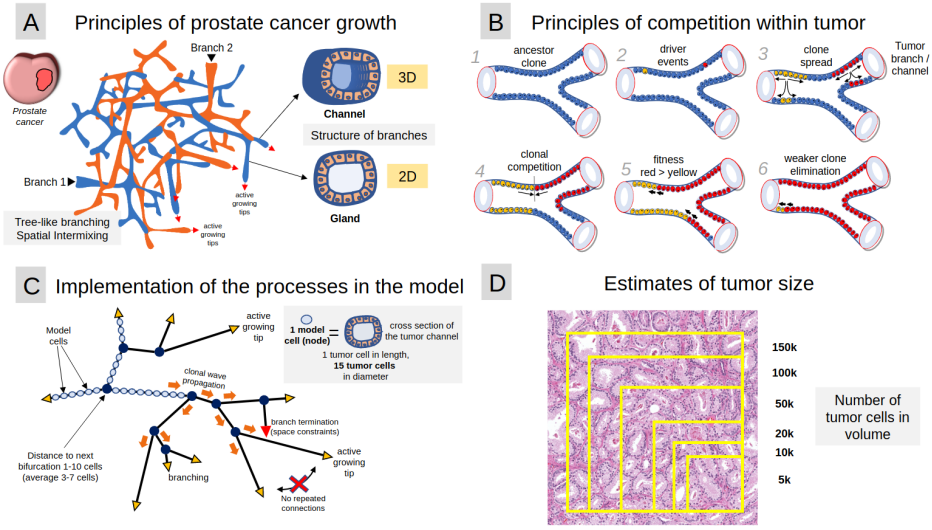

Figure C.1: ***Principles of prostate cancer growth, clonal development and their implementation in the developed mathematical model.*** ***A****. Most prostate cancer (PCA) tumours that are well and moderately differentiated grow in tree-forming branches according to the rules of branching morphogenesis. These branches are highly intermixed spatially and represent hollow structures (i.e. channels) in three dimensions, lined by tumour epithelial cells. In the regular pathological sections, the channels look like glands.* ***B****. Competition between clonal populations in PCA presumably occurs on the luminal surface of glands, with the propagation of the 'stronger' clone along the pre-formed branches. An example of competition between two populations (steps 1–6) is provided.* ***C****. During our simultaneous implementation of 1) tumour growth and 2) genetic/clonal evolution, we reduced one dimension of the architecture (the hollow nature of channels). Every model cell represents a cross-section of such channel, with a natural length of one cell but incorporating on average 15 real tumour cells lining the lumen. The branching occurs only through bifurcations and only at active growth tips within a distance calculated from morphological analysis. Branch termination occurs if there is no space for further growth.* ***D****. A typical prostate adenocarcinoma is presented with glands corresponding to channels in three dimensions. Morphological estimation of the number of cells, and of the corresponding tumour volume and morphological visibility was performed, which is important for the definition of the clinically relevant clonal population (definition of clone to be used later). The estimation is made in thousands (k) of tumour cells for a cube of a given size.*

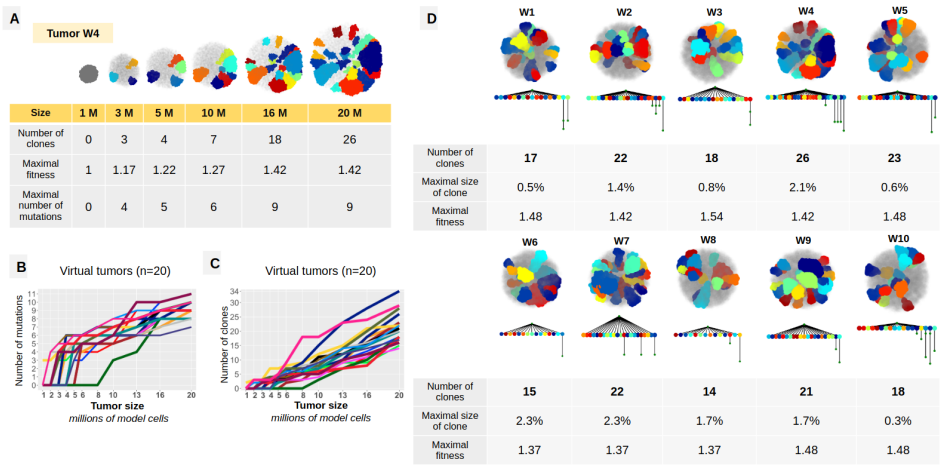

Size	1 M	3 M	5 M	10 M	16 M	20 M
Number of clones	0	3	4	7	18	26
Maximal fitness	1	1.17	1.22	1.27	1.42	1.42
Maximal number of mutations	0	4	5	6	9	9

	W1	W2	W3	W4	W5
Number of clones	17	22	18	26	23
Maximal size of clone	0.5%	1.4%	0.8%	2.1%	0.6%
Maximal fitness	1.48	1.42	1.54	1.42	1.48

	W6	W7	W8	W9	W10
Number of clones	15	22	14	21	18
Maximal size of clone	2.3%	2.3%	1.7%	1.7%	0.3%
Maximal fitness	1.37	1.37	1.37	1.48	1.48

Figure C.2: ***Evaluation of clonality in 20 synthetic tumours (W1–W20) from a model with only a 'weak' type of genetic alteration.*** *'Weak' genetic alterations (different types of alteration called mutation) provide small fitness increments for the birth–death ratio (0.04). The clone definition was set as a branch in the clonal hierarchy with size > 10.000 model cells (> 150.000 real tumour cells; being readily distinguishable morphologically, Figure C.1 D).* ***A****. Example of the development of tumour W4 from a size of 1 mln up to the end size of the simulation corresponding to the average size of a clinically relevant prostate cancer tumour (20 mln model cells).* ***B****. Dynamics of the number of consecutive mutations in the most advanced clone according to the course of tumour development. Some stochastic variations in the early stages of development (up to the size of 8 mln model cells) are evident, with similar trends shown later.* ***C****. Dynamics in the number of clones in the course of tumour development.* ***D****. Spatial orientation of clones, clonal hierarchy (larger coloured circles: clones according to the definition; smaller green circles: prominent daughter populations not reaching a clone size of 10.000 model cells) and metrics for the first ten tumours (W1–W10). Importantly, due to the prominent spatial intermixing of populations, the volume on the spatial maps seems larger than that measured as number of cells (provided in % of the whole tumour). The tumour architecture is a major bottleneck in the case of only 'weak' mutations. It precludes the development of clonal sweeps with dominant clones of substantial sizes and divergent/branching evolution evident from previous studies using patient samples.*

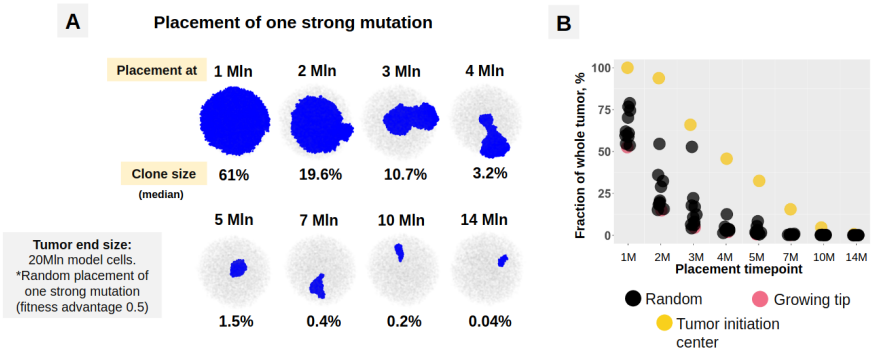

Figure C.3: ***Investigation of the clonal sweeps resulting from the isolated placement of one 'strong' mutation at different tumour sizes.*** *Ten simulations for every placement at tumour sizes of 1, 2, 3, 4, 5, 7, 10 and 14 mln model cells: eight with randomly positioned mutations and two with fixed positions (at the actively growing tip and in the tumour initiation centre). Fitness of background cells in the tumour: 1.0. Fitness increment for strong mutation: 0.5. Importantly, due to the prominent spatial intermixing of populations, the volume on the spatial maps seems larger than that measured as number of cells (provided in % of the whole tumour).* ***A****. A substantial clone/sweep size can be achieved only by the very early emergence of strong mutation (1–3 mln model cells, approximately corresponding to 10% of the final, clinically detectable tumour size). The tumour architecture is a major bottleneck for effective clonal spread even in the case of strong mutations.* ***B****. Ten simulations with placement at different tumour sizes with the resulting clone fraction (% of the whole tumour) at the end of the simulation (20 mln model cells). The most beneficial emergence position is in the tumour initiation centre (yellow). The most disadvantageous position is at the active tip (red).*

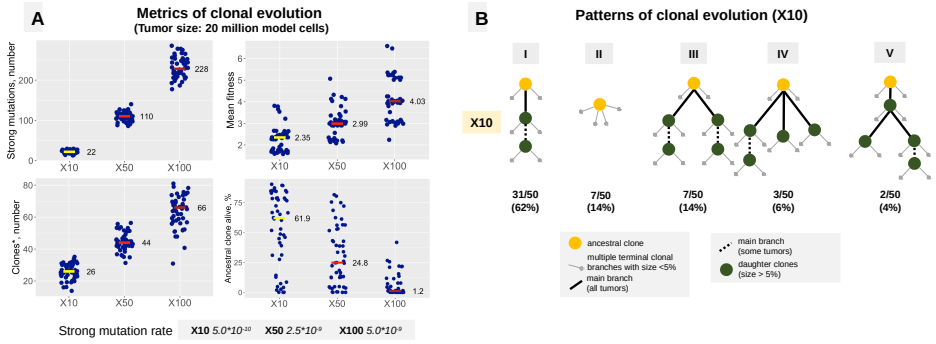

Figure C.4: ***Metrics of clonal development and patterns of clonal evolution in synthetic tumours with two types of mutation (weak and strong) and three different levels of strong mutation rate (X10).*** *Synthetic tumour groups X10, X50 and X100 represent three different strong mutation rates, with the weak mutation rate the same as that initially.* ***A****. Overall number of strong mutations in single tumours, mean fitness of the most advanced clone, number of clones in the tumour (using the initial definition of a clone as a branch* > 10.000 *cells) and % of ancestral clone alive (as a metric of intensity of the clonal-sweep processes in the tumour).* ***B****. Five patterns of clonal evolution evident in the X10 synthetic tumours. The definition of clone was changed to a clinically relevant one: a branch in the clonal hierarchy with a size* $> 5\%$ *of the final tumour size. The green circles represent clones and the yellow circle represents an ancestral clone (see Figure Legends). Only dominant clones with leading fitness levels were used in the classification of patterns. In all the tumours, there was an evidence of multiple small populations (shown as small grey branches).*

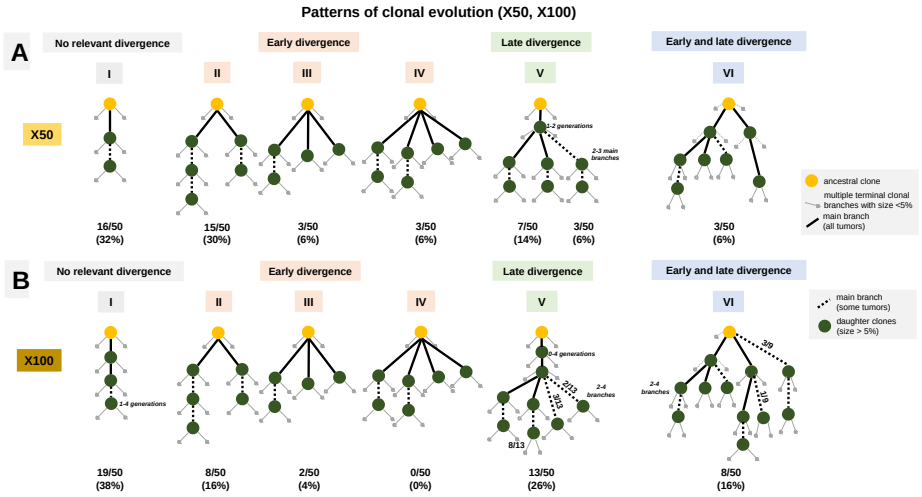

Figure C.5: ***Patterns of clonal evolution in synthetic tumours with two types of mutation (weak and strong) and different levels of strong mutation rate: A. X50 group. B. X100 group.*** *A finite number of clonal-evolution patterns was evident in the synthetic tumours from groups X50 and X100, classified as (1) no relevant divergence, (2) early divergence, (3) late divergence or (4) early and late divergence. Importantly, even with a high strong mutation rate (X100), there was a limited number of divergent clonal-hierarchy branches (up to five; most of the tumours had one to three dominant branches). In both groups X50 and X100, approximately one third of the tumours showed only one dominant clone, without relevant divergence.*

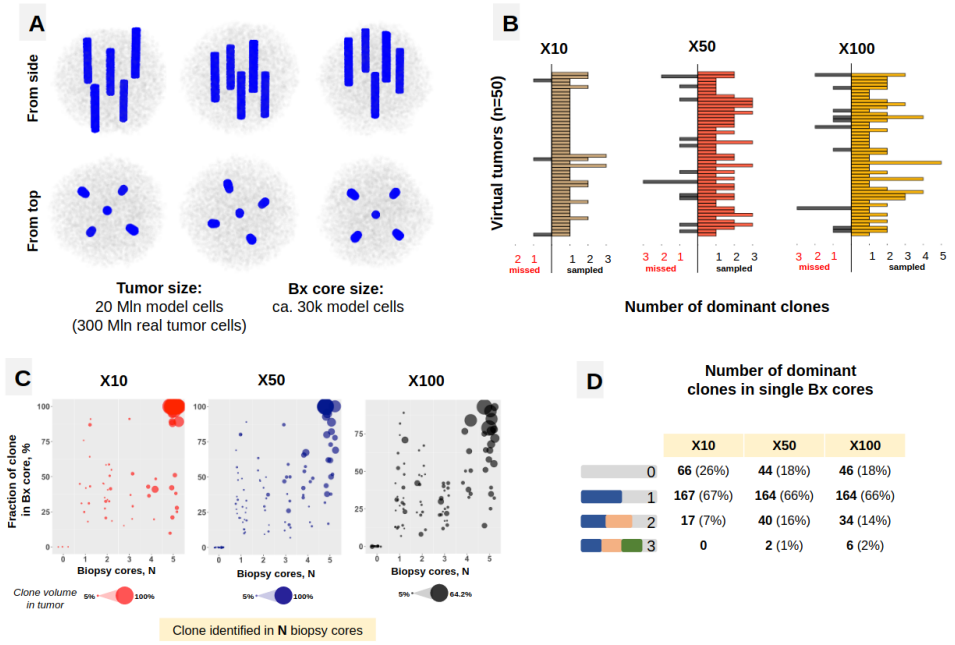

Figure C.6: ***Results of the biopsy experiments.*** ***A****. Three representative examples of the synthetic-tumour biopsy setup. Five cores were used, each sampling approximately 30.000-35.000 model cells (corresponding to real clinical prostate biopsies). One core was placed centrally and four cores were situated equidistant at the periphery. The penetration depth was selected randomly. Biopsies were performed in all the X10, X50 and X100 tumours at the final size of 20 mln model cells.* ***B****. Results of the biopsy experiments: numbers of caught and missed dominant clones in each tumour (groups X10, X50 and X100).* ***C****. All the dominant clones were identified in zero (missed) to five biopsy cores. The plots demonstrate the dominant clone size (% of the whole tumour; diameter of the circles) and the median fraction of this clone in single biopsy cores (y-axis) depending on in how many of the five biopsy cores the clone was found (x-axis).* ***D****. Number of sampled dominant clones in the single biopsy cores (groups X10, X50 and X100). A substantial number of cores in all the groups contained two or more dominant clones.*

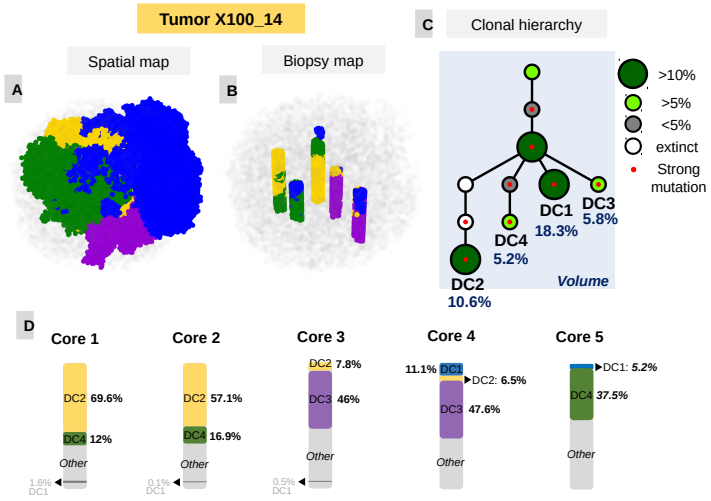

Figure C.7: ***Biopsy results of the synthetic tumour X100-14.*** ***A****. Spatial map of the distribution of four dominant clones with evidence of typical clonal intermixing in prostate cancer (the colours correspond to the colours of the tumours in B and D, respectively). Importantly, due to the prominent spatial intermixing and growth in the small outrunner branches, the volume on the spatial maps seems larger than that measured as number of cells (provided in % of the whole tumour in C).* ***B****. Five-core biopsy of the tumour with delineation of core content concerning sampled clones.* ***C****. Clonal hierarchy of the tumour with the four dominant clones DC1–DC4.* ***D****. Detailed distribution of dominant clones in five biopsy cores. 'Other' refers to the cells from other populations with low fitness or with comparable fitness but whose population size does not meet the clone criteria (> 5% of the whole tumour). For further information regarding the frequency of single mutations, small populations in the biopsy cores, and temporal dynamics of clonal evolution in Tumour X100-14 see Figures C.20, C.21.*

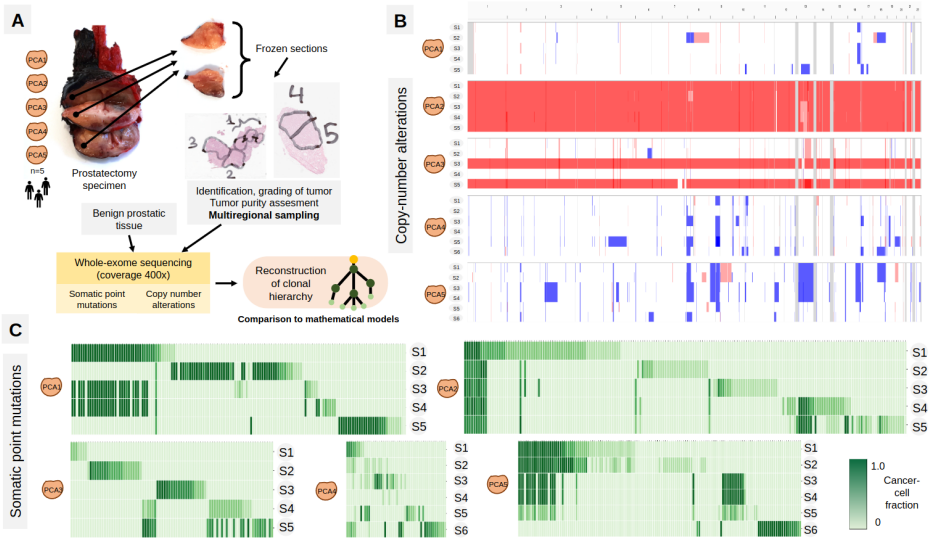

Figure C.8: ***Design of the next-generation sequencing validation study and results of multiregional sequencing of five prostate cancer.*** ***A****. Five prostatectomy specimens from patients with low- and intermediate risk prostate cancers were processed (local variations of Gleason score for five tumours 3+3 to 4+3). At least five different tumour regions (S1, S2, etc.) and one benign sample / specimen under control of frozen sections were harvested for DNA extraction. Deep whole exome sequencing with coverage of up to 400x was performed on each sample. Somatic point alterations and copy number alterations were used for the reconstruction of clonal hierarchy and studies of tumour development processes.* ***B****. Copy-number alterations for multiregional samples of five prostate cancers (PCA1-PCA5). Blue – areas of deletion, red – areas of amplification, gray – areas with limited coverage / low quality of calls. PCA2 and PCA3 cancers show clonal (PCA2) and subclonal (PCA3) whole-genome duplication event.* ***C****. Somatic point mutations calls for PCA1-PCA5 tumours (per sample analyzed). Different shades of green represent differences in cancer-cell fractions (see Legend).*

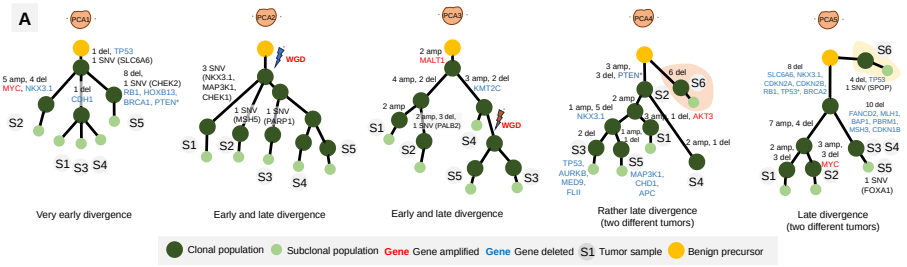

B Number of discernible subclonal populations / sample

	S1	S2	S3	S4	S5	S6
PCA 1	4	4	3	3	3	-
PCA 2	4	4	4	4	4	-
PCA 3	1	3	3	2	2	-
PCA 4	3	2	4	2	4	5
PCA 5	4	4	3	3	3	3

C Virtually reproduced tumor samples (similar to NGS study)

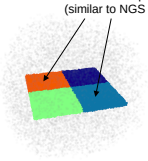

Number of discernible subclonal populations / sample

	Mean	Std
10X tumors	1.6	0.9
50X tumors	2.9	1.4
100X tumors	3.8	1.7

Figure C.9: ***Clonal hierarchies of the PCA1-PCA5 tumours reconstructed from somatic point mutation and copy number alterations data and analysis of number of discernible subclonal populations per sample.*** ***A****. Reconstruction of clonal hierarchies of five tumours (PCA1-5). The information to genetic alterations evident at trunk and branches is provided. When the genes with clearly established role for development of prostate cancer could be identified, they are provided as well: red – amplification, blue – deletion of the gene. At some amplifications and deletion no genes with clearly established functional role could be identified. Patterns of clonal divergence are summarized per tumour. In Cases PCA4 and PCA5 branch in different colour represents a genetically completely indepdent second tumour focus identified immediately adjacent to the main tumour focus. Abbreviations: SNV – somatic nucleotide variant, del – deletion, amp – amplification, * - NGS calls with low quality.* ***B****. Number of discernible subclonal populations in single tumour samples based on cancer cell frequencies from Figure 8C.* ***C****. Principle of sampling of virtual tumours that exactly reproduces the samples of human tumours concerning location, form, and number of tumour cells is shown above. Below provided a summary of the number of discernible subclonal populations per sample, tightly resembling those of human samples (B).*

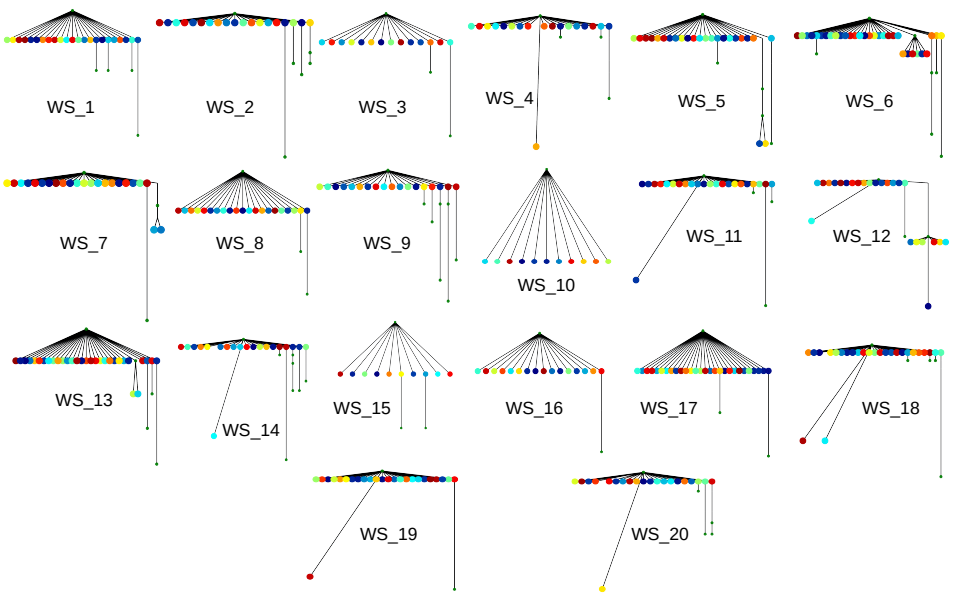

Figure C.10: Clonal hierarchies of 20 synthetic tumours modelled with a combined implementation of weak and strong mutations (named WS group). An initial strong mutation rate of $5.0 \cdot 10^{-11}$ *was used for strong mutations. Initial definition of clone (larger coloured circles): a branch in the clonal hierarchy with number of cells* $>$ *10.000. The smaller green circles represent prominent daughter populations not reaching the threshold of 10.000 cells for clone definition. Most of the strong mutations appeared too late to generate even local clonal sweeps due to architecture bottlenecks and the presence of many counteracting populations with multiple consecutive weak mutations and comparable fitness levels. Among the 20 synthetic tumours in this setting, only five (tumours 5, 6, 7, 12 and 13) demonstrated divergent/branching evolution to some extent (those where strong mutations appeared earlier).*

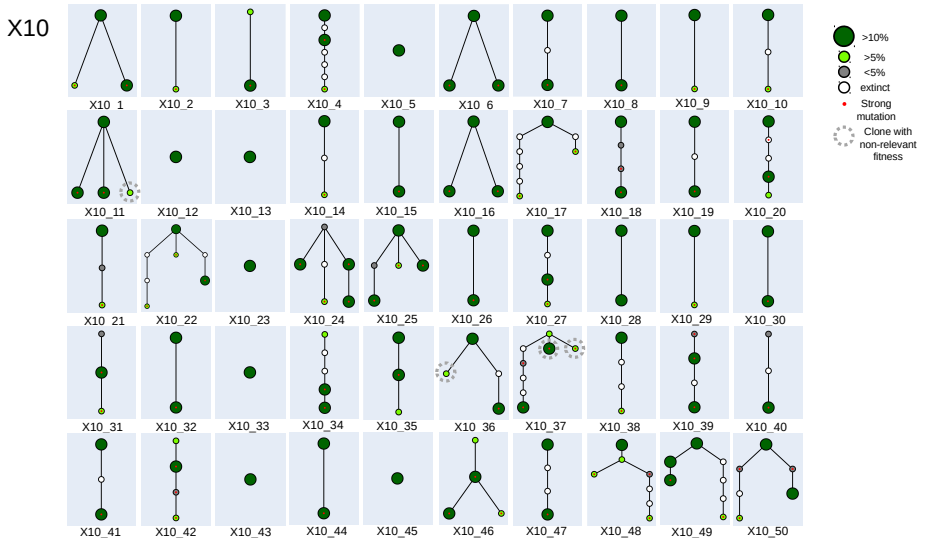

Figure C.11: Clonal hierarchies for the synthetic tumours in group X10 (strong mutation rate $5.0 \cdot 10^{-10}, n = 50$*. Adjusted, the clinically relevant definition of clone was used: a branch in the hierarchy with a size* $> 5\%$ *of the whole tumour volume.*

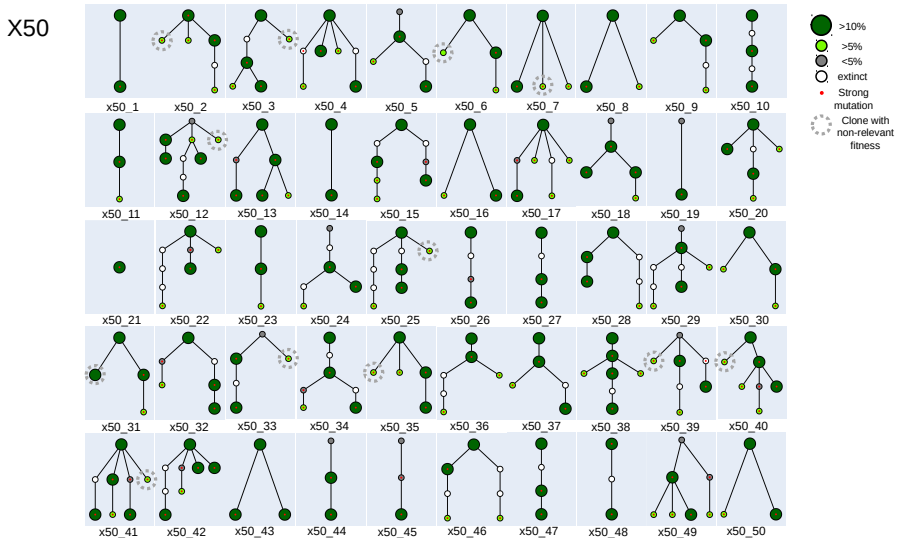

Figure C.12: Clonal hierarchies for the synthetic tumours in group X50 (strong mutation rate $2.5 \cdot 10^{-9}, n = 50$*. Adjusted, the clinically relevant definition of clone was used: a branch in the hierarchy with a size* $> 5\%$ *of the whole tumour volume.*

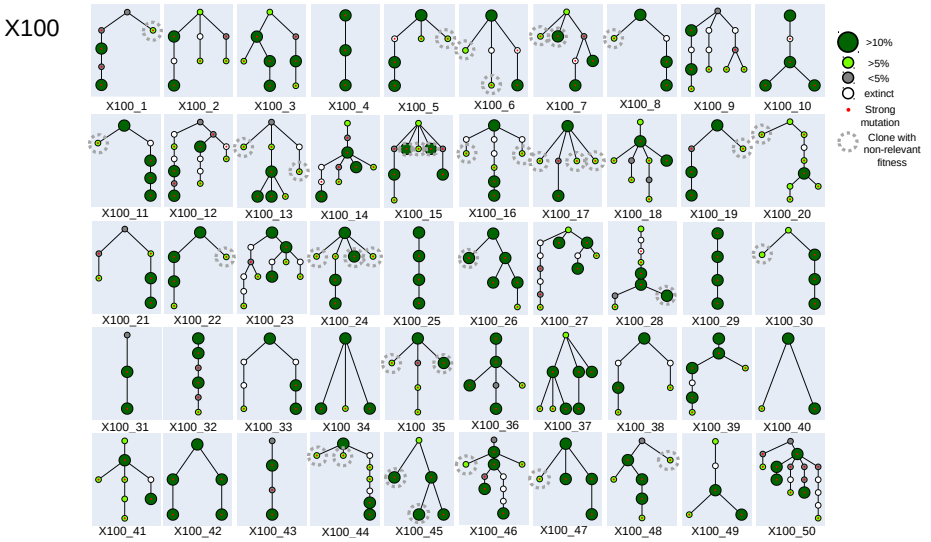

Figure C.13: Clonal hierarchies for the synthetic tumours in group X100 (strong mutation rate $5 \cdot 10^{-9}, n = 50$. Adjusted, the clinically relevant definition of clone was used: a branch in the hierarchy with a size $> 5\%$ of the whole tumour volume.

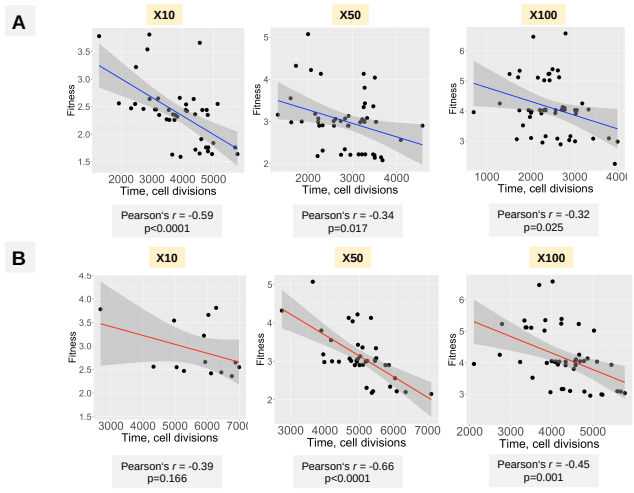

*Figure C.14: Dependence of the final fitness of the most advanced clone in the tumour on the time of emergence of the first (**A**) and second consecutive (**B**) strong mutations in synthetic tumour groups X10, X50 and X100, respectively. Time measured in cell cycles (cell divisions). A clear positive correlation was found between time of emergence of the first and second consecutive strong mutations and higher fitness of the dominant clone at the end of the simulation.*

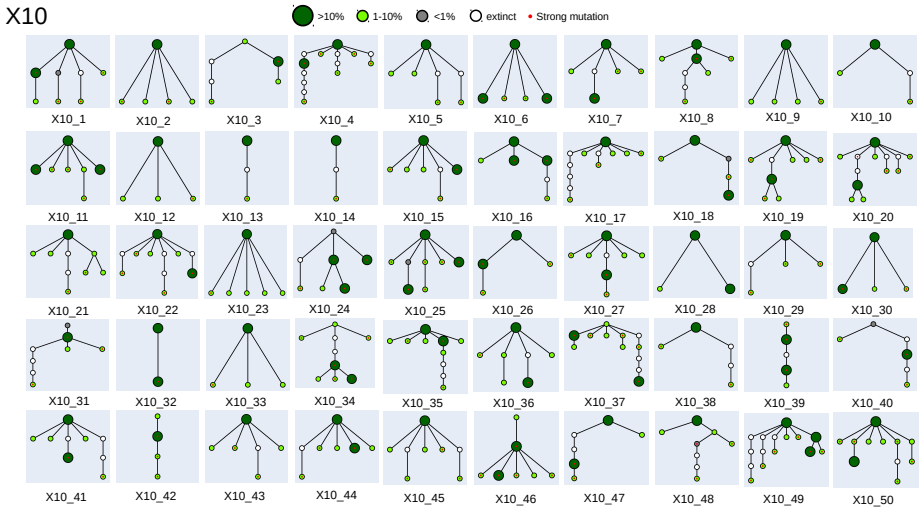

Figure C.15: Clonal hierarchies for the synthetic tumours in group X10 (strong mutation rate $5.0 \cdot 10^{-10}, n = 50$*. Multiple small populations are evident, often with a fitness level comparable to that of the dominant clone(s) when the clone definition is relaxed to hierarchy branch size* $> 1\%$ *at the end of the simulation. The clinical relevance of such small clonal populations is unclear.*

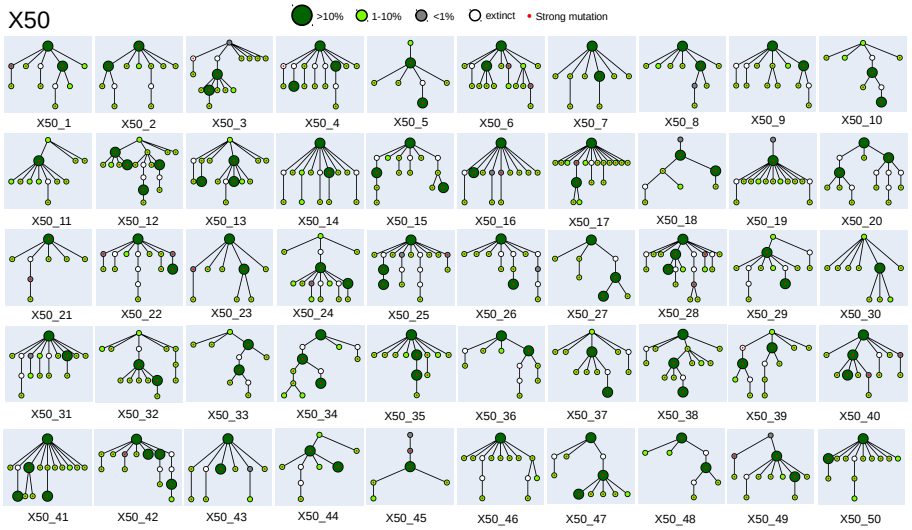

Figure C.16: Clonal hierarchies for the synthetic tumours in group X50 (strong mutation rate $2.5 \cdot 10^{-9}, n = 50$*. Multiple small populations are evident, often with a fitness level comparable to that of the dominant clone(s) when the clone definition is relaxed to hierarchy branch size* $> 1\%$ *at the end of the simulation. Clinical relevance of such small clonal populations is unclear.*

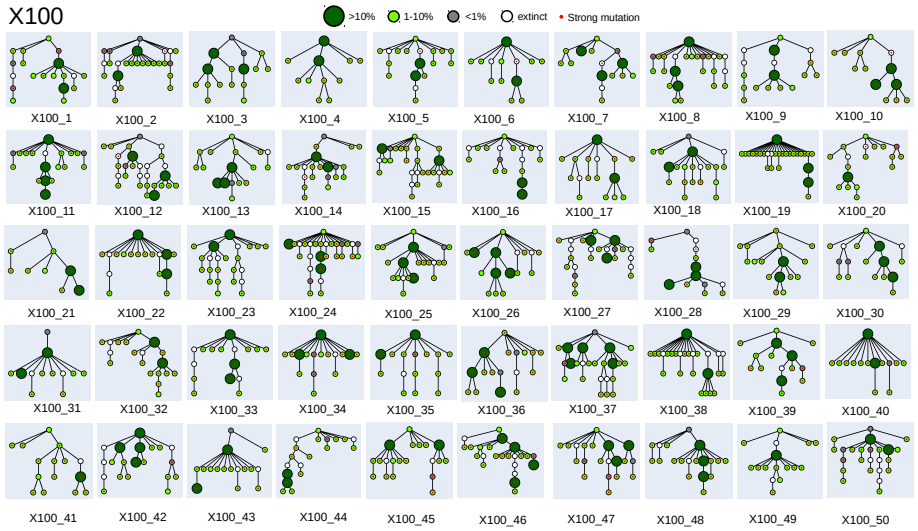

Figure C.17: Clonal hierarchies for the synthetic tumours in group X100 (strong mutation rate $5.0 \cdot 10^{-9}, n = 50$. Multiple small populations are evident, often with a fitness level comparable to that of the dominant clone(s) when the clone definition is relaxed to hierarchy branch size $> 1\%$ at the end of the simulation. The clinical relevance of such small clonal populations is unclear.

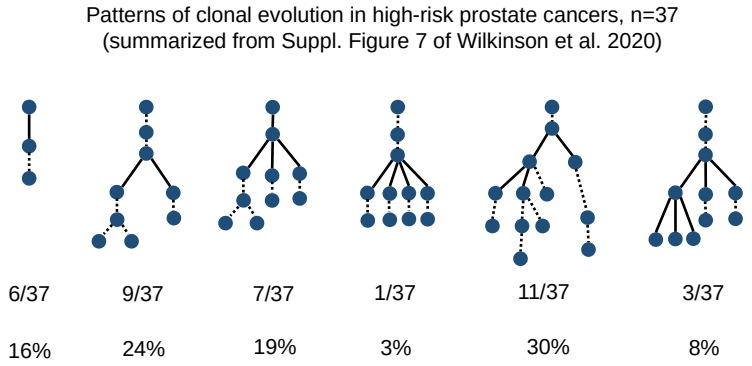

Figure C.18: Patterns of clonal evolution in high-risk prostate cancers, $n = 37$ (summarised from Suppl. Figure 7 of Wilkinson et al. [161]). Wilkinson et al.'s study is one of the largest studies on intratumoural heterogeneity based on multiregional analysis, with available reconstructions of clonal hierarchies for 37 patients (high-risk patients only). The patterns of clonal evolution are highly similar to our findings (Figures C.4B, C.5A,B).

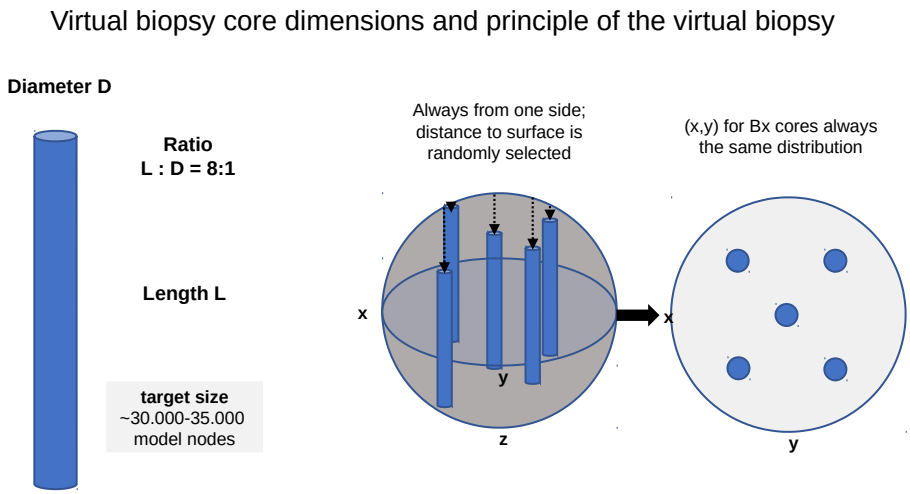

Figure C.19: Virtual biopsy core dimensions and principle of virtual biopsy.

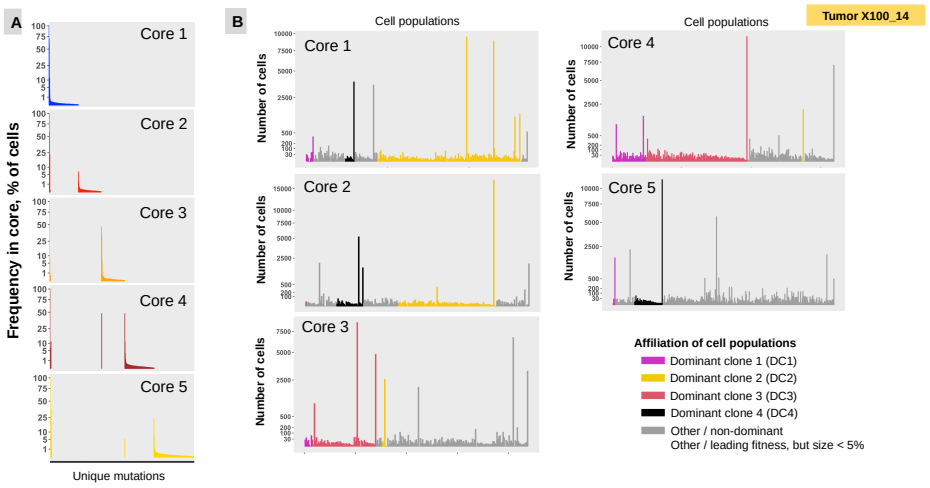

Figure C.20: Detailed information about frequency of single genetic alterations (mutations) and cellular populations with a unique genotype in five biopsy cores of the X100-14 synthetic tumour (refer to Figure 7). ***A****. Frequency of unique mutations in single cores (% of the cells). On the left side of the plots, from cores 1 to 5, the spikes correspond to trunk mutations (100%). The other high spikes correspond to the founder mutations of dominant clones. A large number of other unique mutations with low frequency is evident.* ***B****. Cell populations with unique genotypes in cores 1–5. Some of them (affiliated with dominant clones) are daughter subpopulations developing on the basis of dominant clones. The grey bars correspond to other populations not affiliated with the dominant clones. Some of them stem from populations or clones with non-dominant and non-relevant fitness. However, there are also cell fractions stemming from clonal populations with dominant fitness, but with a size $< 5\%$ (not fulfilling the clone criteria). The clinical relevance of such cell populations (especially with a size of 1–5% of the whole tumour) is unclear. Some of the other cell populations are of a substantial size (several thousands of cells) and can therefore interfere with the correct, next-generation sequencing-based evaluation of the genetic formula of the dominant clone for clinical decision making.*

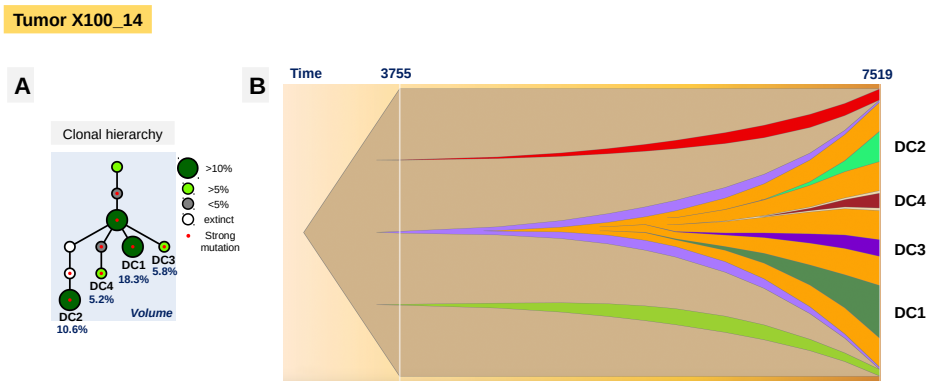

Figure C.21: ***A****. Clonal hierarchy scheme from case study C.7.* ***B****. Corresponding fishplot of temporal dynamics of clonal evolution (Tumour X100-14). Timeline corresponds to cell division cycles.*

Supplementary: Detailed review of published studies on intratumoural heterogeneity in prostate cancer.

Nr	Study	Number of patients	Technique	Sampling Type	Main results
1	[4]	11 (9 tumor samples)	SNS, low-pass DNAseq (only CNV analysis)	Biopsy, 2-8 tumor samples/patient	1) In 3/6 cases multiple clones in single Bx cores 2) Clonal hierarchy reconstruction in 6 cases (cell-level): one to three clonal branches (no information about their genetics)
2	[9]	57	WGS	Prostatectomy, 1 sample / patient	1) Chromoplexy as a "strong" genetic event leading to punctuated evolution rather than gradual acquisition of genetic alterations. 2) Several major alterations (PTEN, CDKN2B, CHD1; also, chromoplexy) are subclonal. 3) No case level reconstructions of clonal hierarchy
3	[18]	5	WGS	Prostatectomy, In total 23 distinct regions from 5 pts, 2-9 samples/tumor	1) Substantial intratumoral heterogeneity 2) Some important driver alterations, including therapy-relevant, are subclonal (TP53, BRCA, CHD1, BRCA1, PIK3CA) 3) No reconstructions of clonal hierarchy.
4	[25]	5 All aggressive, high-stage cancers (e.g. 3/5 GS 4+5, 2/5 tertiary GP5)	Illumina HumanMethylation450 BeadChip array (only CNV analysis)	Prostatectomy, up to 10 samples / tumor	1) Detailed reconstruction of hierarchy: two or three main clonal branches with early and late divergence. 2) No estimates of aggressivity / functional impact of identified subclones. Some of them maybe not relevant. 3) No saturation with used number of samples (all single samples from one tumor contain different clones).
5	[33]	3	WGS	Prostatectomy, in total 12 tumor samples from 3 pts (3 of them from low-grade secondary cancer focus), 3-5 samples / patient	1) Significant inter-sample heterogeneity. 2) Alterations counted, but not named. Although alterations of unknown or no significance (passengers). 3) Detailed reconstruction of hierarchy: one, three, and three main branches (including low-grade clones lacking clinical significance), early and late divergence patterns. 4) No saturation with used number of samples (all single samples from one tumor contain different clones). 5) Large number of alterations in benign tissue.
6	[40]	2	WES	Prostatectomy 1 tumor sample / patient	1) Every sample contains more than one clone (spatial coexistence / intermixing of clones). 2) PTEN and TP53 alterations are subclonal.

7	[59]	8 highly selected population of early onset cancers	WGS	Prostatectomy, number of samples / tumor not clearly specified	1) Detailed reconstruction of clonal hierarchy, however, reconstructions not linked to samples (Bayesian mixture model). 2) Estimation of aggressivity of every identified clone (probabilistic modeling) 3) In all cases short trunk and two main clonal branches with late divergence. 4) Late divergence in many cases with a number of clones without relevant genetic alterations and with low estimated aggressivity. 5) In 2 cases TP53 as clonal event, in 4 cases subclonal. RB1, PTEN, BRCA1, BRCA2 alterations are often subclonal. 6) TP53 alterations are very infrequent in primary PCA, here in 6/8. Also 6/8 RB1 alterations. Highly selected population.
8	[70]	1	Targeted DNAseq	Prostatectomy, 9 samples from primary tumor	PTEN and TP53 as subclonal events (identified in 1/9 tumor samples)
9	[78]	4	WGS, targeted resequencing	1, 1, 2, and 6 primary tumor samples / case	1) Of four patients two with MSH2 and BRCA2 (probably, special trajectories for clonal evolution). Two patients additional with POLE mutation. Highly selected population. 2) Reconstruction of clonal hierarchy unreliable in 3/4 patients due to low number of primary tumor samples. 3) In one patient with MSH2 mutation probably one dominant branch. 4) p53 often subclonal and important for metastatic process.
10	[95]	11	Panel DNAseq (289 genes)	Multifocal tumors, 2-3 samples / patient (prostatectomy); 1-3 preop core biopsies / patient	1) Only one sample pro focus of multifocal tumor; also, non-dominant foci sampled. Almost all cases with GS 7. 2) Prominent interfocal heterogeneity (intratumoral heterogeneity is not estimated due to sampling of 1 sample / tumor) 3) High levels of under-sampling of relevant genetic rearrangements when only biopsies analyzed.
11	[100]	25 clinically high-risk tumors (ca. 50% with M1 disease)	WGS/WES	Biopsy samples, 2-4 tumor samples / patient	1) Prominent levels of intratumoral heterogeneity (more on the CNV level). 2) Naturally, no control for spatial localization of samples. 3) No phylogenetic reconstructions.
12	[101]	1 high-stage, high-grade	Low-pass WGS, breakpoint analysis	Prostatectomy, 25 tumor areas, laser-capture microdissection	1) Detailed reconstruction of clonal hierarchy in 1 case based on CNV breakpoints. 2) Three main clonal branches with early and late divergence (no analysis of relevance of identified branches or subclones; some of them might be of no relevance). 3) No saturation reached with used number of samples (all single samples from one tumor contain different clones).
13	[104]	23 (with 2 samples from one focus)	WES		1) Main focus of study is interfocal heterogeneity in multifocal prostate cancer. 2) 23 patients with only 2 samples / focus, which showed substantial heterogeneity. 3) No detailed phylogenetic reconstructions.

14	[43], [52]	293 (97% clinically intermediate tumors)	WGS	1 sample / patient: prostatectomy sample or Bx core from patients for radiation therapy	1) All analyses 1 sample / patient. 2) 119 (41%) monoclonal, 135 (46%) biclonal, 35 (12%) tri-clonal in one sample: prominent spatial mixing of clones. 3) Sampling bias (1 sample/tumor; sample size not reported). Low sequencing coverage (bias). 4) Many tumors classified as high prognostic risk based on subclonal alterations (clinical relevance).
15	[52]	11 (5 BRCA2 carriers, 6 sporadic)	WGS	2 samples / tumor (one – invasive, one – intraductal carcinoma)	1) Selection bias: high-stage, high-grade cancers with intraductal carcinoma. 2) No systematic multi-region sampling of tumors. 3) BRCA2 tumors have distinct evolutionary trajectories due to large number of driver alterations early in course. 4) No significant information about intratumoral heterogeneity: invasive carcinoma and intraductal carcinoma of common origin.
16	[151]	4	WES	Prostatectomy, 2-3 samples / case (probably multiple foci also)	1) Substantial divergence and heterogeneity 2) Early divergence (maybe multifocal tumors). Also, late divergence in 2 tumors. 3) No detailed analysis of single mutations or relevance of subclones. No analysis of CNA.
17	[152]	10	WES, low-pass WGS	Prostatectomy, 5-9 samples / tumor (index lesion)	1) Selection bias for higher grade / higher stage tumors. 2) High levels of intratumoral heterogeneity. 3) No saturation reached with used number of samples (all single samples from one tumor contain genetically different sub-clones). 4) Both early and late divergence evolutionary patterns. 5) Two or three main clonal branches. No analysis of relevance of single sub-clones. In three cases evidence of rather one dominant branch with late divergence. 6) Evidence for prominent and complex spatial intermixing of divergent clones. 7) BRCA1, BRCA2 both clonal and subclonal, ATM subclonal. TP53, RB1 both clonal and subclonal. PTEN often subclonal. 8) CNVs are often subclonal (especially gains).
18	[165]	16 (6 pts with M1, bias for higher-stage, higher-grade disease)	WES	Biopsy, 1-4 cores / index lesion	1) High levels of intratumoral heterogeneity at different levels. 2) Naturally, no control for spatial localization of samples. 3) Evidence for early and late divergence. 4) Two to five main branches, but no analysis of branch or clonal relevance, only number of SNVs (not CNVs). Probably some branches are of no relevance (not dominant).
19	[160]	4 (bias for higher stage/grade disease)	WES	Biopsy, 3 cores from index lesion, up to 4 cores from smaller lesions	1) High levels of intratumoral heterogeneity. 2) Clinical significance of branch mutations unclear. 3) Phylogenetic trees generated based on somatic mutations. Mainly 2 branches with late divergence in sub-clones of unclear relevance.

20	[164]	10 (lethal metastatic disease)	WGS, targeted DNAseq	Autopsy samples, in total 33 samples from prostate, 1-8 samples / patient	1) Only 4 patients with prostatectomy before autopsy, all other samples – heavily pretreated, harvested at time of prostatectomy. 2) Detailed phylogenetic reconstructions based on targeted sequencing (higher coverage, but only selected alterations identified previously using WGS). 3) High levels of intratumoral heterogeneity in the prostate. 4) Prominent spatial intermixing of subclones in the prostate, also during spread to local organs. 5) Intraprostatic clonal evolution: one or two main branches with late divergence in 2 tumors. 6) Monoclonal or biclonal (mostly from one intraprostatic branch) seeding of metastasis. 7) Conclusion: "It is likely that metastatic trigger events are rare and arise stochastically, which means it will be difficult to predict the lineage that will eventually metastasize."
21	[161]	37 (intermediate/high clinical risk disease)	WES	Biopsy samples (MRI: 48 foci), microdissected, median 4 Foci/patient	1) Possible sampling bias (biopsy from foci identified by MRI). 2) Detailed reconstruction of clonal hierarchy trees in all patients. 3) Two patterns of clonal evolution: linear and branching. 4) Branching in 86% of poor responders to neoadjuvant therapy, and in 73% of exceptional responders to this therapy. 5) Evidence for early and late divergence. See Figure C.18 for a detailed analysis of clonal evolution patterns

Abbreviations used in the table:

ADT androgen deprivation therapy
CNV copy-number variation
GP Gleason pattern
GS Gleason Score
MRI magnet-resonance investigation
SNS single nucleus sequencing
SNV single-nucleotide variants
WES whole-exome sequencing
WGS whole-genome sequencing

C.7 Supplementary mathematical methods

C.7.1 Tumour geometry and growth

Essentially, the following stochastic self-avoiding branching process was introduced and discussed in detail by Hannezo et al. [73, 74], as a model for the branching morphogenesis of several healthy tissues: the authors compare their numerical results with biological data from the mouse mammary gland, kidney, and the human prostate. We earlier reported the same self-avoiding structures in PCA [146], and only slightly modify the dynamics in [73] to the present case. As explained in the following, we increase the capability of the process to grow in spatially densely packed regions, reflecting the malignant nature of the tumor.

To begin with, the length of an edge in the network represents the diameter of a single cell, normed to $l(e) \equiv 1$. Each node of the network represents a cross-section of 15 cells of the tubular tumour-structure (Fig. C.1). The radial thickness of the structure is set to $d_{rad} = 4$, representing 15 round cells which form the boundary of a squeezed tube. Each node v has a specific three-dimensional coordinate $x(v) \in \mathbb{R}^3$ and is represented by a ball of radius $r = d_{rad}/2 = 2$ with center $x(v)$. The self-avoidance is implemented such that it depends only on the nodes (Fig. C.22), which have to respect a minimal distance of $2r$ if their network-distance (shortest path via edges) is more than $d_{net} = 1 + 3r$ (rounded down to the next integer if necessary). This way, two branches can separate after a branch-event and nodes on the same branch do not impede their neighbours. With the chosen parameters, this node-avoidance provides a sufficient approximation of non-intersecting round tubes while being fast to compute. This approximation is necessary if we consider networks consisting of 10^7 nodes.

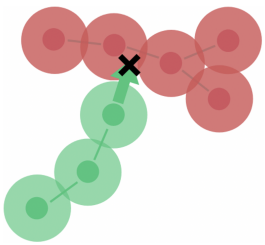

Figure C.22: Self-avoidance based on the radial size r of the vertices. Vertices with a network-distance of more than $d = 1 + 3r$ have to respect the resulting minimal distance of $2r$. All edges have length $l(e) = 1$. With the chosen radius $r = 2$ this gives a sufficient approximation of a round tube (for better visualization, the figure shows the case for $r = 0.7$).

The growth-rate $R_g(v, t)$ and the branch-rate $R_b(v, t)$ at node v at time t are only positive if the node is active, indicated by its growth- and branch-

activity $A_g(v,t)$ and $A_b(v,t)$. Both indicators can independently be either zero or one. We set

$$\begin{aligned} R_g(v,t) &= A_g(v,t) \cdot f(v,t) \cdot C_g, \\ R_b(v,t) &= A_b(v,t) \cdot f(v,t) \cdot C_b. \end{aligned} \tag{C.7}$$

The constants $C_g, C_b \geq 0$ represent the number of cell-divisions that result in a longitudinal growth or a branching of the tubule. We used physiological data from a previous study (Fig. C.1), translating into a fixed ratio of branching compared to normal growth-events: $C_g/C_b = 1/4$. The resulting total growth-constant is set to $C_g + C_b = 1/10$, reflecting the slow growth of low-grade PCA. The total growth-constant $C_g + C_b$ should be clearly less than one, as the spatial pressure exerted by the surrounding healthy and cancerous tissue impedes growth, as well as does their consumption of nutrients. We are aware of the fact that we can not validate the effective speed of growth numerically, but we refer to the end of this subsection for an estimate on the time it takes a tumor to grow to full size.

At a growth event, a new coordinate in front of v is drawn randomly, then it is verified if this potential position for a new vertex respects the prescribed distance rules. Therefore, a random growth direction is chosen uniformly from a cone around the previous growth direction (Figure C.23). The maximal possible deviation from the previous direction is set to $\alpha = 60°$, which allows the growing branch to evade possible obstacles without perturbing the growth direction too much (on average) and fits the morphological analysis in [146]. If the newly sampled position is not too close to any other existing nodes, a new node w is placed there and connected to v via an edge. The new node w is set as fully active, meaning that both $A_g(w,t) = 1$ and $A_b(w,t) = 1$. If the chosen coordinate is blocked, a new one is sampled i.i.d. to the previous one. After N_g unsuccessful trials, we irreversibly set $A_g(v,t) = 0$, the growth-event is considered to have failed due to spatial restrictions. We allow for a possible branching event afterwards, not changing $A_b(w,t)$ after a failed growth event, and vice versa.

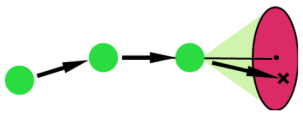

Figure C.23: At a growth event, the direction is drawn uniformly from the pink set, which is a cone around the current direction.

At a branching event, two new coordinates in front of v are drawn randomly, then it is verified if both respect the prescribed distant rules. Therefore, two opposing random growth directions are chosen uniformly under the following restrictions: they have an angle of $\beta = 60°$ to the mean growth direction and an angle of 2β towards each other, (Figure C.24). If both resulting new positions are unoccupied, two new nodes are placed and each is

connected to v via an edge, both new nodes are set as fully active. Otherwise, two new coordinates are sampled. After N_b unsuccessful trials, we set $A_b(v,t) = 0$. In this case, since we think of branching as excessive growth, a growth event follows if $A_g(v,t) = 1$.

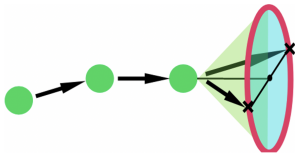

Figure C.24: At a branching event, the new direction is drawn uniformly from the pink set, which is a circle in a plane rectangular to the current direction. The new branches point in opposing directions.

The allowed number of growth-trials is set to $N_g = 5$ (differing from [73], where $N_g = 1$). This proved to be a good value for creating the effect of dense regions in the simulations, where no more growth is possible, but still allowed growing branches to evade other branches. For a branching event, we simply set $N_b = N_g^2$, even though the two proposed coordinates are clearly not independent.

As a self-avoiding process, all growing branches of the tree can get trapped, then growth stops. For the tested branching rates, the empirical probability of such an event was negligible, further this extinction occured only in the initial steps. We ignored such rare cases and simply restarted the simulation.

We estimated the number of tumour cells at the time of diagnosis from ten prostatectomy cases with small, intermediate and large tumours. This was done by calculating the amount of tumour cells in the tumour focus in one histological slide (Using QuPath software [10]), given the thickness of a standard tumour piece in a block of 4mm, with median tumour cell size of 20 µm, and typical number of blocks with tumour tissue in radical prostatectomy specimens. At that, we received an average number of cells 70 mln, 300 mln, and 800 mln for small, intermediate, and very large tumours, corresponding to the number of cells derived from tumour volume estimates from Salomon et al. [127]. We stopped our simulations at a size of 20 mln model nodes, corresponding to tumours with intermediate size of 300 mln real cells.

In the present model and with the above parameters, this size was reached after a time corresponding to 6000-8500 cell cycles of cells with fitness 1.0 (varying with the appearance of strong driver mutations). The average length of a cell-cycle is given by the inverse of the rate of cell-division $f(v,t)^{-1}$. Assumed that tumour cell divisions happen in a time range of 2-7 days dependent on tumour aggressivity [133], this translates the above 6000-8500 cell cycles into a real-time estimate of the order of 33-46 years

or 115-160 years, respectively. Prostate cancer is known to grow very slow in comparison to other malignant tumours, see for example Schmid et al. [133]. We are aware of the fact that this reasoning provides merely an estimate as we do not account for several factors (e.g. tumour interaction with microenvironment).

C.7.2 Mutations

In order to reduce the computational costs, we reformulate the entire process of mutation and competition in terms of an *effective rate of mutation* and *effective rate of competition*. Some published models take into account drift effects of clonal evolution, for example [139]. However, for computing such models, that additionally incorporate also the spatial structure of the tumor, cells are structured into deems, locally well-mixed populations consisting of several hundreds or thousands of cells, interacting with each other only on the higher level of deems. These deems typically lay on a grid. We adopt this idea, but do compute the internal cellular composition of the deems. The PCAs under investigation form a self-avoiding branched tubular structure. Therefore, we estimated the number of mutations that survive the early fluctuations, and studied their spreading over the tubular network. The smallest unit in our simulations (which reflects the idea of a deem) is a single node of the network. The rate for mutations resulting in a fitness advantage for tumours has long been and still is a subject for investigations and discussions. We adopt the estimate also used in [139, 21] and set the probability for such an event to be equal to $P_\mu = 10^{-5}$ per cell division. Since every node in our model hosts 15 cells, we set the rate of (weaker) driver mutations to $R_\mu(v,t) = 1.5 \cdot 10^{-4} \cdot f(v,t)$. We simulate only such mutations that survive the early fluctuations. Hence, we need to estimate the resulting rate of *effective mutations*. In a large well-mixed population which is in equilibrium, a new trait with small fitness advantage $\Delta > 0$ (in this setting equal to the effective growth rate during the initial growth phase) survives the early fluctuations and fixates with probability

$$P_{fix} \approx 1 - \left(\frac{1}{2}\frac{2+\Delta}{1+\Delta}\right) + \sqrt{\left(\frac{1}{2}\frac{2+\Delta}{1+\Delta}\right)^2 - \frac{1}{1+\Delta}} \approx \Delta. \tag{C.8}$$

The second approximation is good for small , the presented formula yields the survival probability of a supercritical branching process (e.g. [11]). Hence, we define the effective rate of (weaker) driver mutations as

$$R_{\mu,eff}(v,t) = R_\mu \cdot \Delta = 1.5 \cdot 10^{-4} \cdot f(v,t) \cdot \Delta. \tag{C.9}$$

We use this rate for all simulations. The fitness advantage of such a mutation was chosen quite large: $\Delta_f = 4\%$ is to be interpreted as an upper bound, for existing literature see [21, 139]. This upper bound yields certainty when stating that weak drivers cannot be the important evolutionary mechanism.

C.7.3 Competition

Under the assumption of a static interior of the tumour with fixed population size, each cell division must induce a local competition process. If two neighbouring nodes w and v host genotypes with fitness $f(w) = k > 0$ and $f(v) = k + \Delta > k$, respectively, the genotype at v has a fitness advantage. Figure C.25 shows two possibilities to model this. In the microscopic approach where each cell is tracked, a cell divides with either rate $f = k$ and $f = k + \Delta$, respectively. Under the assumption of a fixed population size, a local competition process must take place. This can be modeled by choosing a neighbouring site of the cell that just divided and by replacing the resident cell. Simulating each cell-division would be time-consuming, so we only simulate the resulting advance of the fitter genotype. We already took into account the extinction of the fitter genotype due to early fluctuations by resorting to the effective rate of mutations. Then, in our approach of modeling the effective advance of the fitter genotype, the fitter genotype at v spreads over to its neighbour w with rate

$$R_c(v, w, t) = \frac{f(v, t) f(w, t)}{N(v, t)}, \tag{C.10}$$

where $N(v, t)$ is the number of edges adjacent to v. In the example shown in Figure C.25, the effective speed of advance in this direction is given by $R_c(v, w, t) = \Delta/2$.

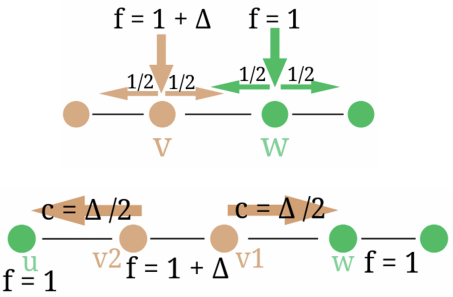

Figure C.25: Competition as a contact process. Cell-divisions occur with fitness $f = 1.0$ and $f = 1.0 + \Delta$, respectively, and result in a replacement of the genotype in one of the neighbouring cells. We model the resulting competition, an advance of the fitter genotype with speed $\Delta/2$.

C.7.4 Strong driver mutations

For simplicity and reproducibility of the results we implement only two different types of mutations with fixed fitness advantages $\Delta_f = 4\%$ and $\Delta_f = 50\%$. The latter value was chosen empirically so that these mutations can spread

with sufficient speed. Such strong mutations have already been reported, for example by Vermeulen et al. [154], even though they investigate the fitness of the first cancer stem cells in intestinal carcinoma. In this study, the authors also conclude that due to a competition process, a gradual clonal development might be not efficient in terms of clonal evolution.

We initially estimated the rate of strong mutations using the incidence of events involving "potent" genes. Their incidence was extracted from published large-scale molecular genetic characterization studies for tumours still growing via branching (i.e. tumours with Gleason-Score $< 4 + 4$): PTEN deletion/mutation (26.8%), TP53 mutation (6%) or deletion (26%) [28], and chromotrypsis (20%) by tumours from 3+3 up to 4+3 [52].

We considered the overall occurrence rate for any of such strong genetic alterations to be about 50% in mid-size tumours of 10 mln vertices that have the branching architecture we modeled. Of those tumours, approximately 20% of tumours show 2 or more of such strong mutation events. For reaching a detectable size, those mutation-events must have occurred at some timepoint before the molecular genetic evaluation of the tumour.

To translate these findings into the model, we assume that rare mutations have a small, fixed probability per cell-division P^s_μ, which we can estimate. Under this assumption, rare mutations follow the dynamics of a Poisson point process, with rate depending on the fitness of the present cells. Assuming that cells have constant fitness $f(v,t) = 1.0$ before the first driver mutations occurs, the rate of a driver mutation per vertex is given by $R^s_{\mu,eff}(v,t) = P^s_\mu f(v,t) = const.$ By the above literature, the probability for finding no strong mutation in a tumour is roughly given by $1/2 = P_\lambda(0) = e^{-\lambda}$, where λ is the *accumulated effective rate of rare mutations* up to the chosen timepoint. We consider the time when the network reaches the size of 10mln model nodes, thus

$$\lambda = \int_0^{T_{10mln}} \Big[\sum_{v \in V(t)} R^s_{\mu,eff}(v,t) \Big] \, dt. \tag{C.11}$$

By performing several simulations, we estimated the above integral numerically. The result is a first estimate for the effective rate of strong mutations: $R^s_{\mu,eff}(v,t) \approx 5 \cdot 10^{-11} f(v,t)$.

However, simulations with this rate of strong driver mutations do not show any significant divergent clonal evolution since the clones arrive far too late (Section C.2; Fig. C.3, C.4). Hence, in our experiments we tested an increased rate of strong mutations, using values up to $R^s_{\mu,eff}(v,t) \approx 5 \cdot 10^{-9} f(v,t)$: of up to the hundredfold of our original estimate, but still far below the rate of weaker driver mutations.

C.7.5 Saturation of fitness

As a final adjustment, we included a saturation effect into our fitness landscape. Typically, a fitness-advantage Δ induced by a mutation is understood to be multiplicative, meaning $f_{new} = (1+\Delta)f_{old}$. As discussed so far, a large fitness advantage is needed for drivers to be able to spread. On top of that they have to arrive early for having any impact, so the effective rate of strong mutations needs to be rather high. The problem is that this led to very large maximal fitness values of order $f = 1.5^8 \approx 25.6$ – even though those values were reached only by subpopulations occupying 1-5% of the tumour. To address this, we introduce a saturation effect into the fitness-landscape and define

$$f_{new}(v,t) := f_{old}(v,t) \cdot \Big[1 + \Delta \cdot \Big(1 - \frac{f_{old}(v,t)}{f_{max}}\Big)\Big]. \tag{C.12}$$

We set $f_{max} = 10$. We compared the results of this saturation mechanism to the increase of KI-67 in prostate carcinoma, which is an indicator for cell proliferation. Aaltoma et al. [1] found an increase of KI-67 by a factor of three when comparing different patient groups, categorized by survival. Our simulations resulted in a final mean-fitness of $f_{mean} = 1.33$, with rate of strong drivers set to $R^s_{my,eff}(v,t) = 5 \cdot 10^{-10} f(v,t)$ (X10) and $f_{mean} = 2.18$ when setting the rate of strong drivers to $R^s_{my,eff}(v,t) = 5 \cdot 10^{-9} f(v,t)$ (X100). Here, the first node always started with a reference-value of $f = 1$. For the maximal fitness, the simulations resulted in a mean of $f_{max} = 2.80$ (X10) and $f_{max} = 5.04$ (X100) respectively, the latter caused by typically at most 5 consecutive hits. As we model tumours with a range of Gleason scores from 3+3 to 4+3, this seems to be a reasonable range for different fitness values, roughly aligning with the findings of Aaltoma et al. [1].

C.7.6 Evaluation

C.7.6.1 Biopsies

To calculate the dimensions of the virtual biopsy and number of tumour cells in it we have summarized the information from 30 typical prostate biopsies from the archive of the pathological institute of the University Hospital Cologne. Those contain 8-22 cores and a complete range of Gleason Scores. The median number of positive cores is approximately 4.3 (range 1-13). For single cases: the median cumulative tumour length over all positive biopsies per case was 4.2 mm (range 0.75-10 mm). The maximal tumour length per biopsy in single cases was 7.0 mm (range 1-22 mm). Accounting for fixation shrinkage artifacts we select a reference tumour tissue length in a core of 5 mm for modelling. According to these estimations and that the median core diameter was measured to be 0.8 mm, we calculate the number

of tumour cells in a core to be approximately 450.000-525.000 tumour cells, corresponding to approximately 30.000-35.000 model nodes.

Based on this we define a virtual core of the biopsy to be a cylinder, with ratio of length and diameter 8:1, containing roughly 32.000 nodes per core (range 30.000-35.000). A biopsy contains a total of five cores. Their horizontal position is chosen using a fixed pattern (Figure C.19), their vertical distance from the boundary of the tumour is chosen randomly.

C.7.6.2 Clusters

For visualizing the clonal hierarchy in a tumour, we derive a phylogenetic tree for every synthetic tumour (see Fig. C.4, C.5, C.7, C.9), and then perform a rather simple clustering. At that, we order the different mutations in resulting genotypical clusters as follows. Given the full tree, first we ignore all mutations with relative frequency below a chosen threshold C_{min}. Then, we follow the leaves up to the first junction of the reduced ancestral tree. The last trait below this junction is defined as a genotypical cluster (if this trait has not been split up into clusters before).

This procedure has several advantages. We are interested in the more advanced genotypes. Those are represented, at the cost that some possibly larger, but less advanced parts of the tumour do not show up (since the corresponding genotypes lie above a branching that is used for defining a cluster). This approach allows to ignore all mutations present in only few cells. Again, those account for a large part of the tumour, but are not interesting in terms of effective clonal structure. Further, this type of clustering does not dependent on any artificial weighting as we have knowledge of the complete phylogenetic tree. Increasing C_{min} reduces the number of different clusters. The two extreme cases are: 1) $C_{min} = 1$: in this case, all leaves of the original ancestral graph are denoted as clusters. 2) $C_{min} = |V|$, the number of nodes of the tumour network: in this case, the entire tumour is registered as a single cluster. We choose $C_{min} = 0.05 \cdot |V|$. Thereby we ignore any mutations with a relative frequency of less than of 5%, this cut-off is for example also used when evaluating the Gleason Score of a radical prostatectomy specimen. Here, morphologically more advanced parts of the tumour that make less than 5% of the tumour volume are ignored in final classification (tertiary pattern). We further used fishplots [108] to outline temporal dynamics in selected tumours.

C.7.7 Modes and growth of evolution

In this section we are going to discuss that the concrete choices of the growth rate and of the fitness landscape do not impact the main result: only few strong drivers can spread and eventually have an impact on the overall growth of the tumour.

C.7.7.1 Possibility of clonal sweeps

In the simulations, an early phase where clonal sweeps are possible is followed by a phase of a more multiclonal evolution. If the speed of competition for a new mutation is of order R_c, which is smaller than the current speed of growth at the tips, so $R_g + R_b \geq R_c$, this new mutation has a very small chance to reach the growing boundary, except when occurring close to or at the growing tip. The fitness at the tips is thereby a-priori bounded by $R_g + R_b \leq Comp_{max}$, where $Comp_{max}$ is the maximal possible speed of competition between two neighbouring genotypes. Typically, two neighbours differ only in at most one strong mutation (and maybe one or two neglectable smaller ones). Assume now that we have two neighbouring nodes v and w, where w hosts the stronger genotype with one additional strong mutation with increment Δ_f^s compared to v. The speed of competition between those two is regulated via the difference in fitness and given by

$$R_c = \frac{f(w) - f(v)}{2} = \frac{\Delta_f^s}{2}\Big(f(v) - \frac{f(v)^2}{f_{max}}\Big). \tag{C.13}$$

This expression has a maximum at $f_{max}/2$, which is given by $Comp_{max} = \frac{\Delta_f^s \cdot f_{max}}{8}$. With the chosen parameters $\Delta_f^s = 0.5$ and $f_{max} = 10$, this gives an upper bound for the maximal possible growth-speed of $Comp_{max} = 5/8$. When this speed is reached, no more clonal sweeps can occur. Given speed of growth $(C_b + C_g) \cdot f(v,t)$, this maximum is reached when $(C_b + C_g) \cdot f(v,t) = Comp_{max}$. As we set $C_g + C_b = 0.1$, the change formally occurs when the tips reach a fitness $f = 6.25$. However, a more multiclonal development took place in almost all simulations in the cohorts X10, X50 and X100, at most one total clonal sweep occurred, See Fig. C.4, C.5. The presented upper bound is more of theoretical interest. Most driver hits occur too late for resulting in total clonal sweeps, these are also prevented from multiple rivaling fitter clones.

C.7.7.2 Qualitative results and choice of fitness landscape

We present two alternative settings for the overall growth rate and the induced fitness advantages. For the total growth as a sum of branching and growth rate, we previously chose $(C_g + C_b) \cdot f(v,t) = 0.1 \cdot f(v,t)$, call it *linear growth* in the following. The alternative would be a more *additive growth*, written as a function of the fitness: $(C_g + C_b)(f) = f - 0.9$. For the reference value $f = 1$, both approaches lead to an effective initial total growth-speed of 0.1. In the additive setting, an increased fitness leads to bigger increase of the total growth speed. Let us call the fitness landscape with saturation-effect and $f_{max} = 10.0$ *saturated fitness*. Without this saturation-effect, it holds that $f_{new} = (1 + \Delta) \cdot f_{old}$, let us denote this as *multiplicative fitness*.

To understand the different settings, take a look at the table in Fiture C.26. It displays the scenario that a single genotype with one additional

strong driver arises within the tumour and spreads along the edges of the network, with speed of competition roughly given by $R_c(v, w, t) = \frac{f_{new} - f_{old}}{2}$. The genealogical ancestor (that lacks this mutation) occupies the rest of the network and dictates the speed of growth. Each table shows the fitness of a fitter mutant after n consecutive driver hits (from 1-5), the resulting competition-speed in an environment that has only $n - 1$ driver-mutations, and the current growth-speed generated by the less fit type. In both scenarios with additive growth, only one sweep is possible at all, possibly an argument against this scenario. In the scenario with saturated fitness and linear growth (which we chose), competition is theoretically faster than growth given not more than 5 consecutive driver mutations. However, in the simulations, time of appearance and additional rivaling clones prevented total sweeps and instead led to a number of several co-existing fitter clones. At the end of the simulations in our three settings X10, X50, and X100, the most advanced clones had a median of 1, 2, and 3 consecutive strong mutations (range 0-3, 1-3, and 1-5), respectively (Fig. C.11, C.12, C.13). In the scenario with multiplicative fitness advantages and linear growth, the difference between competition speed and growth speed after the first few mutations is not much larger than in the scenario with saturated fitness, leading to a similar behavior in terms of clonal evolution.

saturated fitness | linear growth

Fitness	Competition	Growth
1.45	0.23	0.1
2.07	0.31	0.14
2.89	0.41	0.21
3.92	0.52	0.29
5.11	0.60	0.39

multiplicative fitness | linear growth

Fitness	Competition	Growth
1.5	0.25	0.1
2.25	0.38	0.15
3.38	0.56	0.23
5.06	0.85	0.34
7.59	1.27	0.51

saturated fitness | additive growth

Fitness	Competition	Growth
1.45	0.23	0.1
2.07	0.31	0.55
2.89	0.41	1.17
3.92	0.52	1.99
5.11	0.60	3.02

multiplicative fitness | additive growth

Fitness	Competition	Growth
1.5	0.25	0.1
2.25	0.38	0.55
3.38	0.56	1.17
5.06	0.85	1.99
7.59	1.27	3.02

Figure C.26: Scenarios with different fitness landscapes and growth terms. A genotype with one additional strong driver arises deep within the tumour and spreads. The genealogical ancestor (that lacks this mutation) occupies the rest of the network and dictates the current speed of growth. Each table shows the fitness of a fitter mutant after n consecutive driver hits (from 1-5), the resulting competition-speed in an environment that has only n-1 driver-mutations, and the growth speed that stems from the less fit type. When the growth speed exceeds the competition speed, it has reached its (effective) maximum.

References

[1] S. Aaltomaa, P. Lipponen, S. Vesalainen, M. Ala-Opas, M. Eskelinen, and K. Syrjänen. Value of Ki-67 immunolabelling as a prognostic factor in prostate cancer. *European Urology*, 32(4):410–415, 1997.

[2] W. Abida, J. Armenia, A. Gopalan, et al. Prospective Genomic Profiling of Prostate Cancer Across Disease States Reveals Germline and Somatic Alterations That May Affect Clinical Decision Making. *JCO Precision Oncology*, 2017.

[3] J. Alexander, R. Gardner, and C. Jones. A topological invariant arising in the stability analysis of travelling waves. *Journal fuer die reine und angewandte Mathematik*, 410:167–212, 1990.

[4] J. Alexander, J. Kendall, J. McIndoo, et al. Utility of Single-Cell Genomics in Diagnostic Evaluation of Prostate Cancer. *Cancer Research*, 78(2):348–358, 2017.

[5] J. Armenia, S. Wankowicz, D. Liu, et al. The long tail of oncogenic drivers in prostate cancer. *Nature Genetics*, 50(5):645–651, 2018.

[6] G. Arumugam and J. Tyagi. Keller-Segel Chemotaxis Models: A Review. *Acta Applicandae Mathematicae*, 171(1):6, 2020.

[7] K. Athreya and P. Ney. *Branching Processes*. Grundlehren der mathematischen Wissenschaften. Springer Berlin, Heidelberg, 1 edition, 2011.

[8] S. Athreya and J. Swart. Systems of branching, annihilating, and coalescing particles. *Electronic Journal of Probability*, 17:1 – 32, 2012.

[9] S. Baca, D. Brandi, L. Garraway, et al. Punctuated evolution of prostate cancer genomes. *Cell*, 153(3):666–677, 2013.

[10] P. Bankhead, M. Loughrey, J. Fernández, et al. QuPath: Open source software for digital pathology image analysis. *Scientific Reports*, 7(1):16878, 2017.

[11] V. Bansaye and S. Méléard. *Stochastic Models for Structured Populations*. Mathematical Biosciences Institute Lecture Series. Springer International Publishing, Switzerland, 2015.

[12] B. Barker, J. Humpherys, G. Lyng, and J. Lytle. Evans function computation for the stability of travelling waves. *Philosophical Transactions of the Royal Society A: Mathematical, Physical and Engineering Sciences*, 376(2117):20170184, 2018.

[13] B. Barker, J. Humpherys, and K. Zumbrun. Stablab: A matlab-based numerical library for evans function computation. `https://github.com/nonlinear-waves/stablab_matlab`, 2015.

[14] P. Bates and C. Jones. Invariant Manifolds for Semilinear Partial Differential Equations. In U. Kirchgraber and H. Walther, editors, *Dynamics Reported: A Series in Dynamical Systems and Their Applications*, pages 1–38. Vieweg & Teubner Verlag, Wiesbaden, 1989.

[15] H. Berestycki, B. Nicolaenko, and B. Scheurer. Traveling Wave Solutions to Combustion Models and Their Singular Limits. *SIAM Journal on Mathematical Analysis*, 16(6):1207–1242, 1985.

[16] J. Berestycki, E. Brunet, and B. Derrida. A new approach to computing the asymptotics of the position of Fisher-KPP fronts. *Europhysics Letters (EPL)*, 122(1):10001, 2018.

[17] M. Bogdan and T. Savin. Fingering instabilities in tissue invasion: an active fluid model. *Royal Society Open Science*, 5(12):181579, 2018.

[18] P. Boutros, M. Fraser, N. Harding, et al. Spatial genomic heterogeneity within localized, multifocal prostate cancer. *Nature Genetics*, 47(7):736–745, 2015.

[19] A. Bovier and L. Hartung. The speed of invasion in an advancing population. *Preprint available under arXiv:2204.11072 [math.PR]*, 2022.

[20] W. Boyce, R. DiPrima, and D. Meade. *Elementary Differential Equations*. John Wiley & Sons, Hoboken, New Jersey, 11 edition, 2017.

[21] I. Bozic, T. Antal, H. Ohtsuki, H. Carter, D. Kim, S. Chen, R. Karchin, K. Kinzler, B. Vogelstein, and M. Nowak. Accumulation of driver and passenger mutations during tumor progression. *Proceedings of the National Academy of Sciences of the United States of America*, 107(43):18545–18550, 2010.

[22] M. Bramson. Convergence of solutions of the Kolmogorov equation to travelling waves. *Memoirs of the American Mathematical Society*, 44(285), 1983.

[23] M. Bramson, D. Wan-Ding, and R. Durrett. Annihilating branching processes. *Stochastic Processes and their Applications*, 37(1):1–17, 1991.

[24] N. Britton. *Essential Mathematical Biology*, volume 1 of *Springer Undergraduate Mathematics Series*. Springer-Verlag, London, 2003.

[25] D. Brocks, Y. Assenov, S. Minner, et al. Intratumor DNA methylation heterogeneity reflects clonal evolution in aggressive prostate cancer. *Cell reports*, 8(3):798–806, 2014.

[26] L. Bányai, M. Trexler, K. Kerekes, O. Csuka, and L. Patthy. Use of signals of positive and negative selection to distinguish cancer genes and passenger genes. *eLife*, 10:e59629, 2021.

[27] S. Camazine, J. Deneubourg, N. Franke, J. Sneyd, G. Theraulaz, and E. Bonabeau. *Self-Organization in Biological Systems*, volume 38. Princeton University Press, 2001.

[28] Cancer Genome Atlas Research Network. The Molecular Taxonomy of Primary Prostate Cancer. *Cell*, 163(4):1011–1025, 2015.

[29] J. Cardy and U. Täuber. Theory of Branching and Annihilating Random Walks. *Physical Review Letters*, 77:4780–4783, 1996.

[30] J. Carr. *Applications of Centre Manifold Theory*, volume 35 of *Applied Mathematical Sciences*. Springer-Verlag, New York, 1 edition, 1982.

[31] M. Casás-Selves and J. Degregori. How cancer shapes evolution, and how evolution shapes cancer. *Evolution (NY)*, 4(4):624–634, 2011.

[32] J. Cohen. Mathematics Is Biology's Next Microscope, Only Better; Biology Is Mathematics' Next Physics, Only Better. *PLOS Biology*, 2(12), 2004.

[33] C. Cooper, R. Eeles, D. Wedge, et al. Analysis of the genetic phylogeny of multifocal prostate cancer identifies multiple independent clonal expansions in neoplastic and morphologically normal prostate tissue. *Nature genetics*, 47(4):367–372, 2015.

[34] Y. Coudert, S. Harris, and B. Charrier. Design Principles of Branching Morphogenesis in Filamentous Organisms. *Current Biology*, 29(21):R1149–R1162, 2019.

[35] Cun, Y. and Yang, T. and Achter, V. and Lang, U. and Peifer, M. Copy-number analysis and inference of subclonal populations in cancer genomes using Sclust. *Nature Protocols*, 13(6):1488–1501, 2018.

[36] K. Cyll, E. Ersvær, L. Vlatkovic, et al. Tumour heterogeneity poses a significant challenge to cancer biomarker research. *British Journal of Cancer*, 117(3):367–375, 2017.

[37] J. d'Alessandro, A. Barbier-Chebbah, V. Cellerin, O. Benichou, R. Mège, R. Voituriez, and B. Ladoux. Cell migration guided by long-lived spatial memory. *Nature Communications*, 12(1):4118, 2021.

[38] J. Davies. *Branching Morphogenesis*. Molecular Biology Intelligence Unit. Springer-Verlag, New York, 1 edition, 2005.

[39] S. Dentro, I. Leshchiner, K. Haase, et al. Characterizing genetic intra-tumor heterogeneity across 2,658 human cancer genomes. *Cell*, 184(8):2239–2254.e39, 2021.

[40] N. Donmez, S. Malikic, A. Wyatt, M. Gleave, C. Collins, and S. Sahinalp. Clonality Inference from Single Tumor Samples Using Low-Coverage Sequence Data. *Journal of Computational Biology*, 24(6):515–523, 2017.

[41] A. Ducrot, T. Giletti, and H. Matano. Spreading speeds for multidimensional reaction-diffusion systems of the prey-predator type. *Calculus of Variations and Partial Differential Equations*, 58(4):137, 2019.

[42] J. Epstein, M. Amin, S. Fine, et al. The 2019 Genitourinary Pathology Society (GUPS) White Paper on Contemporary Grading of Prostate Cancer. *Archives of pathology & laboratory medicine*, 145(4):461—493, 2021.

[43] S. Espiritu, L. Liu, P. Boutros, et al. The Evolutionary Landscape of Localized Prostate Cancers Drives Clinical Aggression. *Cell*, 173(4):1003–1013.e15, 2018.

[44] T. Ethier and S. Kurtz. *Markov Processes: Characterization and Convergence*. Wiley-Interscience, 2005.

[45] J. Evans and J. Feroe. Local stability of the nerve impulse. *Mathematical Biosciences*, 37(1):23–50, 1977.

[46] J. Falco, A. Agosti, I. Vetrano, A. Bizzi, F. Restelli, M. Broggi, M. Schiariti, F. DiMeco, P. Ferroli, P. Ciarletta, and F. Acerbi. In Silico Mathematical Modelling for Glioblastoma: A Critical Review and a Patient-Specific Case. *Journal of clinical medicine*, 10(10):2169, 2021.

[47] G. Faye and M. Holzer. Asymptotic stability of the critical Fisher-KPP front using pointwise estimates. *Zeitschrift für angewandte Mathematik und Physik*, 70(1):13, 2018.

[48] G. Faye and M. Holzer. Asymptotic stability of the critical pulled front in a Lotka-Volterra competition model. *Journal of Differential Equations*, 269(9):6559–6601, 2020.

[49] N. Fenichel. Geometric singular perturbation theory for ordinary differential equations. *Journal of Differential Equations*, 31(1):53–98, 1979.

[50] R. Fisher. The Wave of Advance of Advantageous Genes. *Annals of Eugenics*, 7(4):355–369, 1937.

[51] R. FitzHugh. Impulses and Physiological States in Theoretical Models of Nerve Membrane. *Biophysical Journal*, 1(6):445–466, 1961.

[52] M. Fraser, V. Sabelnykova, P. Boutros, et al. Genomic hallmarks of localized, non-indolent prostate cancer. *Nature*, 541(7637):359–364, 2017.

[53] T. Gallay. Local stability of critical fronts in nonlinear parabolic partial differential equations. *Nonlinearity*, 7(3):741–764, 1994.

[54] R. Gardner. Existence and stability of travelling wave solutions of competition models: A degree theoretic approach. *Journal of Differential Equations*, 44(3):343–364, 1982.

[55] R. Gardner and C. Jones. Stability of Travelling Wave Solutions of Diffusive Predator-Prey Systems. *Transactions of the American Mathematical Society*, 327(2):465–524, 1991.

[56] R. Gardner and K. Zumbrun. The gap lemma and geometric criteria for instability of viscous shock profiles. *Communications on Pure and Applied Mathematics*, 51(7):797–855, 1998.

[57] J. Gauthier, A. Vincent, S. Charette, and N. Derome. A brief history of bioinformatics. *Briefings in Bioinformatics*, 20(6):1981–1996, 2018.

[58] J. George, J. Lim, S. Jang, et al. Comprehensive genomic profiles of small cell lung cancer. *Nature*, 524(7563):47–53, 2015.

[59] C. Gerhauser, F. Favero, T. Risch, et al. Molecular Evolution of Early-Onset Prostate Cancer Identifies Molecular Risk Markers and Clinical Trajectories. *Cancer Cell*, 34(6):996–1011.e8, 2018.

[60] M. Gerstung, C. Jolly, I. Leshchiner, et al. The evolutionary history of 2,658 cancers. *Nature*, 578(7793):122–128, February 2020.

[61] A. Ghazaryan. Nonlinear Stability of High Lewis Number Combustion Fronts. *Indiana University Mathematics Journal*, 58(1):181–212, 2009.

[62] A. Ghazaryan, Y. Latushkin, and S. Schecter. Stability of Traveling Waves for Degenerate Systems of Reaction Diffusion Equations. *Indiana University Mathematics Journal*, 60(2):443–471, 2011.

[63] A. Ghazaryan, Y. Latushkin, and S. Schecter. Stability of Traveling Waves in Partly Parabolic Systems. *Mathematical Modelling of Natural Phenomena*, 8(5):31–47, 2013.

[64] A. Ghazaryan, Y. Latushkin, S. Schecter, and A. de Souza. Stability of Gasless Combustion Fronts in One-Dimensional Solids. *Archive for Rational Mechanics and Analysis*, 198(3):981–1030, 2010.

[65] D. Gillespie. Exact stochastic simulation of coupled chemical reactions. *Journal of Physical Chemistry*, 81:2340–2361, 1977.

[66] L. Girardin and K. Lam. Invasion of open space by two competitors: spreading properties of monostable two-species competition-diffusion systems. *Proceedings of the London Mathematical Society*, 119(5), 2019.

[67] J. Guckheimer and P. Holmes. *Nonlinear Oscillations, Dynamical Systems, and Bifurcations of Vector Fields*, volume 1 of *Applied Mathematical Sciences*. Springer-Verlag, New York, 1 edition, 1983.

[68] Y. Guo, M. Sun, A. Garfinkel, and X. Zhao. Mechanisms of Side Branching and Tip Splitting in a Model of Branching Morphogenesis. *PLOS ONE*, 9(7):1–14, 2014.

[69] M. Haffner, A. De Marzo, S. Yegnasubramanian, J. Epstein, and H. Carter. Diagnostic challenges of clonal heterogeneity in prostate cancer. *Journal of Clinical Oncology*, 33(7):e38–40, 2014.

[70] M. Haffner, T. Mosbruger, D. Esopi, et al. Tracking the clonal origin of lethal prostate cancer. *Journal of Clinical Investigation*, 123(11):4918–4922, 2013.

[71] M. Haffner, C. Weier, M. Xu, et al. Molecular evidence that invasive adenocarcinoma can mimic prostatic intraepithelial neoplasia (PIN) and intraductal carcinoma through retrograde glandular colonization. *Journal of pathology*, 238(1):31–41, 2015.

[72] M. Haffner, W. Zwart, M. Roudier, et al. Genomic and phenotypic heterogeneity in prostate cancer. *Nature Reviews Urology*, 18(2):79–92, 2021.

[73] E. Hannezo, C. Scheele, M. Moad, N. Drogo, R. Heer, R. Sampogna, J. van Rheenen, and B. Simons. A Unifying Theory of Branching Morphogenesis. *Cell*, 171(1):242–255.e27, 2017.

[74] E. Hannezo and B. Simons. Statistical theory of branching morphogenesis. *Development, Growth & Differentiation*, 60(9):512–521, 2018.

[75] J. Hendricks, J. Humpherys, G. Lyng, and K. Zumbrun. Stability of Viscous Weak Detonation Waves for Majda's Model. *Journal of Dynamics and Differential Equations*, 27(2):237–260, 2015.

[76] D. Henry. *Geometric Theory of Semilinear Parabolic Equations*. Lecture Notes in Mathematics. Springer Berlin, Heidelberg, 1 edition, 1981.

[77] C. Herling, N. Abedpour, J. Weiss, et al. Clonal dynamics towards the development of venetoclax resistance in chronic lymphocytic leukemia. *Nature Communications*, 9(1):727, 2018.

[78] M. Hong, G. Macintyre, D. Wedge, et al. Tracking the origins and drivers of subclonal metastatic expansion in prostate cancer. *Nature Communications*, 6:6605, 2015.

[79] P. Hsieh and Y. Sibuya. *Basic Theory of Ordinary Differential Equations*. Universitext. Springer-Verlag, New York, 1 edition, 1999.

[80] P. Hunter. Biology is the new physics. *EMBO Rep*, 11(5):350–352, 2010.

[81] D. Iber and D. Menshykau. The control of branching morphogenesis. *Open Biol*, 3(9):130088, 2013.

[82] J. Kübler J. Kaandorp. *The Algorithmic Beauty of Seaweeds, Sponges and Corals*. The Virtual Laboratory. Springer Berlin, Heidelberg, 1 edition, 2001.

[83] S. Jain, B. Ladoux, and R. Mège. Mechanical plasticity in collective cell migration. *Current Opinion in Cell Biology*, 72:54–62, 2021.

[84] C. Jones. Geometric singular perturbation theory. In R. Johnson, editor, *Dynamical Systems. Lecture Notes in Mathematics*, pages 44–118. Springer Berlin, Heidelberg, 1995.

[85] Y. Kan-On and Q. Fang. Stability of monotone travelling waves for competition-diffusion equations. *Japan Journal of Industrial and Applied Mathematics*, 13(2):343–349, 1996.

[86] I. Karatzas and S. Shreve. *Brownian Motion and Stochastic Calculus*. Graduate Texts in Mathematics. Springer-Verlag, New York, 2 edition, 1991.

[87] E. Karsenti. Self-organization in cell biology: a brief history. *Nature Reviews Molecular Cell Biology*, 9(3):255–262, 2008.

[88] E. Keller and L. Segel. Traveling bands of chemotactic bacteria: A theoretical analysis. *Journal of Theoretical Biology*, 30(2):235–248, 1971.

[89] K. Kirchgässner. On the nonlinear dynamics of travelling fronts. *Journal of Differential Equations*, 96(2):256–278, 1992.

[90] U. Kirchgraber and K. Palmer. *Goemetry in the neighborhood of invariant manifolds of maps and flows and linearization*, volume 233 of *Pitman research notes in mathematics*. Longman Group UK Limited, Harlow, UK, 1990.

[91] A. Kolmogorov, I. Petrovskii, and N. Piscunov. A study of the equation of diffusion with increase in the quantity of matter, and its application to a biological problem. *Byul. Moskovskogo Gos. Univ.*, 1(6):1–25, 1937.

[92] F. Kreten. Traveling waves of an FKPP-type model for self-organized growth. *Journal of Mathematical Biology*, 84(6):42, 2022.

[93] F. Kreten. Convective stability of the critical waves of an FKPP growth process. *Preprint available under arXiv:2305.10228 [math.AP]*, 2023.

[94] F. Kreten, R. Büttner, M. Peifer, C. Harder, A. Hillmer, N. Abedpour, A. Bovier, and Y. Tolkach. Tumour architecture and emergence of strong genetic alterations are bottlenecks for clonal evolution in primary prostate cancer. *Unpublished*.

[95] A. Kristiansen, R. Bergström, B. Delahunt, et al. Somatic alterations detected in diagnostic prostate biopsies provide an inadequate representation of multifocal prostate cancer. *The Prostate*, 79(8):920–928, 2019.

[96] C. Lang, L. Conrad, and O. Michos. Mathematical Approaches of Branching Morphogenesis. *Front Genet*, 9:673, 2018.

[97] C. Lattanzio and D. Zhelyazov. Spectral analysis of dispersive shocks for quantum hydrodynamics with nonlinear viscosity. *Mathematical Models and Methods in Applied Sciences*, 31(09):1719–1747, 2021.

[98] J. Lefevre, K. Short, T. Lamberton, O. Michos, D. Graf, I. Smyth, and N. Hamilton. Branching morphogenesis in the developing kidney is governed by rules that pattern the ureteric tree. *Development*, 144(23):4377–4385, 2017.

[99] M. Leroy-Lerêtre, G. Dimarco, M. Cazales, M. Boizeau, B. Ducommun, V. Lobjois, and P. Degond. Are Tumor Cell Lineages Solely Shaped by Mechanical Forces? *Bulletin of Mathematical Biology*, 79(10):2356–2393, 2017.

[100] M. Linch, G. Goh, C. Hiley, et al. Intratumoural evolutionary landscape of high-risk prostate cancer: the PROGENY study of genomic and immune parameters. *Annals of Oncology*, 28(10):2472–2480, 2017.

[101] J. Lindberg, A. Kristiansen, P. Wiklund, H. Grönberg, and L. Egevad. Tracking the Origin of Metastatic Prostate Cancer. *European Urology*, 67(5):819–822, 2015.

[102] G. Lorenzo, T. Hughes, P. Dominguez-Frojan, A. Reali, and H. Gomez. Computer simulations suggest that prostate enlargement due to benign prostatic hyperplasia mechanically impedes prostate cancer growth. *Proceedings of the National Academy of Sciences of the United States of America*, 116(4):1152–1161, 2019.

[103] G. Lorenzo, V. Pérez-García, A. Mariño, L. Pérez-Romasanta, A. Reali, and H. Gomez. Mechanistic modelling of prostate-specific antigen dynamics shows potential for personalized prediction of radiation therapy outcome. *Journal of The Royal Society Interface*, 16(157):20190195, 2019.

[104] M. Løvf, S. Zhao, U. Axcrona, B. Johannessen, A. Bakken, K. Carm, A. Hoff, O. Myklebost, L. Meza-Zepeda, A. Lie, K. Axcrona, R. Lothe, and R. Skotheim. Multifocal Primary Prostate Cancer Exhibits High Degree of Genomic Heterogeneity. *European Urology*, 75(3):498–505, 2019.

[105] N. Madras and G. Slade. *The Self-Avoiding Walk*. Modern Birkhäuser Classics. Birkhäuser New York, NY, 2012.

[106] T. Mammoto and D. Ingber. Mechanical control of tissue and organ development. *Development*, 137(9):1407–1420, 2010.

[107] J. Mathiesen, I. Procaccia, H. Swinney, and M. Thrasher. The universality class of diffusion-limited aggregation and viscous fingering. *Europhysics Letters*, 76(2):257, 2006.

[108] C. Miller, J. McMichael, H. Dang, C. Maher, L. Ding, T. Ley, E. Mardis, and R. Wilson. Visualizing tumor evolution with the fishplot package for R. *BMC Genomics*, 17(1):880, 2016.

[109] T. Misteli. The concept of self-organization in cellular architecture. *Journal of Cell Biology*, 155(2):181–185, 2001.

[110] M. Moad, E. Hannezo, R. Heer, et al. Multipotent Basal Stem Cells, Maintained in Localized Proximal Niches, Support Directed Long-Ranging Epithelial Flows in Human Prostates. *Cell Rep*, 20(7):1609–1622, 2017.

[111] S. Montes-Olivas, L. Marucci, and M. Homer. Mathematical Models of Organoid Cultures. *Frontiers in genetics*, 10:873–873, 2019.

[112] J. Nagumo, S. Arimoto, and S. Yoshizawa. An Active Pulse Transmission Line Simulating Nerve Axon. *Proceedings of the IRE*, 50(10):2061–2070, 1962.

[113] B. Nerger, J. Jaslove, H. Elashal, S. Mao, A. Košmrlj, A. Link, and C. Nelson. Local accumulation of extracellular matrix regulates global morphogenetic patterning in the developing mammary gland. *Current Biology*, 31(9):1903–1917.e6, 2021.

[114] H. Othmer, K. Painter, D. Umulis, and C. Xue. The Intersection of Theory and Application in Elucidating Pattern Formation in Developmental Biology. *Mathematical Modelling of Natural Phenomena*, 4(4):3–82, 2009.

[115] F. Ozbag and S. Schecter. Stability of combustion waves in a simplified gas–solid combustion model in porous media. *Philosophical Transactions of the Royal Society A: Mathematical, Physical and Engineering Sciences*, 376(2117):20170185, 2018.

[116] K. Painter. Mathematical models for chemotaxis and their applications in self-organisation phenomena. *Journal of Theoretical Biology*, 481:162–182, 2019.

[117] A. Pazy. Semigroups of Linear Operators and Applications to Partial Differential Equations. *Journal of Applied Mathematics and Mechanics*, 1983.

[118] R. Pego and M. Weinstein. Asymptotic stability of solitary waves. *Communications in Mathematical Physics*, 164(2):305–349, 1994.

[119] M. Peifer, L. Fernández-Cuesta, M. Sos, et al. Integrative genome analyses identify key somatic driver mutations of small-cell lung cancer. *Nature Genetics*, 44(10):1104–1110, 2012.

[120] B. Perthame. PDE Models for Chemotactic Movements: Parabolic, Hyperbolic and Kinetic. *Applications of Mathematics*, 49(6):539–564, 2004.

[121] B. Perthame, F. Quirós, and J. Vázquez. The Hele-Shaw Asymptotics for Mechanical Models of Tumor Growth. *Archive for Rational Mechanics and Analysis*, 212(1):93–127, 2014.

[122] L. Preziosi and A. Tosin. Multiphase modelling of tumour growth and extracellular matrix interaction: mathematical tools and applications. *Journal of Mathematical Biology*, 58(4):625–656, 2009.

[123] J. Reiter, M. Baretti, J. Gerold, et al. An analysis of genetic heterogeneity in untreated cancers. *Nature Reviews Cancer*, 19(11):639–650, 2019.

[124] J. Rottmann-Matthes. Stability of parabolic-hyperbolic traveling waves. *Dynamics of Partial Differential Equations*, 9:29–62, 2012.

[125] V. Rottschäfer and C. Wayne. Existence and Stability of Traveling Fronts in the Extended Fisher–Kolmogorov Equation. *Journal of Differential Equations*, 176(2):532–560, 2001.

[126] M. Rubin, G. Girelli, and F. Demichelis. Genomic Correlates to the Newly Proposed Grading Prognostic Groups for Prostate Cancer. *European Urology*, 69(4):557–560, 2016.

[127] L. Salomon, O. Levrel, A. Anastasiadis, J. Irani, A. De La Taille, F. Saint, D. Vordos, A. Cicco, A. Hoznek, D. Chopin, and C. Abbou. Prognostic Significance of Tumor Volume after Radical Prostatectomy: A Multivariate Analysis of Pathological Prognostic Factors. *European Urology*, 43(1):39–44, 2003.

[128] R. Sampayo and M. Bissell. Cancer stem cells in breast and prostate: Fact or fiction? *Advances in Cancer Research*, 144:315–341, 2019.

[129] L. Sander. Diffusion-limited aggregation: A kinetic critical phenomenon? *Contemporary Physics*, 41(4):203–218, 2000.

[130] B. Sandstede. Chapter 18 - Stability of Travelling Waves. In B. Fiedler, editor, *Handbook of Dynamical Systems*, volume 2, pages 983–1055. Elsevier Science, Amsterdam, 2002.

[131] B. Sandstede and A. Scheel. Absolute and convective instabilities of waves on unbounded and large bounded domains. *Physica D: Nonlinear Phenomena*, 145(3):233–277, 2000.

[132] D. Sattinger. On the stability of waves of nonlinear parabolic systems. *Advances in Mathematics*, 22(3):312–355, 1976.

[133] H. Schmid, J. McNeal, and T. Stamey. Observations on the doubling time of prostate cancer. The use of serial prostate-specific antigen in patients with untreated disease as a measure of increasing cancer volume. *Cancer*, 71(6):2031–2040, 1993.

[134] R. Schwartz and A. Schäffer. The evolution of tumour phylogenetics: principles and practice. *Nature Reviews Genetics* , 18(4):213–229, 2017.

[135] G. Sell and Y. You. *Dynamics of Evolutionary Equations*. Applied Mathematical Sciences. Springer-Verlag, New York, 1 edition, 2002.

[136] J. Sherratt, A. Dagbovie, and F. Hilker. A Mathematical Biologist's Guide to Absolute and Convective Instability. *Bulletin of Mathematical Biology*, 76(1):1–26, 2014.

[137] R. Siegel, K. Miller, and A. Jemal. Cancer statistics, 2020. *CA: A Cancer Journal for Clinicians*, 70(1):7–30, 2020.

[138] J. Smoller. *Shock Waves and Reaction-Diffusion Equations*, volume 258 of *Grundlehren der mathematischen Wissenschaften*. Springer-Verlag, New York, 2 edition, 1994.

[139] R. Sun, Z. Hu, A. Sottoriva, T. Graham, A. Harpak, Z. Ma, J. Fischer, D. Shibata, and C. Curtis. Between-region genetic divergence reflects the mode and tempo of tumor evolution. *Nature Genetics*, 49(7):1015–1024, 2017.

[140] M. Sznurkowska, E. Hannezo, R. Azzarelli, et al. Defining Lineage Potential and Fate Behavior of Precursors during Pancreas Development. *Developmental Cell*, 46(3):360–375.e5, 2018.

[141] M. Tarabichi, A. Salcedo, A. Deshwar, et al. A practical guide to cancer subclonal reconstruction from DNA sequencing. *Nature Methods*, 18(2):144–155, 2021.

[142] A. Thomson and P. Marker. Branching morphogenesis in the prostate gland and seminal vesicles. *Differentiation*, 74(7):382–392, 2006.

[143] S. Tobias, M. Proctor, and E. Knobloch. Convective and absolute instabilities of fluid flows in finite geometry. *Physica D: Nonlinear Phenomena*, 113(1):43–72, 1998.

[144] Y. Tolkach and G. Kristiansen. Is high-grade prostatic intraepithelial neoplasia (HGPIN) a reliable precursor for prostate carcinoma? Implications for clonal evolution and early detection strategies. *Journal of Pathology*, 244(4):389–393, 2018.

[145] Y. Tolkach and G. Kristiansen. The Heterogeneity of Prostate Cancer: A Practical Approach. *Pathobiology*, 85(1-2):108–116, 2018.

[146] Y. Tolkach, S. Thomann, and G. Kristiansen. Three-dimensional reconstruction of prostate cancer architecture with serial immunohistochemical sections: hallmarks of tumour growth, tumour compartmentalisation, and implications for grading and heterogeneity. *Histopathology*, 72(6):1051–1059, 2018.

[147] A. Turing. The chemical basis of morphogenesis. *Philosophical Transactions of the Royal Society of London B: Biological Sciences*, 237(641):37–72, 1952.

[148] K. Uchiyama. The behavior of solutions of the equation of Kolmogorov-Petrovsky-Piskunov. *Proceedings of the Japan Academy, Series A, Mathematical Sciences*, 53(7), 1977.

[149] E. van Rensburg. *The Statistical Mechanics of Interacting Walks, Polygons, Animals and Vesicles*. Oxford University Press, 2 edition, 2015.

[150] M. van Royen, E. Verhoef, C. Kweldam, et al. Three-dimensional microscopic analysis of clinical prostate specimens. *Histopathology*, 69(6):985–992, 2016.

[151] D. VanderWeele, C. Brown, J. Taxy, et al. Low-grade prostate cancer diverges early from high grade and metastatic disease. *Cancer Science*, 105(8):1079–1085, 2014.

[152] D. VanderWeele, R. Finney, K. Katayama, et al. Genomic Heterogeneity Within Individual Prostate Cancer Foci Impacts Predictive Biomarkers of Targeted Therapy. *European Urology Focus*, 5(3):416–424, 2019.

[153] F. Varas and J. Vega. Linear Stability of a Plane Front in Solid Combustion at Large Heat of Reaction. *SIAM Journal on Applied Mathematics*, 62(5):1810–1822, 2002.

[154] L. Vermeulen, E. Morrissey, M. van der Heijden, A. Nicholson, A. Sottoriva, S. Buczacki, R. Kemp, S. Tavaré, and D. Winton. Defining stem cell dynamics in models of intestinal tumor initiation. *Science*, 342(6161):995–998, 2013.

[155] J. Visvader and G. Lindeman. Cancer stem cells in solid tumours: accumulating evidence and unresolved questions. *Nature Reviews Cancer*, 8(10):755–768, 2008.

[156] V. Volpert and S. Petrovskii. Reaction-diffusion waves in biology. *Physics of Life Reviews*, 6(4):267–310, 2009.

[157] X. Wang, M. Julio, K. Economides, D. Walker, H. Yu, M. Halili, Y. Hu, S. Price, C. Abate-Shen, and M. Shen. A luminal epithelial stem cell that is a cell of origin for prostate cancer. *Nature*, 461(7263):495–500, 2009.

[158] D. Wedge, G. Gundem, T. Mitchell, et al. Sequencing of prostate cancers identifies new cancer genes, routes of progression and drug targets. *Nature Genetics*, 50(5):682–692, 2018.

[159] R. Wedlich-Söldner and T. Betz. Self-organization: the fundament of cell biology. *Philosophical Transactions of the Royal Society B: Biological Sciences*, 373(1747):20170103, 2018.

[160] L. Wei, J. Wang, E. Lampert, et al. Intratumoral and Intertumoral Genomic Heterogeneity of Multifocal Localized Prostate Cancer Impacts Molecular Classifications and Genomic Prognosticators. *European Urology*, 71(2):183–192, 2016.

[161] S. Wilkinson, H. Ye, A. Sowalsky, et al. Nascent Prostate Cancer Heterogeneity Drives Evolution and Resistance to Intense Hormonal Therapy. *European Urology*, 80(6):746–757, 2021.

[162] M. Williams, B. Werner, C. Barnes, T. Graham, and A. Sottoriva. Identification of neutral tumor evolution across cancer types. *Nature Genetics*, 48(3):238–244, 2016.

[163] Witten, T. and Sander, L. Diffusion-limited aggregation. *Physical Review B*, 27:5686–5697, 1983.

[164] D. Woodcock, E. Riabchenko, S. Taavitsainen, et al. Prostate cancer evolution from multilineage primary to single lineage metastases with implications for liquid biopsy. *Nature Communications*, 11(1):5070, 2020.

[165] B. Wu, X. Lu, H. Shen, et al. Intratumoral heterogeneity and genetic characteristics of prostate cancer. *International Journal of Cancer*, 146(12):3369–3378, 2020.

[166] J. Xin. Multidimensional Stability of Traveling Waves in a Bistable Reaction-Diffusion Equation, I. *Communications in Partial Differential Equations*, 17(11-12):1889–1899, 1992.

[167] K. Zumbrun and P. Howard. Pointwise Semigroup Methods and Stability of Viscous Shock Waves. *Indiana University Mathematics Journal*, 47(3):741–871, 1998.